UNIVERSITY OF CALIFORNIA,
IRVINE

Travel Direction as a Fundamental Component of Human Navigation: Integrating Psychophysics, Neuroimaging, and Computational Modeling Approaches

DISSERTATION

submitted in partial satisfaction of the requirements
for the degree of

DOCTOR OF PHILOSOPHY

in Cognitive Sciences

by

You Cheng

Dissertation Committee:
Assistant Professor Elizabeth R. Chrastil, Chair
Professor Jeffrey Krichmar
Professor Emily Grossman
Professor Ramesh Srinivasan
Professor Bruce McNaughton

2022

TABLE OF CONTENTS

LIST OF FIGURES

LIST OF TABLES

Page

ACKNOWLEDGMENTS

I owe my gratitude to a number of people who have supported me throughout graduate school.

First, I am indebted to my primary advisor Dr. Elizabeth R. Chrastil, a conscientious scholar and a generous person, for patiently guiding me through research and for exemplifying what it is to be a scientist. I would like to especially thank her for always keeping her faith in me and being my biggest supporter.

I would like to express my gratitude to Dr. Jeffrey L. Krichmar for introducing me into the world of computational neuroscience. I would like to thank him for not only enriching my knowledge of computational methods, but also demonstrating the importance of approaching research questions through diverse viewpoints and theoretical frameworks.

I thank Drs. Elizabeth R. Chrastil, Jeffrey L. Krichmar, Ramesh Srinivasan, Emily Grossman, and Bruce McNaughton for serving on my advancement committee and dissertation committee and sharing their expertise. Drs. Sam Ling and Chantal Stern from Boston University for constantly providing their feedback over the years to support the growth of my research project. Drs. Mary Hegarty, Daniel Montello, Emily Jacobs, and Steven Gaulin from UCSB for teaching me the value of interdisciplinary work. Dr. Julien Brun from the National Center for Ecological Analysis & Synthesis and Dr. Adish Singla from the Max Planck Institute for Software System for serving as my mentors in the fields of data science and machine learning.

My colleagues from the Spatial Neuroscience Lab that supports me throughout each stage of my graduate school. I would like to especially thank Rie Davis and Nikki Hatamian for their effortless assistance with my data collection, Dr. Vaisakh Puthusseryppady and Dr. Mike Starrett Ambrose for providing insightful research and career advice. I would also like to thank Bailey Tranquado-Torres, Robert Woodry, Alina Tu, Justin Kasowski, Erica Ward, Theo Kapogianis, Daniela Cossio, Marjan Rashidi for the company and for helping to make the lab feel like a family. I would also like to thank all of my past and present undergraduate research assistants who helped with different aspects of my research over the years.

My colleagues from the Cognitive Anteater Robotics Laboratory for sharing their innovative and diverse approach to computational neuroscience. I would like to especially thank Dr. Hirak Kashyap, Kexin Chen and Jingwei Xing for kindly sharing their expertise that helped me to shape my computational modeling project.

My colleagues from UCSB for providing me with endless support, both intellectually and professionally: Dr. Crystal Bae, Dr. Alex Boone, Dr. Peri Gunalp, Dr. Jing Xu, Dr. Rui Zhu, Dr. Erin Wetherley, Dr. Kevin Mwenda, Shuying Yu, Jessica Zisa. I would like to especially thank Carol He, a great collaborator and a good friend, who demonstrates courage and empathy and who is the paradigm of growth mindset.

Community support. Dr. Barbara Sarnecka and the UCI Cognitive Sciences Writing Group

that brought me into the writing world and welcomed me into the UCI community. UCI Center for the Neurobiology of Learning and Memory Ambassador's Program for helping me to find ways to share my interest in brain sciences through various outreach programs. Dr. Phong Leung for helping me stay sane during the pandemic. Dr. Craig Stark for tirelessly providing technical computing support that enables me to complete my fMRI data analyses.

The funding sources that made my dissertation projects possible: National Science Foundation, Institute for Collborative Biotechnologies, and Hellman Family Foundation.

My parents and relatives who allowed me to grow and pursue my dream. I'd especially like to thank my uncle Zhongwei for sharing his positive life attitude and being a model for me.

Dear friends, Xiaoqiang, Xiewen, Huanping, Youjun, Jing, Lilly, Carol, Crystal, Anagha, Zhibin, Xiaoran for sharing interests and being such caring companions who helped me survive throughout graduate school.

My dog, Waguan, for accompanying me during the pandemic and sharing his impressive Frisbee fetching skills.

VITA

You Cheng

EDUCATION

Doctor of Philosophy in Cognitive Sciences with a Concentration in Cognitive Neuroscience — **2022**
University of California, Irvine — *Irvine, CA*

Master of Science in Cognitive Neuroscience — **2020**
University of California, Irvine — *Irvine, CA*

Master of Art in Geography — **2019**
University of California, Santa Barbara — *Santa Barbara, CA*

Bachelor of Science in Psychology — **2014**
South China Normal University — *Guangzhou, China*

RESEARCH EXPERIENCE

Graduate Student Researcher — **2019–2022**
University of California, Irvine — *Irvine, California*

Graduate Student Researcher — **2017–2019**
University of California, Santa Barbara — *Santa Barbara, California*

REFEREED JOURNAL PUBLICATIONS

Cheng, Y., Hegarty, M., Chrastil, E. R.. Telling right from right: the influence of handedness in the mental rotation of hands. — **2020**
Cognitive Research: Principles and Implications, 5, 1-18.

Sun, L., Tan, P. *, Cheng, Y. *, Chen, J., Qu, C.. The effect of altruistic tendency on fairness in third-party punishment. — **2015**
Frontiers in psychology, 6, 820.

*denotes equal authorship

Qu, L., Dou, W., Cheng, Y., Qu, C.. The processing course of conflicts in thirdparty punishment: An even-trelated potential study. — **2014**
PsyCh journal, 3(3), 214-221.

BOOK CHAPTERS

Chrastil, E. R., Cheng, Y.. Central Coordination and Integration of Diverse Information to Form a Single Map. In R. D. Montello & K. M. Curtin (Eds.), **in press**
Collective Spatial Cognition: A Research Agenda. Routledge (Taylor and Francis).

TEACHING EXPERIENCE

Instructor of Record **Summer 2021**
University of California, Irvine *Irvine, CA*

Social Sciences Instructional Fellow **Summer 2020**
University of California, Irvine *Irvine, CA*

Teaching Assistant **2017–2018**
University of California, Santa Barbara *Santa Barbara, CA*

Teaching Assistant **Spring 2016**
Dartmouth College *Hanover, NH*

Instructor of Record **Fall 2013**
Guangzhou 10th Middle School *Guangzhou, China*

SELECT CONFERENCE TALKS

Cheng, Y., Chrastil, E.R.. Sex Differences in Head Direction Signals When Learning a Complex Environment. **Dec., 2021**
Neuromatch Conference 4.0 Flash Talk, Virtual.

Cheng, Y., Chrastil, E.R.. Head Direction Signals During Navigation. **May, 2021**
Virtual Spring CNLM Conference - Memory: It's About Time, Virtual.

Cheng, Y.. Finding the Compass: Head Direction Signals in the Human Brain. **May, 2021**
UCI CNLM Awards Ceremony, Virtual.

Invited. Roger W. Russell Scholar's Award in the Neurobiology of Learning and Memory

Cheng, Y., Chrastil, E.R.. The Emergence of Head Direction Signals in Human Navigation. **April, 2021**
UCI Associated Graduate Students (AGS) Symposium, Virtual.

Audience Choice Award

Cheng, Y., Ling, S., Stern, C. E., Huang, A., Chrastil, E.R.. Travel Direction as a Fundamental Component of Human Navigation. **Oct., 2020**
Neuromatch Conference 3.0, Virtual.

Cheng, Y., Ling, S., Stern, C. E., Huang, A., Chrastil, E.R.. Travel Direction as a Fundamental Component of Human Navigation. **Oct., 2020**
Interdisciplinary Navigation Symposium (iNAV), Virtual.

Cheng, Y.. Travel Direction as a Fundamental Component of Human Navigation. **Jan., 2020**
UCI Cognitive Sciences Department Graduate Student Presentation Bonanza, Irvine, USA

Cheng, Y.. What Are the Sex Differences in Navigation Training? Using the Sea Hero Quest Dataset. **Nov., 2019**
UCSB Crossroads Symposium, Santa Barbara, USA

Downs, M., Davis, F., Brun, J., Huang, T., Cheng, Y.. Greater Than the Sum of the Parts: Collaboration in the U.S. LTER Network. **Sept., 2019**
International Long-Term Ecosystem Research Open Science Meeting (ILTER OSM), Leipzig, Germany

Cheng, Y.. Domain-General Distance Representation. **May, 2019**
Spring Quarter UCSB Geography Department Colloquium, Santa Barbara, USA

Cheng, Y., Chrastil, E.R.. From Individual Cognitive Maps to a Collective Cognitive Map: Prescriptive Guidelines. **April, 2019**
Collective Spatial Cognition Specialist Meeting, Santa Barbara, USA

Cheng, Y.. Left Hand, Right Hand. **May, 2019**
2018 Spatial Lightning Talks, UCSB Center for Spatial Studies, Santa Barbara, USA

Cheng, Y., Liang, Y., Tang, Z., Qu, C., Chen, C.. Mixed Time-Based and Event-Based Prospective Memory: A Behavioral Study. **Nov., 2013**
The 16th National Academic Congress of Psychology, Nanjing, China

SELECT CONFERENCE POSTER PRESENTATIONS

Cheng, Y., Ling, S., Stern, C. E., Huang, A., Chrastil, E.R.. Travel Direction as a Fundamental Component of Human Navigation. **Nov., 2021**
Harvard Women in Psychology's Annual Trends in Psychology Summit (TiPS), Virtual.

Cheng, Y., Chrastil, E.R.. Sex Differences in Head Direction Signals When Learning a Complex Environment. **Nov., 2021**
Society for Neuroscience (SfN), Virtual.

Cheng, Y.*, He C. *, Spiers H., Coutrot A., Hornberger M., Hegarty M., Chrastil, E.R.. Self-Evaluations of Navigation Ability: A Big Data Approach. **Nov., 2021**
Psychonomic Society Annual Meeting, Virtual.

*denotes equal authorship

Cheng, Y., Chrastil, E.R.. Head Direction Signals During Navigation: Comparing Movement And Stationary Periods. **Aug., 2021**
Spatial Cognition, Virtual.

Cheng, Y., Chrastil, E.R.. The Emergence of Head Direction Signals in a Complex Environment. **June, 2021**
Annual Meeting of the Organization for Human Brain Mapping (OHBM), Virtual.

Cheng, Y., Chrastil, E.R.. The Emergence of Head Direction Signals in Human Navigation. **June, 2021**
spatial@ucsb.global2021: Spatial Data Science for a Sustainable Future, Virtual.

Cheng, Y., Chrastil, E.R.. The Emergence of Head Direction Signals in Human Navigation. **March, 2021**
Cognitive Neuroscience Society (CNS) Annual Meeting, Virtual.

Cheng, Y., Chrastil, E.R.. The Emergence of Head Direction Signals in Human Navigation. **Jan., 2021.**
Society for Neuroscience Global Connectome (SfN), Virtual.

Trainee Professional Development Award.

Cheng, Y., Chrastil, E.R.. The Emergence of Head Direction Signals in Human Navigation. **Nov., 2020**
Psychonomic Society Annual Meeting, Virtual.

Downs, M., Brun, J., Huang, T., Cheng, Y.. Greater Than the Sum of the Parts: Collaboration in and Beyond the U.S. LTER Network. **Aug., 2020**
Ecological Society of America Annual Meeting, Virtual.

Cheng, Y., Ling, S., Stern, C. E., Huang, A., Chrastil, E.R.. Travel Direction as a Fundamental Component of Human Navigation. **Nov., 2019**
Psychonomic Society Annual Meeting, Montreal, Canada.

Cheng, Y., Hegarty, M., Chrastil, E.R.. Embodied Experience of the Wrong' Hand, Not World Knowledge, Supports the Mental Rotation of Hands. **Nov., 2018**
Psychonomic Society Annual Meeting, New Orleans, USA.

Cheng, Y., Hegarty, M., Chrastil, E.R.. Performance Discrepancy Between Left-handers and Right-handers Reveals Multisensory Integration in the Mental Rotation of Hands. **Aug., 2018**
Spatial Cognition, Tbingen, Germany.

Cheng, Y., Ling, S., Stern, C. E., Huang, A., Chrastil, E.R.. Travel Direction as a Fundamental Component of Human Navigation. **June, 2018**
Interdisciplinary Navigation Symposium (iNAV), Quebec, Canada.

Cheng, Y., Ling, S., Stern, C. E., Huang, A., Chrastil, E.R.. Are You Getting Closer to the Sun or to the Moon? An Unusual Motion Adaptation Effect of Travel Direction. **June, 2018**
spatial@ucsb.local2018, UCSB Center for Spatial Studies.Santa Barbara, USA

Chrastil, E.R., Nicora, G., Davis, R., Smith, J., Cheng, Y.. The Influence of Decision-Making on Spatial Learning and Memory: An Individual Differences Approach. **Nov., 2017**
Society for Neuroscience Annual Meeting (SfN), Washington DC, USA.

Cheng, Y., Qu, C.. Cost Consideration Driven by Prosociality in Third-party Punishment: Using Feedback Related Negativity. **Oct., 2015**
Society for Neuroscience Annual Meeting (SfN), Chicago, USA

AD HOC JOURNAL REFEREE

Quarterly Journal of Experimental Psychology, Communications Biology, Current Psychology, Qeios

PROGRAMMING SKILLS

R, Python, MATLAB

ABSTRACT OF THE DISSERTATION

Travel Direction as a Fundamental Component of Human Navigation: Integrating Psychophysics, Neuroimaging, and Computational Modeling Approaches

By

You Cheng

Doctor of Philosophy in Cognitive Sciences

University of California, Irvine, 2022

Assistant Professor Elizabeth R. Chrastil, Chair

It is often assumed that travel direction is redundant with head direction, but from first principles it is clear that these two factors provide differing spatial information regarding one's orientation in the environment. Although head direction has been found to be a fundamental component in human navigation, it is unclear whether travel direction also plays a primary role. This dissertation sets out to investigate the role of travel direction in the spatial orientation system in the human brain by combining methodologies in psychophysics, neuroimaging, and computational modeling.

The first study employs a motion adaptation paradigm from visual neuroscience designed to preclude the contribution of head direction. I found high-level aftereffects of perceived travel direction, indicating that travel direction is indeed a fundamental component of human navigation. Interestingly, I discovered a higher frequency of reporting perceived travel toward the adapted direction, as compared to a no-adapt control - an aftereffect which runs contrary to low-level motion aftereffects. This travel aftereffect was maintained after controlling for possible response biases and approaching effects, and it scaled with adaptation duration. These findings represent the first evidence for a pure travel direction signal in humans, independent of head direction.

The second study examines if, when moving to the brain activation level, it is still possible to discriminate between directions using fMRI signals from distributed brain areas, while people navigate complex environments. Using machine learning methods, I discriminated between head and travel directions - i.e., translational movement directions, rotational movement directions, and stationary facing directions - from those fMRI signals, in a study where people were tasked with actively navigating a complex maze. It is worth noting here that while I did not study head and travel direction signals in isolation from one another, my analysis is informative for our understanding of how the human brain represents spatial orientation. The regions of interest (ROIs) primarily include areas in which head direction signals have been previously reported, including the thalamus, retrosplenial cortex, precuneus, extrastriate cortex, and early visual cortex. I also examined signals from the striatum - i.e., caudate, putamen, nucleus accumbens, and pallidum - along with the hippocampus, amygdala, and the auditory cortex. In addition to the present cognitive map, my model was able to classify directions for future and past directions across ROIs during the stationary period. Interestingly, I only observed correlations between classification accuracy and navigation performance during the test phase, but not during the exploration phase. Transitioning from the exploration phase to the test phase, although there was a tendency to rely more on the allocentric frame of reference for navigation, successful navigation seems to rely more on efficient utilization of the egocentric frame of reference. This relationship was found when looking at the past and future movements, which constitute the travel trajectory and could indicate path planning. The results not only shed light on different directional representations in a distributed head and travel direction system during active navigation in a complex environment, they also support the dynamic involvement of both allocentric and egocentric frames of reference, the representations of past, present, and future cognitive maps, as well as individual differences in fMRI signals that relates to navigation performance.

To understand how the travel direction system might work in the human brain, the third study adopted the experimental paradigm from the first study by building a biologically

plausible computational model to simulate the travel direction system. The model predicted the motion aftereffects that I observed experimentally, and was tested with a series of perturbation studies, which brought further support to our understanding of the travel direction system. This study proposed a new approach to simulate the human orientation system by using a recurrent neural network (echo state network).

In summary, I investigated travel direction in human navigation using a combination of psychophysics, neuroimaging, and computational modeling approaches. Each study added an additional level of understanding for travel direction with a different approach. Study 1 provides evidence of what is the role of travel direction in the internal orientation system of human navigation. Study 2 features a distributed travel and head direction system in discriminating directions in a complex navigation task, suggesting where in the human brain travel directions could be represented. Study 3 continues exploring travel direction by demonstrating how the travel direction system might work in the human brain using a computational model. This dissertation suggests a fundamental role of the travel direction system in the human brain, and also illustrates the importance of using multifaceted approaches in understanding neuroscience.

Chapter 1

Introduction

A lady who spent most of her life living in California moved to Chicago after her retirement. While in Chicago, she was unfortunately diagnosed with Alzheimer's disease and got lost quite often. One of the typical mistakes in her wayfinding was that she constantly assumes that the main body of water is to the west, just like in the west coast California; while in Chicago, the main body of water, Lake Michigan, is to the east. Therefore, whenever she thought she was heading north, she was actually heading south: her entire cognitive map is inverted. This was due to misrepresentations of cardinal directions in her brain: her California compass stuck in her mind due to neurodegeneration and was misapplied to the Chicago map[1]. Our wayfinding (i.e., spatial navigation) behavior and the internal orientation system in our brain are so integrated that it is hard to see it until the neural circuit breaks down. So, what does the internal orientation system in the human brain look like? And how does it relate to our navigation behavior?

Edward Tolman was among one of the first to propose the concept of a cognitive map - a representation of external environmental features or landmarks in the brain (Tolman, 1948). The existence of a cognitive map in the rodent brain has been clear since the discoveries of

[1]Credit to Dr. Anna Lysakowski from the University of Illinois Chicago for sharing the case.

cells that correspond to various spatial features in rodent brain, such as place cells that represent a particular location in the environment (O'Keefe, 1976; O'Keefe & Dostrovsky, 1971; OKeefe & Nadel, 1978), grid cells that represent a spatially distributed array of locations (Fyhn, Molden, Witter, Moser, & Moser, 2004; Hafting, Fyhn, Molden, Moser, & Moser, 2005), and head direction cells that represent where a rat is facing momentarily (Chen, Lin, Green, Barnes, & McNaughton, 1994; Cullen & Taube, 2017; Ranck Jr, 1984; Taube, Muller, & Ranck, 1990a, 1990b). Decades of research following these discoveries has been aimed at understanding cognitive maps in different species. As this research has accumulated, it has been clear that there were place-cell-like representations (Ekstrom et al., 2003), grid-cell-like representations (Jacobs et al., 2013), and head direction signals (Baumann, Chan, & Mattingley, 2010; Koch, Li, Polk, & Schuck, 2020; Nau, Schröder, Frey, & Doeller, 2020; Shine, Valdés-Herrera, Hegarty, & Wolbers, 2016; Vass & Epstein, 2013) in the human brain. **But this is not the end of our search for the cognitive map.**

Travel direction, the direction one's body is moving toward, has largely been ignored in previous animal and human research. This is because head and travel directions are typically conflated, as it is often assumed where we are going is where we are facing. However, from first principles, travel direction might be more important than head direction in forming travel trajectories over time. The role that travel direction plays in human navigation remains elusive primarily because it is uncertain whether travel direction is indeed supported by a neural signal independent of head direction. Further, if travel direction is playing a fundamental role in human navigation, where and how is it represented in the brain? Can we discriminate between egocentric movement directions and allocentric movement directions? This research aimed to bridge these gaps by utilizing a combination of approaches to look at travel direction signals at multiple scales, including the behavioral level (psychophysics), the level of group of neural populations (fMRI), and a biological plausible system level (computational neuroscience model). The studies are laid out in following aims:

Aim 1: Differentiate cognitive mechanisms of travel direction from those of head direction to test for the role of travel direction in the internal representation system of human navigation

To test the hypothesis that travel direction is a fundamental component of the internal representation system of human navigation, I utilized a paradigm called *motion adaptation* in a simple virtual hallway. In motion adaptation, neurons selective for visual motion features (e.g., moving downward) will adapt to visual stimuli that correspond to its selective firing properties after being exposed to the same stimuli over time (Barlow, 1990). This adaptation often results in a decrease in the neuron's responsiveness to the same stimuli compared to a normal response. The motion adaptation paradigm - previously only used to test third-person view motions in visual perception - was utilized in this study in a novel way to test the first-person view self-motion in path integration. Throughout the task, we decoupled head direction and travel direction by randomly reversing the head direction, canceling out the possible head direction input from optic flow. Across a series of experiments, I observed robust adaptation effects of travel direction, providing evidence for a travel direction signal in humans that is independent of head direction.

Aim 2: Determine the brain regions that code head and travel direction during active navigation in a complex environment using machine learning methods on fMRI signals

Building upon the assumption that travel direction plays a fundamental role in the internal representation system of human navigation (see Aim 1), Study 2 goes a step further by examining where head and travel directions are represented in the human brain when people actively navigate in a virtual complex environment during fMRI scanning. This task simulates people's wayfinding behavior in daily activities better than the simple virtual hallway in Study 1. To test the hypothesis that head and travel direction is represented in distributed brain areas, I used a machine learning classifier to discriminate between directions from

fMRI signals in a wide range of brain areas, including medial temporal lobe, basal ganglia, visual cortex, thalamus, and parietal cortex. The model could discriminate between directions in varying brain regions depending upon type of movement (i.e., rotating, translating, or stationary), navigation phase (i.e., exploration phase vs. test phase), frame of reference (egocentric vs. allocentric frame of reference), and time (present, future, and past cognitive maps). The results suggest the involvement of a distributed network of brain regions to code head and travel directions that provide information about path planning and trajectories. I also tested individual differences in the strength of these classifiers, finding relationships with performance only in the test phase, suggesting that people use these maps differently when navigating once they have learned.

Aim 3: Develop and test a computational model of travel direction for its ability to support coding of travel direction

Finally, to illuminate the intricacies of how brain regions coordinate to code travel direction from visual input that give rise to wayfinding behaviors, I explored another approach to investigating travel direction by building a biologically plausible model. The model - composed of a recurrent neural network - was proposed to simulate visual aftereffects of travel direction observed in a series of experiments in Study 1. The model was tested by a series of perturbation studies showing the effectiveness of the neural network in predicting travel direction judgment and generating adaptation effects. The model has the potential to be integrated with models for other major neural systems to help understand neurodegenerative diseases with common navigation difficulties. That way, we could help people like the lady with Alzheimer's disease, who constantly mistakes east for west, to eventually return home.

Considering travel direction as a basic navigation component will enrich the knowledge of the field of human spatial navigation, especially for scientists who are devoted to questions related to basic signals such as head direction. This research is well-positioned to inform a number of disparate disciplines ranging from animal behavior to artificial intelligence. For

instance, the results will encourage scientists who study navigation behavior of other species (e.g., rodents, birds, non-human primates, etc.) to look for more direct neurological evidence of travel direction. Alternatively, these results could also be applied to the field of artificial intelligence to enhance navigation performance in robots or other autonomous vehicles.

Chapter 2

(Don't) Look Where You're Going: Evidence for a Travel Direction Signal in Humans that is Independent of Head Direction

2.1 Introduction

In daily navigation, for activities as simple as going to a grocery store, we form a trajectory of our travel paths. How do we use self-motion information to form this travel trajectory? Travel trajectory is derived from time and velocity. Velocity in turn is composed of speed and travel direction, which is the direction of one's body movement. Although *head direction* - the direction that one's head is facing toward (also called facing direction) - is typically assumed to be the direction of travel, in reality these two factors offer different spatial information. For instance, when we walk on the street, we constantly look around at our surroundings, changing our head direction while maintaining a constant travel direction. Thus, from first principles *travel direction*, rather than head direction or facing direction, is the most important component in forming a travel trajectory, as well as in maintaining spatial-vector memory over time (Hulse et al., 2021; Stone et al., 2017).

Only a handful of human and rodent studies have examined whether travel direction is coded separately from heading direction. Although they do not offer the same amount of information, spatially-tuned head direction cells have previously been used as a theoretical basis for the formation of a travel trajectory. Indeed, head direction cells have been discovered in the rats brain, which selectively fire in the direction a rat is facing towards, independent of its location (Chen et al., 1994; Ranck Jr, 1984; Taube, 1995; Taube et al., 1990a), demonstrating that head direction is a fundamental component of the internal orientation system of navigation. These head direction cells are found in thalamus (Taube, 1995), retrosplenial cortex (Chen et al., 1994; Cho & Sharp, 2001), presubiculum (Ranck Jr, 1984), extrastriate cortex (Chen et al., 1994), and entorhinal cortex (Frank, Brown, & Wilson, 2000; Quirk, Muller, Kubie, & Ranck, 1992). Head direction cells could fire independently of whether an animal is moving or motionless (Taube, 1998), whereas travel direction should involve motion, therefore it might be more difficult to record activity related to travel direction. One study that contrasted head and travel direction found that head direction is coded more strongly than

travel direction in a population of rodent entorhinal neurons (Raudies, Brandon, Chapman, & Hasselmo, 2015). Experimental findings in the neural system of other species also suggest the existence of neural signals for travel direction (Lyu, Abbott, & Maimon, 2021; Olson, Tongprasearth, & Nitz, 2017). Taken together, while there is evidence to suggest a dissociation between coding of head direction and travel direction, the role that travel direction plays in the internal representation system of human navigation remains unclear.

The goal of this study was to determine whether there are behavioral signatures of travel direction as a fundamental component of human spatial navigation, independent of facing direction. To test the role of travel direction in human navigation, we utilized a motion adaptation paradigm adopted from vision science. In motion adaptation, neurons selective for visual motion features (e.g., moving downward) will adapt to visual stimuli that corresponds to its selective firing properties after prolonged exposure to the same stimuli (Barlow, 1990). This adaptation often results in a decrease in the neural response to the same stimuli, compared to an unadapted stimulus (S. P. Brown & Masland, 2001; Lisberger & Movshon, 1999; Maffei, Fiorentini, & Bisti, 1973; Miller, Gochin, & Gross, 1991). This neuronal change is represented at the behavioral level as a motion aftereffect (MAE) - a visual phenomenon produced after motion adaptation such that a stationary stimulus will appear to move in the opposite direction of the previously viewed motion. These motion aftereffects are suggested to be associated with an amalgam of adaptation of motion-selective opponency cells at several visuocortical sites (Antal et al., 2004; Ashida & Osaka, 1994; Bach & Ullrich, 1994; Barlow & Hill, 1963; Bex, Metha, & Makous, 1999; Culham et al., 1998; Kohn & Movshon, 2003; G. Mather, Pavan, Campana, & Casco, 2008; Sutherland, 1961; Verstraten, Van Der Smagt, & Van De Grind, 1998). Thus, our study operates under the assumption that if travel direction exhibits adaptation-like effects, then it is a fundamental component of the representation system for human navigation.

In the present study, participants were adapted to travel direction by viewing movement

in a hallway in a constant direction. To dissociate travel direction from head direction, head direction randomly reversed while travel direction was kept constant during adaptation (Figure 2.1). We expected to observe motion aftereffects compared to a control condition with no adaptation. Typically, motion aftereffects are found in the opposite direction to the adapted motion (Anstis, Verstraten, & Mather, 1998; G. E. Mather, Verstraten, & Anstis, 1998), and so we predicted motion aftereffects in the opposite direction of travel. However, high-level motion aftereffects are frequently seen in the same direction as the locally adapted motion because they use non-retinotopic visual features, although they might go in the opposite direction from the globally perceived movement (Culham, Verstraten, Ashida, & Cavanagh, 2000; Dubé & Von Grünau, 1992; Hiris & Blake, 1992; Nishida & Sato, 1995; Von Grünau, 1986). Navigation is considered high-level cognition (Wolbers & Hegarty, 2010) whose information processing generally centers around higher level brain regions rather than visual areas (Chrastil, 2013; OKeefe & Nadel, 1978), and navigation process are typically non-retinotopic (Chrastil, Nicora, & Huang, 2019; Giudice, 2018; Loomis et al., 1993). Thus, we predicted that we could instead observe high-level motion aftereffects in the same direction as the motion adaptation. In addition, as far as we knew, the motion adaptation paradigm has only been used to study motions in the third person view in previous research. Our study was the first to utilize such paradigm to study a first-person view motion - self-motion. This new implementation of the motion adaptation paradigm may also lead to different adaptation effects as we observed in previous visual perception studies. Regardless of the direction of the effect, a motion aftereffect would be the behavioral signature of travel direction selectivity, potentially operating as a fundamental basis function in human navigation.

2.2 Results

2.2.1 High-level motion aftereffects of travel direction

To test whether there is a travel direction signal in humans, we used a visual motion adaptation paradigm in desktop virtual reality (VR), designed to isolate travel direction from the contribution of head direction. In the initial adaptation phase, participants experienced 60 seconds of visual self-motion toward a cardinal direction (towards a sun or towards a moon) along a virtual hallway (Figure 2.1c). In the test phase, participants then experienced a series of visual back and forth movements, toward and away from the initial cardinal direction. We then asked participants to report their net travel direction during the test phase. Importantly, in both adaptation and test phases the heading direction alternated occasionally, cancelling out overall heading direction, to dissociate heading from travel direction. To maintain adaptation state, participants experienced shorter 10-second "top-up" adaptation between each trial. We compared the adaptation condition to a no-adapt control condition, in which participants viewed a static hallway with occasional heading changes; the control condition had the exact same test phase as the adaptation condition. By parametrically manipulating the coherence of global travel direction, we acquired psychometric functions for perceived travel direction, which allowed us to assess whether travel direction adaptation shifted the psychometric function, relative to the control.

In Experiment 1, we recruited 60 participants (31 females). To guard against response bias for one of the cardinal directions, we divided the participants into two groups (random assignment), with each group adapting to either the sun or the moon direction. (Figure 2.1 a - e; Methods Section 2.4.1). The groups were combined for analysis (see Appendix Figure A.3 and Table A.2-A.3 for analysis of each group separately). We observed significant motion aftereffects of travel direction in the adaptation condition compared to the control ($F(1, 59) = 11.38$, $p = 0.001$, $\eta_p^2 = 0.162$, 95% confidence interval (CI) = [0.028, 0.332]) (Figure 2.2a, Appendix Table A.1). Although we found a significant shift in the function with adapta-

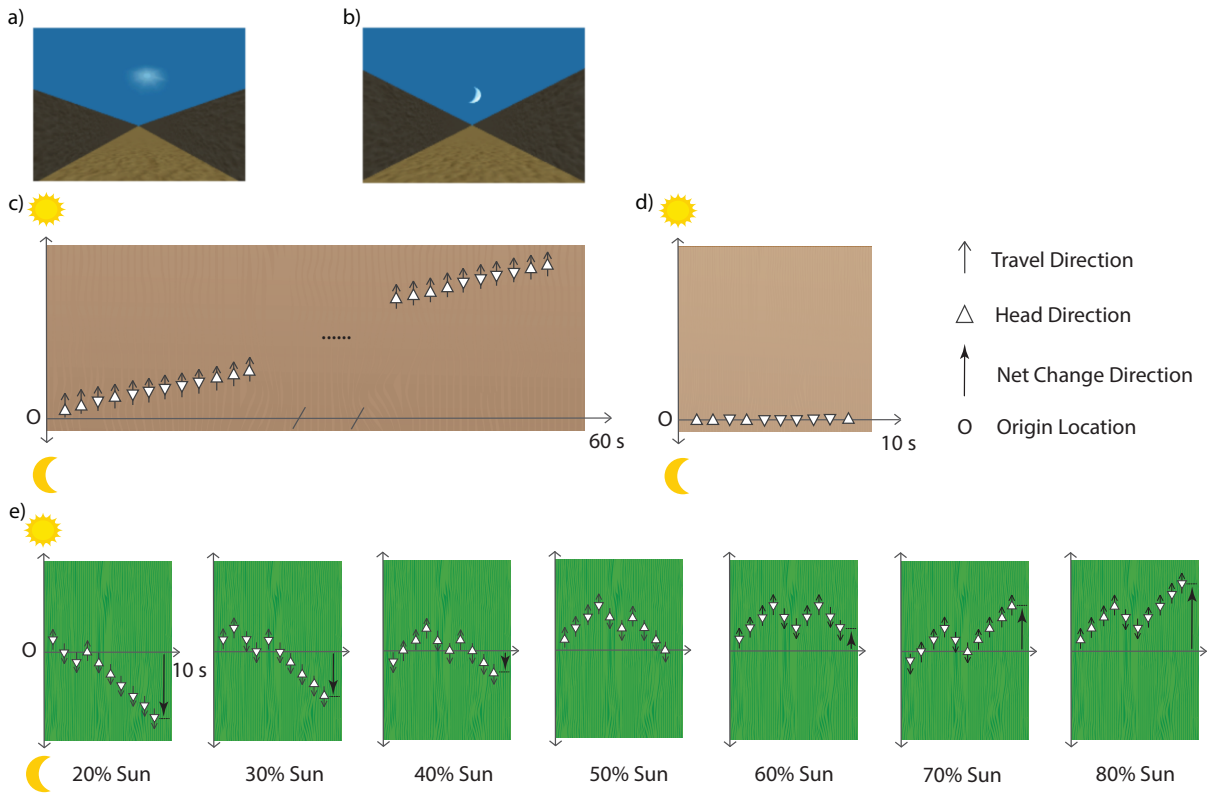

Figure 2.1: Experiment 1. Hallway during the adaptation phase, facing the a) sun or b) moon direction. Note that in the virtual environment, both the sun and the moon were rendered to move with the viewer at a constant distance; the size of the moon and the sun did not change with self-motion and participants could not evaluate distance change based on perceptual changes in either the sun or the moon. The extreme length of the hallway and random textures also precluded using changes in the hallway itself for location cues. The ground for the hallways turned green during the test phase to provide a visual cue for when to start tracking movement direction. c) The 60-second adaptation phase for the sun group. During the adaptation phase, visual movement traveled toward the sun while the facing direction occasionally changed. Half the participants were adapted to a similar moon condition, with travel direction toward the moon. d) The 10-second initial phase for the control session, which was the same for both the sun and moon groups. There was no visual travel, but the facing direction randomly changed. e) The test phase, which was the same for all sessions in all conditions. Visual movement traveled back-and-forth between the sun and the moon during a 10-second interval. Participants were asked to decide whether the total movement was more toward the sun or more toward the moon in that interval. The facing direction randomly changed during the test phase. Here, we show one example from each of the seven test phase conditions of the percent of net movement toward the adaptation direction (20%, 30%, 40%, 50%, 60%, 70%, 80%).

tion, the pattern was not in the initially predicted direction: motion adaptation increased travel estimation in the same direction as the adaptation, instead of producing a traditional opponent-process aftereffect in the opposite direction. As expected, there was a main effect of the actual percentage of motion on perceived direction ($F(2.14,\ 126.49) = 522.34$, $p < 0.001$, $\eta_p^2 = 0.899$, $95\%CI = [0.882,\ 0.912]$), with the perceived percentage of movement in the adaptation direction increased with the actual percentage. There was also an interaction between the experimental condition and the actual percentage of movement ($F(4.22,\ 248.94) = 4.91$, $p < 0.001$, $\eta_p^2 = 0.077$, $95\%CI = [0.021,\ 0.122]$), which indicates that the difference between the adaptation and control conditions depended on the actual percentage of movement in the adaptation direction. Post-hoc analyses revealed that the adaptation significantly increased the perceived percentage of movement in the adaptation direction in several conditions where the actual percentage was below 60%. These planned comparisons further confirmed that the adaptation condition was increased toward the adaptation direction compared to the control condition (Figure 2.2a).

We conducted several additional analyses to preclude possible explanations besides a motion aftereffect. We separately analyzed results from sun and moon adaptation groups and found the same result as the combined data (with somewhat weaker effects for the moon group), which ensured that neither the particular adaptation direction nor response bias disproportionately affected the results (Appendix Figure A.3, Table A.2 - A.3). We also found no serial position effects (i.e., no primacy or recency effects), suggesting that no particular portion of the test phase disproportionately contributed to the reported rate (e.g. participants only paid attention to the last second of the movement) (Appendix Figure A.4 - A.7). We found no reaction time differences between conditions. We only found the expected higher reaction time at the 50%, indicating that participants found the condition with equal amounts of travel in each direction difficult to judge, which is an indication that our task was effective (Appendix Figure A.1). We also specifically analyzed all the initial test trial in each block after the initial adaptation and found similar result patterns as the

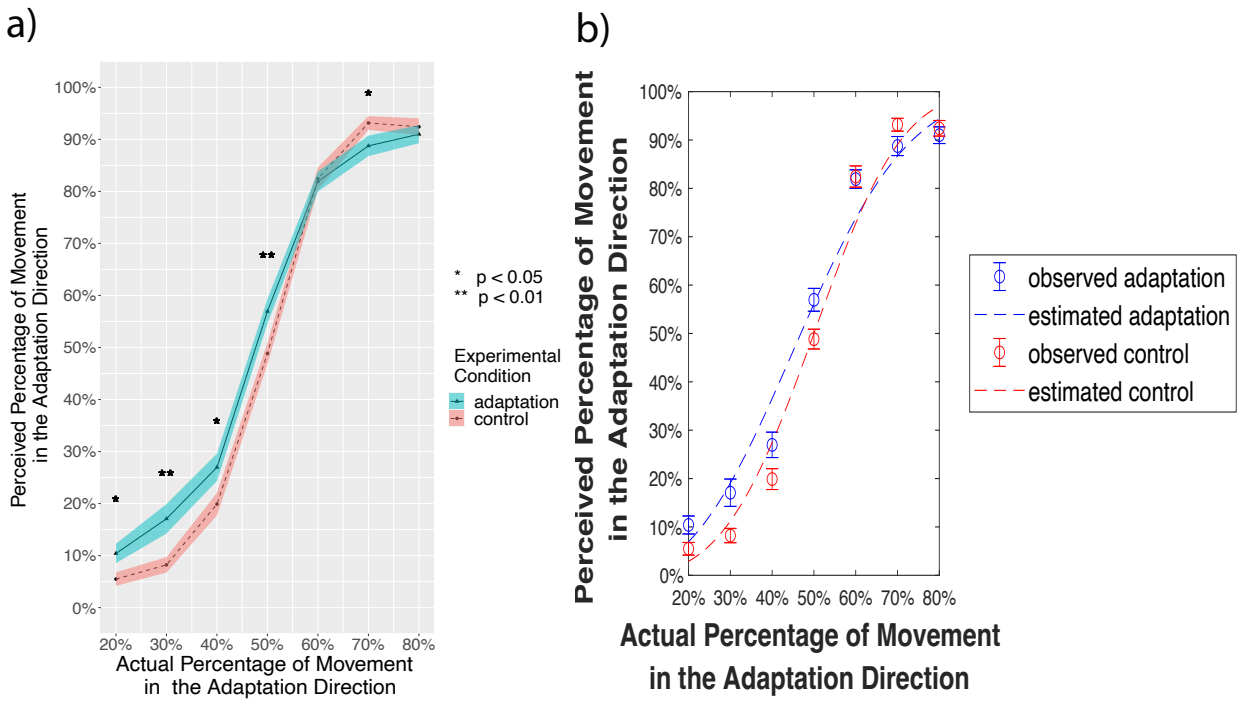

Figure 2.2: Experiment 1. a) The perceived percentage of movement in the adaptation direction compared with the actual percentage for all subjects (n = 60). The adaptation condition had an overall significantly higher reported percentage than the control condition (p = 0.001). The adaptation condition showed significantly higher reported percentages than corresponding control conditions at 20%, 30%, 40%, and 50%, supporting the aftereffect. This result suggests an aftereffect in the same direction of travel. There was also a significant interaction between condition and the actual percentage. Solid lines indicate the grand average value, and the shaded areas indicate 1 standard error of the means. * p $<$ 0.05; ** p $<$ 0.01, Tukey correction. b) The average psychometric Weibull functions for all subjects (n = 60). The bias psychometric function (i.e., α) shifts toward lower percentage of movement toward the adaptation direction when adapted but was not significant (p = 0.252). The uncertainty psychometric function (i.e., β) became more flattened when adapted, indicating that observers' detectability of the difference between the two directions was decreased by adaptation (p = 0.007). Error bars indicate standard errors.

entire data set, suggesting that the opposite motion aftereffect was not due to insufficient adaptation duration during the top-ups (Appendix Figure A.8). In addition, the pattern of results remained after we controlled for strategies in the analyses (see Methods Section 2.4.1; Appendix Section A.6). Finally, we filtered out 9 subjects (around 15% of the subjects; 3 from the sun adaptation group, 6 from the moon adaptation group), based implausible psychometric parameters yielded from the Weibull function (Mood, Graybill, & Boes, 1974) (Appendix Figure A.10 - A.11) and results from the remaining subjects still revealed the same pattern as the raw data, suggesting that the observed opposite motion aftereffect was not due to outlier subjects (see Methods; Appendix Figure A.9, Table A.4).

2.2.2 Higher uncertainty in estimating travel directions after adaptation

To quantify the magnitude of the aftereffect, we fitted each participant's data with a Weibull function (Mood et al., 1974) (Appendix Figure A.2). α and β values were derived for each fitted function: α means a bias to respond to the "sun" or the "moon" direction in the task, while β means the detectability of the difference in the task (Methods). We found no difference in the bias (α) between the adaptation and the control conditions ($t(59) = 1.16$, $p = 0.252$, $Cohen's\, d = 0.196$, $95\%CI$ = [-0.143, 0.536], ns). The detectability (β) in the adaptation condition was significantly lower than in the control condition ($t(59)$ = -2.79, p = 0.007, $Cohen's\, d$ = -0.439, $95\%CI$ = [-0.765, -0.113]), indicating that people have more uncertainty in making judgments in the adaptation condition (Figure 2.2b).

In summary, our first experiment found significantly increased perception of movement toward the direction of adaptation, consistent with a motion aftereffect. Participants also exhibited more uncertainty after the adaptation, compared to control, suggesting that the adaptation was affecting their judgments of movement direction during the test periods. Together, these findings are consistent with a role for travel direction that is independent of

head direction.

2.2.3 Motion aftereffects remain when adaptation heading is orthogonal to travel direction

In Experiment 2 ($n = 30$ participants; 16 females), we attempted to address additional questions about response biases and approaching effects. In Experiment 1, although we separated travel direction from head direction by randomly flipping head direction throughout the task, travel direction was still on the same axis as head direction - the direction that aligns with the front-back body axis. One possible outcome of this alignment of travel direction and head direction is that people might more easily generate a feeling of approaching the adapted travel direction. Thus, to test this alternative possibility and to preclude approaching effects during the adaptation, in Experiment 2 facing direction was changed to be perpendicular to travel direction (Figure 2.3a-e; Methods Section 2.4.2). Because travel direction and facing direction were never aligned, this experiment provides an even more stringent test of our motion aftereffect hypothesis.

We observed a trend for a difference between the perceived percentage in the adaptation and the control conditions, but it was not statistically significant ($F(1, 29) = 2.92$, $p = 0.098$, $\eta_p^2 = 0.092$, $95\%C.I. = [0.000, 0.321]$, ns). As expected, there was a main effect of the actual percentage report ($F(2.10, 60.89) = 232.24$, $p < 0.001$, $\eta_p^2 = 0.889$, $95\%CI = [0.861, 0.909]$) that showed the perceived percentage increased with the actual percentage. There was no interaction between the experimental condition and the actual percentage ($F(3.31, 95.97) = 2.07$, $p = 0.103$, $\eta_p^2 = 0.067$, $95\%C.I. = [0.000, 0.122]$, ns). However, for the planned Tukey HSD paired t-tests between adaptation trials and control trials within each actual percentage, we found that adaptation increased the perceived percentage where the actual percentages were 20% and 40%. These planned comparisons found that the adaptation condition was increased toward the adaptation direction, compared to the control condition

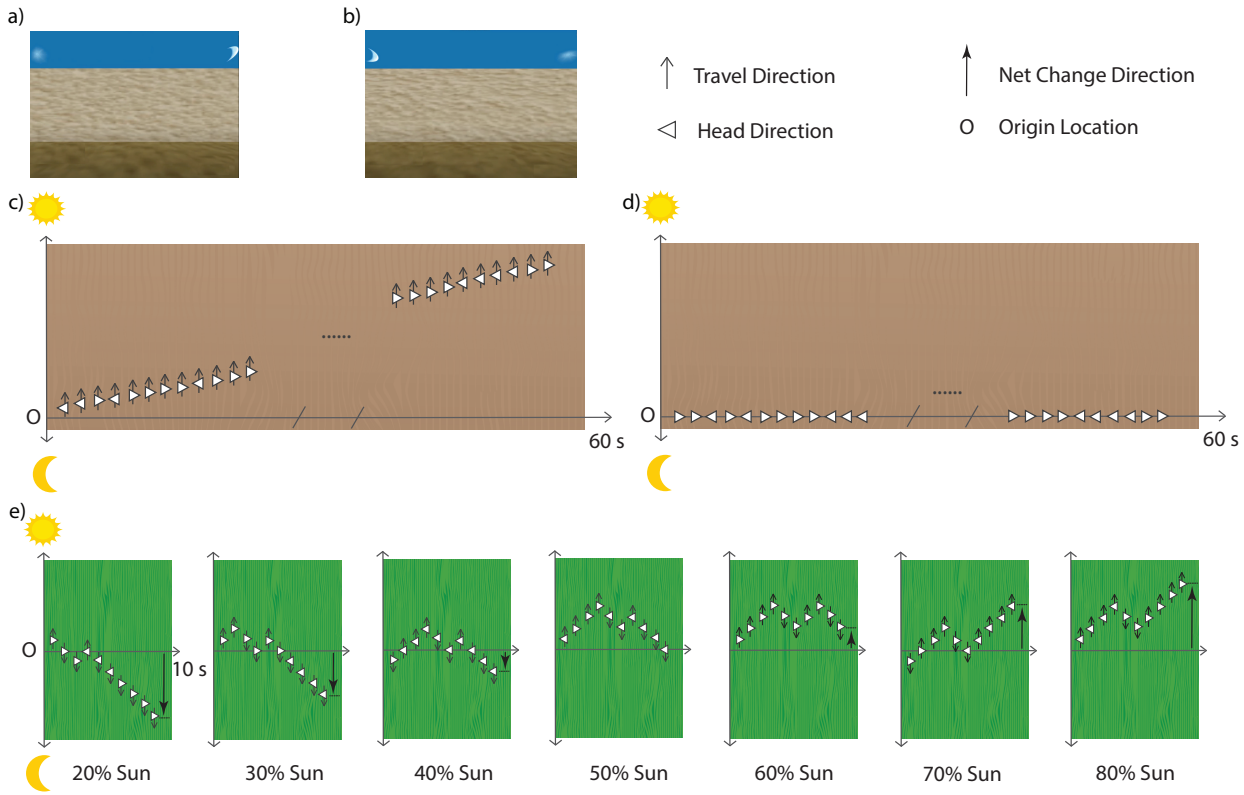

Figure 2.3: Experiment 2. a) Hallway during the adaptation phase, adapting to the sun direction. b) Hallway during the adaptation phase, adapting to the sun direction, opposite facing direction than a). The ground for the hallways turned green during the test phase to provide a visual cue for when to start tracking movement direction. c) The 60-second adaptation phase for the experimental condition. During the adaptation phase, visual movement traveled toward the sun while the facing direction occasionally changed. d) The 60-second initial phase for the control session. There was no visual travel, but the facing direction randomly changed. e) The test phase, which was the same for all sessions in all conditions. Visual movement traveled back-and-forth between the sun and the moon during a 10-second interval. Participants were asked to decide whether the total movement was more toward the sun or more toward the moon in that interval. The facing direction randomly changed during the test phase. Here we show one example from each of the seven test phase conditions of the percent of net movement toward the adaptation direction (20%, 30%, 40%, 50%, 60%, 70%, 80%).

(Figure 2.4a, Appendix Table A.5), consistent with Experiment 1.

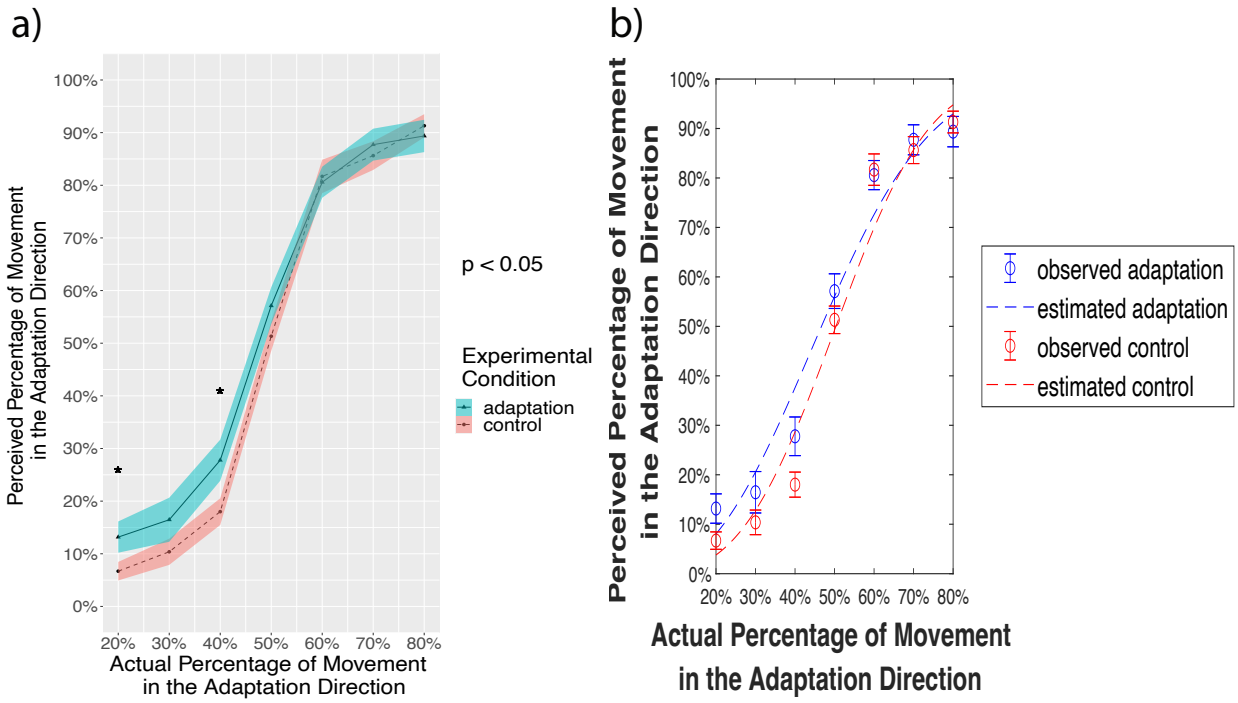

Figure 2.4: Experiment 2. a) The perceived percentage of movement in the adaptation direction compared with the actual percentage for all subjects (n = 30). The adaptation condition showed significantly higher reported percentages than corresponding control conditions at 20% and 40%, supporting the aftereffect. This result suggests an aftereffect in the same direction of travel. Solid lines indicate the grand average value, and the shaded area indicate 1 standard error of means. * $p < 0.05$, Tukey correction. b)The average psychometric Weibull functions for all subjects (n = 30). The bias psychometric function (i.e., α) did not significantly shift when adapted ($p = 0.670$). The uncertainty psychometric function (i.e., β) indicates that observers' detectability of the difference between the two directions was not significantly decreased by adaptation ($p = 0.210$). Error bars indicate standard errors.

Furthermore, after controlling for people's self-reported strategies by including types of strategies (e.g., counting, focusing on part of the environment, and others) as a factor in the analyses (see Methods Section 2.4.2; Appendix Section A.9.3), the difference between the adaptation and the control condition became more distinguishable, such that adaptation increased people's reported rate ($F(1,\ 27) = 5.58,\ p = 0.026,\ \eta_p^2 = 0.171,\ 95\%CI = [0.000, 0.418]$). There was a significant interaction between condition and the actual percentage ($F(3.53,\ 95.40) = 3.23,\ p = 0.020,\ \eta_p^2 = 0.107,\ 95\%CI = [0.012, 0.178]$). Tukey HSD analyses revealed that people reported significantly more travel toward the adap-

tation direction in the adaptation session than in the control session at 20% ($p = 0.003$), 40% ($p = 0.005$), 50% ($p = 0.031$), and marginally more at 30% ($p = 0.070$). The motion aftereffect also got stronger after excluding 7 subjects (about 25% of subjects) with implausible psychometric parameters yielded from the Weibull function (Appendix Figure A.14 - A.16, Table A.6).

We fit each subject's data into the Weibull function as we did in Experiment 1 (Appendix Figure A.13). We found no difference between the adaptation and the control conditions in either response bias (α) ($t(29) = 0.43$, $p = 0.670$, $Cohen's\, d = 0.112$, $95\%CI$ = [-0.409, 0.633], ns) or detectability (β) ($t(29)$ = -1.28, $p = 0.210$, $Cohen's\, d$ = -0.251, $95\%CI$ = [-0.648, -0.147], ns) (Figure 2.4b).

Thus, the observed aftereffects in Experiment 2 were weaker compared with those observed in Experiment 1. Experiment 2 had fewer participants than Experiment 1; the sample size was based on our power analysis from the Experiment 1 results. This weaker aftereffect could be also due to the unusual travel direction in the task: in daily life, people experience walking forward or backward more often than walking laterally. Moreover, especially for the adaptation condition, tracking four directions (front-back for head direction and left-right or sun-moon directions for travel direction) in Experiment 2 was likely more challenging than in Experiment 1, where people only tracked two directions (front-back or sun-moon directions for both travel direction and head direction). After including the strategy as an additional factor or excluding subjects based on implausible parameter estimates from the Weibull function fitting procedure, we observed much stronger motion aftereffects, indicating that we were able to successfully replicate the results from Experiment 1 in this more challenging scenario.

2.2.4 Motion aftereffects scale with duration of adaptation

In Experiment 3 ($n = 28$ participants; 16 females), we attempted to address remaining questions from Experiment 1 and 2 about the adaptation duration. An alternative explanation for the "opposite" adaptation effect is that the adaptation time used in the previous two experiments might be too long or too short to induce a sufficient adaptation effect for travel direction. We initially set the adaptation time (i.e., 60s initial adaptation, 10s top-ups) based on previous visual adaptation studies, but since adaptation effects of travel direction have never been studied before, we had few *a priori* expectations regarding whether adaptation duration would produce larger or smaller effects. Based on previous visual adaptation literature, the magnitude of a classic motion aftereffect should scale depending on the amount of adaptation, as increased adaptation time yields a greater decrease in the neural responsiveness to the same stimuli (Fang & He, 2005; Fang, Murray, Kersten, & He, 2005; Leopold, Rhodes, Müller, & Jeffery, 2005; Vautin & Berkley, 1977). To take a closer look at whether and how adaptation time affects motion aftereffects of travel direction, we conducted an experiment where we tested four adaptation time periods: 18s, 36s, 54s, and 72s. Motion was in the direction of the hallway like in Experiment 1, and for simplicity we only used the sun direction for this study. Because we added more adaptation conditions, we also only tested three levels of percentage of actual movement in the adaptation direction: 30, 50, and 70% (see Methods Section 2.4.3).

We were again able to successfully replicate the primary results from Experiment 1 and Experiment 2. We observed a tendency for a difference between the experimental and control conditions at the 18s adaptation time period ($F(1, 27) = 3.88$, $p = 0.059$, $\eta_p^2 = 0.126$, $95\%C.I. = [0.000, 0.370]$). The effect grew towards significance at 36s ($F(1, 27) = 5.20$, $p = 0.031$, $\eta_p^2 = 0.162$, $95\%C.I. = [0.000, 0.408]$), 54s ($F(1, 27) = 13.25$, $p = 0.001$, $\eta_p^2 = 0.329$, $95\%C.I. = [0.070, 0.555]$), and 72s adaptation time periods ($F(1, 27) = 7.22$, $p = 0.012$, $\eta_p^2 = 0.211$, $95\%C.I. = [0.011, 0.455]$). This suggests that the magnitude of the travel motion aftereffect

scales with adaptation time (Figure 2.5, Appendix Figure A.19, Table A.8).

Next, we made pair-wise comparisons between the different adaptation time conditions at each percentage of actual movement in the adaptation direction (Figure 2.2.4a-f, Appendix Figure A.17, A.20). This analysis revealed that when the actual percentage was at 70%, the 72s adaptation trials had significantly higher perceived percentage than the 36s adaptation trials ($p = 0.014$) (Figure 2.2.4e) and marginally higher than the 54s adaptation trials ($p = 0.055$) (Figure 2.2.4f).

All patterns of results were maintained after after excluding 4 subjects (around 14% of subjects) based on implausible parameter estimates from the Weibull function fitting procedure (Appendix Figure A.21 - A.26, Table A.7). These findings are consistent with motion aftereffects scaling with adaptation time. These findings were replicated in an independent sample of participants ($n = 31$ participants; 16 females), with slightly different instructions and some blocks having adaptation to the moon direction (see Appendix Figure A.31 - A.38). In addition, the main result patterns did not shift after controlling for strategies in the analyses for both Experiment 3 (see Methods Section 2.4.3; Appendix Section A.12) and the replication (see Appendix Section A.13 - A.16).

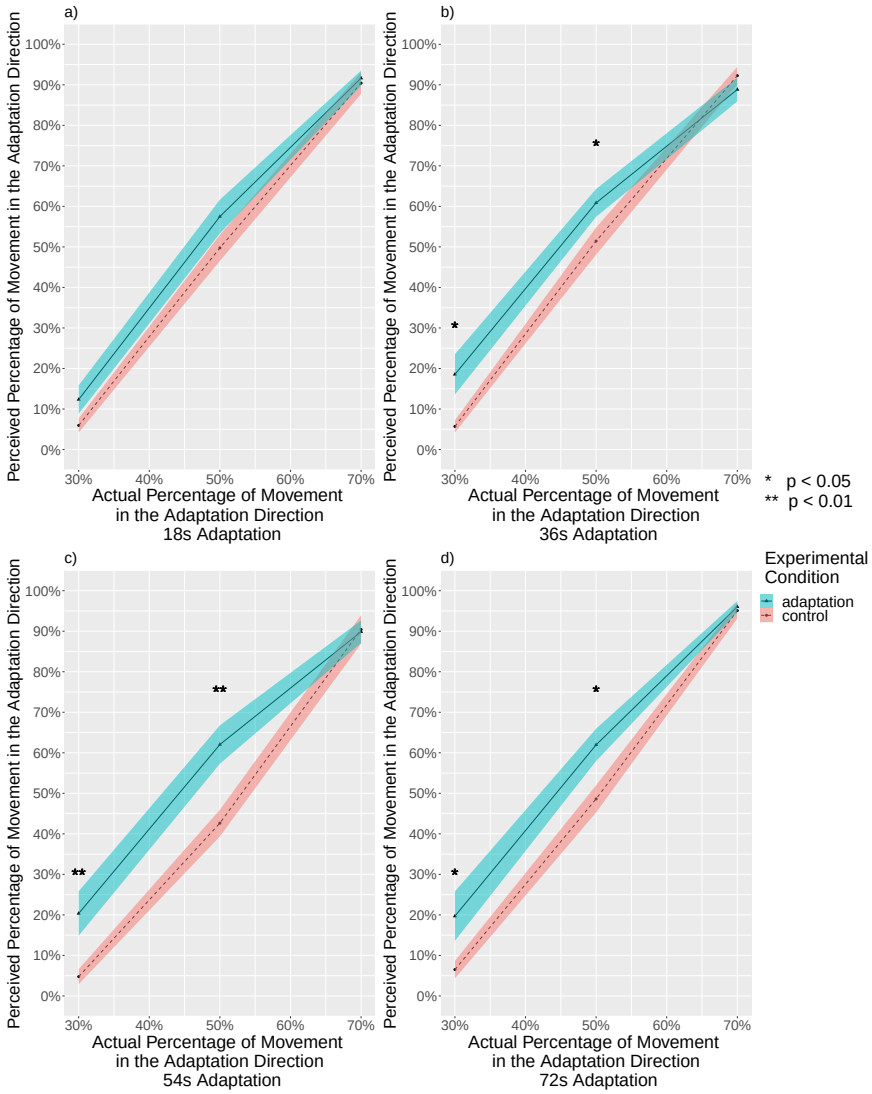

Figure 2.5: Experiment 3. The perceived percentage of movement in the adaptation direction compared with the actual percentage for all subjects, separated by adaptation time periods (n = 28). a) The reported rate for 18s adaptation trials. The adaptation condition showed a trend for higher reported percentages than the control conditions (p = 0.059). b) The reported rate for 36s adaptation trials. The adaptation condition showed significantly overall higher reported percentages than the control conditions (p = 0.031), particularly at 30% (p = 0.015) and 50% (p = 0.032), supporting the aftereffect in the same direction of travel. c) The reported rate for 54s adaptation trials. The adaptation condition showed significantly overall higher reported percentages than the control conditions (p = 0.001), particularly at 30% (p = 0.007) and 50% (p = 0.001), supporting the aftereffect. d) The reported rate for 72s adaptation trials. The adaptation condition showed significantly overall higher reported percentages than the control conditions (p = 0.012), particularly at 30% (p = 0.047) and 50% (p = 0.032), supporting the aftereffect in the same direction of travel. Solid lines indicate the grand average value, and the shaded area indicate 1 standard error of means. * $p < 0.05$, ** $p < 0.01$, Tukey correction.

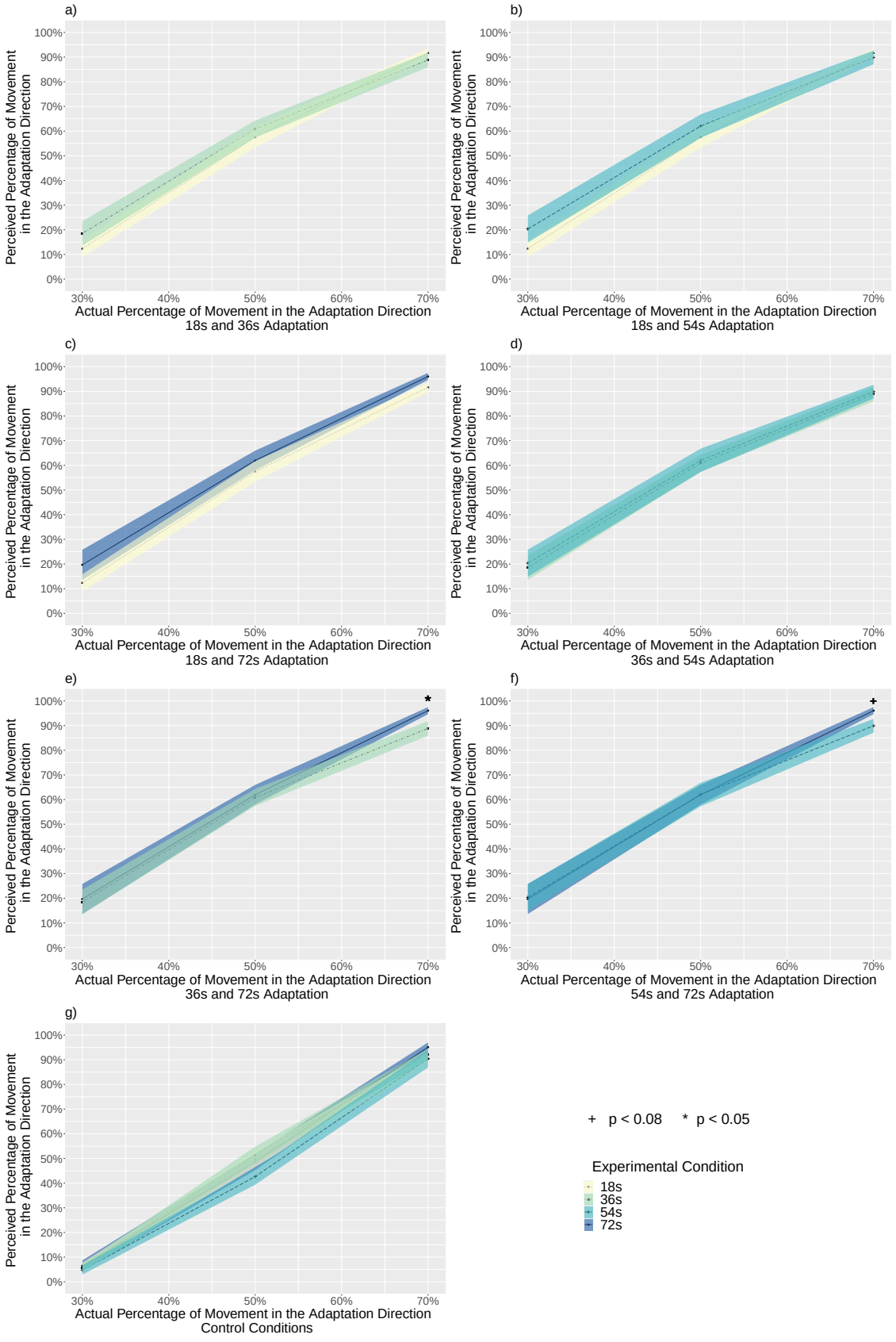
a)
b)
c)
d)
e)
f)
g)
Perceived Percentage of Movement in the Adaptation Direction
100%
90%
80%
70%
60%
50%
40%
30%
20%
10%
0%
30%
40%
50%
60%
70%
Actual Percentage of Movement in the Adaptation Direction
18s and 36s Adaptation
18s and 54s Adaptation
18s and 72s Adaptation
36s and 54s Adaptation
36s and 72s Adaptation
54s and 72s Adaptation
Control Conditions
*
+
+ p < 0.08
* p < 0.05
Experimental Condition
18s
36s
54s
72s

Figure 2.6: Experiment 3. The perceived percentage of movement in the adaptation direction compared with the actual percentage for all subjects, separated by experimental conditions (n = 28). a) The reported rate for the 18s and 36s adaptation conditions. b) The reported rate for the 18s and 54s adaptation conditions. c) The reported rate for the 18s and 72s adaptation conditions. d) The reported rate for the 36s and 54s adaptation conditions. e) The reported rate for the 36s and 72s adaptation conditions. At 70%, 72s adaptation trials had a significantly higher perceived percentage than 36s adaptation trials (p = 0.014), supporting that the aftereffect increased with adaptation time. The aftereffect is in the same direction of travel. f) The reported rate for the 54s and 72s adaptation conditions. At 70%, 72s adaptation trials had slightly higher perceived percentage than 54s adaptation trials (p = 0.055), supporting that the aftereffect increased with adaptation time. The aftereffect is in the same direction of travel. g) The reported rate for all four control conditions. There were no differences between trials with different adaptation time periods within any actual percentage. Solid lines indicate the grand average value, and the shaded area indicate 1 standard error of means. + $p < 0.08$, * $p < 0.05$. All results are reported with the Tukey correction for multiple comparisons.

Further, Weibull analyses showed that when the adaptation time was 54s ($t(27)$ = -2.54, p = 0.017, $Cohen's\, d$ = -0.616, 95%CI = [-1.146, -0.086]) and 72s ($t(27)$ = -1.86, p = 0.074, $Cohen's\, d$ = -0.146, 95%CI = [-0.623, 0.331]), people had significantly more uncertainty in making judgments in the adaptation condition compared to the control condition. When adaptation time was 72s, there was a tendency to bias responses (α) toward the adaptation direction ($t(27)$ = -2.00, p = 0.056, $Cohen's\, d$ = -0.575, 95%CI = [-1.199, 0.048]) (Figure 2.7; Appendix A.18).

Overall, the results in Experiment 3 successfully replicated effects from Experiment 1 and Experiment 2. Importantly, we observed the same "opposite" motion aftereffect of travel direction for differing adaptation time lengths, precluding the alternative explanation that the "opposite" motion aftereffect was due to the adaptation time being too long or too short. Furthermore, the travel aftereffect was scaled with adaptation duration, such that longer adaptation duration tended to have larger aftereffects. Together, these findings provide additional support for a motion aftereffect for travel direction that is independent of head direction.

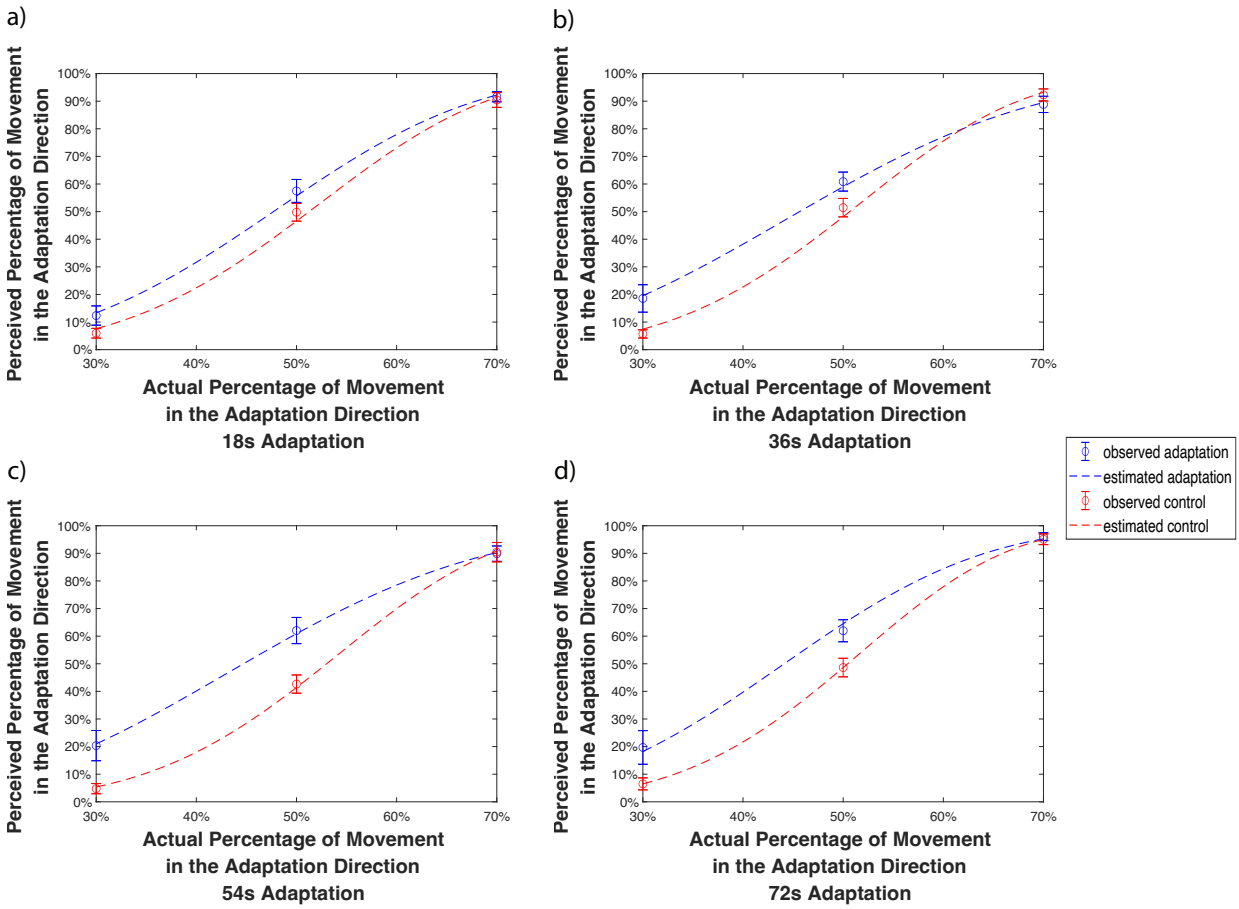

Figure 2.7: Experiment 3. The average psychometric functions by adaptation time periods for all subjects (n = 28). a) The average psychometric functions for 18s adaptation trials. b) The average psychometric functions for 36s adaptation trials. c) The average psychometric functions for 54s adaptation trials. d) The average psychometric functions for 72s adaptation trials. The bias psychometric function (i.e., α) marginally shifted toward a lower percentage of reported movement toward the adaptation direction when adapted at 72s adaptation (p = 0.056) time period, but the shift was not significant at 18s (p = 0.315), 36s (p = 0.407), or 54s (p = 0.669) adaptation time periods. The uncertainty psychometric function (i.e., β) indicates that observers' detectability of the difference between the two directions was decreased by adaptation but were not significant at 18s (p = 0.543) or 36s (p = 0.132) adaptation time periods, but was significant at 54s (p = 0.017) adaptation time period and marginally significant at 72s (p = 0.074) adaptation time period. Error bars indicate standard errors.

2.3 Discussion

How people maintain their travel trajectory during wayfinding has been a long-standing question. The current research attempts to answer this question through understanding the role of travel direction in self-motion. In a series of experiments, we tested travel direction using a motion adaptation paradigm in a visual self-motion task. We observed systematic travel motion aftereffects across all experiments in both raw data (Appendix Figure A.41, Figure A.43) and filtered data (Appendix Figure A.42, Figure A.46). The aftereffect was not due to response bias, approaching effects, or serial position effects. Moreover, the motion aftereffect scaled to a longer adaptation time span.

The aftereffects were observed in the same direction as the adapted travel direction, which fits the characteristics of previous high-level motion aftereffects paradigms (Culham et al., 1998, 2000). First, the adaptation of travel direction we observed was likely high-level, as the possible influence of low-level visual adaptation was designed to be cancelled out due to the constant changes of head direction in the experiment. Second, subjects were instructed to focus on the global net change in position, meaning that they had to integrate their movement over time. Third, the test pattern was dynamic. However, the current task is different from previous motion adaptation experiments in that participants took a first-person (egocentric) perspective to attentively track self-motion instead of simply viewing stimuli move across the screen (e.g. the waterfall effect). Taken together, this makes the effects we observed in the current study unique among high-level motion aftereffects.

This "opposite" motion aftereffect (which is in the same direction of travel) indicates that a non-opponent process underlies the travel direction system. Several previous studies have found similar motion aftereffects but via different sensory modalities, including the *podokinetic aftereffect* where spatial orientation is changed via remodeling somatosensory signals between the trunk and feet (Earhart et al., 2001; Gordon, Fletcher, Jones, & Block, 1995; Weber, Fletcher, Gordon, Jones, & Block, 1998), and the *jogging/running-in-place aftereff-*

fect that involves recalibration of visuomotor control systems (Anstis, 1995; Durgin & Pelah, 1999; Mulavara et al., 2010). Additionally, the cross-modal bias theory hypothesizes a strong association between visual and vestibular pathways as a result of evolution (Bai, He, Jiang, Zhang, & Bao, 2020). The theory suggests that vestibular signals may still integrate with visual input in the current study even though it did not include actual head motion. Such cross-modal bias could lead to a suppression of the neural system to maintain the actual motion.

What could be the possible relationship between the head direction system and the travel direction system in the brain? It is difficult to find direct answers to this question because, as mentioned in the introduction, the two direction systems have typically been conflated. However, we may get some clues from studies in which head direction and travel direction are perfectly aligned. Several studies have investigated heading direction using adaptation paradigms or repetition suppression in fMRI to look at the sensitivity to heading direction of various cortical visual motion areas (Baumann et al., 2010; Cardin, Hemsworth, & Smith, 2012; Shine et al., 2016). Researchers observed clear head direction adaptation in MT, MST (Cardin et al., 2012), medial parietal lobe (Baumann et al., 2010), as well as bilateral retrosplenial cortex, thalamus, and precuneus (Shine et al., 2016). We can take from these results that when head direction and travel direction are aligned, there is still adaptation taking place in the brain. The brain areas that demonstrate adaptation are higher-level motion systems, suggesting that these systems are involved in encoding heading direction in the human brain.

Possible travel direction pathways are more speculative. They could involve independent sensory inputs (e.g., vision, somatosensation) and feed-forward high-level motion processing pathways (e.g., MST, parietal lobe, hippocampus, etc.). Recent findings of bi-directional cells in rodent dysgranular retrosplenial cortex (Jacob et al., 2017) may also be a good candidate for cells that are sensitive to travel direction. Further research using fMRI and

computational modeling is needed to shed light on the relationship between the travel direction and head direction systems in the human brain, and the degree to which they have independent circuitry.

One limitation of our study is that participants did not actually change their head direction or travel direction during the experiment: all participants were sitting still, facing a computer screen, during the entire experiment. Although all subjects experienced visual self-motion (i.e., vection) purely from the desktop virtual reality visual input, it is admittedly different from real-life self-motion. To more effectively test the aftereffect of visually-guided travel direction, other sensory modalities (e.g., motor efference copy, vestibular signal, proprioception, etc.) should be included. That said, the fact that we observed these effects with visual inputs alone is a testament to the potential power of this adaptation paradigm.

In conclusion, in this study we found high-level motion aftereffects of travel direction using a motion adaptation paradigm, which suggests that travel direction is a fundamental component of human navigation. Interestingly, the aftereffect is in the opposite direction to traditional motion aftereffects, suggesting that adapting to a travel direction will result in greater perception of moving towards the adapting direction. Critically, we dissociated head direction from travel direction across all experiments, indicating that travel direction has separate neural mechanisms from head direction in the human brain. Considering travel direction as a basic navigation component provides a new path to understanding the question of how people form their a sense of direction. Furthermore, the results will encourage scientists who study navigation behavior of other species (rodents, birds, insects, etc.) to look for more direct neurological evidence of travel direction, rather than head direction.

2.4 Methods

2.4.1 Experiment 1

Participants

Participants consisted of 77 University of California, Santa Barbara (UCSB) undergraduates who participated in return for course credit or monetary incentive ($12/hour). Our task is novel, thus there is limited previous data to use for a power analysis. Therefore, we based our sample size on previous studies of movement adaptation that used within-subjects designs (Culham et al., 2000; Earhart et al., 2001) and desktop navigation tasks (Weisberg & Newcombe, 2016; Weisberg, Schinazi, Newcombe, Shipley, & Epstein, 2014). These studies yielded a target of 30 participants per condition. We used the outcomes of Experiment 1 for power analysis of subsequent experiments. The four criteria for prescreening participants were 1) no history or a current condition of psychiatric problems, 2) no learning disability or attention deficit disorder, 3) not currently taking psychoactive drugs, and 4) no history of head trauma.

Participants were discarded for either not completing both control and adaptation sessions ($n = 15$), responding with the same key all the time ($n = 1$), or responding too slowly ($RT > 10$ s; $n = 1$). The final pool consisted of 60 participants (29 males, 31 females), with 30 participants randomly assigned in the moon condition virtual environment (16 males, 14 females) and 30 participants randomly assigned in the sun condition virtual environment (13 males, 17 females). Ages of the remaining 60 participants ranged from 18 to 30 (mean 20.32). All participants signed an informed consent form in agreement with the UCSB Institutional Review Board requirements in accordance with the Declaration of Helsinki.

Stimuli

The virtual environment was generated on a PC (Origin, NVIDIA GeForce GTX 980 graphics card, 15-inch display, 1920 1080 pixels display resolution) using Vizard software (WorldViz) to render the images. Participants experienced visual self-motion in a long (8566 virtual units) landmark-free virtual hallway (see Figure 2.1). The hallway was long enough such that the visual angle to the end of the hallway did not change during movement and therefore could not act as a cue to distance traveled. The translational speed of self-motion was randomly sampled from 10 - 15 virtual units/second in each trial. The rotational speed of self-motion was randomly sampled from 130° - 150°/second. Speeds for adaptation and test phases were sampled separately in each trial. The hallway consisted of two walls and a ground surface with coarse grained texture; the textures were designed to prevent participants using them for location cues during movement. The walls were always colored dark brown, while the ground was colored light brown during the adaptation phase and was colored green during the test phase (see Figure 2.1a - b). At one end of the hallway, in the sky, there was a sun and at the other end there was a moon. The sun and the moon were designed to be cardinal frames of reference and were rendered to move with the viewer at a constant distance. Therefore, the size of the moon and the sun did not change with self-motion, and participants could not evaluate distance change based on perceptual changes in either the sun or moon. In the moon condition, participants would initially move toward the moon frame of reference, and vice versa for the sun condition.

Task

The task consisted of an adaptation period followed by test trials (see Figure 2.1c-e). In the adaptation phase for both the sun and the moon adaptation groups, each block started with 60 seconds of virtual travel toward the sun or the moon as the global travel direction, depending on their group (see Figure 2.1c). During the adaptation phase, participants were instructed to pay attention to the movement in the hallway on the computer screen.

To dissociate travel direction from heading direction, we included occasional 180° turns to change the local facing direction while maintaining the constant global travel direction. The number of turns in all experiments were randomly sampled from a range varied by the time length of each trial (0-2 turns for 10s trials, 5-7 turns for 60s initial adaptation phase).

The control was the same for both groups, where the "adaptation" phase consisted of a still screen without movement. This phase only lasted 10 seconds, but with occasional 180° turns to change the facing direction (see Figure 2.1d).

Immediately after the adaptation phase was a 10-second test phase. The test phase was the same for all conditions. The ground in the hallway would turn green, signifying the 10-second test period. In the test phase, the travel direction would change, such that participants experienced back-and-forth movement toward both the sun and the moon. The facing direction changed during the test phase, just like in the adaptation phase, with between 0 and 2 turns. The amount of back-and-forth movement on each trial was expressed in terms of a percentage of movement toward one of the two cardinal frames of reference (see Figure 2.1e). The percentage of movement in one direction is complementary to the other direction such that they add up to 100%. For example, 20% of virtual movement toward the sun is equivalent to 80% of virtual movement toward the moon. In order to compare the sun and the moon conditions, all analyses are described as oriented toward the sun direction so that we could easily see the effect of adaptation in each condition.

In addition to the experimental condition (adaptation vs. control), this percentage of virtual movement was the primary independent variable in the study, ranging from 20% to 80% in 10% steps. Participants were instructed to pay attention to the overall direction they traveled in during the test period. When the movement in the test period stopped, on-screen text asked participants to judge whether their movement during the test period was overall more toward the sun or more toward the moon direction. They used their left hand to press the D key to indicate that they moved closer to the sun and used their right hand to press the

K key to indicate that they moved closer to the moon. Although the task was untimed, participants were instructed to respond as quickly and accurately as possible.

As soon as participants pressed a response key, the hallway would turn brown again for 10 seconds as a top-up adaptation phase. The top-up adaptation of the next trial started with the same facing direction as the last screen of the previous testing trial so that participants could have a more coherent experience in the virtual environment. During the 10-second top-up phase, participants would experience the same movement as the initial 60-second adaptation (i.e., the same initial travel direction with occasional changes of facing directions) but for a shorter time length. Then, participants would be given another 10-second test of travel direction. In the control condition, the top-up was 10 seconds in the hallway without movement, but with occasional facing changes. The task continued alternating between the original travel direction top-up adaptations (brown) and test phase (green) until the block ended, and then participants could take a break (up to 5 minutes). Reported direction and reaction time for each trial were recorded.

Design

A 2 (experimental condition: adaptation, control; within subjects) $\times$ 7 (actual percentage of movement toward the sun: 20%, 30%, 40%, 50%, 60%, 70%, 80% rate; within subjects) within-subjects design was used. Each test condition was repeated for 12 trials, for a total of 84 trials (7 test conditions 12 trials/test condition). These 84 trials were randomly separated into 3 blocks with a short break between blocks. A new 60-second adaptation occurred after each break to reinstate the adaptation. All stimuli were presented in random order for all participants.

In order to control for the influence of a particular adapting direction and of response bias, half of subjects were randomly assigned to the sun adaptation group, and the other half were assigned to the moon adaptation group. We combined the sun and moon adaptation groups

for analysis, although we also analyzed them separately (see Supplemental Information). The experiment was conducted over two sessions for each participant, with one session the experimental task and the other session as the control. The order of completing these two sessions were counterbalanced among participants within each group.

Procedure

Participants first were greeted in the lab, given information about the study, and given consent forms to sign. They then completed a participant screening form and were given an instruction sheet to learn about the task.

Next, they performed the motion adaptation task. Participants sat approximately 50 cm in front of the computer screen. Before beginning the formal experiment, they were given additional instructions and the experimenter answered any questions. They completed 5 practice trials (the adaptation time and test conditions were different from the experimental trials), and then any additional questions were answered.

Each session lasted approximately 1 hour. Participants completed the two sessions on two separate days to prevent fatigue, with no more than one week between sessions.

Finally, after each session, participants were asked to rate the difficulty of the task based on a 1 - 7 Likert scale (1 meant very easy and 7 meant very difficult) and to respond to an open-ended question about their strategy.

Data Analysis

R-studio and MATLAB were used for data analysis. We first removed outlier trials that were 3 standard deviations above or below of the mean of each subject's reaction time. Approximately 0.33% of trials were removed: no trials were removed in the sun group, and in the moon group 0.04% trials were removed from the experimental session and 1.27% trials were removed from the control session. From the remaining trials for each participant, we

calculated the reported percentage of movement toward the adaptation direction (i.e., sun or moon direction) as well as mean reaction time for each percentage level.

First, we conducted a 2 (experimental condition: adaptation, control; within subjects) $\times$ 7 (actual percentage toward the adaptation direction: 20% - 80% rate of actual movement toward the adaptation direction; within subjects) repeated-measures analysis of variance (ANOVA). The primary comparison was the difference between the adaptation and the control conditions within each actual percentage of movement since a motion aftereffect would lead to a shift in the curve for the adaptation conditions. Because this difference between adaptation and control was the primary outcome measure, we also conducted Tukey HSD paired t-tests between adaptation trials and control trials within each actual percentage of movement.

We then analyzed the data by fitting results with a Weibull function. In the current study, the Weibull function assumes that the perceived movement contrast between the moon and the sun scales proportionally to the signal-to-noise ratio of the actual movement contrast that supports the perception. Separate Weibull functions were fit to individual participants's data for each experimental condition (adaptation and control) and each percentage of movement in the adaptation direction (20% - 80%) using Palamedes toolbox in MATLAB (Prins & Kingdom, 2018). Two parameters were derived for each fitted function: the α value (i.e., the point of subjective equality) measures a bias to respond the sun or the moon direction in the task, and the β value reflects the detectability of the difference in the task. We then filtered 9 subjects' data (3 from the sun adaptation group, 6 from the moon adaptation group) whose α or β value were beyond 2 standard deviations above or below the mean, and conducted paired t-tests of the α and β values between the adaptation and control condition. In addition, we re-ran the same ANOVAs of reported rate and reaction time on the filtered data.

Based on post-study questionnaires, participants generally reported the same strategies for

both adaptation and control sessions. More specifically, more than half of the subjects ($n = 36$) reported using counting strategies (e.g., mentally counting time, counting steps, physically counting by tapping fingers, etc.). The next set of subjects ($n = 18$) reported keeping focus on a certain part of the environment (e.g., wall, hallway, ground, sky, etc.) for distance estimation. Each of the remaining people ($n = 6$) used a unique strategy. For the filtered data, there were still subjects using counting ($n = 31$), focusing on a part of the environment ($n = 14$), and a unique strategy ($n = 6$). We controlled for the influence of strategies by adding strategy as a factor in the above ANOVA analyses for reported rate and reaction time.

2.4.2 Experiment 2

Participants

The sample size in Experiment 2 was determined based on power analysis using the results of Experiment 1. We used G*Power software (http://www.gpower.hhu.de/) (Erdfelder, Faul, & Buchner, 1996) with an $\alpha = 0.05$, $power = 0.8$, and $Cohen's f$ measurement of effect size $= 0.176$ which is based on the weakest effect size (i.e., the interaction effect of the moon condition, see Appendix Figure A.3c) from Experiment 1. The resulting sample size for within-group comparison was 24. Using this power analysis, we recruited 33 participants for Experiment 2, which is more than adequate for the main objectives of this study and which matched closely with the participant numbers from the Experiment 1 sun condition. Participants consisted of 33 University of California, Irvine (UCI) students who participated in return for monetary incentive ($12/hour). Three participants were discarded for misunderstanding the task instruction ($n = 1$), wrongly pressing the reverse response buttons ($n = 1$), or not completing both control and adaptation sessions ($n = 1$). The final pool consisted of 30 participants (14 males, 16 females). Ages of the remaining 30 participants ranged from 18 to 34 (mean 22.93). All participants signed an informed consent form in agreement with the UCI Institutional Review Board requirements in accordance with the Declaration

of Helsinki.

The Stimuli, Task, Design, and Procedure were the same as Experiment 1, except that tasks were modified such that the head direction was always orthogonal to the travel direction (see Figure 2.3). For simplicity, we only conducted adaptation to the sun direction. The initial control adaptation period lasted 60s in Experiment 2.

Data Analysis

The analysis was largely the same as Experiment 1. We first removed outlier trials that were 3 standard deviations above or below of the mean of each subject's reaction time. Approximately 2.12% of trials were removed: 2.18% trials were removed from the experimental session and 2.06% trials were removed from the control session. From the remaining trials for each participant, we calculated the reported percentage of movement toward the sun as well as mean reaction time for each percentage level.

First, we conducted a 2 (experimental condition: adaptation, control; within subjects) $\times$ 7 (actual sun percentage: 20% - 80% rate of actual movement toward the sun; within subjects) repeated-measures analysis of variance (ANOVA) analysis. Because the primary comparison was the difference between the adaptation and the control conditions within each actual percentage of movement, we also conducted Tukey HSD paired t-tests between adaptation trials and control trials within each actual percentage of movement. We then filtered 7 subjects' data and analyzed the data using parameters derived from Weibull fits, similar to Experiment 1.

Based on post-study questionnaires, participants generally reported the same strategies for both adaptation and control sessions. Same as we had observed in Experiment 1, people reported three main types of strategies in Experiment 2: counting strategies ($n = 13$), keeping focus on a certain part of the environment for distance estimation ($n = 7$), and a unique strategy ($n = 10$). For the filtered data, there were still subjects using counting ($n = 12$),

focusing on a part of the environment ($n = 4$), and a unique strategy ($n = 7$). Again, we controlled for the influence of strategies by adding strategy as a factor in the above ANOVA analyses for reported rate and reaction time.

2.4.3 Experiment 3

Participants

Similar to Experiment 2, we calculated a sample size of 24 for within-group comparison in Experiment 3 determined based on power analysis using G*Power software (http://www.gpower.hhu.de/)(Erdfelder et al., 1996) based on the weakest effect size from Experiment 1 (Appendix Figure A.3c). We recruited 28 participants for Experiment 3 (12 males, 16 females), which is more than adequate for the main objectives of this study. All participants were UCI students who participated in return for monetary incentive ($12/hour). Ages of the participants ranged from 18 to 30 (mean 24.71). All participants signed an informed consent form in agreement with the UCI Institutional Review Board requirements in accordance with the Declaration of Helsinki.

The Stimuli and Procedure were the same as Experiment 1.

Task

The Task was the same as Experiment 1, except for the following:

1. Each block started with different initial adaptation time periods (18s, 36, 54s, or 72s), correspondingly followed by different top-up time periods (3s, 6s, 9s, or 12s). The control adaptation phases and top-up periods had the same corresponding time lengths. For convenience, we refer to all adaptation trials in terms of their initial adaptation time.

2. Corresponding to the change in the time length for the adaptation phases, we also changed the range of the number of turns of the facing direction that each top-up and adaptation

period was sampled from: 0-1 turn for 3s top-ups, 0-2 turns for 6s top-ups, 0-2 turns for 9s top-ups, 0-2 turns for 12s top-ups, 1-3 turns for 18s adaptation periods, 3-5 turns for 36s adaptation periods, 4-6 turns for 54s adaptation periods, 6-8 turns for 72s adaptation periods. Ranges were calculated based on the following equations:

$$N_{max} = \lfloor \alpha t + 1 \rceil \tag{2.1}$$

$$N_{min} = \begin{cases} \lfloor \alpha t - 1 \rceil, & \text{if } t \geq 10 \\ 0, & \text{otherwise} \end{cases} \tag{2.2}$$

N denotes number of turns. α is a coefficient which was set to 0.1. t denotes the number of time step in the trial (either the adaptation or the test phase). $\lfloor \rceil$ denotes round to the nearest integer.

3. To keep the experiment within two sessions, we used three percentages of virtual movement (30%, 50%, and 70%) and reduced the number of trials in each percentage to 9.

Design

A 2 (experimental condition: adaptation, control; within subjects) × 4 (adaptation time blocks: 3s top-up with 18s initial adaptation, 6s top-up with 36s initial adaptation, 9s top-up with 54s initial adaptation, 12s top-up with 72s initial adaptation; within subjects) × 3 (actual percentage of movement toward the sun: 30%, 50%, 70% rate; within subjects) within-subject design was used. Each test condition was repeated for 9 trials, for a total of 108 trials (4 blocks x 3 percentages/block 9 trials/percentage, not including the initial trial

of each block). Each of the 4 blocks corresponded to one adaptation time condition. The order of the 4 blocks was counterbalanced across subjects. The trials with the 3 different percentages of actual movement toward the sun were presented in random order within each block. There was a short break between blocks. A new initial adaptation period occurred after each break to initiate adaptation of a different magnitude.

The experiment was conducted over two sessions for each participant, with one session the experimental task and the other session as the control. The order of completing these two sessions was counterbalanced.

Data Analysis

The analysis was largely the same as Experiment 1. We first removed outlier trials that were 3 standard deviations above or below of the mean of each subject's reaction time. Approximately 1.93% of trials were removed: 1.79% trials were removed from the experimental session and 2.08% trials were removed from the control session. From the remaining trials for each participant, we calculated the reported percentage of movement toward the sun as well as mean reaction time for each percentage level at each adaptation condition (the initial adaptation trial in each block were not included).

First, we conducted a 2 (experimental condition: adaptation, control; within subjects) $\times$ 3 (actual sun percentage: 30%, 50%, 70% rate of actual movement toward the sun; within subjects) repeated-measures ANOVA for each adaptation time periods (18s, 36s, 54s, or 72s) separately. Because the primary comparison was the difference between the adaptation and the control conditions within each actual percentage of movement, we also conducted Tukey HSD paired t-tests between adaptation trials and control trials within each actual percentage of movement.

Next, we conducted a 4 (adaptation time periods: 18s, 36s, 54s, or 72s; within subjects) $\times$ 3 (actual sun percentage: 30%, 50%, 70% rate of actual movement toward the sun; within

subjects) repeated-measures ANOVA for each experimental condition (control, adaptation) separately. Because the primary comparison was the difference between different adaptation time periods within each actual percentage of movement, we also conducted Tukey HSD paired t-tests between different adaptation time periods within each actual percentage of movement. We then filtered and analyzed the data using the Weibull function, similar to Experiment 1. We filtered 4 subjects' data from all conditions based on subjects whose results were excluded by more than one adaptation time period condition.

Same as we have observed in Experiment 1 and 2, people reported three main types of strategies in Experiment 3: counting strategies ($n = 13$), keeping focus on a certain part of the environment for distance estimation ($n = 13$), and a unique strategy ($n = 2$). For the filtered data, there were still subjects using counting ($n = 10$), focusing on a part of the environment ($n = 12$), and a unique strategy ($n = 2$). Again, we controlled for the influence of strategies by adding strategy as a factor in the above ANOVA analyses for reported rate and reaction time.

Chapter 3

The Distributed Head and Travel Direction System in the Human Brain During Active Navigation: Past, Present, and Future

3.1 Introduction

Each person may see the same environment in different ways. Individual differences in the internal representation of the external environment - the cognitive map (Tolman, 1948) - may generate a broad range of navigation abilities (Wolbers & Hegarty, 2010). While we all want to navigate efficiently and avoid getting lost, it is essential to first understand what the cognitive map looks like, and then to detect fingerprints on the cognitive map that shape our navigation abilities.

Decades of research has revealed a menagerie of spatial cells - centered in and around the medial temporal lobe - that are the basic building blocks of the cognitive map (Moser, Moser, & McNaughton, 2017). Neurons such as place cells - found in hippocampal CA1, CA3, and dentate gyrus - that represent location signals (O'Keefe, 1976; O'Keefe & Dostrovsky, 1971; OKeefe & Nadel, 1978) and grid cells - found in entorhinal cortex - that represent metric signals (Fyhn et al., 2004; Hafting et al., 2005) are basic coordinates of the cognitive map. Head direction cells, which represent the direction an animal is facing momentarily, complement place cells and grid cells as the internal compass of the cognitive map. Head direction cells are widely distributed around the medial temporal lobe. In the rodent brain, head direction cells are found in the thalamus, presubiculum, subiculum, and retrosplenial cortex (Chen et al., 1994; Cullen & Taube, 2017; Ranck Jr, 1984; Taube et al., 1990a, 1990b). In humans, head direction signals have been observed in the thalamus (Shine et al., 2016), retrosplenial cortex (Koch et al., 2020; Marchette, Vass, Ryan, & Epstein, 2014; Nau et al., 2020; Shine et al., 2016), precuneus (Baumann et al., 2010; Shine et al., 2016), presubiculum (Vass & Epstein, 2013), extrastriate cortex (Sherrill et al., 2015a), and early visual cortex (Koch et al., 2020; Nau et al., 2020).

One critical question in human spatial neuroscience is whether we have a single internal compass tuned for allocentric (world-centered) directions, or many internal compasses that are attuned to different aspects of navigation. For example, could we use signals in the

human brain to discriminate between moving north from moving south, as well as turning left from turning right?

This question has not been answered in previous studies. On the one hand, previous fMRI studies detected head direction signals with repetition suppression (Grill-Spector & Malach, 2001) in brain regions that are sensitive to changes in head direction in complex environments. For example, studies have found decreased fMRI signals after viewing pictures of objects located in the same direction in a learned environment. However, repetition suppression only reveals brain activation related to processing head directions in general (Baumann et al., 2010; Shine et al., 2016), but not in discriminating one direction from another. In contrast, firing for a particular direction is the hallmark of head direction cells in animals (Ranck Jr, 1984; Taube et al., 1990a, 1990b). On the other hand, studies on head direction signals in the human brain that used machine learning methods to discriminate one direction from another direction only focused on open field tasks where the environment is an open space with a horizon-like boundary (Koch et al., 2020; Nau et al., 2020) or static images (Vass & Epstein, 2013). In open field tasks, directions could only be defined and thus be discriminated in a single way (e.g., discriminating 30° from 60°) due to a lack of external reference points. However, it is important to examine these signals in complex, dynamic, and naturalistic environments that are more like the environments that people experience in daily life.

To address this lacuna, our lab designed a virtual navigation task in a complex maze that aligns with four cardinal directions (arbitrarily defined as north, south, east, west; see Figure 3.1; see Methods). First, participants freely explored the maze to learn it. Then, in the test task, the lab asked participants to navigate to goals through a series of translations and rotations; this setup allows us to look at active goal-directed navigation. With this complex environment, I aim to conduct direction classification on brain signals for three types of

directions: static head direction, translating, and rotating[1].

Another critical question in understanding the cognitive map is what the roles of different frames of reference are. There are two main frames of reference. The egocentric frame of reference is based on a viewer-centered representation of the environment, such that spatial information is formed with respect to oneself, such as right and left. The allocentric frame of reference is formed independently of the observer's view, for example, cardinal directions of north, south, etc. Navigation strategies based on the egocentric frame of reference are also sometimes called *response-learning* or *route-based strategies*. Navigation strategies based on the allocentric frame of reference are sometimes called place-learning. Distinct neural circuits have been shown to be recruited for these different navigation strategies: the medial temporal lobe - especially hippocampus - is involved in the allocentric strategy, while a striatal pathway - especially caudate - is involved in coding the egocentric strategy (Berke, Breck, & Eichenbaum, 2009; Doeller, King, & Burgess, 2008; Geerts, Chersi, Stachenfeld, & Burgess, 2020; Hartley, Maguire, Spiers, & Burgess, 2003). Previous studies also reported different frames of reference during self-motion (Clark & Harvey, 2016; Robertson, Rolls, Georges-François, & Panzeri, 1999).

These previous studies leave many open questions: During active navigation, will all brain regions adopt the same reference frame? Or will they split between egocentric or allocentric representations, switch back and forth between representations, or adopt both representations simultaneously? In this study, I also aim to look at this question by comparing classifier performance on brain signals defined according to egocentric and allocentric frames of reference (see Methods). This analysis is possible because translations and rotations have both allocentric and egocentric interpretations in the task. For example, a clockwise turn could be defined egocentrically as turning right or allocentrically as turning from north to east.

[1]I specifically call head and travel direction signals "movement directions" (i.e., translating and rotating) because the head direction (the direction someone is facing) and the travel direction (the direction of one's body movement) were conflated during self-motion in this study, but provide separate signals in the internal representation system in human navigation (for details, see Chapter 2).

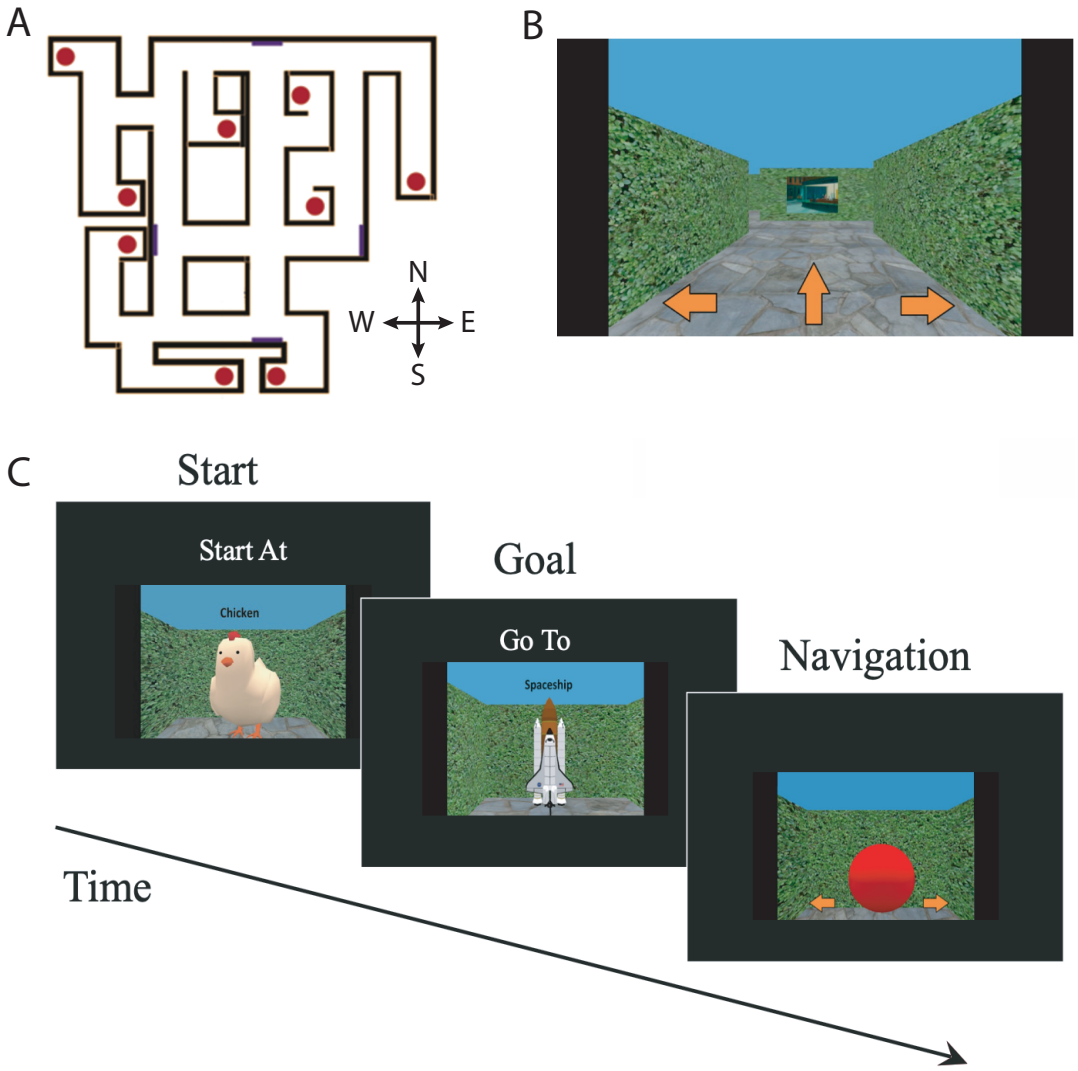

Figure 3.1: Task Overview. (A) Topographical view of the virtual maze environment, which participants never saw. Red dots represent the locations of objects. Purple lines along the walls represent the locations of paintings in the hallways that could be utilized as navigational landmarks. The maze was arbitrarily defined to be aligned with north (N), east (E), south (S), west (W). (B) Navigating the virtual environment: Participants were given a button box and were presented with options at each intersection. Here, the participant has the option of going left, right, or continuing forward. During the exploration phase, participants were given a total of 16 minutes to freely explore the maze environment by choosing from any of the options at each intersection, making a button press to indicate their choice. (C) During the test phase, participants were started at one object, then instructed to navigate to a second object within a 45-second time limit. After the prompt, all objects were replaced with red spheres and the participant had to navigate to the target object from memory.

To support my classification of head direction signals in both egocentric and allocentric frames of reference, I selected regions of interest (ROIs) that were found to be important or related to areas coding for allocentric strategies and egocentric strategies in addition to brain areas where head direction signals have been reported. These regions include the hippocampus, basal ganglia (caudate, putamen, pallidum, nucleus accumbens), visual cortex (extrastriate cortex and early visual cortex), thalamus, and parietal lobe (retrosplenial cortex, precuneus). I selected the auditory cortex as a reference area (see Figure 3.2; Methods).

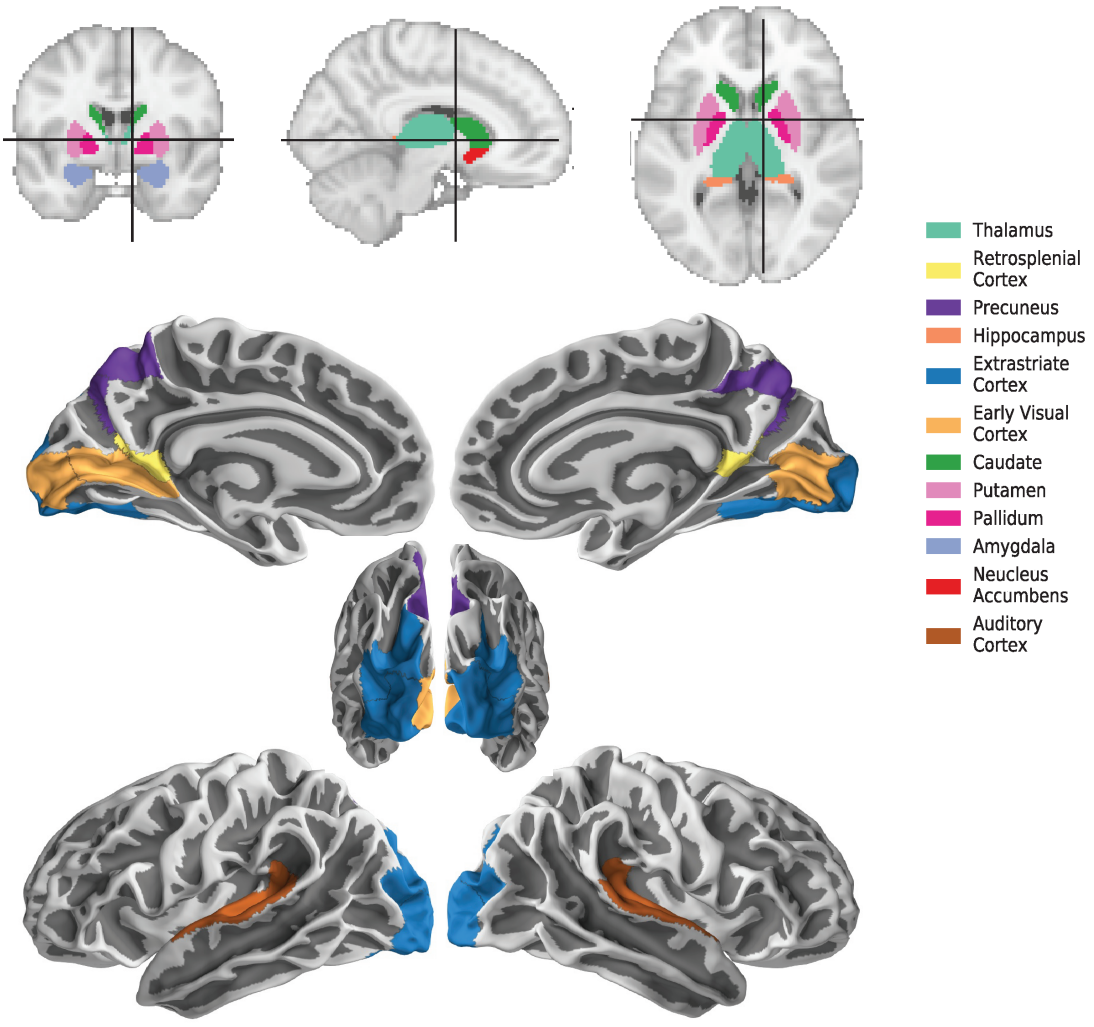

Figure 3.2: Regions of Interest (ROIs). Subcortical regions (upper) were based on the Harvard-Oxford subcortical atlas. Cortical regions (lower) were based on the Schaefer 17 network cortical parcellation (2018).

In addition to representing the position and direction a person is currently experiencing

(the present cognitive map), are there also cognitive maps that predict the next movement (the future cognitive map) or track the previous movement (the past cognitive map)? In rodent research, researchers have reported hippocampal replays - similar firing sequences in place cells during spatial behaviors and the sleep afterwards - that conjectured to consolidate memory of past events (Wilson & McNaughton, 1994), providing support for a past cognitive map. Furthermore, researchers have also reported hippocampal preplay - similar firing sequences in place cells during sleep or rest and the afterwards spatial behaviors (Dragoi & Tonegawa, 2011), providing support for a future cognitive map. Additional support for a future cognitive map comes from goal-directed navigation studies that reported simulations of prospective navigational states in hippocampus that relate to planning in both rodents (Johnson & Redish, 2007; Wikenheiser & Redish, 2015) and humans (T. I. Brown et al., 2016; Hassabis et al., 2009; Spiers & Gilbert, 2015), as well as predicting future heading directions in the hippocampus in an open field task (Huxter, Senior, Allen, & Csicsvari, 2008). In this study, I plan to look at possible representations of future and past cognitive maps in the head direction signals in humans. Critically, this analysis is possible because multiple directional representations might take place during the stationary period in the task: not only the current allocentric direction represented, but also the next movement that subjects would make (both egocentric and allocentric), as well as the previous movement that was just completed (see Methods).

How do head direction signals come on board? Previous fMRI studies on head direction signals in humans only looked at well-learned environments (Baumann et al., 2010; Koch et al., 2020; Nau et al., 2020; Shine et al., 2016; Vass & Epstein, 2013), so it remains elusive whether head direction signals could still be discriminated when learning the environment. My task was designed to include an environmental exploration phase before the test phase which enabled us to see the emergence of head direction signals (see Methods).

Finally, I will return to the initial question to investigate individual differences in head

direction signals by conducting correlation analyses between classification accuracy of brain signals and navigation performance across all aforementioned dimensions (i.e., different types of directions, two frames of reference, cognitive maps of present, future and past, as well as exploration and test phases). This correlation analysis is possible due to our large sample size (98 subjects).

Here, I offer following hypotheses of head and travel direction representation during active navigation:

1. The classifier will be able to discriminate between different signals associated with head and travel directions in brain areas where head direction signals have been found before, including the thalamus, retrosplenial cortex, precuneus, and visual cortex.

2. Allocentric head and travel directions would be represented in the hippocampus, thalamus, and retrosplenial cortex, and visual cortex; while egocentric head and travel directions would be represented in the basal ganglia, parietal lobe, and visual cortex.

3. Alternatively, I might observe wide representations of head and travel directions beyond the regions hypothesized above (e.g., in the amygdala and auditory cortex) due to a highly connected internal orientation network that might be activated during active navigation.

4. Head and travel direction signals will have stronger representations (either more widely distributed or stronger signals, or both) during self-motion than during the stationary period.

5. Head and travel direction signals will have stronger representations (either more widely distributed or stronger signals, or both) during the test phase than during the exploration phase.

6. The classifier will be able to discriminate between different signals associated with past

and future head and travel directions in brain regions where head directions signals have been reported before (e.g., the thalamus, retrosplenial cortex, precuneus, visual cortex) as well as the hippocampus.

3.2 Results

3.2.1 Navigation performance

Subjects were scored by their proportion of correct trials. Trials were considered "correct" if the participant ended at the target object, regardless of whether they pressed the "selection" button or whether they ran out of time when just reaching the target. Proportion correct scores range from 2.08% - 100.00% (see Figure 3.3). Detailed behavioral analysis is done elsewhere (see Lawson et al., *in prep*).

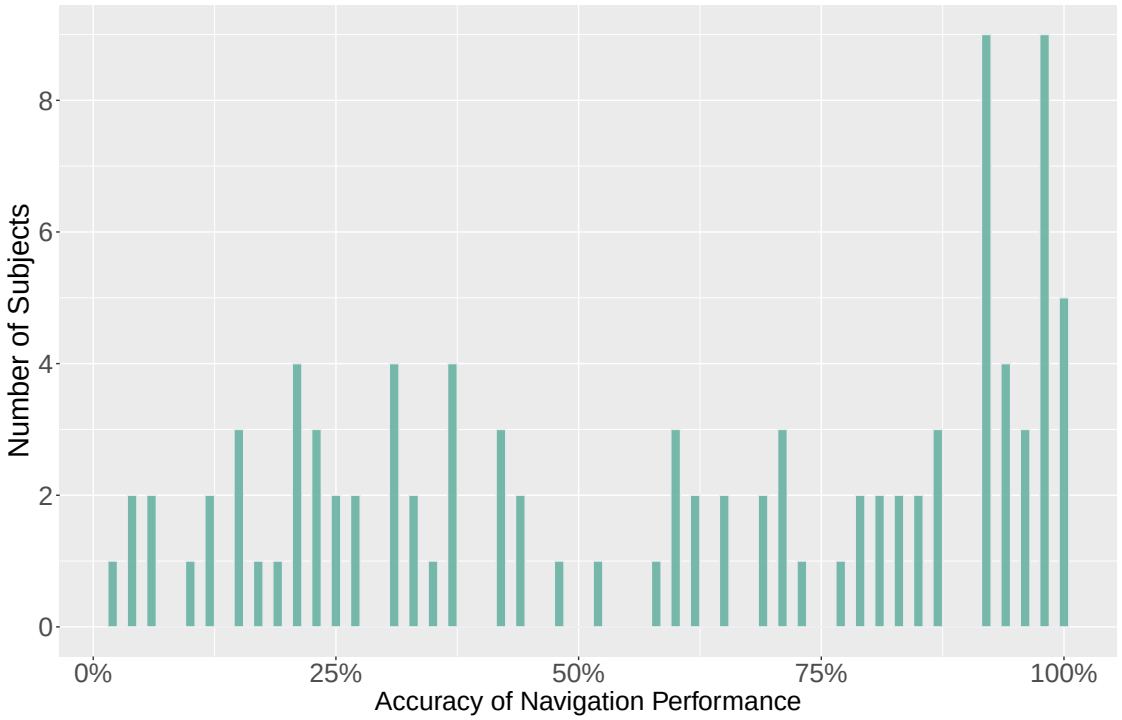

Figure 3.3: Histogram of the accuracy of navigation performance for all subjects (N = 98). Bin size was set to 1%.

For a result summary of all fMRI analyses (details below), please see Figure 3.24.

3.2.2 The present cognitive map: allocentric stationary facing directions

To test the hypothesis that allocentric stationary facing directions (i.e., north, south, east, and west) could be discriminated from signals in distributed brain areas, I conducted pattern classifications in beta series signals for each participant, separated by regions of interest (ROIs) and navigation phases (i.e., exploration and testing).

During the exploration phase, I successfully decoded allocentric facing directions from thalamus, retrosplenial cortex, precuneus, hippocampus, caudate, putamen, and pallidum (all $pFDRs < 0.05$), with marginally significantly better than chance classification performance in nucleus accumbens and auditory cortex (all $pFDRs < 0.08$) (see multivariate pattern analysis in Methods; Fig. 3.4a; Table 3.1). However, I could not successfully discriminate stationary facing directions from the extrastriate cortex, early visual cortex, or amygdala. All the results mentioned above were using empirical baseline based on random permutation, while discrimination scores for all ROIs compared with theoretical baselines were significant (all $pFDRs < 0.001$). I then conducted correlation analyses between classification accuracy and navigation performance. However, I did not observe correlation within any ROI, suggesting no individual differences in ROIs for discriminating stationary facing directions when learning the environment (all $pFDRs > 0.05$) (Figure 3.4c).

During the test phase, I could successfully discriminate between stationary facing directions in the early visual cortex ($pFDR < 0.001$) (Figure 3.4b; Table 3.2), but not in thalamus, retrosplenial cortex, precuneus, hippocampus, extrastriate cortex, caudate, putamen, pallidum, amygdala, nucleus accumbens, or auditory cortex (all $pFDRs > 0.05$). Discrimination scores for all ROIs compared with theoretical baselines were significant (all $pFDRs < 0.001$). I then conducted correlation analyses between classification accuracy and navigation performance. Interestingly, I found significant negative correlation between the classification accuracy in most ROIs and navigation performance (all $pFDRs < 0.05$) except marginally significant for

extrastriate cortex ($pFDR = 0.067$), suggesting higher classification accuracy for stationary facing directions were related to worse navigation performance during the test phase (Figure 3.4d).

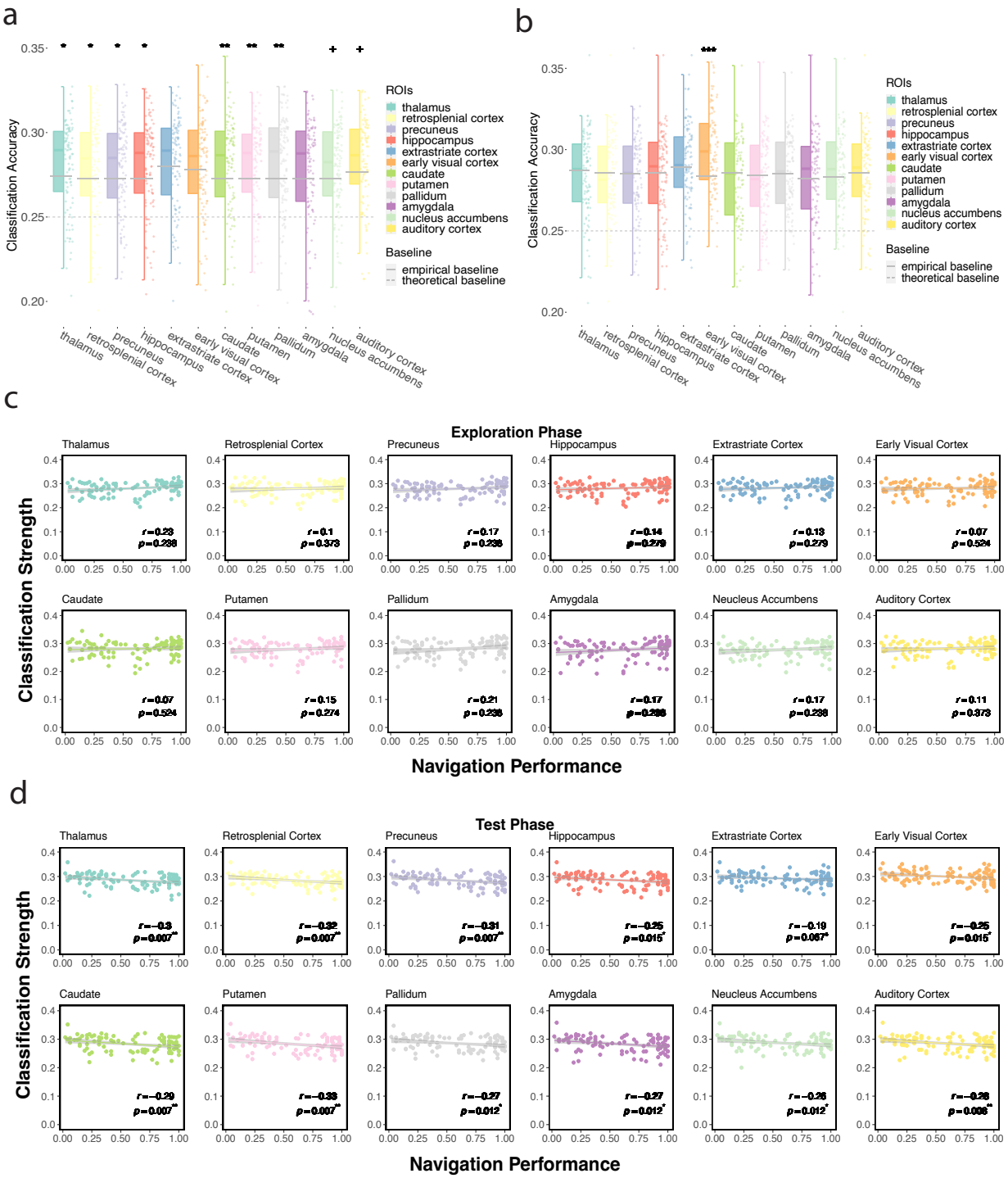

Figure 3.4: Classification accuracy for allocentric stationary facing directions. a. Model performance for all participants in all ROIs during the exploration phase. I plot single-participant data and group-level whiskerboxplots (center, median; box, 25th to 75th percentiles; whiskers, n = 98 participants). I observed significant classification model performance from signals in thalamus, retrosplenial cortex, precuneus, hippocampus, caudate, putamen, pallidum using empirical baseline (gray solid line). Significant classification of allocentric stationary directions was observed in all ROIs using theoretical baseline (gray dashed line, significance not labeled in the figure) b. similar to a., I plot model performance for all participants in all ROIs during the test phase. I observed significant classification model performance from signals in the early visual cortex using empirical baseline. Significant classification of allocentric stationary directions was observed in all ROIs using theoretical baseline (significance not labeled in the figure). c. Correlation between classification accuracy and navigation performance for data from all participants in all ROIs during the exploration phase. Significant classification of allocentric stationary directions in the exploration phase was not related to navigation performance. d. Correlation between classification accuracy and navigation performance for data from all participants in all ROIs during the test phase. Significant classification of allocentric stationary directions in the test phase in most ROIs (marginally significant for extrastriate cortex) depends on navigation performance. Note: + p < 0.08, * p < 0.05, ** p < 0.01, *** p < 0.001, FDR-corrected.

ROIs	*df*	*t*	*p*	*pFDR*	*Cohen's d*	*C.I.*
Thalamus	97	2.65	0.009^{**}	0.023^{*}	0.267	[0.276, 0.286]
Retrosplenial Cortex	97	2.23	0.028^{*}	0.049^{*}	0.225	[0.274, 0.285]
Precuneus	97	2.35	0.021^{*}	0.041^{*}	0.238	[0.274, 0.285]
Hippocampus	97	3.17	0.002^{**}	0.01^{*}	0.321	[0.276, 0.287]
Extrastriate Cortex	97	1.2	0.234	0.255	0.121	[0.278, 0.288]
Early Visual Cortex	97	0.88	0.383	0.383	0.089	[0.275, 0.286]
Caudate	97	3.04	0.003^{**}	0.01^{*}	0.307	[0.276, 0.287]
Putamen	97	3.01	0.003^{**}	0.01^{*}	0.304	[0.275, 0.286]
Pallidum	97	3.02	0.003^{**}	0.01^{*}	0.305	[0.276, 0.287]
Amygdala	97	1.63	0.107	0.128	0.165	[0.271, 0.284]
Nucleus Accumbens	97	2.06	0.042^{*}	0.062^{+}	0.208	[0.273, 0.284]
Auditory Cortex	97	2.02	0.046^{*}	0.062^{+}	0.204	[0.277, 0.287]

Notes: ** $p < 0.01$, * $p < 0.05$; * $pFDR < 0.05$, + $pFDR < 0.08$

Table 3.1: The present cognitive map: model performance on allocentric facing directions in the exploration phase

ROIs	df	t	p	$pFDR$	$Cohen's\, d$	$C.I.$
Thalamus	97	-1.26	0.209	0.618	-0.128	[0.279, 0.289]
Retrosplenial Cortex	97	-1.02	0.312	0.618	-0.103	[0.278, 0.288]
Precuneus	97	-0.91	0.363	0.618	-0.092	[0.278, 0.288]
Hippocampus	97	-0.49	0.623	0.831	-0.05	[0.279, 0.29]
Extrastriate Cortex	97	0.94	0.347	0.618	0.095	[0.287, 0.296]
Early Visual Cortex	97	6.33	$< 0.001^{***}$	$< 0.001^{***}$	0.639	[0.295, 0.305]
Caudate	97	-1.19	0.236	0.618	-0.12	[0.277, 0.288]
Putamen	97	-0.82	0.412	0.618	-0.083	[0.277, 0.287]
Pallidum	97	-0.15	0.881	0.919	-0.015	[0.28, 0.29]
Amygdala	97	0.1	0.919	0.919	0.01	[0.277, 0.288]
Nucleus Accumbens	97	1.2	0.233	0.618	0.121	[0.281, 0.291]
Auditory Cortex	97	-0.38	0.702	0.842	-0.039	[0.28, 0.29]

Notes: *** $p < 0.001$; *** $pFDR < 0.001$

Table 3.2: The present cognitive map: model performance on allocentric facing directions in the test phase

3.2.3 The present cognitive map: allocentric translations

To test the hypothesis that allocentric translations (i.e., north, south, east, and west) could be discriminated from signals in distributed brain areas, I conducted pattern classifications in beta series signals for each participant, separated by regions of interest (ROIs) and navigation phases (i.e., exploration and testing).

During the exploration phase, I successfully decoded allocentric translations from all ROIs (all $pFDRs < 0.001$) (Fig. 3.5a, Table 3.3). Same results were observed using the theoretical baseline. I then conducted correlation analyses between classification accuracy and navigation performance. However, I did not observe significant correlation between classification accuracy of any ROI and navigation performance, suggesting no individual differences observed in brain signals for translations when learning the environment (all $pFDRs > 0.05$) (Fig. 3.5c).

During the test phase, I could also successfully discriminate between translations in all ROIs (all $pFDRs < 0.001$) (Fig. 3.5b, Table 3.4). Same results were observed using the theoretical baseline. I then conducted correlation analyses between classification accuracy and navigation performance. However, I did not observe significant correlation between classification accuracy of any ROI and navigation performance, suggesting no individual differences observed in brain signals for translations when tested with navigation in the environment (all $pFDRs > 0.05$) (Fig. 3.5d).

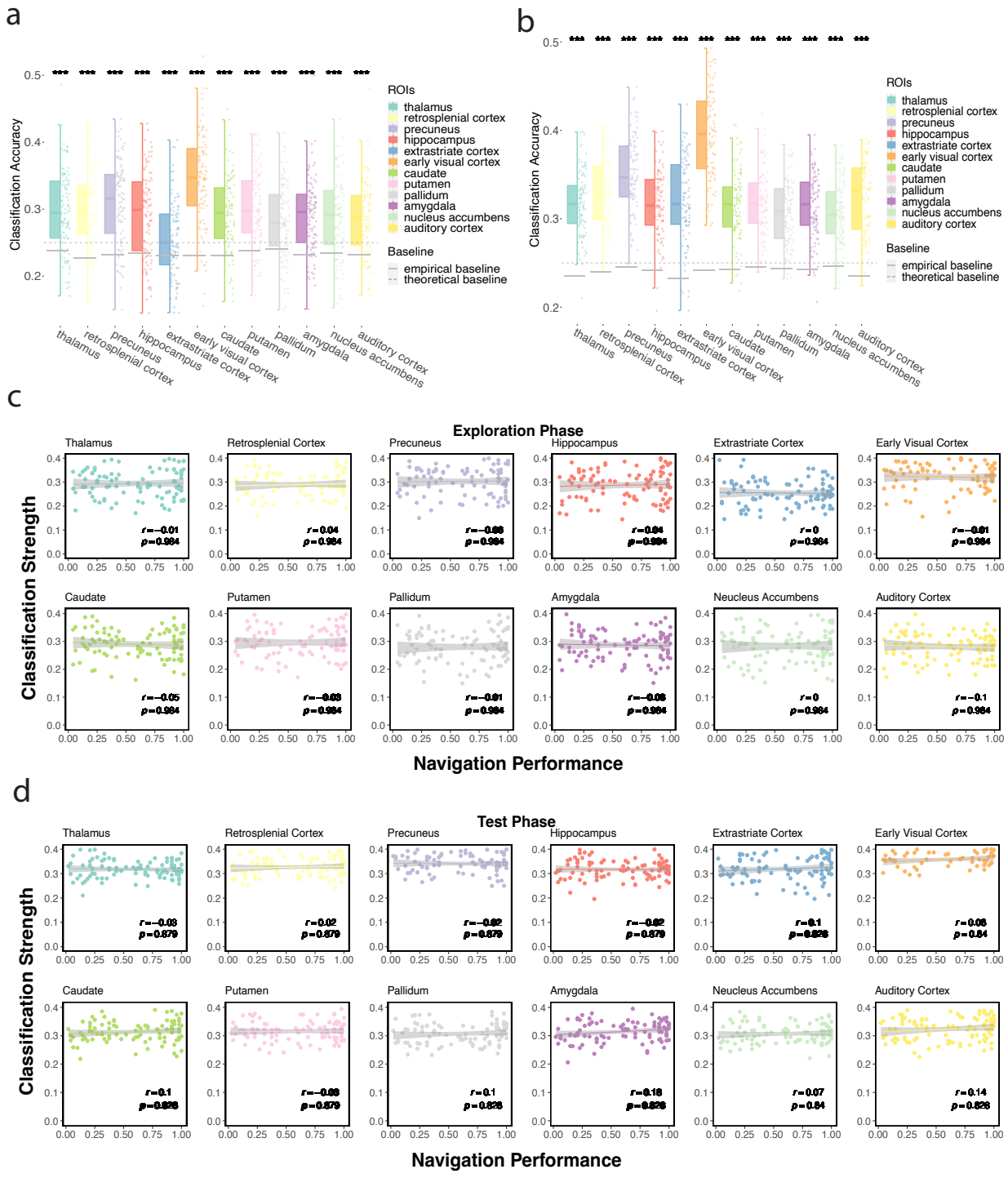
a
b
Classification Accuracy
ROIs
thalamus
retrosplenial cortex
precuneus
hippocampus
extrastriate cortex
early visual cortex
caudate
putamen
pallidum
amygdala
nucleus accumbens
auditory cortex
Baseline
empirical baseline
theoretical baseline
c
Exploration Phase
Classification Strength
Navigation Performance
Thalamus
Retrosplenial Cortex
Precuneus
Hippocampus
Extrastriate Cortex
Early Visual Cortex
Caudate
Putamen
Pallidum
Amygdala
Neucleus Accumbens
Auditory Cortex
d
Test Phase
Classification Strength
Navigation Performance

Figure 3.5: Classification accuracy for allocentric translations. a. Model performance for all participants in all ROIs during the exploration phase. I plot single-participant data and group-level whiskerboxplots (center, median; box, 25th to 75th percentiles; whiskers, n=98 participants). I observed significant model classification performance from signals in all ROIs using empirical baseline (gray solid line). Significant model classification performance was also observed in signals from all ROIs using theoretical baseline (gray dashed line, significance not labeled in the figure) b. similar to a., I plot model performance for all participants in all ROIs during the test phase. I observed significant model classification performance from signals in all ROIs using empirical baseline. Significant model classification performance was also observed in signals from all ROIs using theoretical baseline (significance not labeled in the figure). c. Correlation between classification accuracy and navigation performance for all participants in all ROIs during the exploration phase. Classification accuracy in the exploration phase was not related to navigation performance. d. Correlation between classification accuracy and navigation performance for all participants in all ROIs during the test phase. Classification accuracy in the test phase was not related to navigation performance. Note: *** p < 0.001, FDR-corrected.

ROIs	*df*	*t*	*p*	*pFDR*	*Cohen's d*	*C.I.*
Thalamus	97	9.58	$< 0.001^{***}$	$< 0.001^{***}$	0.967	[0.285, 0.31]
Retrosplenial Cortex	97	11.88	$< 0.001^{***}$	$< 0.001^{***}$	1.2	[0.289, 0.314]
Precuneus	97	12.31	$< 0.001^{***}$	$< 0.001^{***}$	1.244	[0.297, 0.322]
Hippocampus	97	8.59	$< 0.001^{***}$	$< 0.001^{***}$	0.867	[0.278, 0.304]
Extrastriate Cortex	97	4.39	$< 0.001^{***}$	$< 0.001^{***}$	0.443	[0.245, 0.267]
Early Visual Cortex	97	16.11	$< 0.001^{***}$	$< 0.001^{***}$	1.627	[0.331, 0.359]
Caudate	97	11.36	$< 0.001^{***}$	$< 0.001^{***}$	1.148	[0.283, 0.305]
Putamen	97	10.83	$< 0.001^{***}$	$< 0.001^{***}$	1.094	[0.291, 0.315]
Pallidum	97	7.37	$< 0.001^{***}$	$< 0.001^{***}$	0.744	[0.271, 0.293]
Amygdala	97	10.49	$< 0.001^{***}$	$< 0.001^{***}$	1.06	[0.279, 0.301]
Nucleus Accumbens	97	8.64	$< 0.001^{***}$	$< 0.001^{***}$	0.873	[0.274, 0.298]
Auditory Cortex	97	9.71	$< 0.001^{***}$	$< 0.001^{***}$	0.981	[0.274, 0.295]

Notes: *** $p < 0.001$; *** $pFDR < 0.001$

Table 3.3: The present cognitive map: model performance on allocentric translations in the exploration phase

ROIs	df	t	p	$pFDR$	$Cohen's\, d$	$C.I.$
Thalamus	97	22.84	$< 0.001^{***}$	$< 0.001^{***}$	2.307	[0.31, 0.325]
Retrosplenial Cortex	97	22.8	$< 0.001^{***}$	$< 0.001^{***}$	2.304	[0.321, 0.336]
Precuneus	97	23.79	$< 0.001^{***}$	$< 0.001^{***}$	2.404	[0.341, 0.358]
Hippocampus	97	19.8	$< 0.001^{***}$	$< 0.001^{***}$	2	[0.309, 0.324]
Extrastriate Cortex	97	17.99	$< 0.001^{***}$	$< 0.001^{***}$	1.817	[0.311, 0.33]
Early Visual Cortex	97	30.64	$< 0.001^{***}$	$< 0.001^{***}$	3.095	[0.386, 0.406]
Caudate	97	19.04	$< 0.001^{***}$	$< 0.001^{***}$	1.923	[0.308, 0.323]
Putamen	97	19.65	$< 0.001^{***}$	$< 0.001^{***}$	1.985	[0.31, 0.325]
Pallidum	97	17.97	$< 0.001^{***}$	$< 0.001^{***}$	1.816	[0.3, 0.314]
Amygdala	97	19.97	$< 0.001^{***}$	$< 0.001^{***}$	2.017	[0.307, 0.322]
Nucleus Accumbens	97	18.09	$< 0.001^{***}$	$< 0.001^{***}$	1.827	[0.3, 0.314]
Auditory Cortex	97	21.45	$< 0.001^{***}$	$< 0.001^{***}$	2.167	[0.315, 0.332]

Notes: $^{***}\, p < 0.001$; $^{***}\, pFDR < 0.001$

Table 3.4: The present cognitive map: model performance on allocentric translations in the test phase

3.2.4 The present cognitive map: allocentric rotations

To test the hypothesis that allocentric rotations (i.e., from north to east, east to south, south to west, west to north, north to west, west to south, south to east, and east to north) could be discriminated from signals in distributed brain areas, I conducted pattern classifications in beta series signals for each participant, separated by regions of interest (ROIs) and navigation phases (i.e., exploration and testing).

In the exploration phase, I could not discriminate directions from any ROIs (all $pFDRs > 0.05$) (Fig. 3.6a, Table 3.5). Discrimination scores for all ROIs compared with theoretical baselines were significant (all $pFDRs < 0.001$). I then conducted correlation analyses between classification accuracy and navigation performance. However, I did not observe significant correlation between classification accuracy of allocentric rotations in any ROI and navigation performance, suggesting no individual differences observed in brain signals for translations when learning the environment (all $pFDRs > 0.05$) (Fig. 3.6c).

In the test phase, I could successfully discriminate directions from all ROIs (all $pFDRs < 0.01$) (Fig. 3.6b, Table 3.6). Discrimination scores for all ROIs compared with theoretical baselines were also significant (all $pFDRs < 0.001$). I then conducted correlation analyses between classification accuracy and navigation performance. I only observed negative correlation between navigation performance and classification accuracy in extrastriate cortex ($pFDR = 0.036$), suggesting higher classification accuracy in extrastriate relates to worse navigation (Fig. 3.6d).

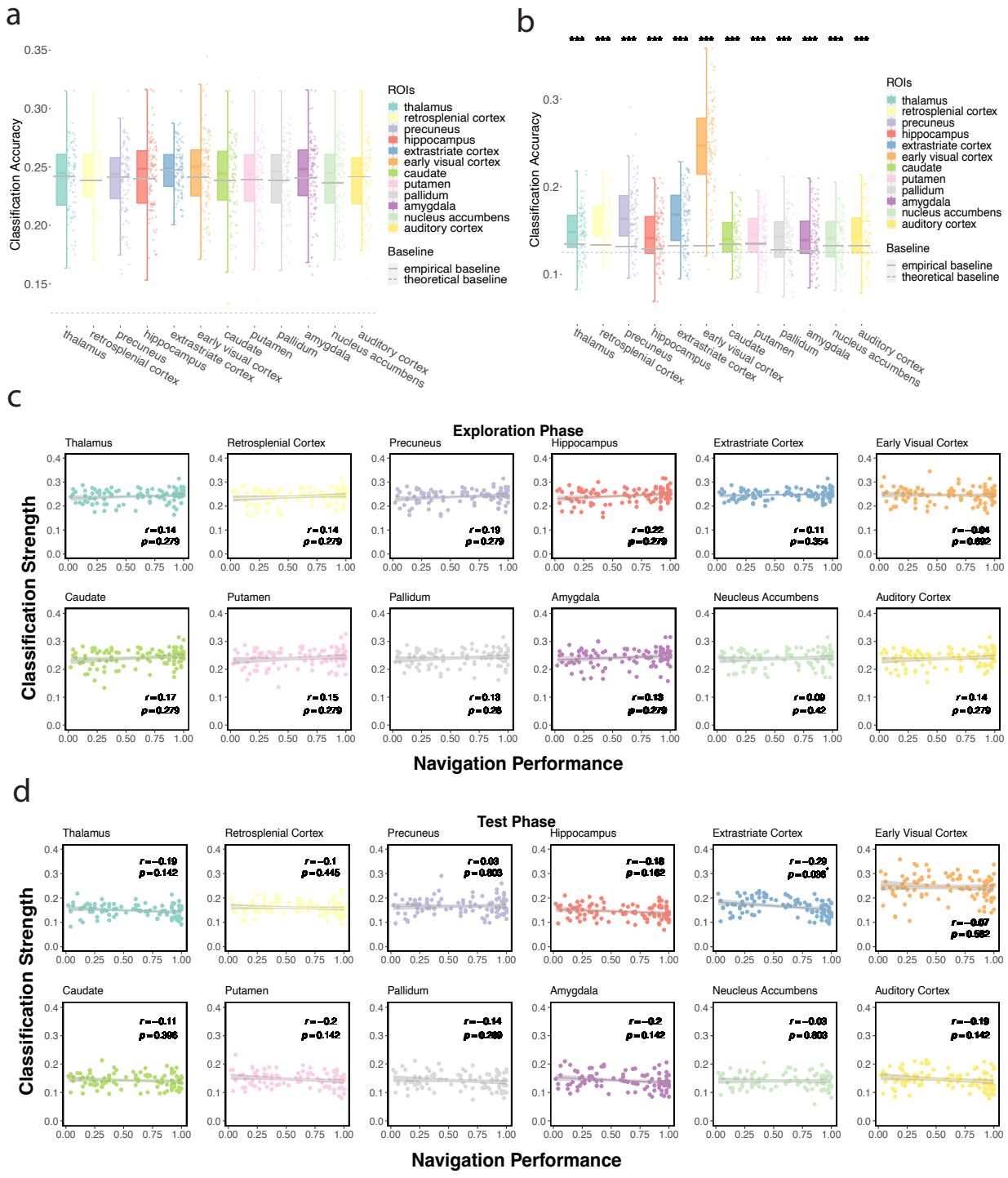
a
b
c
d
Classification Accuracy
ROIs
thalamus
retrosplenial cortex
precuneus
hippocampus
extrastriate cortex
early visual cortex
caudate
putamen
pallidum
amygdala
nucleus accumbens
auditory cortex
Baseline
empirical baseline
theoretical baseline
Exploration Phase
Test Phase
Classification Strength
Navigation Performance
Thalamus
Retrosplenial Cortex
Precuneus
Hippocampus
Extrastriate Cortex
Early Visual Cortex
Caudate
Putamen
Pallidum
Amygdala
Neucleus Accumbens
Auditory Cortex

Figure 3.6: Classification accuracy for allocentric rotations. a. Model performance for all participants in all ROIs during the exploration phase. I plot single-participant data and group-level whiskerboxplots (center, median; box, 25th to 75th percentiles; whiskers, n=98 participants). I did not observed classification accuracy in any ROI using empirical baseline (gray solid line). Classification accuracy was observed in all ROIs using theoretical baseline (gray dashed line, significance not labeled in the figure) b. similar to a., I plot model performance for all participants in all ROIs during the test phase. I observed classification accuracy in all ROIs using empirical baseline. Classification accuracy was also observed in all ROIs using a theoretical baseline (significance not labeled in the figure). c. Correlation between classification accuracy strength and navigation performance for all participants in all ROIs during the exploration phase. Classification accuracy in the exploration phase was not related to navigation performance. d. Correlation between classification accuracy strength and navigation performance for all participants in all ROIs during the test phase. Classification accuracy in the test phase was negatively correlated to navigation performance in extrastriate cortex. Note: * $p < 0.05$, *** $p < 0.001$, FDR-corrected.

ROIs	*df*	*t*	*p*	*pFDR*	*Cohen's d*	*C.I.*
Thalamus	97	-0.37	0.709	0.902	-0.038	[0.235, 0.246]
Retrosplenial Cortex	97	0.32	0.752	0.902	0.032	[0.233, 0.246]
Precuneus	97	-0.57	0.569	0.853	-0.058	[0.233, 0.245]
Hippocampus	97	0.92	0.358	0.853	0.093	[0.237, 0.249]
Extrastriate Cortex	97	0.01	0.994	0.994	0.001	[0.243, 0.252]
Early Visual Cortex	97	1.43	0.157	0.853	0.144	[0.239, 0.252]
Caudate	97	0.66	0.509	0.853	0.067	[0.234, 0.247]
Putamen	97	0.09	0.928	0.994	0.009	[0.233, 0.246]
Pallidum	97	0.86	0.391	0.853	0.087	[0.235, 0.247]
Amygdala	97	0.58	0.561	0.853	0.059	[0.236, 0.249]
Nucleus Accumbens	97	0.91	0.365	0.853	0.092	[0.233, 0.245]
Auditory Cortex	97	-0.85	0.396	0.853	-0.086	[0.233, 0.245]

Table 3.5: The present cognitive map: model performance on allocentric rotations in the exploration phase

ROIs	df	t	p	$pFDR$	$Cohen's\ d$	$C.I.$
Thalamus	97	5.02	$< 0.001^{***}$	$< 0.001^{***}$	0.507	[0.143, 0.153]
Retrosplenial Cortex	97	9.58	$< 0.001^{***}$	$< 0.001^{***}$	0.967	[0.154, 0.165]
Precuneus	97	9.61	$< 0.001^{***}$	$< 0.001^{***}$	0.97	[0.159, 0.173]
Hippocampus	97	4.95	$< 0.001^{***}$	$< 0.001^{***}$	0.5	[0.138, 0.15]
Extrastriate Cortex	97	9.06	$< 0.001^{***}$	$< 0.001^{***}$	0.915	[0.158, 0.172]
Early Visual Cortex	97	21.63	$< 0.001^{***}$	$< 0.001^{***}$	2.185	[0.235, 0.255]
Caudate	97	2.98	0.004^{**}	0.004^{**}	0.301	[0.137, 0.147]
Putamen	97	3.97	$< 0.001^{***}$	$< 0.001^{***}$	0.401	[0.14, 0.151]
Pallidum	97	4.63	$< 0.001^{***}$	$< 0.001^{***}$	0.468	[0.135, 0.147]
Amygdala	97	4.86	$< 0.001^{***}$	$< 0.001^{***}$	0.491	[0.136, 0.148]
Nucleus Accumbens	97	2.92	0.004^{**}	0.004^{**}	0.295	[0.135, 0.146]
Auditory Cortex	97	3.79	$< 0.001^{***}$	$< 0.001^{***}$	0.383	[0.139, 0.151]

Notes: *** $p < 0.001$, ** $p < 0.01$; *** $pFDR < 0.001$, ** $pFDR < 0.01$

Table 3.6: The present cognitive map: model performance on allocentric rotations in the test phase

To make sure the model discriminating between allocentric directions were not only just classify signals in an egocentric way (e.g., north to east instead of just turning right/clockwise), I conducted model classification on all clockwise and counterclockwise rotations, separately.

The present cognitive map: allocentric clockwise rotations

To test the hypothesis that allocentric clockwise rotations (i.e., from north to east, east to south, south to west, west to north) could be discriminated from signals in distributed brain areas, I conducted pattern classifications in beta series signals for each participant, separated by regions of interest (ROIs) and navigation phases (i.e., exploration and testing).

For the exploration phase, I could successfully classify between clockwise directions in all ROIs (all $pFDRs < 0.01$) (Figure 3.7a, Table 3.7). Analyses using theoretical baselines yield the same results. I then conducted correlation analyses between classification accuracy and navigation performance. I did not observe any correlations between allocentric current rotation classification accuracy in any ROI and navigation performance during the exploration phase (all $pFDRs > 0.05$) (Figure 3.7c).

For the test phase, I could successfully classify directions in all ROIs (all $pFDRs < 0.05$) (Figure 3.7b, Table 3.8). Analyses using theoretical baselines yield the same results. I then conducted correlation analyses between classification accuracy and navigation performance. I did not observe any correlations between allocentric current rotation classification accuracy in any ROI and navigation performance during the test phase (all $pFDRs > 0.05$) (Figure 3.7d).

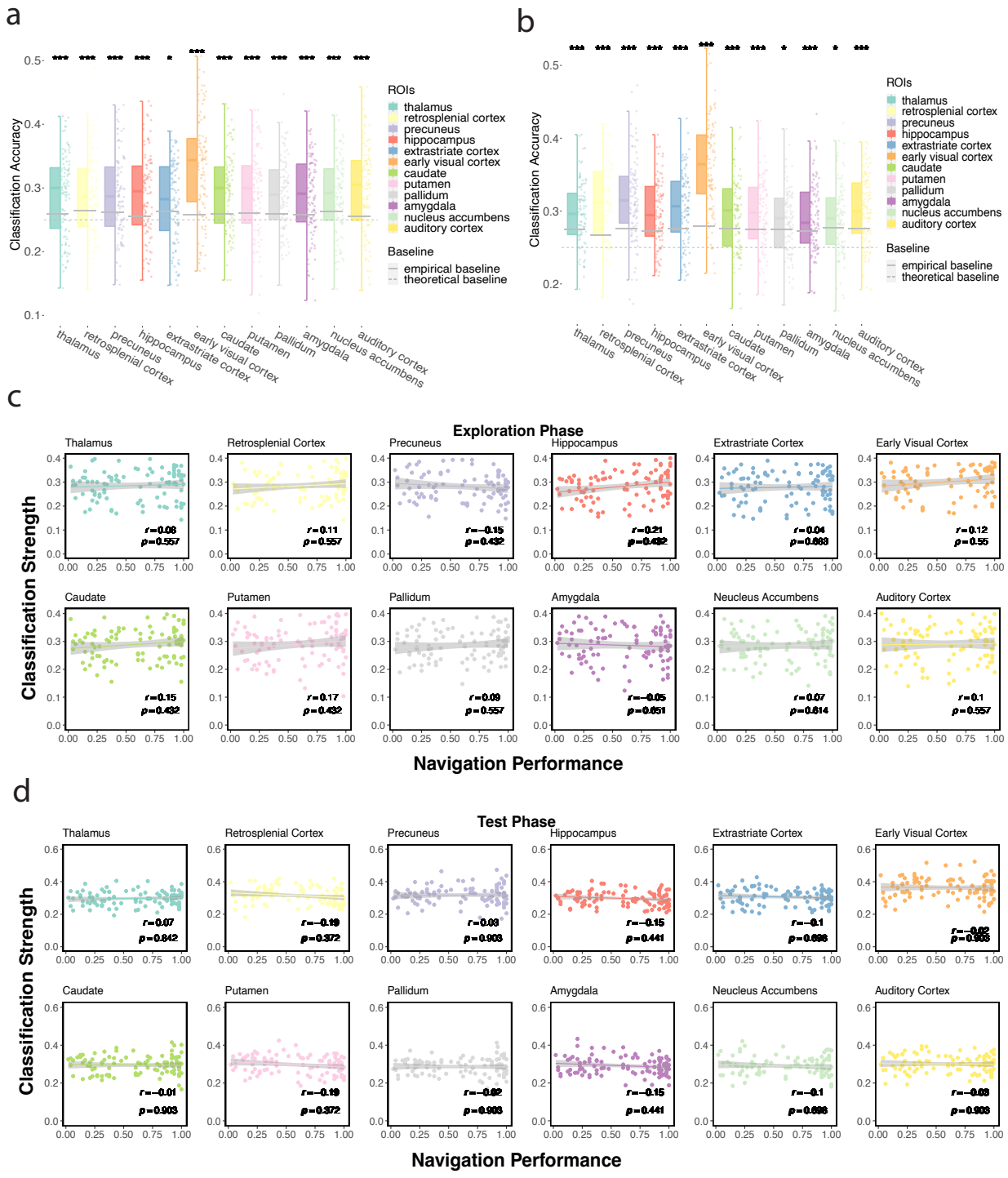
a
b
Classification Accuracy
ROIs
thalamus
retrosplenial cortex
precuneus
hippocampus
extrastriate cortex
early visual cortex
caudate
putamen
pallidum
amygdala
nucleus accumbens
auditory cortex
Baseline
empirical baseline
theoretical baseline
c
Exploration Phase
Classification Strength
Navigation Performance
Thalamus
Retrosplenial Cortex
Precuneus
Hippocampus
Extrastriate Cortex
Early Visual Cortex
Caudate
Putamen
Pallidum
Amygdala
Neucleus Accumbens
Auditory Cortex
r = 0.08
p = 0.557
r = 0.11
p = 0.557
r = −0.15
p = 0.432
r = 0.21
p = 0.432
r = 0.04
p = 0.683
r = 0.12
p = 0.55
r = 0.15
p = 0.432
r = 0.17
p = 0.432
r = 0.09
p = 0.557
r = −0.05
p = 0.651
r = 0.07
p = 0.614
r = 0.1
p = 0.557
d
Test Phase
Classification Strength
Navigation Performance
r = 0.07
p = 0.842
r = −0.19
p = 0.372
r = 0.03
p = 0.903
r = −0.15
p = 0.441
r = −0.1
p = 0.686
r = −0.02
p = 0.903
r = −0.01
p = 0.903
r = −0.19
p = 0.372
r = −0.02
p = 0.903
r = −0.15
p = 0.441
r = −0.1
p = 0.686
r = −0.03
p = 0.903

Figure 3.7: Classification accuracy for clockwise rotations. a. Model performance for all participants in all ROIs during the exploration phase. I plot single-participant data and group-level whiskerboxplots (center, median; box, 25th to 75th percentiles; whiskers, n=98 participants). Classification accuracy was observed in all ROIs using empirical baseline (gray solid line). Classification accuracy was observed in all ROIs using theoretical baseline (gray dashed line, significance not labeled in the figure) b. similar to a., I plot model performance for all participants in all ROIs during the test phase. I observed classification accuracy in all ROIs using empirical baseline. Classification accuracy was also observed in all ROIs using theoretical baseline (significance not labeled in the figure). c. Correlation between classification accuracy strength and navigation performance for all participants in all ROIs during the exploration phase. Classification accuracy in the exploration phase was not related to navigation performance. d. Correlation between classification accuracy strength and navigation performance for all participants in all ROIs during the test phase. Classification accuracy in the test phase was not related to navigation performance. Note: * $p < 0.05$, *** $p < 0.001$, FDR-corrected.

ROIs	*df*	*t*	*p*	*pFDR*	*Cohen's d*	*C.I.*
Thalamus	97	4.6	$< 0.001^{***}$	$< 0.001^{***}$	0.465	[0.277, 0.302]
Retrosplenial Cortex	97	4.06	$< 0.001^{***}$	$< 0.001^{***}$	0.41	[0.277, 0.302]
Precuneus	97	4.01	$< 0.001^{***}$	$< 0.001^{***}$	0.405	[0.275, 0.301]
Hippocampus	97	5.09	$< 0.001^{***}$	$< 0.001^{***}$	0.515	[0.276, 0.303]
Extrastriate Cortex	97	2.37	0.02^{*}	0.02^{*}	0.24	[0.266, 0.291]
Early Visual Cortex	97	9.11	$< 0.001^{***}$	$< 0.001^{***}$	0.92	[0.317, 0.349]
Caudate	97	5.58	$< 0.001^{***}$	$< 0.001^{***}$	0.564	[0.281, 0.306]
Putamen	97	4.95	$< 0.001^{***}$	$< 0.001^{***}$	0.5	[0.28, 0.307]
Pallidum	97	5.36	$< 0.001^{***}$	$< 0.001^{***}$	0.541	[0.278, 0.301]
Amygdala	97	4.72	$< 0.001^{***}$	$< 0.001^{***}$	0.477	[0.275, 0.3]
Nucleus Accumbens	97	4.13	$< 0.001^{***}$	$< 0.001^{***}$	0.417	[0.276, 0.3]
Auditory Cortex	97	6	$< 0.001^{***}$	$< 0.001^{***}$	0.606	[0.285, 0.313]

Notes: *** $p < 0.001$, * $p < 0.05$; *** $pFDR < 0.001$, * $pFDR < 0.05$

Table 3.7: The present cognitive map: model performance on allocentric clockwise rotations in the exploration phase

ROIs	df	t	p	$pFDR$	$Cohen's\ d$	$C.I.$
Thalamus	97	5.19	$< 0.001^{***}$	$< 0.001^{***}$	0.524	[0.289, 0.306]
Retrosplenial Cortex	97	9.02	$< 0.001^{***}$	$< 0.001^{***}$	0.911	[0.304, 0.324]
Precuneus	97	7.41	$< 0.001^{***}$	$< 0.001^{***}$	0.748	[0.306, 0.329]
Hippocampus	97	5.35	$< 0.001^{***}$	$< 0.001^{***}$	0.54	[0.288, 0.306]
Extrastriate Cortex	97	5.87	$< 0.001^{***}$	$< 0.001^{***}$	0.593	[0.296, 0.316]
Early Visual Cortex	97	13.04	$< 0.001^{***}$	$< 0.001^{***}$	1.317	[0.351, 0.376]
Caudate	97	3.9	$< 0.001^{***}$	$< 0.001^{***}$	0.394	[0.285, 0.305]
Putamen	97	4.44	$< 0.001^{***}$	$< 0.001^{***}$	0.448	[0.286, 0.305]
Pallidum	97	2.64	0.01^{*}	0.01^{*}	0.267	[0.278, 0.295]
Amygdala	97	3.91	$< 0.001^{***}$	$< 0.001^{***}$	0.395	[0.282, 0.301]
Nucleus Accumbens	97	2.51	0.014^{*}	0.014^{*}	0.253	[0.28, 0.3]
Auditory Cortex	97	5.26	$< 0.001^{***}$	$< 0.001^{***}$	0.531	[0.291, 0.31]

Notes: $^{***}\ p < 0.001$, $^{*}\ p < 0.05$; $^{***}\ pFDR < 0.001$, $^{*}\ pFDR < 0.05$

Table 3.8: The present cognitive map: model performance on allocentric clockwise rotations in the test phase

The present cognitive map: allocentric counterclockwise rotations

To test the hypothesis that allocentric clockwise rotations (i.e., north to west, west to south, south to east, and east to north) could be discriminated from signals in distributed brain areas, I conducted pattern classifications in beta series signals for each participant, separated by regions of interest (ROIs) and navigation phases (i.e., exploration and testing).

For the exploration phase, I could successfully discriminate counterclockwise directions in all ROIs (all $pFDRs < 0.001$) (Figure 3.8a, Table 3.9). Analyses using theoretical baselines yield the same results. I then conducted correlation analyses between classification accuracy and navigation performance. I did not observe correlation between allocentric current counterclockwise rotation classification accuracy in any ROI and navigation performance during the test phase (all $pFDRs > 0.05$) (Figure 3.8c).

For the test phase, I could successfully discriminate counterclockwise directions in most ROIs (all $pFDRs < 0.01$) except nucleus accumbens ($pFDR = 0.257$) (Figure 3.8b, Table 3.10). Analyses using theoretical baselines yield the same results (all $pFDRs < 0.001$) except also show significance for nucleus accumbens ($pFDR = 0.015$). I then conducted correlation analyses between classification accuracy and navigation performance. I did not observe correlation between allocentric current counterclockwise rotation classification accuracy in any ROI and navigation performance during the test phase (all $pFDRs > 0.05$) (Figure 3.8d).

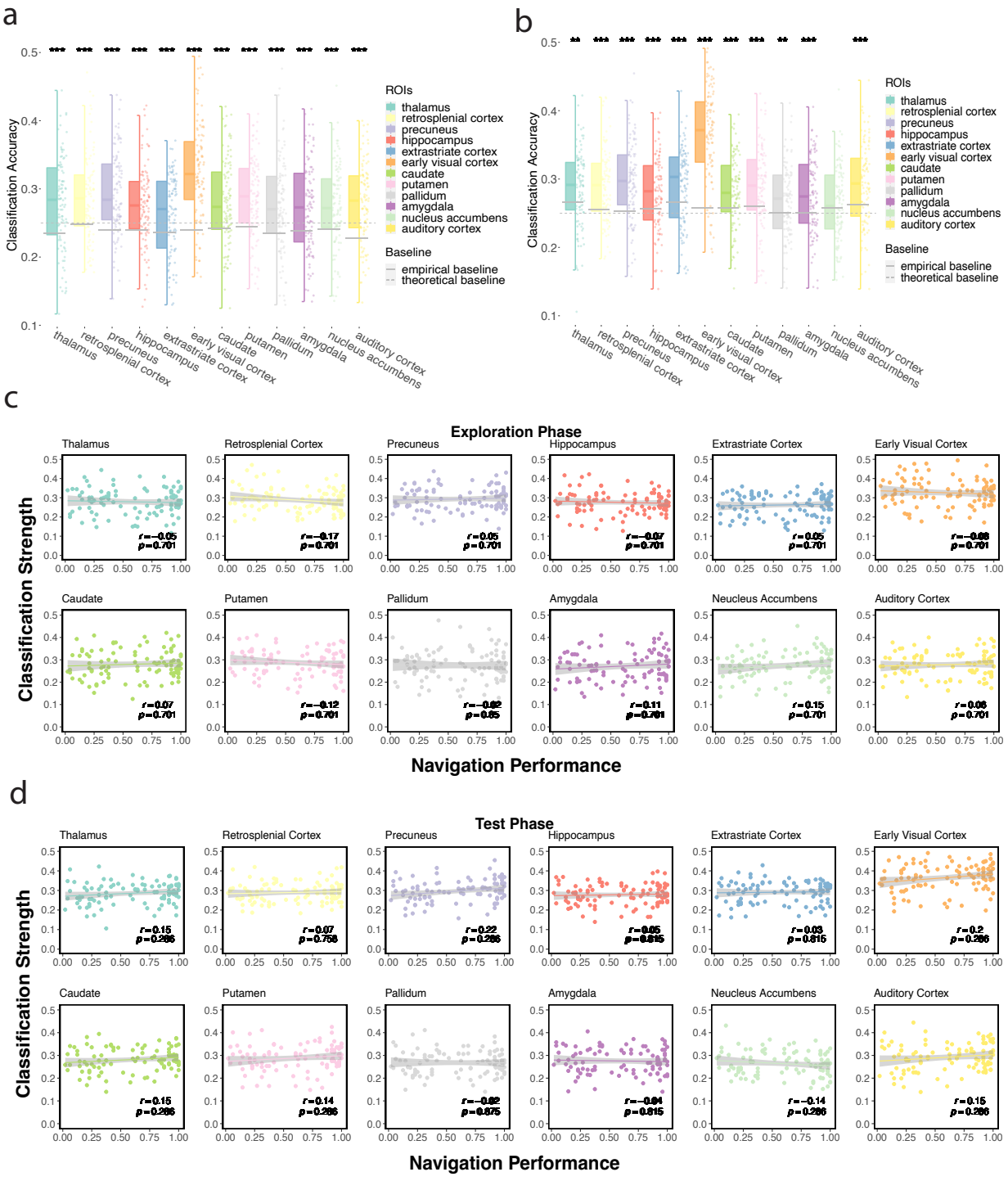
a
b
Classification Accuracy
ROIs
thalamus
retrosplenial cortex
precuneus
hippocampus
extrastriate cortex
early visual cortex
caudate
putamen
pallidum
amygdala
nucleus accumbens
auditory cortex
Baseline
empirical baseline
theoretical baseline
c
Exploration Phase
Classification Strength
Navigation Performance
Thalamus
Retrosplenial Cortex
Precuneus
Hippocampus
Extrastriate Cortex
Early Visual Cortex
Caudate
Putamen
Pallidum
Amygdala
Neucleus Accumbens
Auditory Cortex
d
Test Phase
Classification Strength
Navigation Performance

Figure 3.8: Classification accuracy for counterclockwise rotations. a. Model performance for all participants in all ROIs during the exploration phase. I plot single-participant data and group-level whiskerboxplots (center, median; box, 25th to 75th percentiles; whiskers, n=98 participants). Classification accuracy was observed in all ROIs using empirical baseline (gray solid line). Classification accuracy was observed in all ROIs using theoretical baseline (gray dashed line, significance not labeled in the figure) b. similar to a., I plot model performance for all participants in all ROIs during the test phase. I observed classification accuracy in most ROIs except nucleus accumbens using empirical baseline. Classification accuracy was also observed in all ROIs using a theoretical baseline (significance not labeled in the figure). c. Correlation between classification accuracy strength and navigation performance for all participants in all ROIs during the exploration phase. Classification accuracy in the exploration phase was not related to navigation performance. d. Correlation between classification accuracy strength and navigation performance for all participants in all ROIs during the test phase. Classification accuracy in the test phase was not related to navigation performance. Note: ** p < 0.01, *** p < 0.001, FDR-corrected.

ROIs	*df*	*t*	*p*	*pFDR*	*Cohen's d*	*C.I.*
Thalamus	97	6.29	$< 0.001^{***}$	$< 0.001^{***}$	0.636	[0.265, 0.292]
Retrosplenial Cortex	97	6.27	$< 0.001^{***}$	$< 0.001^{***}$	0.634	[0.275, 0.3]
Precuneus	97	8.82	$< 0.001^{***}$	$< 0.001^{***}$	0.891	[0.281, 0.306]
Hippocampus	97	6.23	$< 0.001^{***}$	$< 0.001^{***}$	0.629	[0.264, 0.287]
Extrastriate Cortex	97	4.4	$< 0.001^{***}$	$< 0.001^{***}$	0.445	[0.251, 0.274]
Early Visual Cortex	97	12.04	$< 0.001^{***}$	$< 0.001^{***}$	1.216	[0.311, 0.34]
Caudate	97	6.05	$< 0.001^{***}$	$< 0.001^{***}$	0.611	[0.268, 0.293]
Putamen	97	7.3	$< 0.001^{***}$	$< 0.001^{***}$	0.737	[0.276, 0.299]
Pallidum	97	5.88	$< 0.001^{***}$	$< 0.001^{***}$	0.594	[0.262, 0.289]
Amygdala	97	5.12	$< 0.001^{***}$	$< 0.001^{***}$	0.517	[0.259, 0.285]
Nucleus Accumbens	97	5.42	$< 0.001^{***}$	$< 0.001^{***}$	0.547	[0.262, 0.287]
Auditory Cortex	97	8.68	$< 0.001^{***}$	$< 0.001^{***}$	0.877	[0.267, 0.29]

Notes: *** $p < 0.001$; *** $pFDR < 0.001$

Table 3.9: The present cognitive map: model performance on allocentric counterclockwise rotations in the exploration phase

ROIs	*df*	*t*	*p*	*pFDR*	*Cohen's d*	*C.I.*
Thalamus	97	3.44	0.001^{**}	0.001^{**}	0.348	[0.275, 0.297]
Retrosplenial Cortex	97	6.54	$< 0.001^{***}$	$< 0.001^{***}$	0.661	[0.279, 0.3]
Precuneus	97	7.58	$< 0.001^{***}$	$< 0.001^{***}$	0.766	[0.285, 0.308]
Hippocampus	97	4.13	$< 0.001^{***}$	$< 0.001^{***}$	0.417	[0.268, 0.289]
Extrastriate Cortex	97	4.4	$< 0.001^{***}$	$< 0.001^{***}$	0.445	[0.28, 0.303]
Early Visual Cortex	97	15.15	$< 0.001^{***}$	$< 0.001^{***}$	1.531	[0.351, 0.379]
Caudate	97	4.61	$< 0.001^{***}$	$< 0.001^{***}$	0.466	[0.271, 0.292]
Putamen	97	4.74	$< 0.001^{***}$	$< 0.001^{***}$	0.478	[0.277, 0.3]
Pallidum	97	3.37	0.001^{**}	0.001^{**}	0.34	[0.258, 0.279]
Amygdala	97	4.54	$< 0.001^{***}$	$< 0.001^{***}$	0.459	[0.264, 0.287]
Nucleus Accumbens	97	1.14	0.257	0.257	0.115	[0.253, 0.274]
Auditory Cortex	97	4.78	$< 0.001^{***}$	$< 0.001^{***}$	0.483	[0.28, 0.304]

Notes: $^{***}\ p < 0.001$, $^{**}\ p < 0.01$; $^{***}\ pFDR < 0.001$, $^{**}\ pFDR < 0.01$

Table 3.10: The present cognitive map: model performance on allocentric counterclockwise rotations in the test phase

3.2.5 The present cognitive map: egocentric rotations

To test the hypothesis that egocentric rotations (i.e., left/counterclockwise and right/clockwise) could be discriminated from signals in distributed brain areas, I conducted pattern classifications in beta series signals for each participant, separated by regions of interest (ROIs) and navigation phases (i.e., exploration and testing).

During the exploration phase, I successfully decoded egocentric rotations from most ROIs (all $pFDRs < 0.05$) except marginally significant in thalamus ($pFDR = 0.051$) and not significant in auditory cortex ($pFDR = 0.087$) (Figure 3.9a, Table 3.11). Discrimination scores for all ROIs compared with theoretical baselines were significant (all $pFDRs < 0.01$). I then conducted correlation analyses between classification accuracy and navigation performance. However, I did not observe significant correlation between classification accuracy of egocentric rotations in any ROI and navigation performance, suggesting no individual differences observed in brain signals for egocentric rotations when learning the environment (all $pFDRs > 0.05$) (Fig. 3.9c).

During the test phase, I successfully decoded egocentric rotations from some ROIs: retrosplenial cortex, precuneus, hippocampus, extrastriate cortex, early visual cortex, putamen, amygdala, and auditory cortex (all $pFDRs < 0.05$). However, I could not discriminate between egocentric rotations from thalamus, caudate, pallidum, or nucleus accumbens (all $pFDRs > 0.05$) (Figure 3.9b, Table 3.12). Analyses using the theoretical baseline yield the same result except significant in pallidum ($pFDR = 0.018$) and marginally significant in thalamus, caudate, amygdala (all $pFDRs < 0.08$). I then conducted correlation analyses between classification accuracy and navigation performance. I observed negative correlation between navigation performance and classification accuracy in thalamus, retrosplenial cortex, hippocampus, extrastriate cortex, caudate, and auditory cortex (all $pFDRs < 0.05$), suggesting higher classification performance on brain signals from these brain regions were related to worse navigation performance (see Fig. 3.9d).

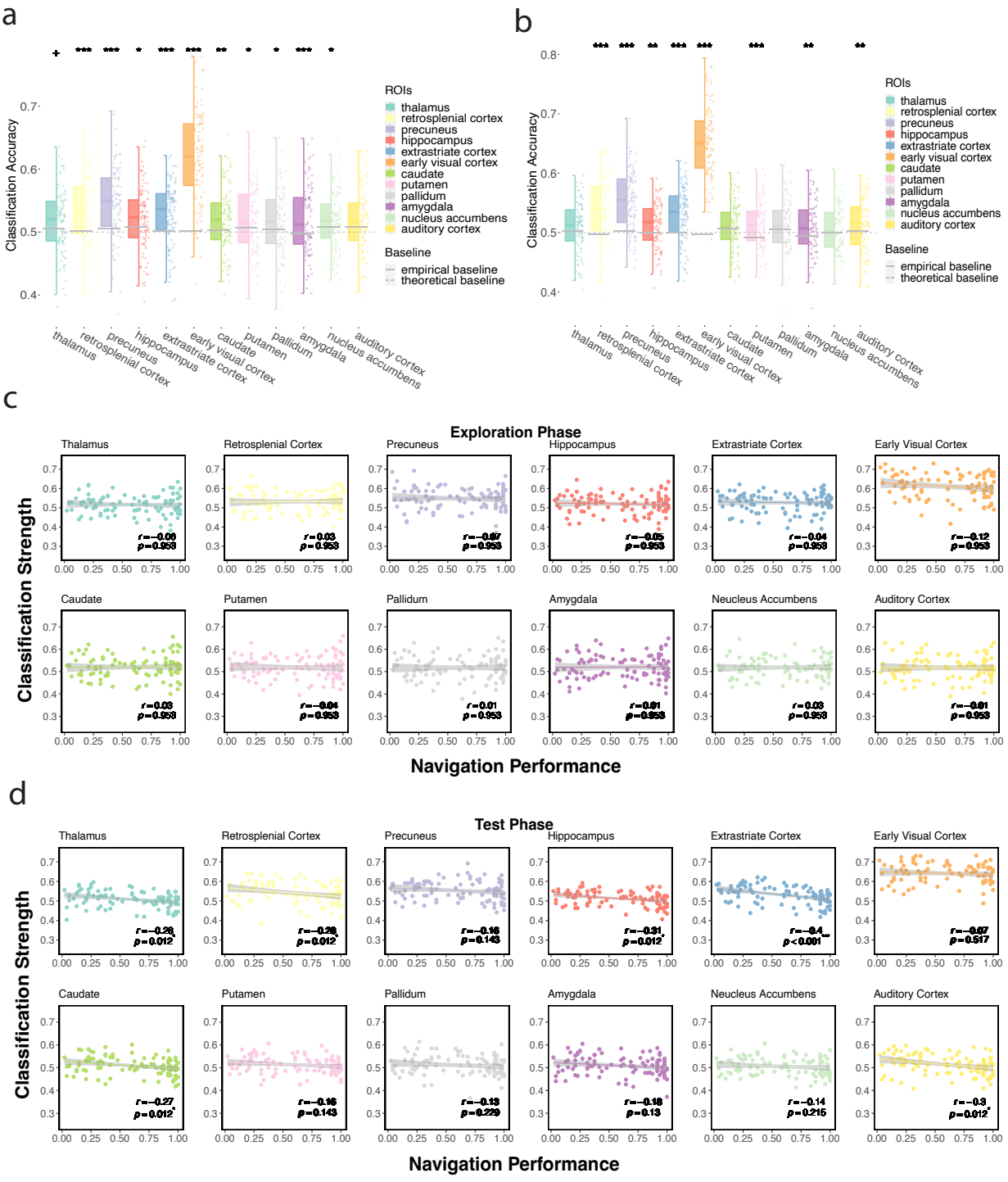
a
b
Classification Accuracy
ROIs
thalamus
retrosplenial cortex
precuneus
hippocampus
extrastriate cortex
early visual cortex
caudate
putamen
pallidum
amygdala
nucleus accumbens
auditory cortex
Baseline
empirical baseline
theoretical baseline
c
Exploration Phase
Classification Strength
Navigation Performance
Thalamus
Retrosplenial Cortex
Precuneus
Hippocampus
Extrastriate Cortex
Early Visual Cortex
Caudate
Putamen
Pallidum
Amygdala
Neucleus Accumbens
Auditory Cortex
d
Test Phase
Classification Strength
Navigation Performance

Figure 3.9: Classification accuracy for egocentric rotations. a. Model performance for all participants in all ROIs during the exploration phase. I plot single-participant data and group-level whiskerboxplots (center, median; box, 25th to 75th percentiles; whiskers, n=98 participants). I observed classification accuracy in retrosplenial cortex, precuneus, hippocampus, extrastriate cortex, early visual cortex, caudate, putamen, pallidum, amygdala, and nucleus accumbens using empirical baseline (gray solid line). Classification accuracy was also observed in all ROIs using theoretical baseline (gray dashed line, significance not labeled in the figure) b. similar to a., I plot model performance for all participants in all ROIs during the test phase. I observed classification accuracy in retrosplenial cortex, precuneus, hippocampus, extrastriate cortex, early visual cortex, putamen, amygdala, and auditory cortex using empirical baseline. Classification accuracy was also observed in all ROIs using theoretical baseline (significance not labeled in the figure). c. Correlation between classification accuracy strength and navigation performance for all participants in all ROIs during the exploration phase. Classification accuracy in the exploration phase was not related to navigation performance. d. Correlation between classification accuracy strength and navigation performance for all participants in all ROIs during the test phase. Classification accuracy in the test phase was negatively correlated to navigation performance in thalamus, retrosplenial cortex, hippocampus, extrastriate cortex, caudate, and auditory cortex. Note: + p $<$ 0.08, * p $<$ 0.05, ** p $<$ 0.01, *** p $<$ 0.001, FDR-corrected.

ROIs	*df*	*t*	*p*	*pFDR*	*Cohen's d*	*C.I.*
Thalamus	97	2.01	0.047^{*}	0.051^{+}	0.203	[0.506, 0.526]
Retrosplenial Cortex	97	5.74	$< 0.001^{***}$	$< 0.001^{***}$	0.58	[0.522, 0.543]
Precuneus	97	7.31	$< 0.001^{***}$	$< 0.001^{***}$	0.738	[0.536, 0.559]
Hippocampus	97	2.31	0.023^{*}	0.032^{*}	0.233	[0.51, 0.53]
Extrastriate Cortex	97	4.98	$< 0.001^{***}$	$< 0.001^{***}$	0.503	[0.517, 0.537]
Early Visual Cortex	97	16.17	$< 0.001^{***}$	$< 0.001^{***}$	1.633	[0.603, 0.632]
Caudate	97	3.21	0.002^{**}	0.004^{**}	0.324	[0.51, 0.53]
Putamen	97	2.16	0.033^{*}	0.039^{*}	0.219	[0.508, 0.529]
Pallidum	97	2.41	0.018^{*}	0.031^{*}	0.243	[0.507, 0.528]
Amygdala	97	4.11	$< 0.001^{***}$	$< 0.001^{***}$	0.415	[0.509, 0.531]
Nucleus Accumbens	97	2.3	0.024^{*}	0.032^{*}	0.232	[0.51, 0.527]
Auditory Cortex	97	1.73	0.087	0.087	0.175	[0.507, 0.528]

Notes: *** $p < 0.001$, ** $p < 0.01$, * $p < 0.05$; *** $pFDR < 0.001$, ** $pFDR < 0.01$, * $pFDR < 0.05$, + $pFDR < 0.08$

Table 3.11: The present cognitive map: model performance on egocentric rotations in the exploration phase

ROIs	df	t	p	$pFDR$	$Cohen's\, d$	$C.I.$
Thalamus	97	1.21	0.227	0.248	0.123	[0.5, 0.517]
Retrosplenial Cortex	97	8.02	$< 0.001^{***}$	$< 0.001^{***}$	0.81	[0.53, 0.551]
Precuneus	97	10.01	$< 0.001^{***}$	$< 0.001^{***}$	1.012	[0.543, 0.563]
Hippocampus	97	3.27	0.001^{**}	0.003^{**}	0.331	[0.505, 0.519]
Extrastriate Cortex	97	6.6	$< 0.001^{***}$	$< 0.001^{***}$	0.667	[0.522, 0.54]
Early Visual Cortex	97	24.88	$< 0.001^{***}$	$< 0.001^{***}$	2.513	[0.64, 0.665]
Caudate	97	0.4	0.687	0.687	0.041	[0.501, 0.516]
Putamen	97	5.77	$< 0.001^{***}$	$< 0.001^{***}$	0.583	[0.505, 0.52]
Pallidum	97	1.26	0.21	0.248	0.128	[0.502, 0.52]
Amygdala	97	3.41	0.001^{**}	0.002^{**}	0.345	[0.5, 0.517]
Nucleus Accumbens	97	1.36	0.177	0.237	0.137	[0.497, 0.513]
Auditory Cortex	97	2.51	0.014^{*}	0.021^{*}	0.253	[0.505, 0.523]

Notes: *** $p < 0.001$, ** $p < 0.01$, * $p < 0.05$; *** $pFDR < 0.001$, ** $pFDR < 0.01$, * $pFDR < 0.05$

Table 3.12: The present cognitive map: model performance on egocentric rotations in the test phase

3.2.6 The future cognitive map: allocentric movements

To test the hypothesis that allocentric future movements (i.e., turning from north to east, east to south, south to west, west to north, north to west, west to south, south to east, east to north, or moving straight toward north, south, east, or west) were represented in the brain when people were stationarily standing at an intersection planning for the next step, I conducted pattern classification analyses for allocentric future movements in beta series signals for each participant, separate by regions of interest (ROIs) and navigation phases (i.e., exploration and testing).

For the exploration phase, I could successfully discriminate allocentric future movements in most ROIs (all $pFDRs < 0.05$) except nucleus accumbens ($pFDR = 0.083$) and pallidum ($pFDR = 0.107$) (see Fig. 3.10a, Table 3.13). Analyses using theoretical baselines yield the same results except also showing significance in pallidum and nucleus accumbens (all $pFDRs < 0.001$). I then conducted correlation analyses between classification accuracy and navigation performance (see Fig. 3.10c). I did not observe correlation between egocentric past movement classification accuracy in any ROI and navigation performance during the exploration phase (all $pFDRs > 0.05$).

For the test phase, I could successfully discriminate allocentric future movements in most ROIs: thalamus, retrosplenial cortex, precuneus, hippocampus, extrastriate cortex, early visual cortex, caudate, pallidum, auditory cortex (all $pFDRs < 0.05$), but the classifications were marginally significant in putamen ($pFDR = 0.069$) and nucleus accumbens ($pFDR = 0.079$), and was not significant in amygdala ($pFDR = 0.164$) (see Fig. 3.10b, Table 3.14). Analyses using theoretical baselines yield the same results except also showing significance in putamen, nucleus accumbens, and amygdala (all $pFDRs < 0.001$). I then conducted correlation analyses between classification accuracy and navigation performance (see Fig. 3.10d). I observed negative correlations between allocentric future movement classification accuracy in most ROIs and navigation performance during the test phase (all $pFDRs < 0.05$)

except marginally significant in precuneus, extrastriate cortex, and caudate (all $pFDRs < 0.08$).

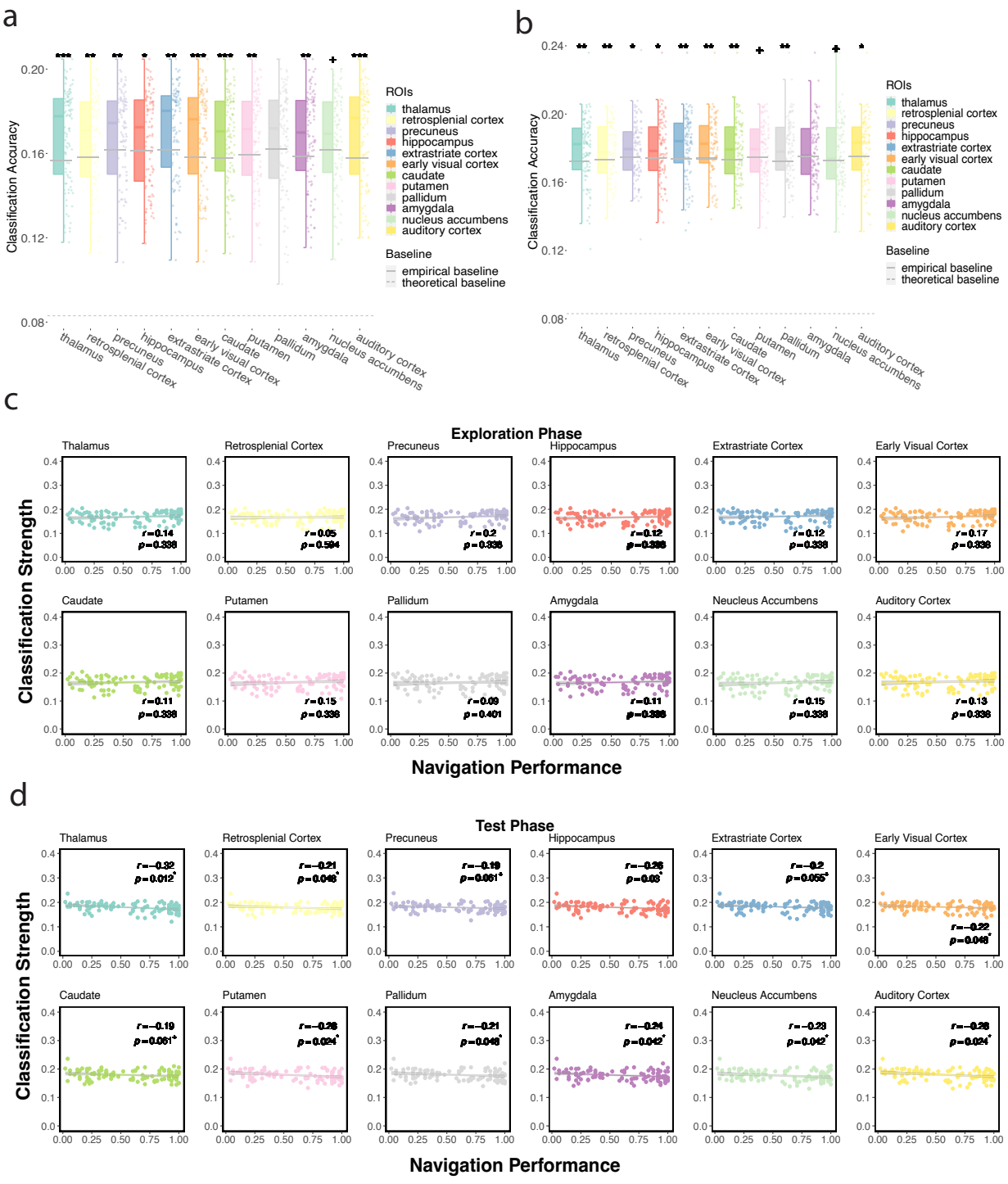

Figure 3.10: Classification accuracy for allocentric future movements. a. Model performance for all participants in all ROIs during the exploration phase. I plot single-participant data and group-level whiskerboxplots (center, median; box, 25th to 75th percentiles; whiskers, n=98 participants). I observed classification accuracy in most ROIs except pallidum (non-significant) and nucleus accumbens (marginally significant) using empirical baseline (gray solid line). Classification accuracy was also observed in all ROIs using theoretical baseline (gray dashed line, significance not labeled in the figure) b. similar to a., I plot model performance for all participants in all ROIs during the test phase. I observed significant classification accuracy in most ROIs except marginally significant in putamen, nucleus accumbens, and not significant amygdala. Classification accuracy was observed in all ROIs using theoretical baseline (gray dashed line, significance not labeled in the figure) c. Correlation between classification accuracy strength and navigation performance for all participants in all ROIs during the exploration phase. Classification accuracy in the exploration phase was not related to navigation performance. d. Correlation between classification accuracy strength and navigation performance for all participants in all ROIs during the test phase. I observed negative correlations between navigation performance and classification accuracy of performance on signals from most ROIs except marginally significant in precuneus, extrastriate cortex, and caudate. Note: + p < 0.08, * p < 0.05, ** p < 0.01, *** p < 0.001, FDR-corrected.

ROIs	*df*	*t*	*p*	*pFDR*	*Cohen's d*	*C.I.*
Thalamus	97	5.26	$< 0.001^{***}$	$< 0.001^{***}$	0.532	[0.164, 0.173]
Retrosplenial Cortex	97	3.69	$< 0.001^{***}$	0.001^{**}	0.373	[0.162, 0.171]
Precuneus	97	2.84	0.006^{**}	0.007^{**}	0.287	[0.164, 0.173]
Hippocampus	97	2.35	0.021^{*}	0.025^{*}	0.238	[0.162, 0.171]
Extrastriate Cortex	97	3.84	$< 0.001^{***}$	0.001^{**}	0.388	[0.166, 0.175]
Early Visual Cortex	97	4.47	$< 0.001^{***}$	$< 0.001^{***}$	0.451	[0.164, 0.173]
Caudate	97	4.26	$< 0.001^{***}$	$< 0.001^{***}$	0.43	[0.163, 0.172]
Putamen	97	3.26	0.002^{**}	0.002^{**}	0.329	[0.162, 0.172]
Pallidum	97	1.63	0.107	0.107	0.164	[0.161, 0.171]
Amygdala	97	3.77	$< 0.001^{***}$	0.001^{**}	0.381	[0.163, 0.172]
Nucleus Accumbens	97	1.79	0.076^{+}	0.083	0.181	[0.161, 0.171]
Auditory Cortex	97	4.81	$< 0.001^{***}$	$< 0.001^{***}$	0.485	[0.164, 0.174]

Notes: *** $p < 0.001$, ** $p < 0.01$, * $p < 0.05$; *** $pFDR < 0.001$, ** $pFDR < 0.01$, * $pFDR < 0.05$

Table 3.13: Future cognitive map: model performance on allocentric directions in the exploration phase

ROIs	df	t	p	$pFDR$	$Cohen's\, d$	$C.I.$
Thalamus	97	3.64	$< 0.001^{***}$	0.001^{**}	0.367	[0.175, 0.183]
Retrosplenial Cortex	97	2.72	0.008^{**}	0.016^{*}	0.274	[0.175, 0.182]
Precuneus	97	2.58	0.011^{*}	0.02^{*}	0.261	[0.176, 0.182]
Hippocampus	97	2.46	0.015^{*}	0.023^{*}	0.249	[0.175, 0.182]
Extrastriate Cortex	97	4.17	$< 0.001^{***}$	0.001^{**}	0.422	[0.178, 0.185]
Early Visual Cortex	97	3.95	$< 0.001^{***}$	0.001^{**}	0.399	[0.177, 0.184]
Caudate	97	2.97	0.004^{**}	0.009^{**}	0.3	[0.175, 0.182]
Putamen	97	1.92	0.057^{+}	0.069^{+}	0.194	[0.175, 0.182]
Pallidum	97	3.87	$< 0.001^{***}$	0.001^{**}	0.391	[0.176, 0.183]
Amygdala	97	1.4	0.164	0.164	0.142	[0.174, 0.181]
Nucleus Accumbens	97	1.82	0.072^{+}	0.079^{+}	0.184	[0.173, 0.18]
Auditory Cortex	97	2.21	0.029^{*}	0.039^{*}	0.223	[0.176, 0.183]

Notes: *** $p < 0.001$, ** $p < 0.01$, * $p < 0.05$, + $p < 0.08$; ** $pFDR < 0.01$, * $pFDR < 0.05$, + $pFDR < 0.08$

Table 3.14: Future cognitive map: model performance on allocentric directions in the test phase

The future cognitive map: allocentric translations

To test the hypothesis that allocentric future translations (i.e., north, south, east, and west) could be discriminated from signals in distributed brain areas, I conducted pattern classifications in beta series signals for each participant, separated by regions of interest (ROIs) and navigation phases (i.e., exploration and testing).

For the exploration phase, I could not discriminate between directions in any ROI (all $pFDRs > 0.05$) (See Fig. 3.11a, Table 3.15). Analyses using theoretical baselines yield the same results except show significance in extrastriate cortex ($pFDR < 0.001$) and early visual cortex ($pFDR = 0.031$). I then conducted correlation analyses between classification accuracy and navigation performance (see Fig. 3.11c). I did not observe any correlations during the exploration phase between allocentric future translations classification accuracy in any ROI and navigation performance (all rest $pFDRs > 0.05$).

For the test phase, I could discriminate between directions in most ROIs (all $pFDRs < 0.05$) except auditory cortex ($pFDR = 0.593$)(See Fig. 3.11b, Table 3.16). Discrimination scores for all ROIs compared with theoretical baselines were significant in all ROIs ($pFDR < 0.001$). I then conducted correlation analyses between classification accuracy and navigation performance (see Fig. 3.11d). I did not observe correlation between allocentric future translations classification accuracy in any ROI and navigation performance during the test phase (all rest $pFDRs > 0.05$).

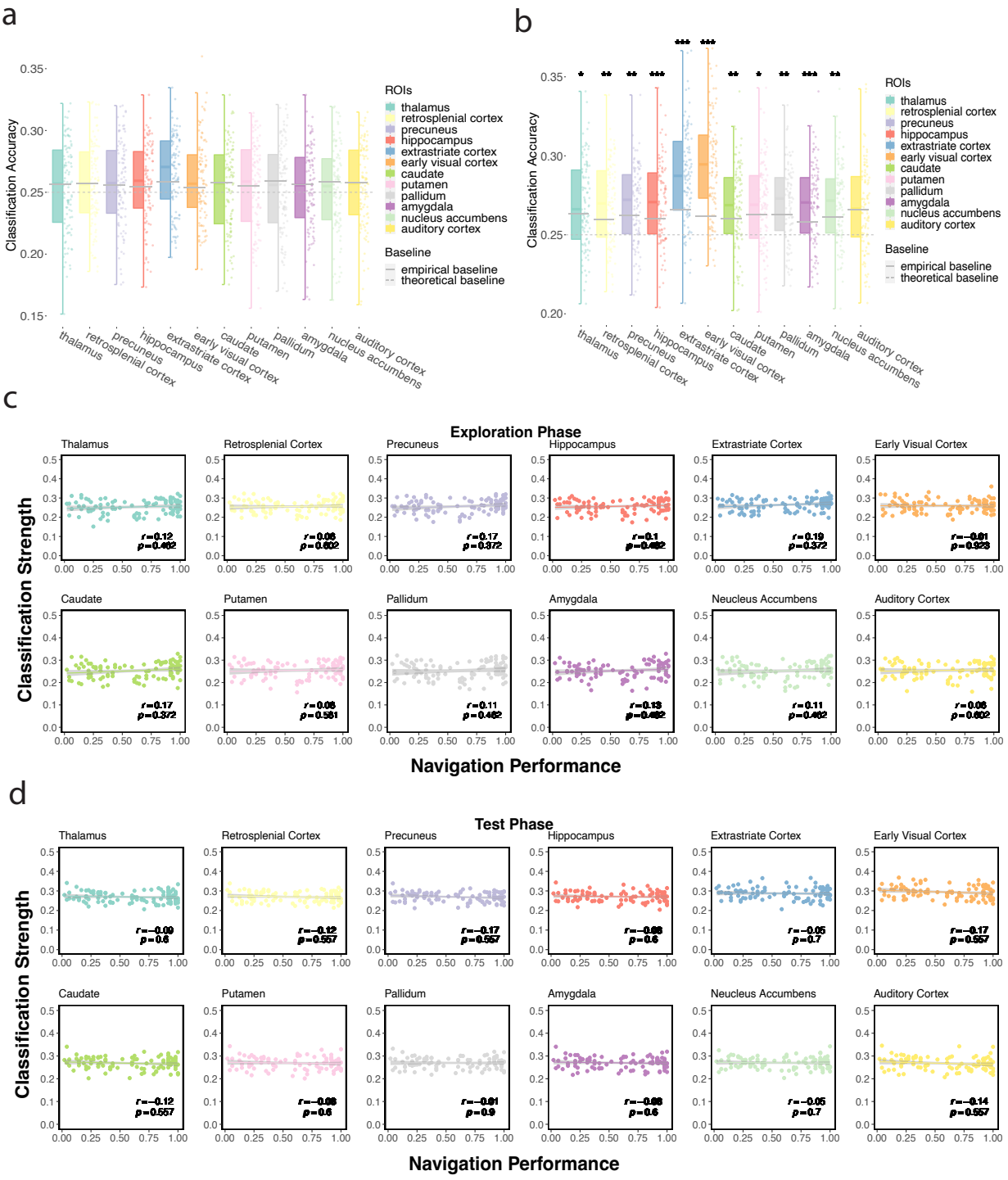
a
b
Classification Accuracy
ROIs
thalamus
retrosplenial cortex
precuneus
hippocampus
extrastriate cortex
early visual cortex
caudate
putamen
pallidum
amygdala
nucleus accumbens
auditory cortex
Baseline
empirical baseline
theoretical baseline
c
Exploration Phase
Classification Strength
Navigation Performance
d
Test Phase
Classification Strength
Navigation Performance

Figure 3.11: Classification accuracy of future translations. a. Model performance for all participants in all ROIs during the exploration phase. I plot single-participant data and group-level whiskerboxplots (center, median; box, 25th to 75th percentiles; whiskers, n=98 participants). I did not observe classification accuracy in any ROI using empirical baseline (gray solid line). Classification accuracy was observed in extrastriate and early visual cortex using theoretical baseline (gray dashed line, significance not labeled in the figure) b. similar to a., I plot model performance for all participants in all ROIs during the test phase. I observed significant classification accuracy in most ROIs except the auditory cortex. Classification accuracy was observed in all ROIs using theoretical baseline (gray dashed line, significance not labeled in the figure) c. Correlation between classification accuracy strength and navigation performance for all participants in all ROIs during the exploration phase. Classification accuracy in the exploration phase was not related to navigation performance. d. Correlation between classification accuracy strength and navigation performance for all participants in all ROIs during the test phase. Classification accuracy in the test phase was not related to navigation performance. Note: * $p < 0.05$, ** $p < 0.01$, *** $p < 0.001$, FDR-corrected.

ROIs	*df*	*t*	*p*	*pFDR*	*Cohen's d*	*C.I.*
Thalamus	97	-0.79	0.432	0.591	-0.08	[0.246, 0.261]
Retrosplenial Cortex	97	-0.25	0.805	0.852	-0.025	[0.25, 0.263]
Precuneus	97	0.27	0.791	0.852	0.027	[0.25, 0.263]
Hippocampus	97	0.97	0.336	0.575	0.098	[0.251, 0.264]
Extrastriate Cortex	97	2.01	0.047*	0.349	0.203	[0.259, 0.271]
Early Visual Cortex	97	1.72	0.088	0.349	0.174	[0.253, 0.266]
Caudate	97	-1.42	0.158	0.38	-0.144	[0.246, 0.26]
Putamen	97	-0.19	0.852	0.852	-0.019	[0.248, 0.262]
Pallidum	97	-1.58	0.116	0.349	-0.16	[0.246, 0.26]
Amygdala	97	-0.77	0.443	0.591	-0.078	[0.247, 0.26]
Nucleus Accumbens	97	-1.72	0.088	0.349	-0.174	[0.245, 0.259]
Auditory Cortex	97	-1	0.321	0.575	-0.101	[0.248, 0.261]

Notes: * $p < 0.05$

Table 3.15: Future cognitive map: model performance on allocentric translations in the exploration phase

ROIs	df	t	p	$pFDR$	$Cohen's\, d$	$C.I.$
Thalamus	97	2.13	0.035^{*}	0.039^{*}	0.215	[0.264, 0.275]
Retrosplenial Cortex	97	3.59	0.001^{**}	0.001^{**}	0.362	[0.264, 0.275]
Precuneus	97	2.78	0.007^{**}	0.009^{**}	0.281	[0.264, 0.274]
Hippocampus	97	4.13	$< 0.001^{***}$	$< 0.001^{***}$	0.418	[0.266, 0.276]
Extrastriate Cortex	97	7.08	$< 0.001^{***}$	$< 0.001^{***}$	0.715	[0.281, 0.293]
Early Visual Cortex	97	10.23	$< 0.001^{***}$	$< 0.001^{***}$	1.034	[0.288, 0.3]
Caudate	97	2.91	0.004^{**}	0.008^{**}	0.294	[0.263, 0.273]
Putamen	97	2.18	0.032^{*}	0.038^{*}	0.22	[0.263, 0.274]
Pallidum	97	2.84	0.006^{**}	0.008^{**}	0.287	[0.265, 0.274]
Amygdala	97	4.65	$< 0.001^{***}$	$< 0.001^{***}$	0.47	[0.265, 0.275]
Nucleus Accumbens	97	3.52	0.001^{**}	0.001^{**}	0.356	[0.265, 0.275]
Auditory Cortex	97	0.54	0.593	0.593	0.054	[0.262, 0.273]

Notes: *** $p < 0.001$, ** $p < 0.01$, * $p < 0.05$; *** $pFDR < 0.001$, ** $pFDR < 0.01$, * $pFDR < 0.05$

Table 3.16: Future cognitive map: model performance on allocentric translations in the test phase

The future cognitive map: allocentric rotations

To test the hypothesis that future allocentric rotations (i.e., from north to east, east to south, south to west, west to north, north to west, west to south, south to east, and east to north) could be discriminated from signals in distributed brain areas, I conducted pattern classifications in beta series signals for each participant, separated by regions of interest (ROIs) and navigation phases (i.e., exploration and testing).

For the exploration phase, I could not discriminate between directions in any ROI (all $pFDRs > 0.05$) (See Fig. 3.12a, Table 3.17). Analyses using theoretical baselines revealed significance in all ROIs (all $pFDRs < 0.001$). I then conducted correlation analyses between classification accuracy and navigation performance (see Fig. 3.12c). I did not observe correlation between allocentric future rotations classification accuracy in any ROI and navigation performance during the exploration phase (all $pFDRs > 0.05$).

For the test phase, I could discriminate between directions in all ROIs (all $pFDRs < 0.01$) (See Fig. 3.12b, Table 3.18). Analyses using theoretical baselines yield the same results. I then conducted correlation analyses between classification accuracy and navigation performance (see Fig. 3.12d). I did not observe correlation between allocentric future rotations classification accuracy in any ROI and navigation performance during the test phase (all $pFDRs > 0.05$).

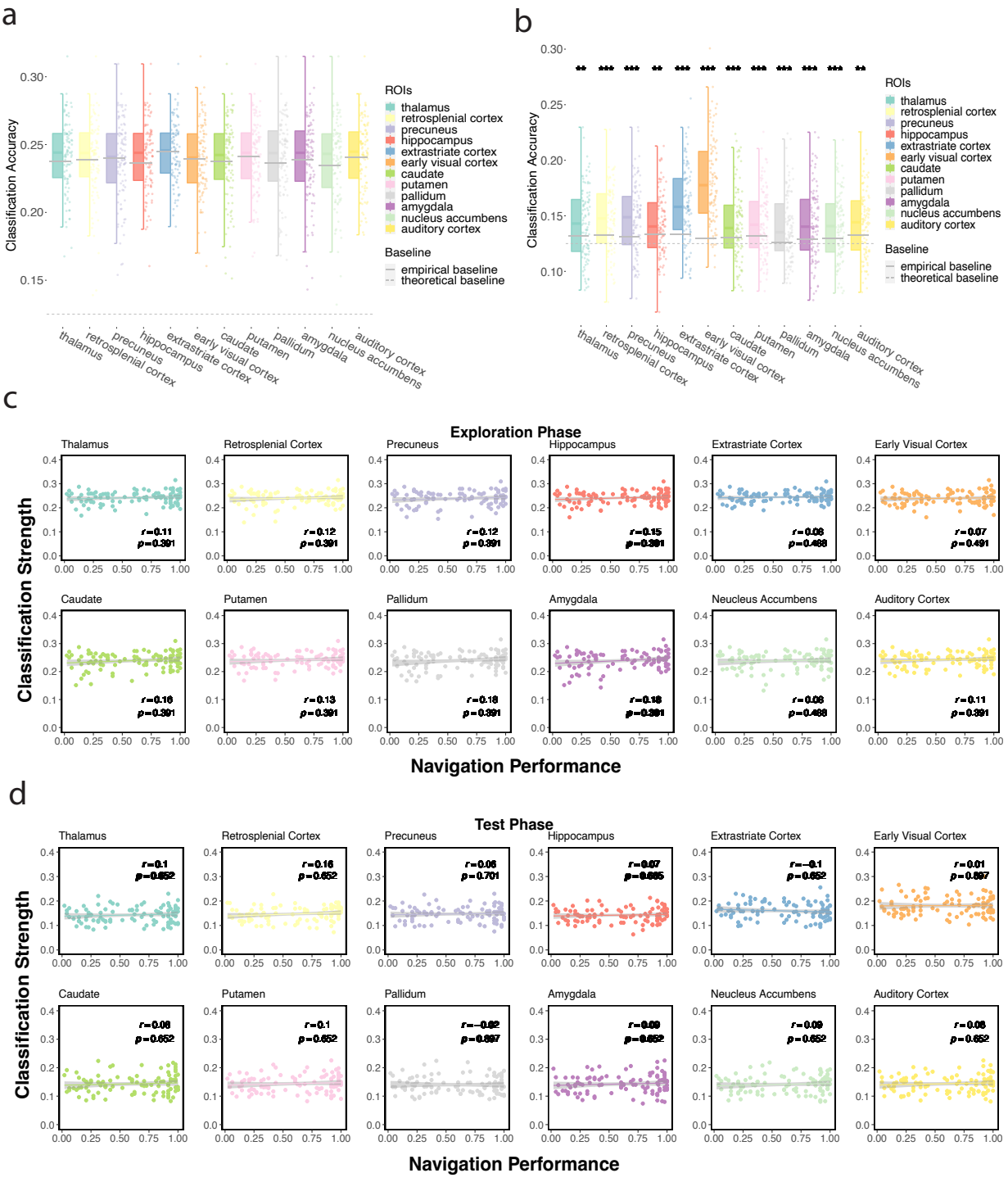
a
b
c
d
Classification Accuracy
ROIs
thalamus
retrosplenial cortex
precuneus
hippocampus
extrastriate cortex
early visual cortex
caudate
putamen
pallidum
amygdala
nucleus accumbens
auditory cortex
Baseline
empirical baseline
theoretical baseline
Exploration Phase
Test Phase
Classification Strength
Navigation Performance
Thalamus
Retrosplenial Cortex
Precuneus
Hippocampus
Extrastriate Cortex
Early Visual Cortex
Caudate
Putamen
Pallidum
Amygdala
Neucleus Accumbens
Auditory Cortex

Figure 3.12: Classification accuracy for future allocentric rotations. a. Model performance for all participants in all ROIs during the exploration phase. I plot single-participant data and group-level whiskerboxplots (center, median; box, 25th to 75th percentiles; whiskers, n=98 participants). I did not observe classification accuracy in any ROI using empirical baseline (gray solid line). Classification accuracy was observed in all ROIs using theoretical baseline (gray dashed line, significance not labeled in the figure) b. similar to a., I plot model performance for all participants in all ROIs during the test phase. I observed significant classification accuracy in all ROIs. Classification accuracy was observed in all ROIs using theoretical baseline (gray dashed line, significance not labeled in the figure) c. Correlation between classification accuracy strength and navigation performance for all participants in all ROIs during the exploration phase. Classification accuracy in the exploration phase was not related to navigation performance. d. Correlation between classification accuracy strength and navigation performance for all participants in all ROIs during the test phase. Classification accuracy in the test phase was not related to navigation performance. Note: ** $p < 0.01$, *** $p < 0.001$, FDR-corrected.

ROIs	*df*	*t*	*p*	*pFDR*	*Cohen's d*	*C.I.*
Thalamus	97	1.69	0.093	0.56	0.171	[0.237, 0.247]
Retrosplenial Cortex	97	0.36	0.719	0.929	0.036	[0.234, 0.246]
Precuneus	97	-0.37	0.712	0.929	-0.037	[0.233, 0.245]
Hippocampus	97	1.76	0.082	0.56	0.178	[0.236, 0.246]
Extrastriate Cortex	97	-0.17	0.868	0.929	-0.017	[0.24, 0.249]
Early Visual Cortex	97	0.09	0.929	0.929	0.009	[0.234, 0.245]
Caudate	97	0.57	0.57	0.929	0.058	[0.233, 0.245]
Putamen	97	0.18	0.855	0.929	0.019	[0.236, 0.247]
Pallidum	97	1.11	0.271	0.812	0.112	[0.234, 0.245]
Amygdala	97	0.19	0.853	0.929	0.019	[0.233, 0.245]
Nucleus Accumbens	97	1.21	0.23	0.812	0.122	[0.232, 0.245]
Auditory Cortex	97	0.59	0.556	0.929	0.06	[0.237, 0.248]

Table 3.17: Future cognitive map: model performance on allocentric rotations in the exploration phase

ROIs	*df*	*t*	*p*	*pFDR*	*Cohen's d*	*C.I.*
Thalamus	97	3.42	0.001^{**}	0.001^{**}	0.345	[0.137, 0.15]
Retrosplenial Cortex	97	4.79	$< 0.001^{***}$	$< 0.001^{***}$	0.484	[0.141, 0.153]
Precuneus	97	5.01	$< 0.001^{***}$	$< 0.001^{***}$	0.506	[0.141, 0.153]
Hippocampus	97	3.08	0.003^{**}	0.003^{**}	0.311	[0.137, 0.148]
Extrastriate Cortex	97	7.79	$< 0.001^{***}$	$< 0.001^{***}$	0.787	[0.153, 0.166]
Early Visual Cortex	97	13.31	$< 0.001^{***}$	$< 0.001^{***}$	1.345	[0.173, 0.189]
Caudate	97	3.87	$< 0.001^{***}$	$< 0.001^{***}$	0.391	[0.137, 0.15]
Putamen	97	4.01	$< 0.001^{***}$	$< 0.001^{***}$	0.405	[0.138, 0.15]
Pallidum	97	4.74	$< 0.001^{***}$	$< 0.001^{***}$	0.478	[0.134, 0.146]
Amygdala	97	4.25	$< 0.001^{***}$	$< 0.001^{***}$	0.429	[0.136, 0.149]
Nucleus Accumbens	97	3.72	$< 0.001^{***}$	$< 0.001^{***}$	0.375	[0.135, 0.147]
Auditory Cortex	97	3.46	0.001^{**}	0.001^{**}	0.349	[0.137, 0.15]

Notes: *** $p < 0.001$, ** $p < 0.01$; *** $pFDR < 0.001$, ** $pFDR < 0.01$

Table 3.18: Future cognitive map: model performance on allocentric rotations in the test phase

To confirm that the rotation classification was truely for allocentric directions instead of only classifying in an egocentric manner, I separately classified the four allocentric directions within clockwise direction and counterclockwise direction.

The future cognitive map: allocentric clockwise rotations To test the hypothesis that future allocentric clockwise rotations (i.e., from north to east, east to south, south to west, west to north) could be discriminated from signals in distributed brain areas, I conducted pattern classifications in beta series signals for each participant, separated by regions of interest (ROIs) and navigation phases (i.e., exploration and test).

For the exploration phase, I could not discriminate between directions in any ROI (all $pFDRs > 0.05$) (Figure 3.13a, Table 3.19). Analyses using theoretical baselines yielded the same results except significant in the extrastriate cortex ($pFDR = 0.005$) and early visual cortex (pFDR = 0.005). I then conducted correlation analyses between classification accuracy and navigation performance (see Fig. 3.13c). I did not observe correlation between allocentric future clockwise movement classification accuracy in any ROI and navigation performance during the exploration phase (all $pFDRs > 0.05$).

For the test phase, I could discriminate between directions in some ROIs: thalamus, extrastriate cortex, early visual cortex, and caudate (all $pFDRs < 0.05$) (Figure 3.13b, Table 3.20). The classification accuracy was marginally significant in precuneus and hippocampus (all $pFDRs < 0.08$), and was not significant in retrosplenial cortex, putamen, pallidum, amygdala, nucleus accumbens, auditory cortex (all $pFDRs > 0.05$). Analyses using theoretical baselines yielded the same results except also showed significance in all other ROIs: precuneus, hippocampus, retrosplenial cortex, putamen, pallidum, amygdala, nucleus accumbens, auditory cortex (all $pFDRs < 0.001$). I then conducted correlation analyses between classification accuracy and navigation performance (see Fig. 3.13d). I did not observe correlation between allocentric future clockwise movement classification accuracy in any ROI

and navigation performance during the test phase (all $pFDRs > 0.05$).

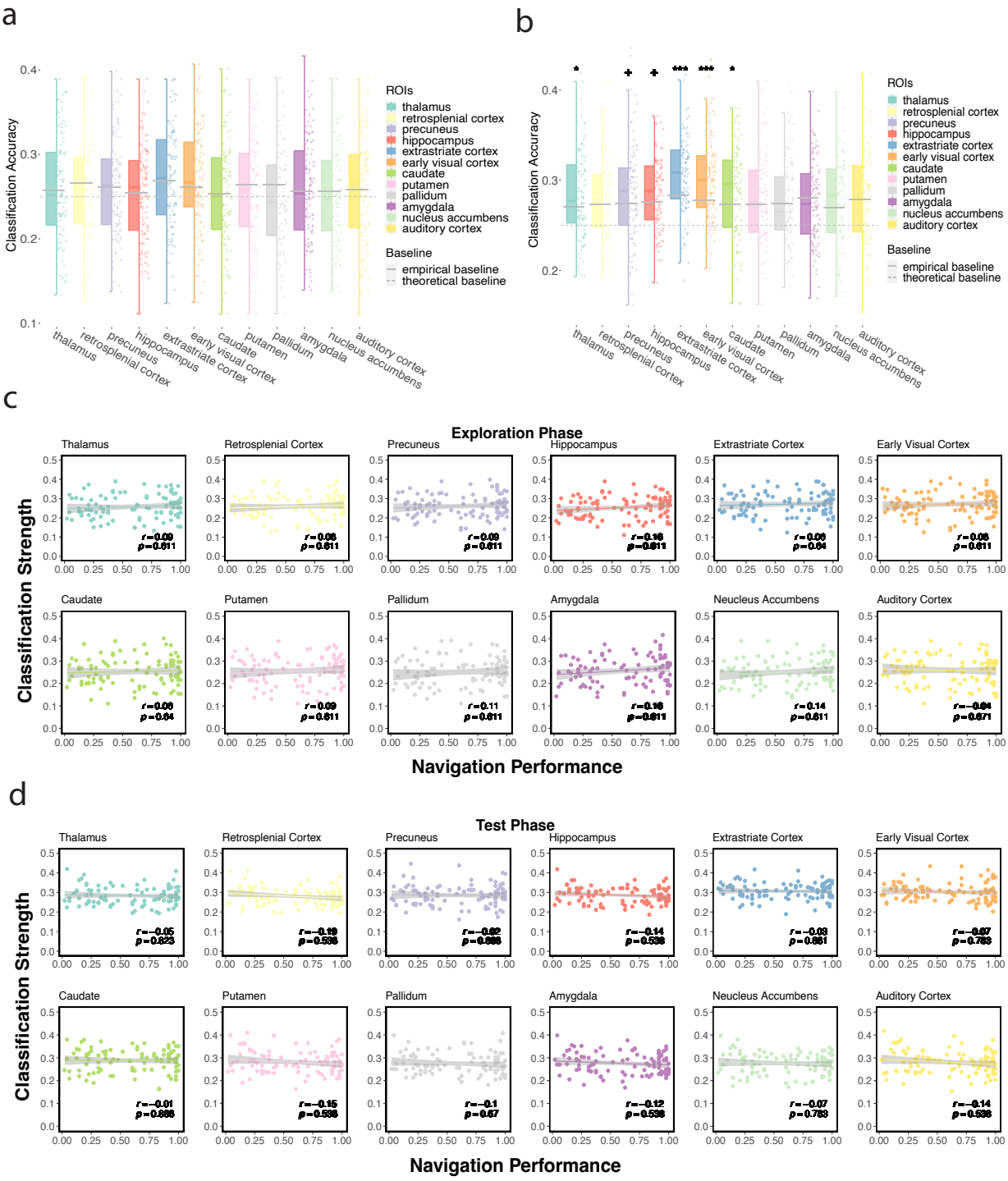

Figure 3.13: Classification accuracy for allocentric future clockwise rotations. a. Model performance for all participants in all ROIs during the exploration phase. I plot single-participant data and group-level whiskerboxplots (center, median; box, 25th to 75th percentiles; whiskers, n=98 participants). I did not observe classification accuracy in any ROI using empirical baseline (gray solid line). Classification accuracy was not significant in most ROIs except extrastriate cortex and early visual cortex using theoretical baseline (gray dashed line, significance not labeled in the figure) b. similar to a., I plot model performance for all participants in all ROIs during the test phase. I observed significant classification accuracy in thalamus, extrastriate cortex, early visual cortex, and caudate, and marginally significant in precuneus and hippocampus . Classification accuracy was observed in all ROIs using theoretical baseline (gray dashed line, significance not labeled in the figure) c. Correlation between classification accuracy strength and navigation performance for all participants in all ROIs during the exploration phase. Classification accuracy in the exploration phase was not related to navigation performance. d. Correlation between classification accuracy strength and navigation performance for all participants in all ROIs during the test phase. Classification accuracy in the test phase was not related to navigation performance. Note: + $p < 0.08$, * $p < 0.05$, *** $p < 0.001$, FDR-corrected.

ROIs	*df*	*t*	*p*	*pFDR*	*Cohen's d*	*C.I.*
Thalamus	97	0.04	0.964	1	0.005	[0.246, 0.27]
Retrosplenial Cortex	97	-1.01	0.315	0.944	-0.102	[0.248, 0.272]
Precuneus	97	< 0.001	1	1	< 0.001	[0.249, 0.273]
Hippocampus	97	0.03	0.978	1	0.003	[0.243, 0.266]
Extrastriate Cortex	97	0.39	0.7	1	0.039	[0.259, 0.283]
Early Visual Cortex	97	1.49	0.14	0.841	0.15	[0.259, 0.283]
Caudate	97	0.05	0.962	1	0.005	[0.241, 0.266]
Putamen	97	-1.21	0.229	0.915	-0.122	[0.244, 0.269]
Pallidum	97	-2.03	0.045	0.539	-0.205	[0.238, 0.263]
Amygdala	97	0.18	0.859	1	0.018	[0.245, 0.27]
Nucleus Accumbens	97	-0.83	0.411	0.987	-0.083	[0.24, 0.263]
Auditory Cortex	97	0.18	0.858	1	0.018	[0.247, 0.272]

Table 3.19: Future cognitive map: model performance on allocentric clockwise rotations in the exploration phase

ROIs	df	t	p	$pFDR$	$Cohen's\, d$	$C.I.$
Thalamus	97	2.82	0.006^{**}	0.017^{*}	0.285	[0.274, 0.293]
Retrosplenial Cortex	97	1.46	0.148	0.222	0.147	[0.271, 0.289]
Precuneus	97	2.18	0.032^{*}	0.063^{+}	0.22	[0.275, 0.296]
Hippocampus	97	2.25	0.027^{*}	0.063^{+}	0.227	[0.277, 0.294]
Extrastriate Cortex	97	5.64	$< 0.001^{***}$	$< 0.001^{***}$	0.57	[0.298, 0.315]
Early Visual Cortex	97	5.31	$< 0.001^{***}$	$< 0.001^{***}$	0.537	[0.293, 0.312]
Caudate	97	2.92	0.004^{**}	0.017^{*}	0.295	[0.278, 0.298]
Putamen	97	1.53	0.128	0.22	0.155	[0.271, 0.291]
Pallidum	97	0.23	0.82	0.82	0.023	[0.265, 0.284]
Amygdala	97	-0.99	0.322	0.387	-0.1	[0.266, 0.285]
Nucleus Accumbens	97	1.3	0.196	0.261	0.132	[0.266, 0.285]
Auditory Cortex	97	0.38	0.703	0.766	0.039	[0.271, 0.291]

Notes: *** $p < 0.001$, ** $p < 0.01$, * $p < 0.05$; *** $pFDR < 0.001$, * $pFDR < 0.05$, + $pFDR < 0.08$

Table 3.20: Future cognitive map: model performance on allocentric clockwise rotations in the test phase

The future cognitive map: allocentric counterclockwise rotations To test the hypothesis that future allocentric counterclockwise rotations (i.e., north to west, west to south, south to east, and east to north) could be discriminated from signals in distributed brain areas, I conducted pattern classifications in beta series signals for each participant, separated by regions of interest (ROIs) and navigation phases (i.e., exploration and test).

For the exploration phase, I could not discriminate between directions in most ROIs (all $pFDRs > 0.05$) except in amygdala ($pFDR = 0.033$) where I observed a lower than chance level classification score (see Fig. 3.14a, Table 3.21). Analyses using theoretical baselines yielded the significance in most ROIs (all $pFDRs < 0.05$) except extrastriate cortex ($pFDR = 0.322$) and early visual cortex (pFDR = 0.308). I then conducted correlation analyses between classification accuracy and navigation performance (see Fig. 3.14c). I did not observe correlation between allocentric future counterclockwise movement classification accuracy in any ROI and navigation performance during the exploration phase (all $pFDRs > 0.05$).

For the test phase, I could discriminate between directions in precuneus ($pFDR = 0.002$) and early visual cortex ($pFDR < 0.001$) (see Fig. 3.14b, Table 3.22). Analyses using theoretical baselines yielded the same result except also show significance in thalamus, retrosplenial cortex, extrastriate cortex, putamen, and auditory cortex (all $pFDRs < 0.05$). I then conducted correlation analyses between classification accuracy and navigation performance (see Fig. 3.14d). I did not observe correlation between allocentric future counterclockwise movement classification accuracy in any ROI and navigation performance during the test phase (all $pFDRs > 0.05$).

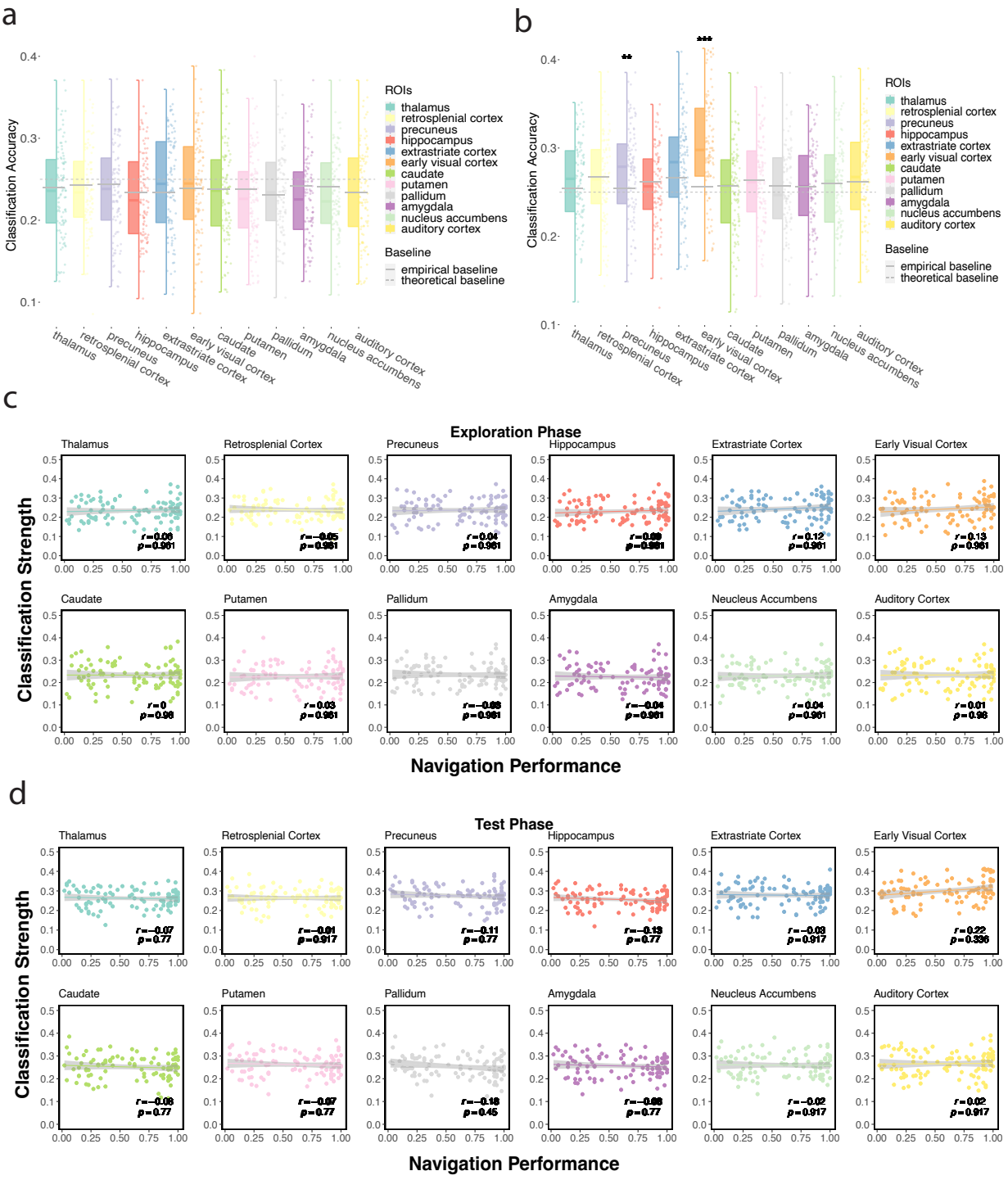
a
b
Classification Accuracy
ROIs
thalamus
retrosplenial cortex
precuneus
hippocampus
extrastriate cortex
early visual cortex
caudate
putamen
pallidum
amygdala
nucleus accumbens
auditory cortex
Baseline
empirical baseline
theoretical baseline
**
***
c
Exploration Phase
Classification Strength
Navigation Performance
Thalamus
Retrosplenial Cortex
Precuneus
Hippocampus
Extrastriate Cortex
Early Visual Cortex
Caudate
Putamen
Pallidum
Amygdala
Neucleus Accumbens
Auditory Cortex
d
Test Phase
Classification Strength
Navigation Performance

Figure 3.14: Classification accuracy for future counterclockwise rotations. a. Model performance for all participants in all ROIs during the exploration phase. I plot single-participant data and group-level whiskerboxplots (center, median; box, 25th to 75th percentiles; whiskers, n=98 participants). I did not observe classification accuracy in any ROI using empirical baseline (gray solid line). Classification accuracy was significant in most ROIs except extrastriate cortex and early visual cortex using theoretical baseline (gray dashed line, significance not labeled in the figure) b. similar to a., I plot model performance for all participants in all ROIs during the test phase. I observed significant classification accuracy in precuneus and early visual cortex . Classification accuracy was observed in thalamus, retrosplenial cortex, precuneus, extrastriate cortex, early visual cortex, putamen, and auditory cortex using theoretical baseline (gray dashed line, significance not labeled in the figure) c. Correlation between classification accuracy strength and navigation performance for all participants in all ROIs during the exploration phase. Classification accuracy in the exploration phase was not related to navigation performance. d. Correlation between classification accuracy strength and navigation performance for all participants in all ROIs during the test phase. Classification accuracy in the test phase was not related to navigation performance. Note: ** $p < 0.01$, *** $p < 0.001$, FDR-corrected.

ROIs	*df*	*t*	*p*	*pFDR*	*Cohen's d*	*C.I.*
Thalamus	97	-0.85	0.4	0.624	-0.085	[0.224, 0.246]
Retrosplenial Cortex	97	-0.84	0.401	0.624	-0.085	[0.228, 0.249]
Precuneus	97	-1.3	0.198	0.476	-0.131	[0.225, 0.248]
Hippocampus	97	-0.54	0.592	0.645	-0.054	[0.22, 0.242]
Extrastriate Cortex	97	1.67	0.099	0.296	0.168	[0.232, 0.256]
Early Visual Cortex	97	0.55	0.586	0.645	0.055	[0.23, 0.256]
Caudate	97	-0.82	0.416	0.624	-0.082	[0.221, 0.245]
Putamen	97	-1.91	0.059	0.234	-0.193	[0.216, 0.238]
Pallidum	97	0.63	0.528	0.645	0.064	[0.224, 0.245]
Amygdala	97	-3.07	0.003	0.033	-0.31	[0.214, 0.236]
Nucleus Accumbens	97	-1.95	0.055	0.234	-0.197	[0.22, 0.241]
Auditory Cortex	97	-0.04	0.966	0.966	-0.004	[0.222, 0.246]

Notes: classification accuracy for signals in putamen, amygdala, and nucleus accumbens were significantly or marginally significantly lower than chance levels, so I do not label these classification scores as successful classification.

Table 3.21: Future cognitive map: model performance on allocentric counterclockwise rotations in the exploration phase

ROIs	df	t	p	$pFDR$	$Cohen's\, d$	$C.I.$
Thalamus	97	1.62	0.108	0.323	0.164	[0.253, 0.272]
Retrosplenial Cortex	97	-0.81	0.417	0.556	-0.082	[0.254, 0.273]
Precuneus	97	3.79	$< 0.001^{***}$	0.002^{**}	0.382	[0.264, 0.284]
Hippocampus	97	-1.35	0.181	0.434	-0.136	[0.247, 0.265]
Extrastriate Cortex	97	2.29	0.024^{*}	0.097	0.231	[0.268, 0.289]
Early Visual Cortex	97	7.61	$< 0.001^{***}$	$< 0.001^{***}$	0.769	[0.29, 0.313]
Caudate	97	-1.02	0.308	0.556	-0.103	[0.241, 0.262]
Putamen	97	-0.41	0.684	0.821	-0.041	[0.252, 0.272]
Pallidum	97	-0.84	0.403	0.556	-0.085	[0.243, 0.263]
Amygdala	97	0.06	0.95	0.95	0.006	[0.247, 0.266]
Nucleus Accumbens	97	-0.13	0.901	0.95	-0.013	[0.249, 0.269]
Auditory Cortex	97	0.86	0.392	0.556	0.087	[0.255, 0.277]

Notes: *** $p < 0.001$, * $p < 0.05$; *** $pFDR < 0.001$, ** $pFDR < 0.01$

Table 3.22: Future cognitive map: model performance on allocentric counterclockwise rotations in the test phase

3.2.7 The future cognitive map: egocentric movements

To test the hypothesis that egocentric future movements (i.e., moving forward, turning left, turning right) were represented in the brain when people were stationarily standing at an intersection planning for the next step, I conducted pattern classification analyses for egocentric future movements in beta series signals for each participant, separated by regions of interest (ROIs) and navigation phases (i.e., exploration and testing).

For the exploration phase, I could successfully discriminate between egocentric future movements in all ROIs (all $pFDRs < 0.001$) (Figure 3.15a, Table 3.23). Analyses using theoretical baselines yield the same results. I then conducted correlation analyses between classification accuracy and navigation performance. I did not observe correlation between egocentric future movement classification accuracy in any ROI and navigation performance during the exploration phase (all $pFDRs > 0.05$) (Figure 3.15c).

For the test phase, I could successfully discriminate between future egocentric movement directions in some ROIs: retrosplenial cortex, precuneus, extrastriate cortex, early visual cortex (all $pFDRs < 0.001$) (Figure 3.15b, Table 3.24). Analyses using theoretical baselines yield the same results except also found significance in all other regions: thalamus, hippocampus, caudate, putamen, pallidum, amygdala, nucleus accumbens, auditory cortex (all $pFDRs < 0.001$). I then conducted correlation analyses between classification accuracy and navigation performance. I observed positive correlation between egocentric future movement classification accuracy and navigation performance during the test phase in thalamus, hippocampus, extrastriate cortex, caudate, putamen, pallidum, amygdala, nucleus accumbens, and auditory cortex (all $pFDRs < 0.01$) (Figure 3.15d).

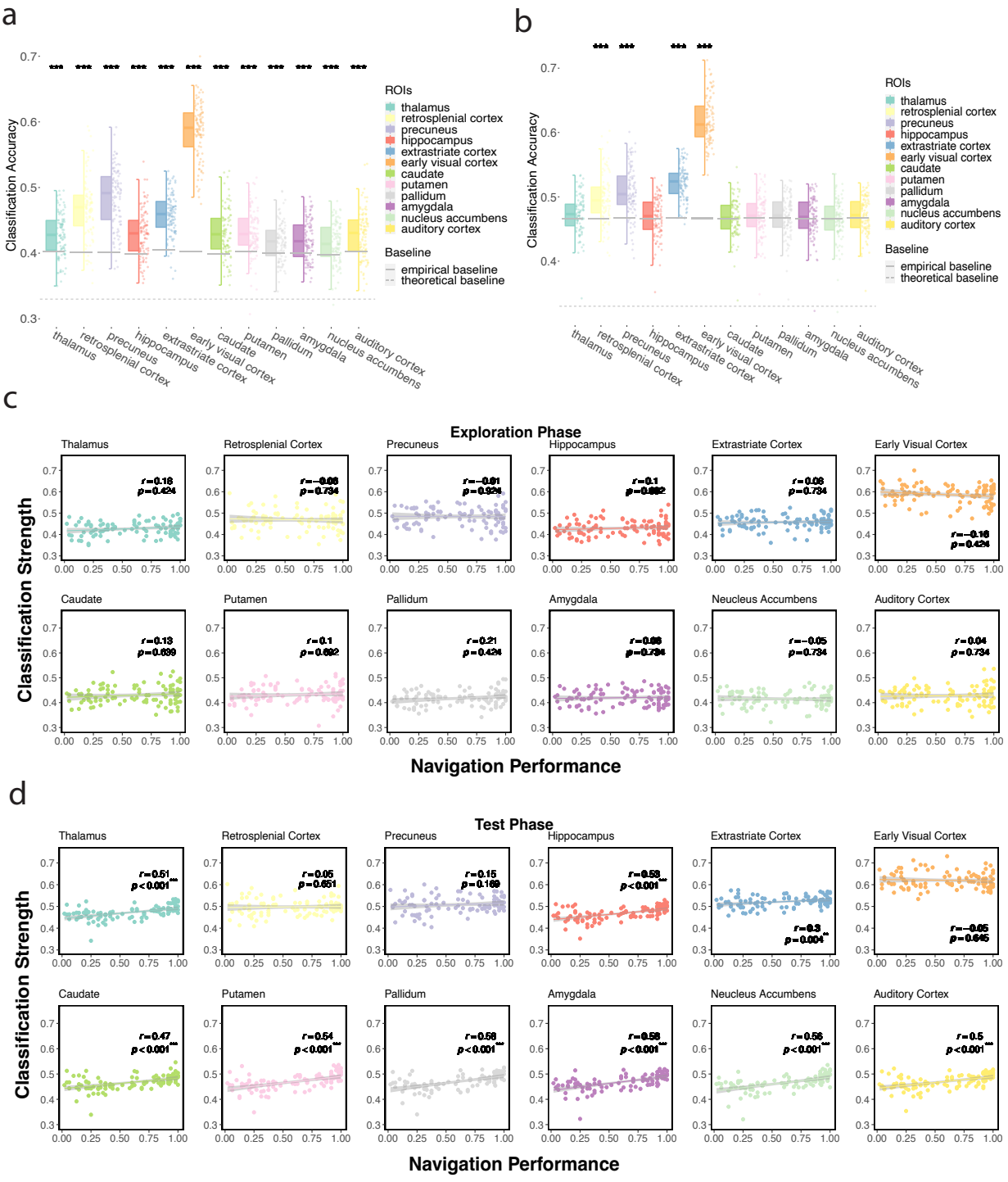
a
b
c
d
Classification Accuracy
ROIs
thalamus
retrosplenial cortex
precuneus
hippocampus
extrastriate cortex
early visual cortex
caudate
putamen
pallidum
amygdala
nucleus accumbens
auditory cortex
Baseline
empirical baseline
theoretical baseline
Exploration Phase
Test Phase
Classification Strength
Navigation Performance
Thalamus
Retrosplenial Cortex
Precuneus
Hippocampus
Extrastriate Cortex
Early Visual Cortex
Caudate
Putamen
Pallidum
Amygdala
Neucleus Accumbens
Auditory Cortex

Figure 3.15: Classification accuracy for egocentric future movements. a. Model performance for all participants in all ROIs during the exploration phase. I plot single-participant data and group-level whiskerboxplots (center, median; box, 25th to 75th percentiles; whiskers, n=98 participants). I observed classification accuracy in all ROIs using empirical baseline (gray solid line). Classification accuracy was also observed in all ROIs using theoretical baseline (gray dashed line, significance not labeled in the figure) b. similar to a., I plot model performance for all participants in all ROIs during the test phase. I observed classification accuracy in retrosplenial cortex, precuneus, extrastriate cortex, and early visual cortex using empirical baseline. Classification accuracy was also observed in all ROIs using a theoretical baseline (significance not labeled in the figure). c. Correlation between classification accuracy strength and navigation performance for all participants in all ROIs during the exploration phase. Classification accuracy in the exploration phase was not related to navigation performance. d. Correlation between classification accuracy strength and navigation performance for all participants in all ROIs during the test phase. Classification accuracy in the test phase was positively correlated to navigation performance in thalamus, hippocampus, extrastriate cortex, caudate, putamen, pallidum, amygdala, nucleus accumbens, and auditory cortex. Note: ** p < 0.01, *** p < 0.001, FDR-corrected.

ROIs	*df*	*t*	*p*	*pFDR*	*Cohen's d*	*C.I.*
Thalamus	97	7.46	$< 0.001^{***}$	$< 0.001^{***}$	0.754	[0.421, 0.434]
Retrosplenial Cortex	97	14.6	$< 0.001^{***}$	$< 0.001^{***}$	1.475	[0.46, 0.478]
Precuneus	97	18.26	$< 0.001^{***}$	$< 0.001^{***}$	1.844	[0.475, 0.493]
Hippocampus	97	8.27	$< 0.001^{***}$	$< 0.001^{***}$	0.835	[0.422, 0.437]
Extrastriate Cortex	97	16.09	$< 0.001^{***}$	$< 0.001^{***}$	1.625	[0.452, 0.465]
Early Visual Cortex	97	43	$< 0.001^{***}$	$< 0.001^{***}$	4.343	[0.578, 0.595]
Caudate	97	8.43	$< 0.001^{***}$	$< 0.001^{***}$	0.852	[0.423, 0.437]
Putamen	97	8.4	$< 0.001^{***}$	$< 0.001^{***}$	0.849	[0.425, 0.439]
Pallidum	97	5.77	$< 0.001^{***}$	$< 0.001^{***}$	0.583	[0.412, 0.424]
Amygdala	97	6.29	$< 0.001^{***}$	$< 0.001^{***}$	0.635	[0.414, 0.426]
Nucleus Accumbens	97	5.42	$< 0.001^{***}$	$< 0.001^{***}$	0.547	[0.409, 0.421]
Auditory Cortex	97	6.85	$< 0.001^{***}$	$< 0.001^{***}$	0.692	[0.421, 0.435]

Notes: *** $p < 0.001$; *** $pFDR < 0.001$

Table 3.23: Future cognitive map: model performance on egocentric directions in the exploration phase

ROIs	df	t	p	$pFDR$	$Cohen's\ d$	$C.I.$
Thalamus	97	2.13	0.036^{*}	0.086	0.215	[0.467, 0.479]
Retrosplenial Cortex	97	8.41	$< 0.001^{***}$	$< 0.001^{***}$	0.849	[0.49, 0.505]
Precuneus	97	10.53	$< 0.001^{***}$	$< 0.001^{***}$	1.064	[0.5, 0.516]
Hippocampus	97	0.52	0.607	0.728	0.052	[0.462, 0.474]
Extrastriate Cortex	97	20.6	$< 0.001^{***}$	$< 0.001^{***}$	2.081	[0.517, 0.527]
Early Visual Cortex	97	40.74	$< 0.001^{***}$	$< 0.001^{***}$	4.115	[0.613, 0.628]
Caudate	97	0.36	0.718	0.759	0.037	[0.461, 0.473]
Putamen	97	0.88	0.382	0.603	0.089	[0.463, 0.476]
Pallidum	97	0.84	0.402	0.603	0.085	[0.464, 0.476]
Amygdala	97	0.66	0.514	0.685	0.066	[0.462, 0.474]
Nucleus Accumbens	97	-0.31	0.759	0.759	-0.031	[0.459, 0.471]
Auditory Cortex	97	1.41	0.162	0.324	0.142	[0.465, 0.477]

Notes: $^{***}\ p < 0.001$, $^{*}\ p < 0.05$; $^{***}\ pFDR < 0.001$

Table 3.24: Future cognitive map: model performance on egocentric directions in the test phase

The future cognitive map: rotations

To test the hypothesis that future egocentric rotations (i.e., left and right or counterclockwise and clockwise) could be discriminated from signals in distributed brain areas, I conducted pattern classifications in beta series signals for each participant, separated by regions of interest (ROIs) and navigation phases (i.e., exploration and testing).

For the exploration phase, I could discriminate between directions in all ROIs (all $pFDRs < 0.01$) (Figure 3.16a, Table 3.25). Analyses using theoretical baselines yield the same results. I then conducted correlation analyses between classification accuracy and navigation performance. I did not observe correlation between egocentric future movement classification accuracy in any ROI and navigation performance during the exploration phase (all $pFDRs > 0.05$) (Figure 3.16c).

For the test phase, I could discriminate directions from most ROIs (all $pFDRs < 0.05$) except pallidum ($pFDR = 0.57$) (Figure 3.16b, Table 3.26). Analyses using theoretical baselines yield the same results except also not significant in nucleus accumbens ($pFDR = 0.202$). I then conducted correlation analyses between classification accuracy and navigation performance. I observed negative correlation between egocentric future rotations classification accuracy and navigation performance during the test phase in extrastriate cortex ($pFDR < 0.001$) and early visual cortex ($pFDRs = 0.024$) (Figure 3.16d).

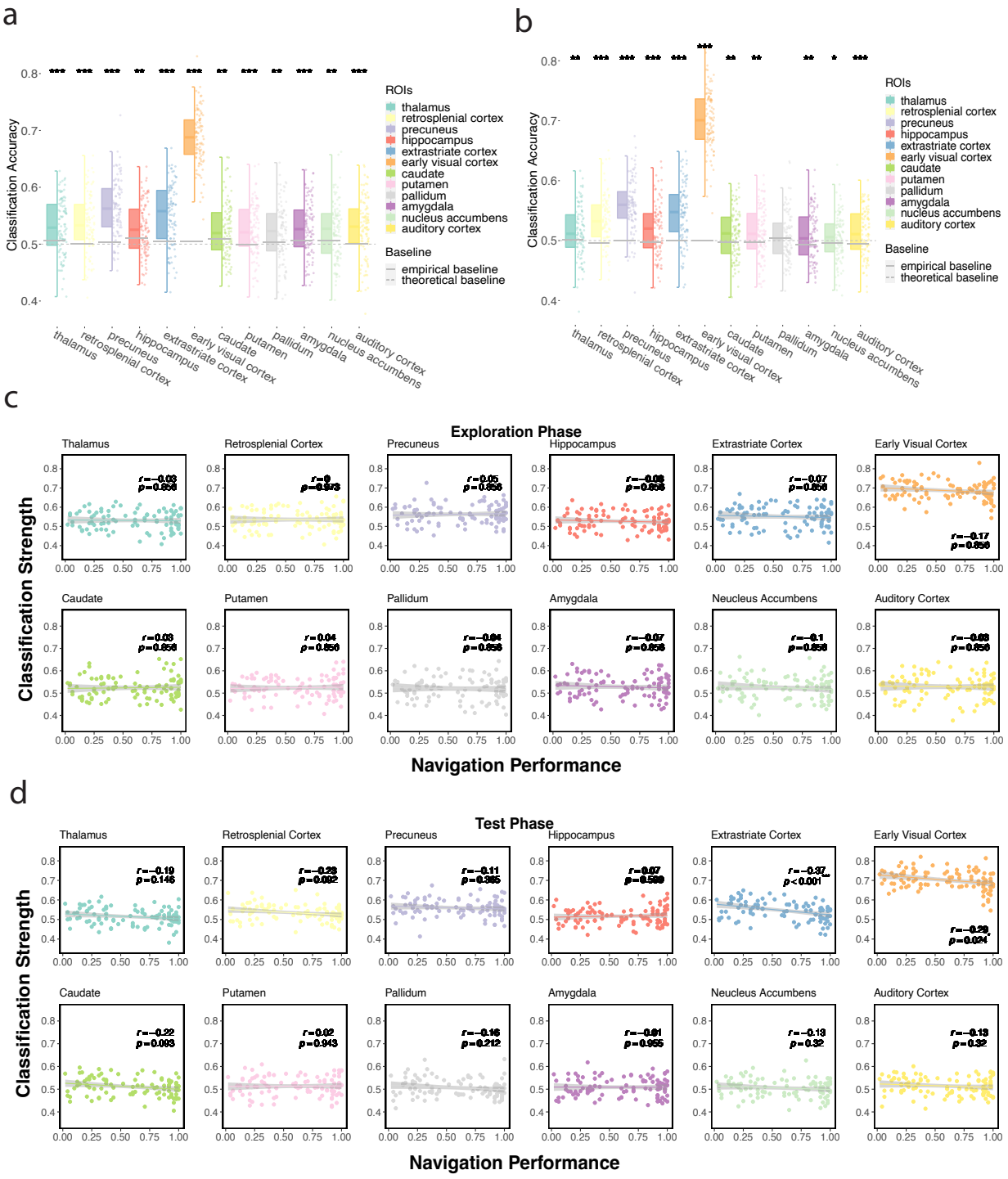
a
b
Classification Accuracy
ROIs
thalamus
retrosplenial cortex
precuneus
hippocampus
extrastriate cortex
early visual cortex
caudate
putamen
pallidum
amygdala
nucleus accumbens
auditory cortex
Baseline
empirical baseline
theoretical baseline
c
Exploration Phase
Classification Strength
Navigation Performance
Thalamus
Retrosplenial Cortex
Precuneus
Hippocampus
Extrastriate Cortex
Early Visual Cortex
Caudate
Putamen
Pallidum
Amygdala
Neucleus Accumbens
Auditory Cortex
d
Test Phase
Classification Strength
Navigation Performance

Figure 3.16: Classification accuracy for future egocentric rotations. a. Model performance for all participants in all ROIs during the exploration phase. I plot single-participant data and group-level whiskerboxplots (center, median; box, 25th to 75th percentiles; whiskers, n=98 participants). I observed classification accuracy in all ROIs using empirical baseline (gray solid line). Classification accuracy was also observed in all ROIs using theoretical baseline (gray dashed line, significance not labeled in the figure) b. similar to a., I plot model performance for all participants in all ROIs during the test phase. I observed classification accuracy in most ROIs except pallidum using empirical baseline. Classification accuracy was also observed in most ROIs except pallidum and nucleus accumbens using a theoretical baseline (significance not labeled in the figure). c. Correlation between classification accuracy strength and navigation performance for all participants in all ROIs during the exploration phase. Classification accuracy in the exploration phase was not related to navigation performance. d. Correlation between classification accuracy strength and navigation performance for all participants in all ROIs during the test phase. Classification accuracy in the test phase was negatively correlated to navigation performance in the extrastriate cortex and early visual cortex. Note: * p $<$ 0.05, ** p $<$ 0.01, *** p $<$ 0.001, FDR-corrected.

ROIs	*df*	*t*	*p*	*pFDR*	*Cohen's d*	*C.I.*
Thalamus	97	5.06	$< 0.001^{***}$	$< 0.001^{***}$	0.511	[0.521, 0.541]
Retrosplenial Cortex	97	6.68	$< 0.001^{***}$	$< 0.001^{***}$	0.675	[0.525, 0.546]
Precuneus	97	11.94	$< 0.001^{***}$	$< 0.001^{***}$	1.206	[0.553, 0.573]
Hippocampus	97	3.52	0.001^{**}	0.001^{**}	0.355	[0.517, 0.536]
Extrastriate Cortex	97	8.36	$< 0.001^{***}$	$< 0.001^{***}$	0.845	[0.54, 0.561]
Early Visual Cortex	97	37.43	$< 0.001^{***}$	$< 0.001^{***}$	3.781	[0.677, 0.696]
Caudate	97	3.06	0.003^{**}	0.003^{**}	0.309	[0.514, 0.534]
Putamen	97	5.42	$< 0.001^{***}$	$< 0.001^{***}$	0.547	[0.515, 0.533]
Pallidum	97	3.31	0.001^{**}	0.001^{**}	0.334	[0.51, 0.53]
Amygdala	97	4.37	$< 0.001^{***}$	$< 0.001^{***}$	0.441	[0.518, 0.538]
Nucleus Accumbens	97	3.33	0.001^{**}	0.001^{**}	0.337	[0.513, 0.534]
Auditory Cortex	97	5.36	$< 0.001^{***}$	$< 0.001^{***}$	0.541	[0.518, 0.539]

Notes: *** $p < 0.001$, ** $p < 0.01$; *** $pFDR < 0.001$, ** $pFDR < 0.01$

Table 3.25: Future cognitive map: model performance on egocentric rotations in the exploration phase

ROIs	df	t	p	$pFDR$	$Cohen's\, d$	$C.I.$
Thalamus	97	3	0.003^{**}	0.004^{**}	0.303	[0.505, 0.523]
Retrosplenial Cortex	97	9.44	$< 0.001^{***}$	$< 0.001^{***}$	0.953	[0.526, 0.543]
Precuneus	97	13.5	$< 0.001^{***}$	$< 0.001^{***}$	1.363	[0.551, 0.568]
Hippocampus	97	4.51	$< 0.001^{***}$	$< 0.001^{***}$	0.455	[0.509, 0.526]
Extrastriate Cortex	97	9.48	$< 0.001^{***}$	$< 0.001^{***}$	0.958	[0.536, 0.555]
Early Visual Cortex	97	39.84	$< 0.001^{***}$	$< 0.001^{***}$	4.025	[0.691, 0.712]
Caudate	97	3.18	0.002^{**}	0.003^{**}	0.322	[0.503, 0.519]
Putamen	97	3.66	$< 0.001^{***}$	0.001^{**}	0.37	[0.505, 0.522]
Pallidum	97	0.57	0.57	0.57	0.058	[0.498, 0.514]
Amygdala	97	3.72	$< 0.001^{***}$	0.001^{**}	0.375	[0.501, 0.517]
Nucleus Accumbens	97	2.16	0.033^{*}	0.036^{*}	0.218	[0.497, 0.513]
Auditory Cortex	97	4.76	$< 0.001^{***}$	$< 0.001^{***}$	0.481	[0.506, 0.522]

Notes: *** $p < 0.001$, ** $p < 0.01$, * $p < 0.05$; *** $pFDR < 0.001$, ** $pFDR < 0.01$, * $pFDR < 0.05$

Table 3.26: Future cognitive map: model performance on egocentric rotations in the test phase

3.2.8 The past cognitive map: allocentric movements

To test the hypothesis that allocentric past movementss (i.e., turning from north to east, east to south, south to west, west to north, north to west, west to south, south to east, east to north, moving toward north, south, east, or west) were still represented in the brain when people were stationarily standing at an intersection planning for the next step, I conducted pattern classification analyses for allocentric past movementss in beta series signals for each participant, separate by regions of interest (ROIs) and navigation phases (i.e., exploration and test).

For the exploration phase, I could successfully discriminate between allocentric past movementss in all ROIs (all $pFDRs < 0.01$) (see Fig. 3.17a, Table 3.27). Analyses using theoretical baselines yielded the same result. I then conducted correlation analyses between classification accuracy and navigation performance (see Fig. 3.17c). I did not observe any correlations between allocentric past movement classification accuracy in any ROI and navigation performance during the exploration phase (all $pFDRs > 0.05$).

For the test phase, I could successfully discriminate between allocentric past movementss in all ROIs ($pFDR < 0.05$) (see Fig. 3.17b, Table 3.28). Analyses using theoretical baselines yielded the same result. I then conducted correlation analyses between classification accuracy and navigation performance (see Fig. 3.17d). I observed negative correlations during the exploration phase between allocentric past movement classification accuracy and navigation performance in all ROIs (all $pFDRs < 0.05$) except marginally significant in pallidum ($pFDR = 0.066$) and early visual cortex ($pFDR = 0.05$).

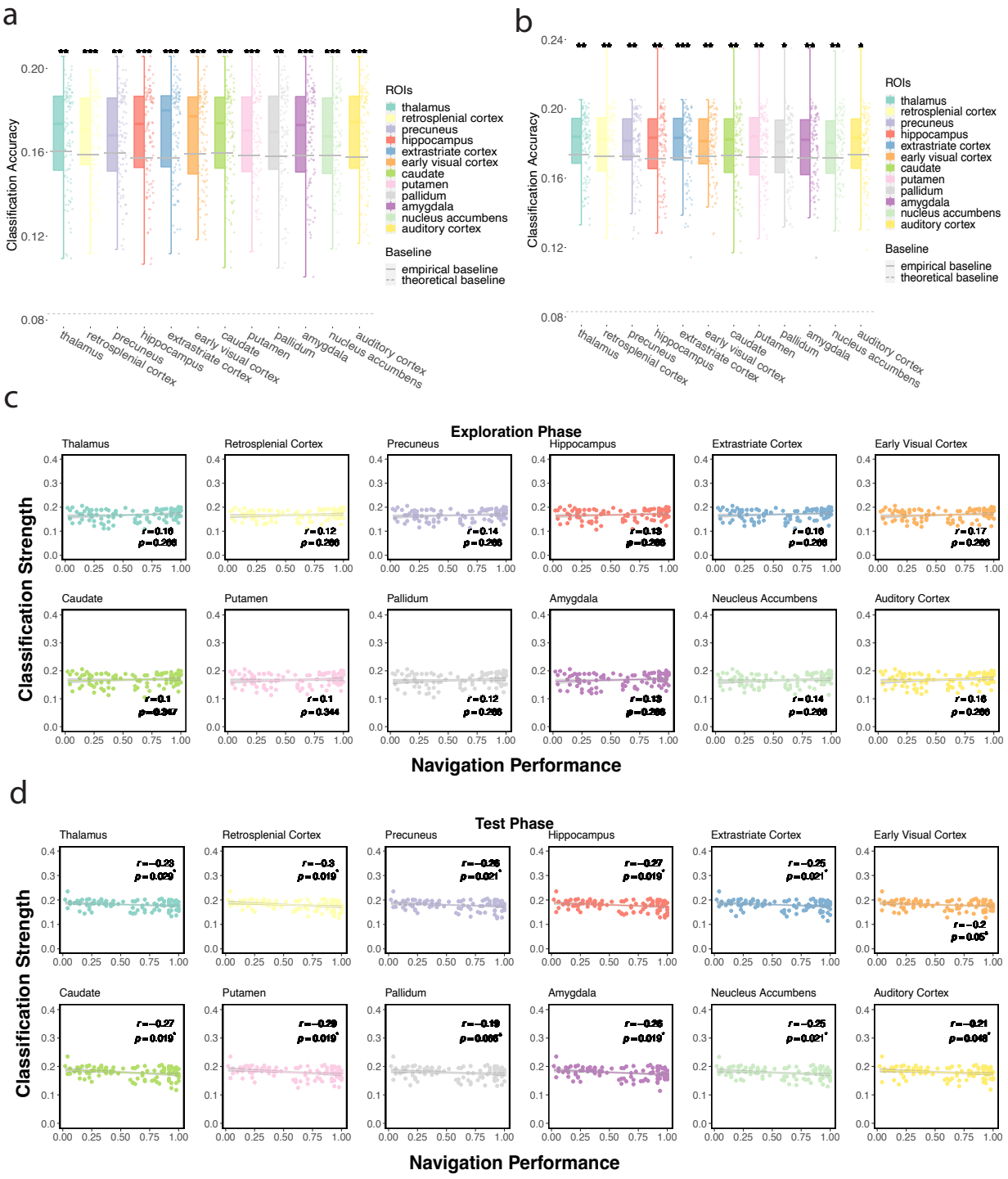
a
b
c
d
Classification Accuracy
ROIs
thalamus
retrosplenial cortex
precuneus
hippocampus
extrastriate cortex
early visual cortex
caudate
putamen
pallidum
amygdala
nucleus accumbens
auditory cortex
Baseline
empirical baseline
theoretical baseline
Exploration Phase
Test Phase
Classification Strength
Navigation Performance
Thalamus
Retrosplenial Cortex
Precuneus
Hippocampus
Extrastriate Cortex
Early Visual Cortex
Caudate
Putamen
Pallidum
Amygdala
Neucleus Accumbens
Auditory Cortex

Figure 3.17: Classification accuracy for allocentric past movementss. a. Model performance for all participants in all ROIs during the exploration phase. I plot single-participant data and group-level whiskerboxplots (center, median; box, 25th to 75th percentiles; whiskers, n=98 participants). I observed classification accuracy in all ROIs using empirical baseline (gray solid line). Classification accuracy was also observed in all ROIs using theoretical baseline (gray dashed line, significance not labeled in the figure) b. similar to a., I plot model performance for all participants in all ROIs during the test phase. I observed significant classification accuracy in all ROIs. Classification accuracy was also observed in all ROIs using theoretical baseline (gray dashed line, significance not labeled in the figure) c. Correlation between classification accuracy strength and navigation performance for all participants in all ROIs during the exploration phase. Classification accuracy in the exploration phase was not related to navigation performance. d. Correlation between classification accuracy strength and navigation performance for all participants in all ROIs during the test phase. Classification accuracy in the test phase was negatively correlated to navigation performance in all ROIs (marginally significant in pallidum and early visual cortex). Note: + $p < 0.08$, * $p < 0.05$, ** $p < 0.01$, *** $p < 0.001$, FDR-corrected.

ROIs	*df*	*t*	*p*	*pFDR*	*Cohen's d*	*C.I.*
Thalamus	97	3.24	0.002^{**}	0.002^{**}	0.327	[0.163, 0.173]
Retrosplenial Cortex	97	4.22	$< 0.001^{***}$	$< 0.001^{***}$	0.426	[0.163, 0.172]
Precuneus	97	3.16	0.002^{**}	0.002^{**}	0.32	[0.162, 0.171]
Hippocampus	97	5.1	$< 0.001^{***}$	$< 0.001^{***}$	0.515	[0.164, 0.173]
Extrastriate Cortex	97	5.93	$< 0.001^{***}$	$< 0.001^{***}$	0.599	[0.166, 0.175]
Early Visual Cortex	97	3.89	$< 0.001^{***}$	$< 0.001^{***}$	0.393	[0.164, 0.173]
Caudate	97	3.8	$< 0.001^{***}$	$< 0.001^{***}$	0.384	[0.164, 0.173]
Putamen	97	3.95	$< 0.001^{***}$	$< 0.001^{***}$	0.399	[0.163, 0.172]
Pallidum	97	3.55	0.001^{**}	0.001^{**}	0.359	[0.162, 0.171]
Amygdala	97	3.99	$< 0.001^{***}$	$< 0.001^{***}$	0.403	[0.163, 0.172]
Nucleus Accumbens	97	3.62	$< 0.001^{***}$	0.001^{**}	0.365	[0.162, 0.171]
Auditory Cortex	97	4.79	$< 0.001^{***}$	$< 0.001^{***}$	0.484	[0.164, 0.173]

Notes: *** $p < 0.001$, ** $p < 0.01$; *** $pFDR < 0.001$, ** $pFDR < 0.01$

Table 3.27: Past cognitive map: model performance on allocentric directions in the exploration phase

ROIs	df	t	p	$pFDR$	$Cohen's\, d$	$C.I.$
Thalamus	97	3.39	0.001^{**}	0.002^{**}	0.342	[0.176, 0.184]
Retrosplenial Cortex	97	3.36	0.001^{**}	0.002^{**}	0.339	[0.175, 0.183]
Precuneus	97	2.94	0.004^{**}	0.006^{**}	0.297	[0.175, 0.183]
Hippocampus	97	3.46	0.001^{**}	0.002^{**}	0.35	[0.174, 0.182]
Extrastriate Cortex	97	3.88	$< 0.001^{***}$	0.002^{**}	0.392	[0.175, 0.183]
Early Visual Cortex	97	3.43	0.001^{**}	0.002^{**}	0.347	[0.176, 0.183]
Caudate	97	2.38	0.019^{*}	0.019^{*}	0.241	[0.174, 0.182]
Putamen	97	3.52	0.001^{**}	0.002^{**}	0.356	[0.175, 0.183]
Pallidum	97	2.65	0.009^{**}	0.01^{*}	0.267	[0.173, 0.182]
Amygdala	97	3.03	0.003^{**}	0.005^{**}	0.306	[0.174, 0.182]
Nucleus Accumbens	97	2.75	0.007^{**}	0.009^{**}	0.278	[0.173, 0.181]
Auditory Cortex	97	2.67	0.009^{**}	0.01^{*}	0.27	[0.175, 0.183]

Notes: *** $p < 0.001$, ** $p < 0.01$, * $p < 0.05$; ** $pFDR < 0.01$, * $pFDR < 0.05$

Table 3.28: Past cognitive map: model performance on allocentric directions in the test phase

The past cognitive map: allocentric translations

To test the hypothesis that allocentric past translations (i.e., north, south, east, and west) could be discriminated from signals in distributed brain areas, I conducted pattern classifications in beta series signals for each participant, separated by regions of interest (ROIs) and navigation phases (i.e., exploration and test).

For the exploration phase, I could not discriminate between directions in any ROI (all $pFDRs > 0.05$) (see Figure 3.18a, Table 3.29). Analyses using theoretical baselines yielded the same result except showed significance in extrastriate cortex ($pFDR = 0.045$) and marginally significant in early visual cortex ($pFDR = 0.070$). I then conducted correlation analyses between classification accuracy and navigation performance (see Fig. 3.18c). I did not observe any correlations between allocentric past translations classification accuracy in any ROIs and navigation performance during the exploration phase ($pFDRs > 0.05$).

For the test phase, I could discriminate between directions in some ROIs: extrastriate cortex, early visual cortex, and auditory cortex (all $pFDRs < 0.01$), but the discrimination was only marginally significant in retrosplenial cortex, caudate, and putamen (all $pFDRs < 0.08$) (see Fig. 3.18b, Table 3.30). Analyses using theoretical baselines yielded the same result except showed significance in all other ROIs: thalamus, retrosplenial cortex, precuneus, hippocampus, caudate, putamen, pallidum, amygdala, and nucleus accumbens (all $pFDRs < 0.001$). I then conducted correlation analyses between classification accuracy and navigation performance (see Fig. 3.18d). I observed negative correlations during the test phase between allocentric past translations classification accuracy and navigation performance in thalamus, precuneus, putamen, amygdala, auditory cortex (all $pFDRs < 0.05$) and the correlation was marginally significant in retrosplenial cortex, hippocampus, early visual cortex, caudate, pallidum, and nucleus accumbens (all $pFDRs < 0.08$), but was not significant in extrastriate cortex ($pFDRs = 0.153$).

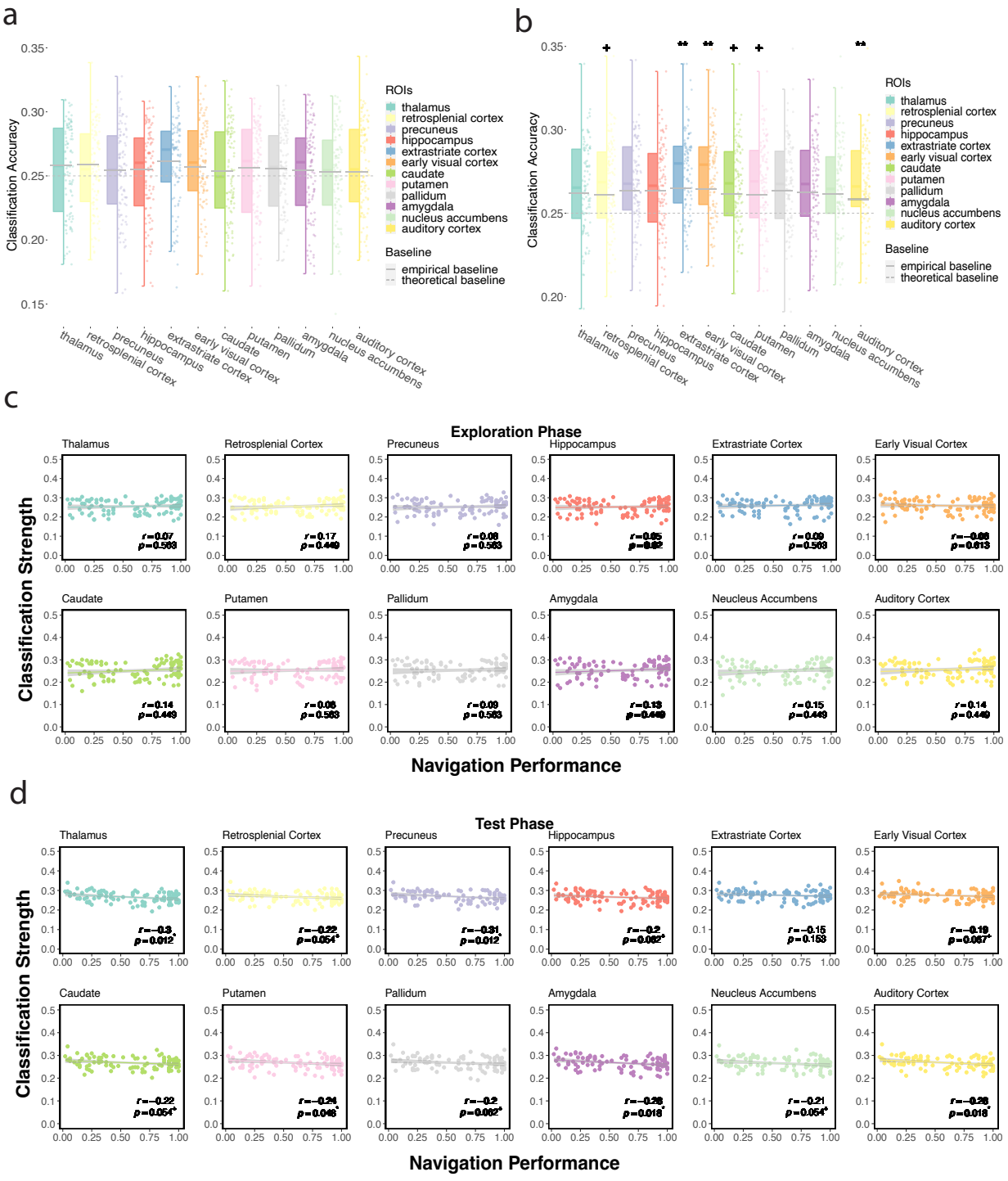
a
b
Classification Accuracy
ROIs
thalamus
retrosplenial cortex
precuneus
hippocampus
extrastriate cortex
early visual cortex
caudate
putamen
pallidum
amygdala
nucleus accumbens
auditory cortex
Baseline
empirical baseline
theoretical baseline
c
Exploration Phase
Classification Strength
Navigation Performance
Thalamus
Retrosplenial Cortex
Precuneus
Hippocampus
Extrastriate Cortex
Early Visual Cortex
Caudate
Putamen
Pallidum
Amygdala
Neucleus Accumbens
Auditory Cortex
d
Test Phase
Classification Strength
Navigation Performance

Figure 3.18: Classification accuracy of past translations. Model performance for all participants in all ROIs during the exploration phase. I plot single-participant data and group-level whiskerboxplots (center, median; box, 25th to 75th percentiles; whiskers, n=98 participants). I did not observe classification accuracy in any ROIs using empirical baselines (gray solid line). Classification accuracy was not observed in most ROIs (except extrastriate cortex and early visual cortex) using theoretical baseline (gray dashed line, significance not labeled in the figure) b. similar to a., I plot model performance for all participants in all ROIs during the test phase. I observed significant classification accuracy in the extrastriate cortex, early visual cortex, and auditory cortex, marginally significant accuracy in retrosplenial cortex, caudate, and putamen. Classification accuracy was also observed in all ROIs using theoretical baseline (gray dashed line, significance not labeled in the figure) c. Correlation between classification accuracy strength and navigation performance for all participants in all ROIs during the exploration phase. Classification accuracy in the exploration phase was not related to navigation performance. d. Correlation between classification accuracy strength and navigation performance for all participants in all ROIs during the test phase. Classification accuracy in the signals from thalamus, precuneus, putamen, amygdala, auditory cortex and marginally significance in retrosplenial cortex, hippocampus, early visual cortex, caudate, pallidum, and nucleus accumbens in the test phase were negatively related to navigation performance. Note: + $p < 0.08$, * $p < 0.05$, ** $p < 0.01$, FDR-corrected.

ROIs	df	t	p	$pFDR$	$Cohen's\, d$	$C.I.$
Thalamus	97	-0.83	0.409	0.682	-0.084	[0.248, 0.262]
Retrosplenial Cortex	97	-1.02	0.308	0.682	-0.104	[0.249, 0.262]
Precuneus	97	-0.44	0.658	0.682	-0.045	[0.245, 0.26]
Hippocampus	97	-0.71	0.481	0.682	-0.072	[0.245, 0.259]
Extrastriate Cortex	97	-0.43	0.669	0.682	-0.043	[0.253, 0.267]
Early Visual Cortex	97	0.56	0.579	0.682	0.056	[0.252, 0.265]
Caudate	97	-0.73	0.465	0.682	-0.074	[0.244, 0.259]
Putamen	97	-0.67	0.504	0.682	-0.068	[0.247, 0.261]
Pallidum	97	-0.6	0.549	0.682	-0.061	[0.247, 0.261]
Amygdala	97	-0.41	0.682	0.682	-0.042	[0.245, 0.26]
Nucleus Accumbens	97	-0.58	0.562	0.682	-0.059	[0.244, 0.258]
Auditory Cortex	97	1.07	0.285	0.682	0.109	[0.25, 0.264]

Table 3.29: Past cognitive map: model performance on allocentric translations in the exploration phase

ROIs	df	t	p	$pFDR$	$Cohen's\, d$	$C.I.$
Thalamus	97	1.25	0.214	0.261	0.126	[0.26, 0.271]
Retrosplenial Cortex	97	2.14	0.035^{*}	0.07^{+}	0.216	[0.262, 0.272]
Precuneus	97	1.82	0.072^{+}	0.124	0.183	[0.263, 0.273]
Hippocampus	97	0.65	0.518	0.518	0.066	[0.26, 0.271]
Extrastriate Cortex	97	3.88	$< 0.001^{***}$	0.001^{**}	0.392	[0.27, 0.28]
Early Visual Cortex	97	4.02	$< 0.001^{***}$	0.001^{**}	0.406	[0.27, 0.28]
Caudate	97	2.3	0.024^{*}	0.07^{+}	0.232	[0.262, 0.272]
Putamen	97	2.19	0.031^{*}	0.07^{+}	0.222	[0.262, 0.273]
Pallidum	97	1.23	0.223	0.261	0.124	[0.262, 0.272]
Amygdala	97	1.53	0.129	0.193	0.155	[0.261, 0.272]
Nucleus Accumbens	97	1.18	0.239	0.261	0.12	[0.259, 0.27]
Auditory Cortex	97	3.81	$< 0.001^{***}$	0.001^{**}	0.385	[0.263, 0.273]

Notes: $^{***}\, p < 0.001$, $^{*}\, p < 0.05$, $^{+}\, p < 0.08$; $^{**}\, pFDR < 0.01$, $^{+}\, pFDR < 0.08$

Table 3.30: Past cognitive map: model performance on allocentric translations in the test phase

The past cognitive map: allocentric rotations

To test the hypothesis that past allocentric rotations (i.e., from north to east, east to south, south to west, west to north, north to west, west to south, south to east, and east to north) could be discriminated from signals in distributed brain areas, I conducted pattern classifications in beta series signals for each participant, separated by regions of interest (ROIs) and navigation phases (i.e., exploration and test).

During the exploration phase, I could not discriminate directions from any ROI (all $pFDRs > 0.05$) (see Fig. 3.19a, Table 3.31). Analyses using theoretical baselines yielded significant results in all ROIs (all $pFDRs < 0.001$). I then conducted correlation analyses between classification accuracy and navigation performance (see Fig. 3.19c). I did not observe any correlations between allocentric past rotations classification accuracy in any ROI and navigation performance during the exploration phase (all $pFDRs > 0.05$).

For the test phase, I could discriminate directions for all ROIs (all $pFDRs < 0.01$)(see Fig. 3.19b, Table 3.32). Analyses using theoretical baselines yielded the same results. I then conducted correlation analyses between classification accuracy and navigation performance (see Fig. 3.19d). I did not observe any correlations between allocentric past rotational movement classification accuracy in any ROI and navigation performance during the test phase (all $pFDRs > 0.05$).

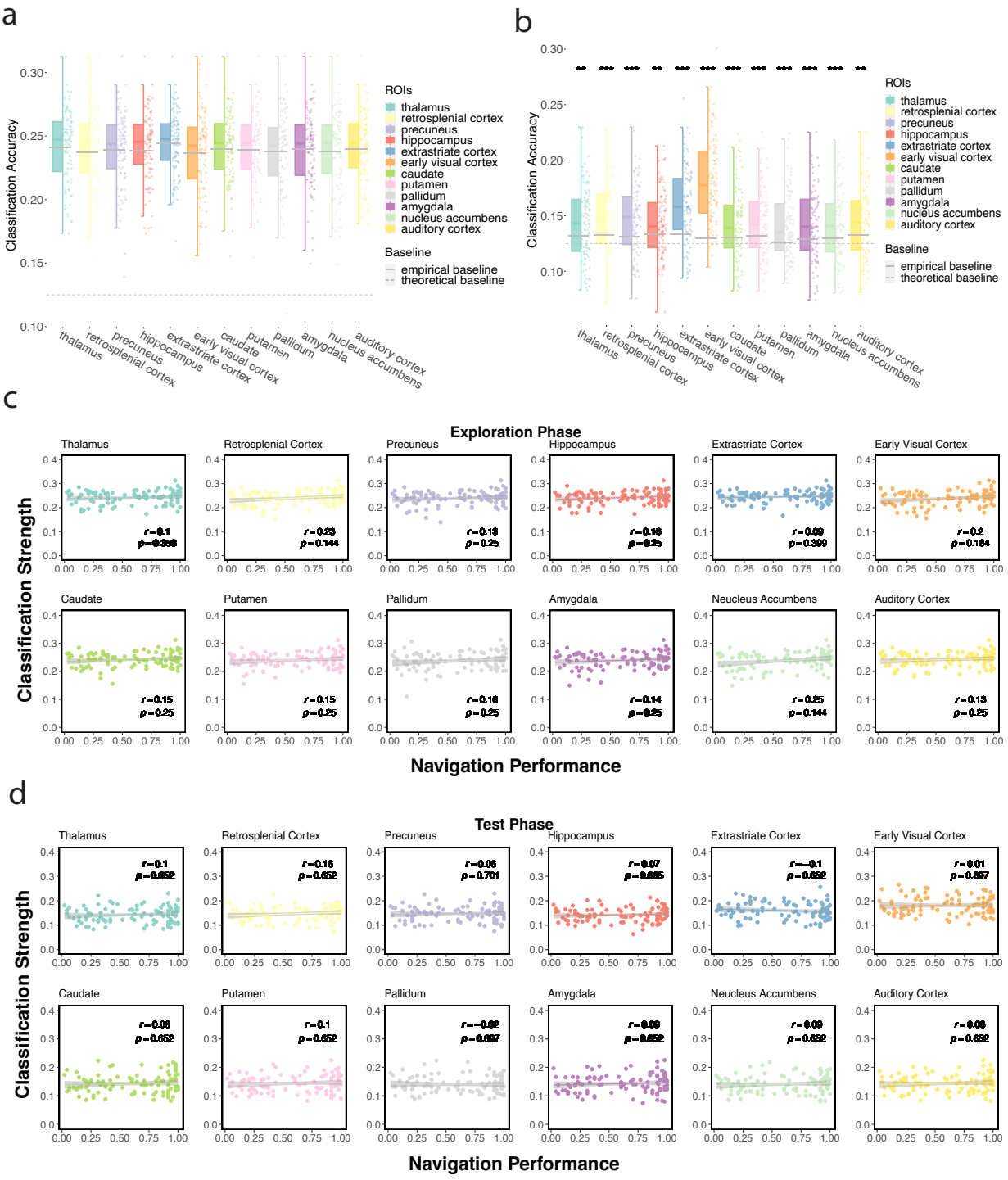
a
b
c
d
Classification Accuracy
ROIs
thalamus
retrosplenial cortex
precuneus
hippocampus
extrastriate cortex
early visual cortex
caudate
putamen
pallidum
amygdala
nucleus accumbens
auditory cortex
Baseline
empirical baseline
theoretical baseline
Exploration Phase
Test Phase
Classification Strength
Navigation Performance
Thalamus
Retrosplenial Cortex
Precuneus
Hippocampus
Extrastriate Cortex
Early Visual Cortex
Caudate
Putamen
Pallidum
Amygdala
Neucleus Accumbens
Auditory Cortex

Figure 3.19: Classification accuracy of past rotations. Model performance for all participants in all ROIs during the exploration phase. I plot single-participant data and group-level whiskerboxplots (center, median; box, 25th to 75th percentiles; whiskers, n=98 participants). I did not observe classification accuracy in any ROIs using empirical baselines (gray solid line). Classification accuracy was observed in all ROIs using theoretical baseline (gray dashed line, significance not labeled in the figure) b. similar to a., I plot model performance for all participants in all ROIs during the test phase. I observed significant classification accuracy in all ROIs. Classification accuracy was also observed in all ROIs using theoretical baseline (gray dashed line, significance not labeled in the figure) c. Correlation between classification accuracy strength and navigation performance for all participants in all ROIs during the exploration phase. Classification accuracy in the exploration phase was not related to navigation performance. d. Correlation between classification accuracy strength and navigation performance for all participants in all ROIs during the test phase. Classification accuracy in the exploration phase was not related to navigation performance. Note: ** $p < 0.01$, *** $p < 0.001$, FDR-corrected.

ROIs	*df*	*t*	*p*	*pFDR*	*Cohen's d*	*C.I.*
Thalamus	97	0.36	0.719	0.984	0.036	[0.237, 0.248]
Retrosplenial Cortex	97	1.06	0.291	0.984	0.107	[0.235, 0.246]
Precuneus	97	0.09	0.929	0.984	0.009	[0.234, 0.245]
Hippocampus	97	1.26	0.21	0.984	0.128	[0.236, 0.247]
Extrastriate Cortex	97	0.25	0.802	0.984	0.025	[0.24, 0.25]
Early Visual Cortex	97	0.5	0.617	0.984	0.051	[0.232, 0.245]
Caudate	97	1.08	0.281	0.984	0.11	[0.237, 0.247]
Putamen	97	0.42	0.679	0.984	0.042	[0.235, 0.246]
Pallidum	97	0.13	0.893	0.984	0.014	[0.232, 0.245]
Amygdala	97	-0.02	0.984	0.984	-0.002	[0.234, 0.245]
Nucleus Accumbens	97	0.2	0.844	0.984	0.02	[0.233, 0.245]
Auditory Cortex	97	0.91	0.368	0.984	0.091	[0.237, 0.247]

Table 3.31: Past cognitive map: model performance on allocentric rotations in the exploration phase

ROIs	df	t	p	$pFDR$	$Cohen's\, d$	$C.I.$
Thalamus	97	3.42	0.001^{**}	0.001^{**}	0.345	[0.137, 0.15]
Retrosplenial Cortex	97	4.79	$< 0.001^{***}$	$< 0.001^{***}$	0.484	[0.141, 0.153]
Precuneus	97	5.01	$< 0.001^{***}$	$< 0.001^{***}$	0.506	[0.141, 0.153]
Hippocampus	97	3.08	0.003^{**}	0.003^{**}	0.311	[0.137, 0.148]
Extrastriate Cortex	97	7.79	$< 0.001^{***}$	$< 0.001^{***}$	0.787	[0.153, 0.166]
Early Visual Cortex	97	13.31	$< 0.001^{***}$	$< 0.001^{***}$	1.345	[0.173, 0.189]
Caudate	97	3.87	$< 0.001^{***}$	$< 0.001^{***}$	0.391	[0.137, 0.15]
Putamen	97	4.01	$< 0.001^{***}$	$< 0.001^{***}$	0.405	[0.138, 0.15]
Pallidum	97	4.74	$< 0.001^{***}$	$< 0.001^{***}$	0.478	[0.134, 0.146]
Amygdala	97	4.25	$< 0.001^{***}$	$< 0.001^{***}$	0.429	[0.136, 0.149]
Nucleus Accumbens	97	3.72	$< 0.001^{***}$	$< 0.001^{***}$	0.375	[0.135, 0.147]
Auditory Cortex	97	3.46	0.001^{**}	0.001^{**}	0.349	[0.137, 0.15]

Notes: *** $p < 0.001$, ** $p < 0.01$; *** $pFDR < 0.001$, ** $pFDR < 0.01$

Table 3.32: Past cognitive map: model performance on allocentric rotations in the test phase

The past cognitive map: allocentric clockwise rotations To test the hypothesis that past allocentric clockwise rotations (i.e., from north to east, east to south, south to west, west to north) could be discriminated from signals in distributed brain areas, I conducted pattern classifications in beta series signals for each participant, separated by regions of interest (ROIs) and navigation phases (i.e., exploration and test).

For the exploration phase, I could successfully classify directions in the early visual cortex ($pFDR = 0.013$) and nucleus accumbens ($pFDR = 0.029$) (see Fig. 3.20a, Table 3.33). Analyses using theoretical baselines yielded same results except also revealed significance in retrosplenial cortex, precuneus, hippocampus, extrastriate cortex, pallidum, putamen, amygdala, auditory cortex (all $pFDRs < 0.05$). I then conducted correlation analyses between classification accuracy and navigation performance (see Fig. 3.20c). I did not observe, during the exploration phase, any correlations between allocentric past clockwise movement classification accuracy in any ROI and navigation performance (all $pFDRs > 0.05$).

For the test phase, I could successfully discriminate directions in all ROIs (all $pFDRs < 0.01$) (see Fig. 3.20b, Table 3.34). Analyses using theoretical baselines yielded the same results. I then conducted correlation analyses between classification accuracy and navigation performance (see Fig. 3.20d). I did not observe, during the test phase, any correlations between allocentric past clockwise movement classification accuracy in any ROI and navigation performance (all $pFDRs > 0.05$).

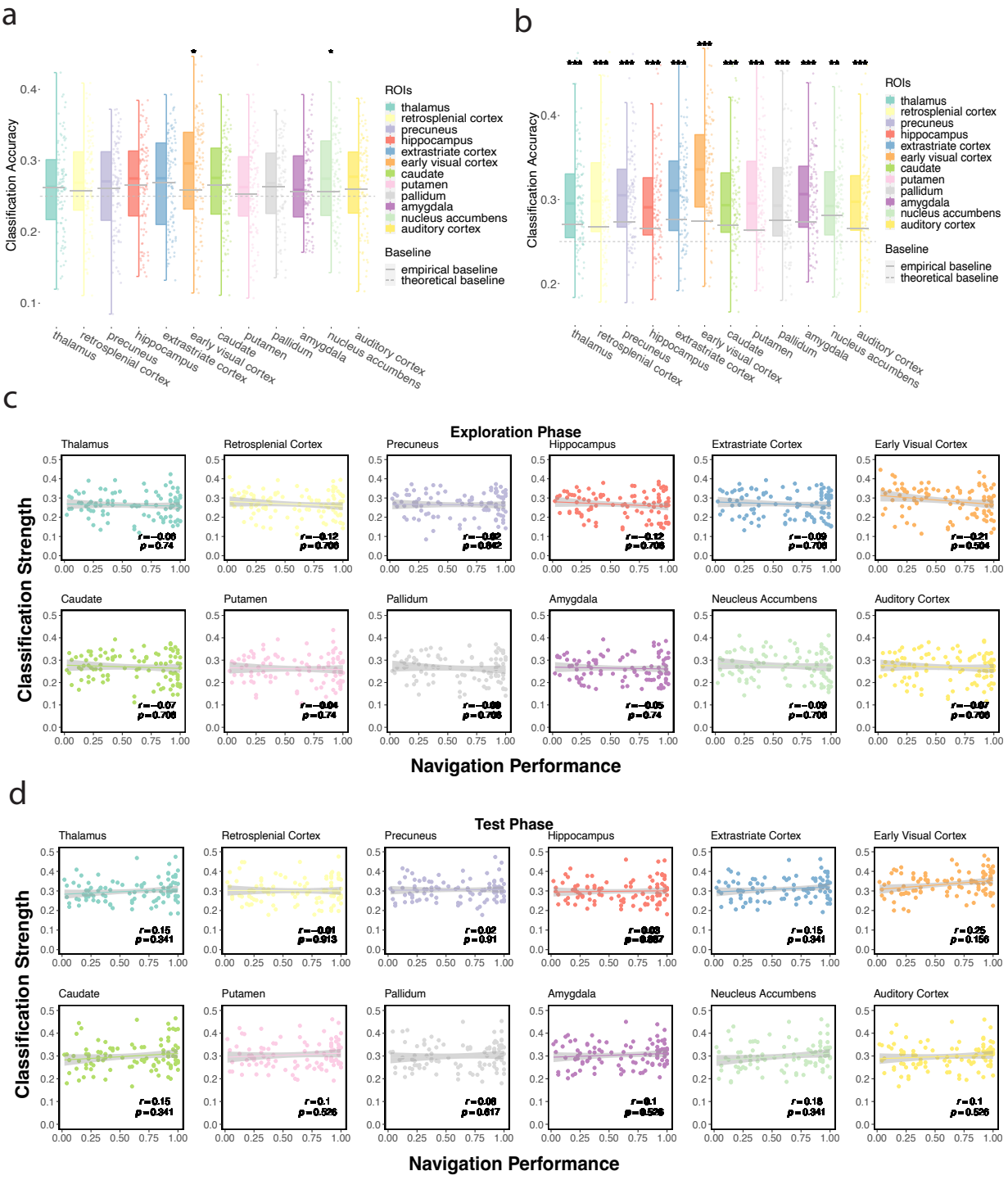
a
b
Classification Accuracy
ROIs
thalamus
retrosplenial cortex
precuneus
hippocampus
extrastriate cortex
early visual cortex
caudate
putamen
pallidum
amygdala
nucleus accumbens
auditory cortex
Baseline
empirical baseline
theoretical baseline
c
Exploration Phase
Classification Strength
Navigation Performance
Thalamus
Retrosplenial Cortex
Precuneus
Hippocampus
Extrastriate Cortex
Early Visual Cortex
Caudate
Putamen
Pallidum
Amygdala
Neucleus Accumbens
Auditory Cortex
d
Test Phase
Classification Strength
Navigation Performance

Figure 3.20: Classification accuracy for past clockwise rotations. a. Model performance for all participants in all ROIs during the exploration phase. I plot single-participant data and group-level whiskerboxplots (center, median; box, 25th to 75th percentiles; whiskers, n=98 participants). I observed classification accuracy in early visual cortex and nucleus accumbens using empirical baseline (gray solid line). Classification accuracy was observed in most ROIs (except thalamus and caudate) using theoretical baseline (gray dashed line, significance not labeled in the figure) b. similar to a., I plot model performance for all participants in all ROIs during the test phase. I observed significant classification accuracy in all ROIs. Classification accuracy was also observed in all ROIs using theoretical baseline (gray dashed line, significance not labeled in the figure) c. Correlation between classification accuracy strength and navigation performance for all participants in all ROIs during the exploration phase. Classification accuracy in the exploration phase was not related to navigation performance. d. Correlation between classification accuracy strength and navigation performance for all participants in all ROIs during the test phase. Classification accuracy in the exploration phase was not related to navigation performance.. Note: * p $<$ 0.05, ** p $<$ 0.01, *** p $<$ 0.001, FDR-corrected.

ROIs	*df*	*t*	*p*	*pFDR*	*Cohen's d*	*C.I.*
Thalamus	97	0.05	0.961	0.98	0.005	[0.25, 0.275]
Retrosplenial Cortex	97	1.43	0.155	0.444	0.145	[0.254, 0.28]
Precuneus	97	0.66	0.508	0.853	0.067	[0.252, 0.277]
Hippocampus	97	0.02	0.98	0.98	0.003	[0.253, 0.279]
Extrastriate Cortex	97	-0.09	0.926	0.98	-0.009	[0.255, 0.282]
Early Visual Cortex	97	3.37	0.001**	0.013*	0.341	[0.27, 0.3]
Caudate	97	0.57	0.569	0.853	0.058	[0.257, 0.282]
Putamen	97	1.23	0.222	0.444	0.124	[0.249, 0.274]
Pallidum	97	0.19	0.848	0.98	0.019	[0.252, 0.276]
Amygdala	97	1.23	0.221	0.444	0.124	[0.253, 0.275]
Nucleus Accumbens	97	2.88	0.005**	0.029*	0.291	[0.262, 0.287]
Auditory Cortex	97	1.32	0.188	0.444	0.134	[0.255, 0.281]

Notes: ** $p < 0.01$; * $pFDR < 0.05$

Table 3.33: Past cognitive map: model performance on allocentric clockwise rotations in the exploration phase

ROIs	*df*	*t*	*p*	*pFDR*	*Cohen's d*	*C.I.*
Thalamus	97	4.84	$< 0.001^{***}$	$< 0.001^{***}$	0.489	[0.287, 0.31]
Retrosplenial Cortex	97	5.26	$< 0.001^{***}$	$< 0.001^{***}$	0.532	[0.288, 0.314]
Precuneus	97	6.07	$< 0.001^{***}$	$< 0.001^{***}$	0.613	[0.295, 0.316]
Hippocampus	97	5.76	$< 0.001^{***}$	$< 0.001^{***}$	0.582	[0.287, 0.31]
Extrastriate Cortex	97	6.03	$< 0.001^{***}$	$< 0.001^{***}$	0.61	[0.299, 0.321]
Early Visual Cortex	97	10.12	$< 0.001^{***}$	$< 0.001^{***}$	1.022	[0.323, 0.347]
Caudate	97	4.84	$< 0.001^{***}$	$< 0.001^{***}$	0.488	[0.287, 0.312]
Putamen	97	6.98	$< 0.001^{***}$	$< 0.001^{***}$	0.706	[0.293, 0.317]
Pallidum	97	4.08	$< 0.001^{***}$	$< 0.001^{***}$	0.412	[0.288, 0.311]
Amygdala	97	5.73	$< 0.001^{***}$	$< 0.001^{***}$	0.578	[0.294, 0.315]
Nucleus Accumbens	97	3.07	0.003^{**}	0.003^{**}	0.311	[0.287, 0.311]
Auditory Cortex	97	5.69	$< 0.001^{***}$	$< 0.001^{***}$	0.575	[0.287, 0.309]

Notes: *** $p < 0.001$, ** $p < 0.01$; *** $pFDR < 0.001$, ** $pFDR < 0.01$

Table 3.34: Past cognitive map: model performance on allocentric clockwise rotations in the test phase

The past cognitive map: allocentric counterclockwise rotations To test the hypothesis that past allocentric counterclockwise rotations (i.e., north to west, west to south, south to east, and east to north) could be discriminated from signals in distributed brain areas, I conducted pattern classifications in beta series signals for each participant, separated by regions of interest (ROIs) and navigation phases (i.e., exploration and test).

For the exploration phase, I could discriminate between directions in several ROIs: retrosplenial cortex, precuneus, extrastriate cortex, early visual cortex (all $pFDRs < 0.05$) (see Fig. 3.21a, Table 3.35). Analyses using theoretical baselines only yielded the same result for early visual cortex ($pFDR = 0.013$). I then conducted correlation analyses between classification accuracy and navigation performance (see Fig. 3.21c). I did not observe any correlations, during the exploration phase, between allocentric past counterclockwise movement classification accuracy in any ROI and navigation performance (all $pFDRs > 0.05$).

For the test phase, I could only discriminate between directions in the extrastriate cortex ($pFDR = 0.002$) and early visual cortex ($pFDR < 0.001$) (see Fig. 3.21b, Table 3.36). Analyses using theoretical baselines only yielded the same results except also found significant results in retrosplenial cortex, precuneus, hippocampus, caudate, putamen, auditory cortex (all $pFDRs < 0.05$) and was marginally significant in thalamus ($pFDR = 0.050$). I then conducted correlation analyses between classification accuracy and navigation performance (see Fig. 3.21d). I did not observe any correlations, during the test phase, between allocentric past counterclockwise movement classification accuracy in any ROI and navigation performance (all $pFDRs > 0.05$).

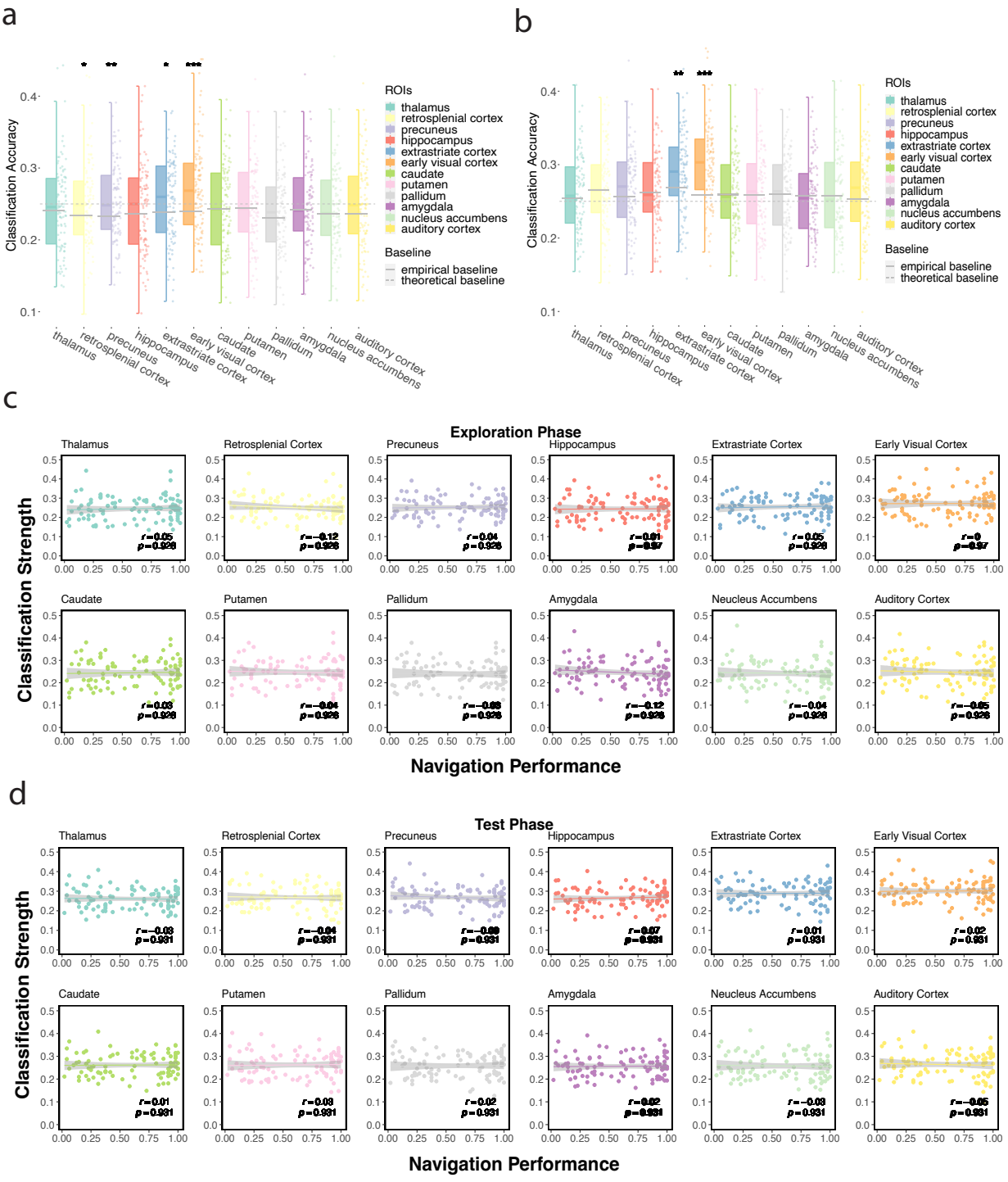
a
b
Classification Accuracy
ROIs
thalamus
retrosplenial cortex
precuneus
hippocampus
extrastriate cortex
early visual cortex
caudate
putamen
pallidum
amygdala
nucleus accumbens
auditory cortex
Baseline
empirical baseline
theoretical baseline
c
Exploration Phase
Classification Strength
Navigation Performance
Thalamus
Retrosplenial Cortex
Precuneus
Hippocampus
Extrastriate Cortex
Early Visual Cortex
Caudate
Putamen
Pallidum
Amygdala
Neucleus Accumbens
Auditory Cortex
d
Test Phase
Classification Strength
Navigation Performance

Figure 3.21: Classification accuracy past allocentric counterclockwise rotations. a. Model performance for all participants in all ROIs during the exploration phase. I plot single-participant data and group-level whiskerboxplots (center, median; box, 25th to 75th percentiles; whiskers, n=98 participants). I observed classification accuracy in retrosplenial cortex, precuneus, extrastriate cortex, and early visual cortex using empirical baseline (gray solid line). Classification accuracy was only observed in the early visual cortex using theoretical baseline (gray dashed line, significance not labeled in the figure) b. similar to a., I plot model performance for all participants in all ROIs during the test phase. I observed significant classification accuracy in the extrastriate cortex and early visual cortex. Classification accuracy was also observed in most ROIs except pallidum, amygdala, and nucleus accumbens using theoretical baseline (gray dashed line, significance not labeled in the figure) c. Correlation between classification accuracy strength and navigation performance for all participants in all ROIs during the exploration phase. Classification accuracy in the exploration phase was not related to navigation performance. d. Correlation between classification accuracy strength and navigation performance for all participants in all ROIs during the test phase. Classification accuracy in the exploration phase was not related to navigation performance.. Note: * p $<$ 0.05, ** p $<$ 0.01, *** p $<$ 0.001, FDR-corrected.

ROIs	*df*	*t*	*p*	*pFDR*	*Cohen's d*	*C.I.*
Thalamus	97	0.71	0.481	0.607	0.071	[0.233, 0.257]
Retrosplenial Cortex	97	2.67	0.009^{**}	0.027^{*}	0.27	[0.239, 0.262]
Precuneus	97	3.8	$< 0.001^{***}$	0.001^{**}	0.384	[0.242, 0.263]
Hippocampus	97	1.27	0.207	0.354	0.128	[0.231, 0.257]
Extrastriate Cortex	97	2.89	0.005^{**}	0.019^{*}	0.292	[0.244, 0.267]
Early Visual Cortex	97	5	$< 0.001^{***}$	$< 0.001^{***}$	0.505	[0.259, 0.285]
Caudate	97	0.31	0.757	0.757	0.031	[0.232, 0.257]
Putamen	97	0.36	0.719	0.757	0.036	[0.235, 0.258]
Pallidum	97	1.56	0.123	0.245	0.157	[0.228, 0.251]
Amygdala	97	0.67	0.506	0.607	0.067	[0.234, 0.257]
Nucleus Accumbens	97	0.86	0.391	0.586	0.087	[0.23, 0.253]
Auditory Cortex	97	1.83	0.071^{+}	0.17	0.184	[0.235, 0.26]

Notes: *** $p < 0.001$, ** $p < 0.01$, + $p < 0.08$; *** $pFDR < 0.001$, ** $pFDR < 0.01$, * $pFDR < 0.05$

Table 3.35: Past cognitive map: model performance on allocentric counterclockwise rotations in the exploration phase

ROIs	df	t	p	$pFDR$	$Cohen's\, d$	$C.I.$
Thalamus	97	1.41	0.163	0.391	0.142	[0.251, 0.272]
Retrosplenial Cortex	97	0.4	0.691	0.899	0.04	[0.257, 0.279]
Precuneus	97	2.08	0.04^{*}	0.16	0.21	[0.257, 0.279]
Hippocampus	97	0.66	0.512	0.899	0.066	[0.256, 0.276]
Extrastriate Cortex	97	3.73	$< 0.001^{***}$	0.002^{**}	0.377	[0.278, 0.3]
Early Visual Cortex	97	7.52	$< 0.001^{***}$	$< 0.001^{***}$	0.759	[0.29, 0.312]
Caudate	97	0.46	0.648	0.899	0.046	[0.252, 0.272]
Putamen	97	0.58	0.564	0.899	0.058	[0.251, 0.273]
Pallidum	97	-0.3	0.765	0.899	-0.03	[0.248, 0.269]
Amygdala	97	-0.22	0.824	0.899	-0.023	[0.246, 0.266]
Nucleus Accumbens	97	0.03	0.973	0.973	0.003	[0.246, 0.269]
Auditory Cortex	97	1.92	0.058	0.175	0.193	[0.253, 0.275]

Notes: *** $p < 0.001$, * $p < 0.05$; *** $pFDR < 0.001$, ** $pFDR < 0.01$

Table 3.36: Past cognitive map: model performance on allocentric counterclockwise rotations in the test phase

3.2.9 The past cognitive map: egocentric movements

To test the hypothesis that egocentric past movementss (i.e., moving forward, turning left, turning right) were still represented in the brain when people were stationarily standing at an intersection planning for the next step, I conducted pattern classification analyses for egocentric past movementss in beta series signals for each participant, separated by regions of interest (ROIs) and navigation phases (i.e., exploration and test).

For the exploration phase, I could successfully discriminate between egocentric past movementss in all ROIs (all $pFDRs < 0.05$) (see Fig. 3.22a, Table 3.37). Analyses using theoretical baselines yielded the same result. I then conducted correlation analyses between classification accuracy and navigation performance (see Fig. 3.22c). I did not observe correlation between egocentric past movement classification accuracy in any ROI and navigation performance during the exploration phase (all $pFDRs > 0.05$).

For the test phase, I successfully discriminated between egocentric past movementss in some ROIs: retrosplenial cortex, precuneus, extrastriate cortex, early visual cortex (all $pFDRs < 0.01$) (see Fig. 3.22b, Table 3.38). Analyses using theoretical baselines yielded the same result except also showing significance in all other ROIs: thalamus, hippocampus, putamen, caudate, pallidum, amygdala, nucleus accumbens, auditory cortex (all $pFDRs < 0.001$). I then conducted correlation analyses between classification accuracy and navigation performance. I observed positive correlation between navigation performance and egocentric past movement classification accuracy in all ROIs except early visual cortex ($pFDR = 0.21$) during the test phase (all rest $pFDRs < 0.05$) (see Fig. 3.22d).

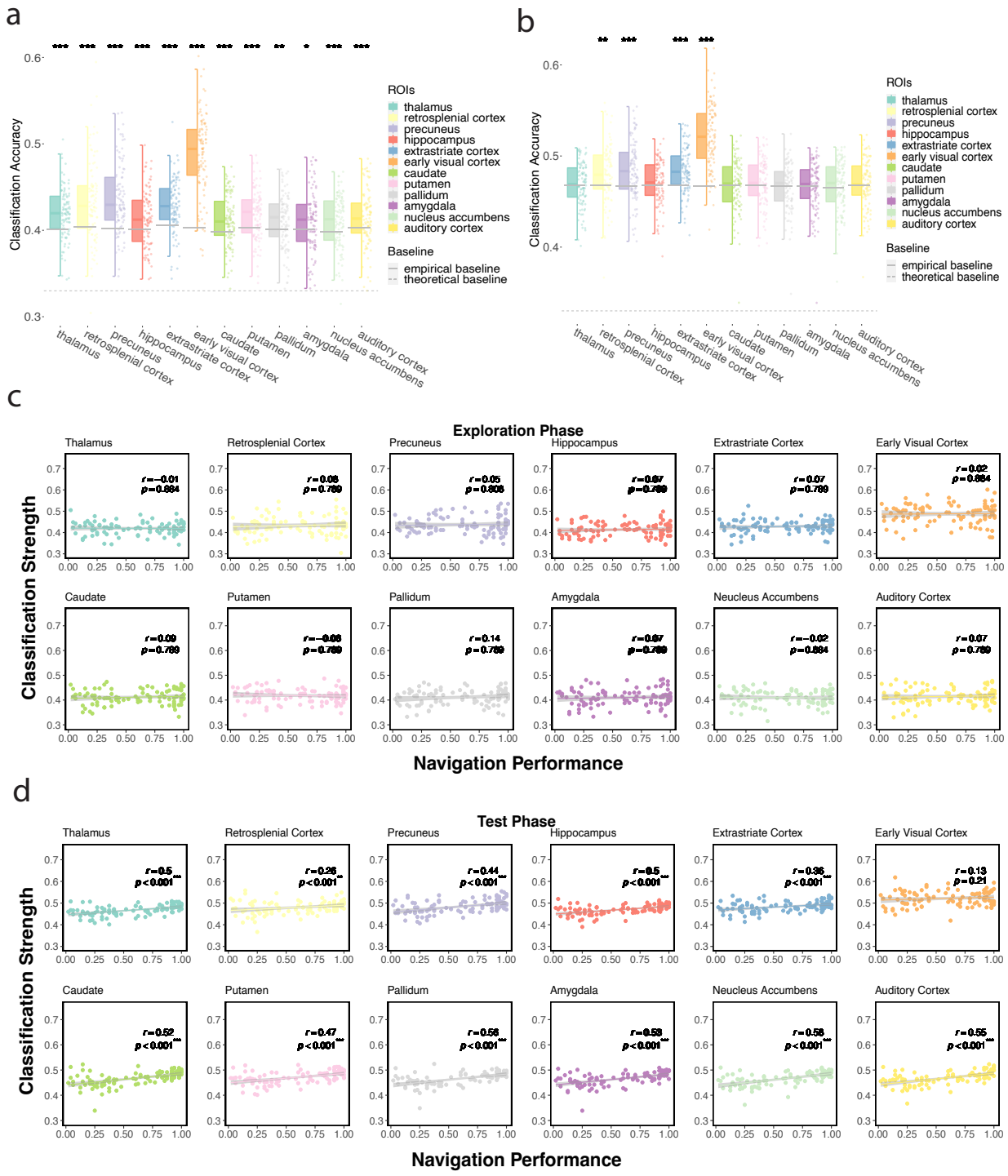
a
b
c
d
Classification Accuracy
ROIs
thalamus
retrosplenial cortex
precuneus
hippocampus
extrastriate cortex
early visual cortex
caudate
putamen
pallidum
amygdala
nucleus accumbens
auditory cortex
Baseline
empirical baseline
theoretical baseline
Exploration Phase
Test Phase
Classification Strength
Navigation Performance
Thalamus
Retrosplenial Cortex
Precuneus
Hippocampus
Extrastriate Cortex
Early Visual Cortex
Caudate
Putamen
Pallidum
Amygdala
Neucleus Accumbens
Auditory Cortex

Figure 3.22: Classification accuracy for egocentric past movementss. a. Model performance for all participants in all ROIs during the exploration phase. I plot single-participant data and group-level whiskerboxplots (center, median; box, 25th to 75th percentiles; whiskers, n=98 participants). I observed classification accuracy in all ROIs using empirical baseline (gray solid line). Classification accuracy was also observed in all ROIs using theoretical baseline (gray dashed line, significance not labeled in the figure) b. similar to a., I plot model performance for all participants in all ROIs during the test phase. I observed classification accuracy in retrosplenial cortex, precuneus, extrastriate cortex, and early visual cortex using empirical baseline. Classification accuracy was also observed in all ROIs using a theoretical baseline (significance not labeled in the figure). c. Correlation between classification accuracy strength and navigation performance for all participants in all ROIs during the exploration phase. Classification accuracy in the exploration phase was not related to navigation performance. d. Correlation between classification accuracy strength and navigation performance for all participants in all ROIs during the test phase. Classification accuracy in the test phase was positively correlated to navigation performance in thalamus, retrosplenial cortex, precuneus, hippocampus, extrastriate cortex, caudate, putamen, pallidum, amygdala, nucleus accumbens, and auditory cortex. Note: * p $<$ 0.05, ** p $<$ 0.01, *** p $<$ 0.001, FDR-corrected.

ROIs	*df*	*t*	*p*	*pFDR*	*Cohen's d*	*C.I.*
Thalamus	97	6.33	$< 0.001^{***}$	$< 0.001^{***}$	0.639	[0.414, 0.426]
Retrosplenial Cortex	97	6.35	$< 0.001^{***}$	$< 0.001^{***}$	0.641	[0.424, 0.443]
Precuneus	97	8.72	$< 0.001^{***}$	$< 0.001^{***}$	0.881	[0.429, 0.445]
Hippocampus	97	3.7	$< 0.001^{***}$	$< 0.001^{***}$	0.374	[0.407, 0.42]
Extrastriate Cortex	97	7.43	$< 0.001^{***}$	$< 0.001^{***}$	0.75	[0.423, 0.435]
Early Visual Cortex	97	18.44	$< 0.001^{***}$	$< 0.001^{***}$	1.863	[0.479, 0.497]
Caudate	97	4.42	$< 0.001^{***}$	$< 0.001^{***}$	0.447	[0.406, 0.418]
Putamen	97	5.06	$< 0.001^{***}$	$< 0.001^{***}$	0.511	[0.412, 0.424]
Pallidum	97	3.47	0.001^{**}	0.001^{**}	0.35	[0.405, 0.418]
Amygdala	97	2.6	0.011^{*}	0.011^{*}	0.263	[0.403, 0.417]
Nucleus Accumbens	97	3.74	$< 0.001^{***}$	$< 0.001^{***}$	0.377	[0.404, 0.416]
Auditory Cortex	97	3.71	$< 0.001^{***}$	$< 0.001^{***}$	0.374	[0.408, 0.421]

Notes: *** $p < 0.001$, ** $p < 0.01$, * $p < 0.05$; *** $pFDR < 0.001$, ** $pFDR < 0.01$, * $pFDR < 0.05$

Table 3.37: Past cognitive map: model performance on egocentric directions in the exploration phase

ROIs	df	t	p	$pFDR$	$Cohen's\ d$	$C.I.$
Thalamus	97	0.36	0.723	0.849	0.036	[0.464, 0.473]
Retrosplenial Cortex	97	3.88	$< 0.001^{***}$	0.001^{**}	0.392	[0.474, 0.486]
Precuneus	97	5.38	$< 0.001^{***}$	$< 0.001^{***}$	0.543	[0.478, 0.49]
Hippocampus	97	1.12	0.267	0.535	0.113	[0.466, 0.475]
Extrastriate Cortex	97	6.41	$< 0.001^{***}$	$< 0.001^{***}$	0.648	[0.479, 0.489]
Early Visual Cortex	97	15.39	$< 0.001^{***}$	$< 0.001^{***}$	1.554	[0.515, 0.529]
Caudate	97	-0.26	0.794	0.849	-0.026	[0.462, 0.473]
Putamen	97	1.47	0.144	0.346	0.149	[0.466, 0.476]
Pallidum	97	-0.48	0.635	0.849	-0.048	[0.461, 0.471]
Amygdala	97	-0.19	0.849	0.849	0.019	[0.461, 0.472]
Nucleus Accumbens	97	0.24	0.81	0.849	0.024	[0.461, 0.472]
Auditory Cortex	97	0.42	0.674	0.849	0.043	[0.464, 0.475]

Notes: *** $p < 0.001$; *** $pFDR < 0.001$, ** $pFDR < 0.01$

Table 3.38: Past cognitive map: model performance on egocentric directions in the test phase

The past cognitive map: egocentric rotations

To test the hypothesis that past egocentric rotations (i.e., left and right or counterclockwise and clockwise) could be discriminated from signals in distributed brain areas, I conducted pattern classifications in beta series signals for each participant, separated by regions of interest (ROIs) and navigation phases (i.e., exploration and test).

For the exploration phase, I could discriminate between directions in most ROIs ($pFDR < 0.05$) except retrosplenial cortex ($pFDR = 0.247$) (see Fig. 3.23a, Table 3.39). Analyses using theoretical baselines yielded the same result except also showed significance in the retrosplenial cortex ($pFDRs = 0.001$). I then conducted correlation analyses between classification accuracy and navigation performance (Figure 3.23c). I did not observe correlation between egocentric past rotations classification accuracy in any ROI and navigation performance during the exploration phase (all $pFDRs > 0.05$).

For the test phase, I could discriminate between directions in most ROIs (all $pFDRs < 0.05$) except pallidum ($pFDR = 0.57$) (see Fig. 3.23b, Table 3.40). Analyses using theoretical baselines yielded the same result except the nucleus accumbens also did not reach significance ($pFDR = 0.202$). I then conducted correlation analyses between classification accuracy and navigation performance (Figure 3.23d). I observed negative correlation between navigation performance and egocentric past movement rotational classification accuracy in extrastriate cortex ($pFDR < 0.001$) and early visual cortex ($pFDR = 0.024$).

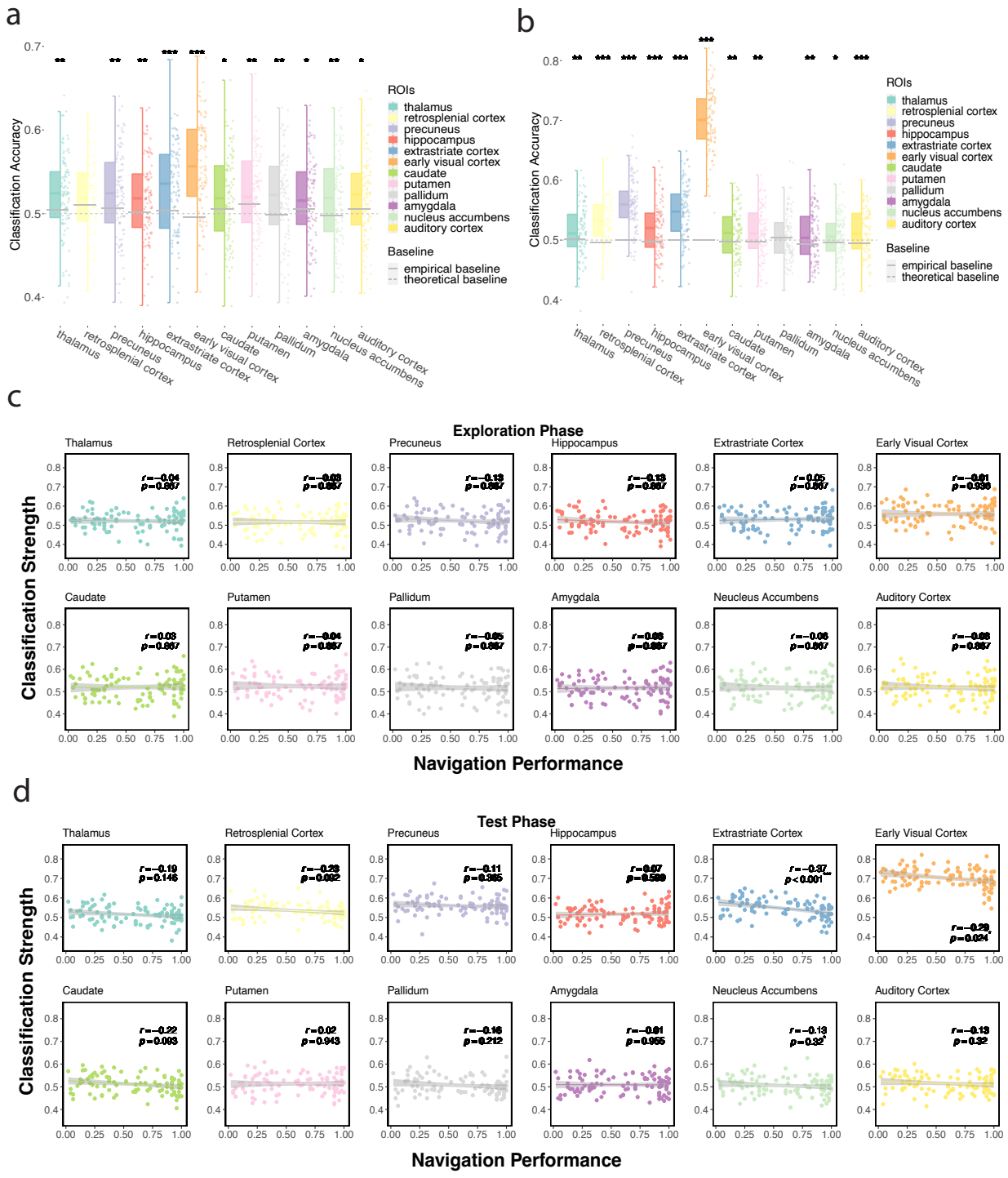
a
b
c
d
Classification Accuracy
ROIs
thalamus
retrosplenial cortex
precuneus
hippocampus
extrastriate cortex
early visual cortex
caudate
putamen
pallidum
amygdala
nucleus accumbens
auditory cortex
Baseline
empirical baseline
theoretical baseline
Exploration Phase
Test Phase
Classification Strength
Navigation Performance
Thalamus
Retrosplenial Cortex
Precuneus
Hippocampus
Extrastriate Cortex
Early Visual Cortex
Caudate
Putamen
Pallidum
Amygdala
Neucleus Accumbens
Auditory Cortex

Figure 3.23: Classification accuracy for past egocentric rotations. a. Model performance for all participants in all ROIs during the exploration phase. I plot single-participant data and group-level whiskerboxplots (center, median; box, 25th to 75th percentiles; whiskers, n=98 participants). I observed classification accuracy in most ROIs (except retrosplenial cortex) using empirical baseline (gray solid line). Classification accuracy was also observed in all ROIs using theoretical baseline (gray dashed line, significance not labeled in the figure) b. similar to a., I plot model performance for all participants in all ROIs during the test phase. I observed classification accuracy in most ROIs except pallidum using empirical baseline. Classification accuracy was also observed in most ROIs except pallidum and nucleus accumbens using a theoretical baseline (significance not labeled in the figure). c. Correlation between classification accuracy strength and navigation performance for all participants in all ROIs during the exploration phase. Classification accuracy in the exploration phase was not related to navigation performance. d. Correlation between classification accuracy strength and navigation performance for all participants in all ROIs during the test phase. Classification accuracy in the test phase was negatively correlated to navigation performance in the extrastriate cortex and early visual cortex. Note: * p $<$ 0.05, ** p $<$ 0.01, *** p $<$ 0.001, FDR-corrected.

ROIs	*df*	*t*	*p*	*pFDR*	*Cohen's d*	*C.I.*
Thalamus	97	3.46	0.001^{**}	0.002^{**}	0.349	[0.512, 0.532]
Retrosplenial Cortex	97	1.16	0.247	0.247	0.118	[0.507, 0.527]
Precuneus	97	3.01	0.003^{**}	0.006^{**}	0.304	[0.512, 0.533]
Hippocampus	97	3.1	0.003^{**}	0.005^{**}	0.314	[0.507, 0.527]
Extrastriate Cortex	97	4.97	$< 0.001^{***}$	$< 0.001^{***}$	0.502	[0.52, 0.541]
Early Visual Cortex	97	11.1	$< 0.001^{***}$	$< 0.001^{***}$	1.121	[0.548, 0.57]
Caudate	97	2.67	0.009^{**}	0.013^{*}	0.269	[0.51, 0.531]
Putamen	97	2.56	0.012^{*}	0.014^{*}	0.259	[0.514, 0.534]
Pallidum	97	3.47	0.001^{**}	0.002^{**}	0.351	[0.507, 0.528]
Amygdala	97	2.16	0.033^{*}	0.036^{*}	0.218	[0.506, 0.526]
Nucleus Accumbens	97	3.36	0.001^{**}	0.003^{**}	0.339	[0.506, 0.527]
Auditory Cortex	97	2.65	0.009^{**}	0.013^{*}	0.268	[0.509, 0.529]

Notes: *** $p < 0.001$, ** $p < 0.01$, * $p < 0.05$; *** $pFDR < 0.001$, ** $pFDR < 0.01$, * $pFDR < 0.05$

Table 3.39: Past cognitive map: model performance on egocentric rotations in the exploration phase

ROIs	*df*	*t*	*p*	*pFDR*	*Cohen's d*	*C.I.*
Thalamus	97	3	0.003^{**}	0.004^{**}	0.303	[0.505, 0.523]
Retrosplenial Cortex	97	9.44	$< 0.001^{***}$	$< 0.001^{***}$	0.953	[0.526, 0.543]
Precuneus	97	13.5	$< 0.001^{***}$	$< 0.001^{***}$	1.363	[0.551, 0.568]
Hippocampus	97	4.51	$< 0.001^{***}$	$< 0.001^{***}$	0.455	[0.509, 0.526]
Extrastriate Cortex	97	9.48	$< 0.001^{***}$	$< 0.001^{***}$	0.958	[0.536, 0.555]
Early Visual Cortex	97	39.84	$< 0.001^{***}$	$< 0.001^{***}$	4.025	[0.691, 0.712]
Caudate	97	3.18	0.002^{**}	0.003^{**}	0.322	[0.503, 0.519]
Putamen	97	3.66	$< 0.001^{***}$	0.001^{**}	0.37	[0.505, 0.522]
Pallidum	97	0.57	0.57	0.57	0.058	[0.498, 0.514]
Amygdala	97	3.72	$< 0.001^{***}$	0.001^{**}	0.375	[0.501, 0.517]
Neucleus Accumbens	97	2.16	0.033^{*}	0.036^{*}	0.218	[0.497, 0.513]
Auditory Cortex	97	4.76	$< 0.001^{***}$	$< 0.001^{***}$	0.481	[0.506, 0.522]

Notes: *** $p < 0.001$, ** $p < 0.01$, * $p < 0.05$; *** $pFDR < 0.001$, ** $pFDR < 0.01$, * $pFDR < 0.05$

Table 3.40: Past cognitive map: model performance on egocentric rotations in the test phase

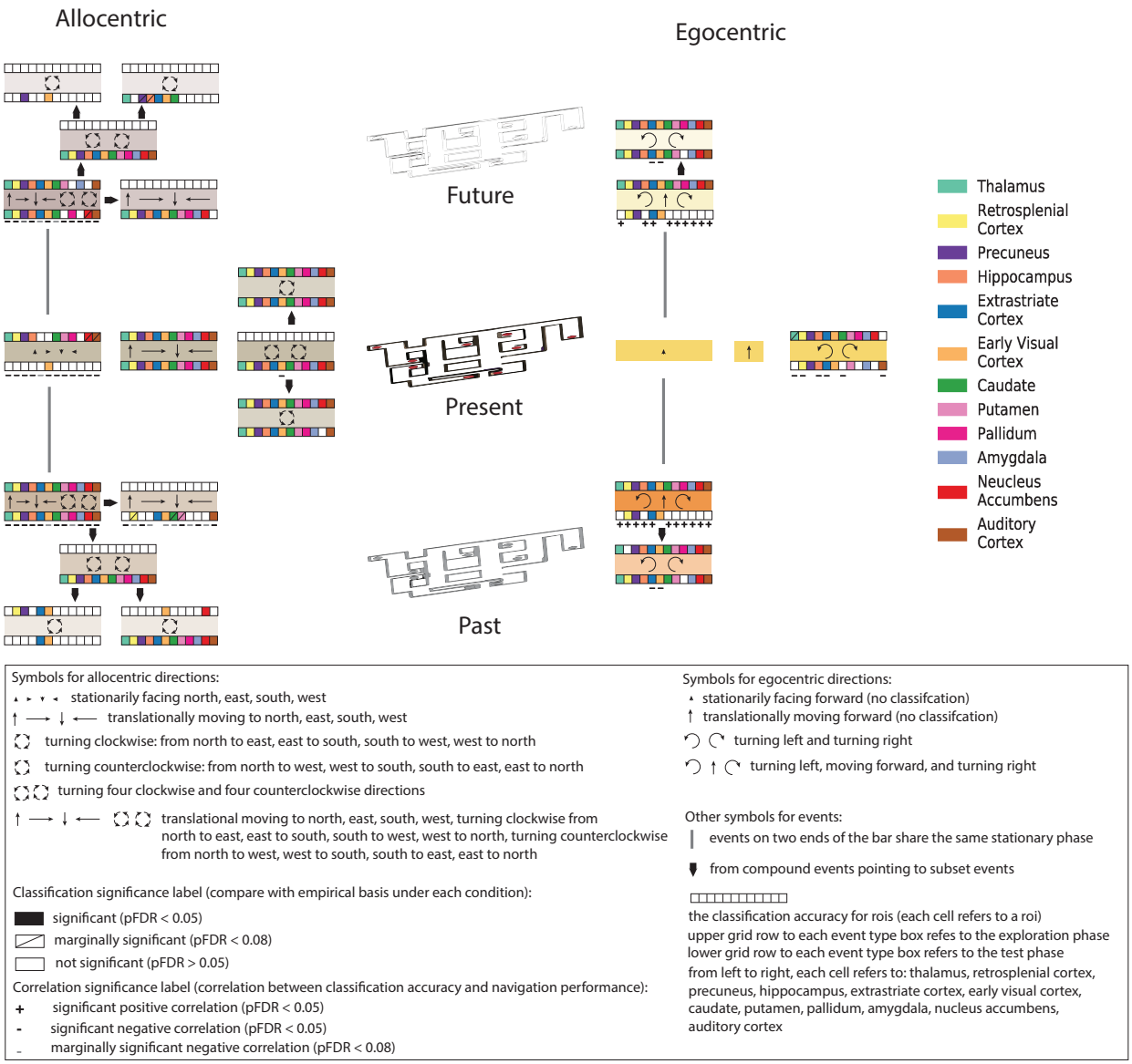

Figure 3.24: Result summary.

3.3 Discussion

In this study, I investigated the distributed head and travel direction representations in the human brain by testing a large group of people (N = 98) actively navigating in a complex virtual environment during fMRI scanning. My model successfully classified both egocentric and allocentric signals. I observed no correlation between classification accuracy and individual navigation performance during the exploration phase, suggesting behavior-independent processes for direction representation during learning when these directional signals could still be emerging. In contrast, I observed correlations between classification accuracy and navigation performance in the test phase, revealing a behavior-dependent process in direction representation. Notably, good navigators have signals that relate to egocentric movements, suggesting that they have converted this information into actionable trajectories, particularly in the past and future.

3.3.1 Signals were detected in the stationary period, but this leaves open questions

The basic question of whether allocentric head directions could be classified might be best addressed by using the stationary phase of the present map. This is supported by an extensively studied pathway for encoding static sense of direction found in rodents (Cullen & Taube, 2017; Yoder & Taube, 2014). Therefore, I first classified the directions where people were facing at the moment during the stationary time period.

During the exploration phase, I could successfully discriminate between allocentric stationary facing directions in some ROIs (thalamus, retrosplenial cortex, precuneus, hippocampus, caudate, putamen, pallidum, and marginally significant in nucleus accumbens and auditory cortex), which replicate previous studies that reported allocentric direction representation in thalamus (Shine et al., 2016), retrosplenial cortex (Shine et al., 2016), and pre-subiculum (hippocampal region)(Vass & Epstein, 2013). During the test phase, however, I could only

successfully discriminate between allocentric stationary facing directions in the early visual cortex, and the classification accuracy was negatively correlated with navigation performance. When considering the exploration phase as cognitive map formation process and the test phase as a cognitive map implementation process, the negative correlation in the early visual cortex in the test phase may indicate that bad navigators were still learning the environment during the test phase. What is interesting and unexpected to me is the result of a weak representation of stationary facing directions (i.e., classification only significant in the early visual cortex) during the test phase. To better understand the stationary phase, I proposed three possible explanations which may independently or simultaneously contribute to the weak representation of head direction signals during the test phase.

The first possibility is the influence of movements in active navigation. Unlike previous studies which classified head direction signals purely on static images (Shine et al., 2016; Vass & Epstein, 2013), our task also has movement periods (i.e., translating or rotating). In rodent studies, two main thalamocortical pathways were found to transmit vestibular information to cortex: the anterior pathway and the posterior pathway (Cullen & Taube, 2017). The anterior pathway was thought to encode head direction signals during static phase or passive motion, but was suppressed during active motion (Cullen & Taube, 2017; Taube & Bassett, 2003). Instead, the posterior pathway, which takes multisensory inputs (including optic flow) instead of purely vestibular input, seems to dominate in detecting active self-motion (Clark & Harvey, 2016; Cullen, 2011, 2012; Cullen & Taube, 2017; Guldin & Grüsser, 1998). Further, visual motion cues were found to influence head direction signals in rodents (Arleo et al., 2013; Blair & Sharp, 1996; Medrea & Cullen, 2013) and humans (Nau et al., 2020). In our task, because each stationary period came after or was followed by a movement period, the static head direction representation could be suppressed. During the exploration phase, the brain may still be updating the head direction network in matching expected sensory feedback to the actual sensory feedback (with only visual input in fMRI) in active navigation in addition to learning the environment, leading to less suppression of

the static head direction network than in the test phase. Therefore, I discriminated head and travel direction signals in ROIs during movement periods. To further understand the role of reference frame in head direction representations, I discriminated movement signals (especially rotations) based on allocentric and egocentric reference frames.

The second possibility for the weak classification accuracy during the stationary periods in the test phase is that ROIs were mainly involved in planning for the *next step*, instead of telling what the *current* direction someone is facing. Further, I speculate if different reference frames could be relied on alternatively or simultaneously in predicting future movements.

The third possibility is that ROIs were mainly involved in tracking the *previous step*, instead of telling what the *current* direction someone is facing. Further, I speculate if different reference frames could be relied on alternatively or simultaneously in tracking past movements.

3.3.2 What about if we move?

I first looked at translations and rotations during present movement. As a result, I could discriminate between directions in movement periods during both exploration and test phases, but the involvement of reference frames seemed to switch dynamically between exploration and test phases across ROIs.

During the exploration phase, I could discriminate between directions in allocentric representations (including allocentric translations, allocentric clockwise rotations, and allocentric counterclockwise rotations) in all ROIs and egocentric representations (i.e., egocentric rotations) in most ROIs. Interestingly, for movement that may involve both reference frames (i.e., in a combination of clockwise and counterclockwise rotations, a turning north to east rotation may be classified allocentrically as a north to east turn or egocentrically as a left turn), the classification was not successful in any ROI. It remains elusive what is happening when the two reference frames have a potential interaction. No correlation was observed

between classification accuracy and navigation performance, suggesting common processes during the exploration phase when head direction signals are emerging.

During the test phase, I could still discriminate between directions in allocentric representations in most ROIs and there seemed to be a variation of egocentric representations across ROIs. More specifically, I could discriminate between directions within egocentric rotations for some ROIs, but not others (thalamus, caudate, pallidum, and nucleus accumbens). Among the ROIs where I could discriminate successfully, the classification accuracy was either negatively related to navigation performance in some ROIs (retrosplenial cortex, hippocampus, extrastriate cortex) or there no correlation in other ROIs (precuneus, early visual cortex, amygdala, and auditory cortex). In contrast to the exploration phase, during the test phase I observed successful classification in combined clockwise and counterclockwise rotations for all ROIs, which may indicate more of an interaction between the two reference frames to increase the flexibility of utilizing navigation strategies.

3.3.3 What about the future?

I next addressed the question of whether the unusal findings in the stationary period could be explained by the past and future path trajectories. For both exploration and test phases, future movements could be discriminated from signals in the stationary period, supporting previous studies about the future cognitive map (T. I. Brown et al., 2016; Dragoi & Tonegawa, 2011; Hassabis et al., 2009; Johnson & Redish, 2007; Spiers & Gilbert, 2015; Wikenheiser & Redish, 2015). The allocentric reference frame was not strongly observed during exploration, but was observed during the test. The egocentric reference frame was observed during both exploration and test.

During the exploration phase, I could not discriminate between directions in any ROIs for purely allocentric future movements (including allocentric translations, allocentric clockwise rotations, and allocentric counterclockwise rotations) but could discriminate between direc-

tions in all ROIs for purely egocentric future movements (including combined egocentric translations and rotations, and egocentric rotations). Inconsistent findings were observed for classification of directions that may involve both reference frames. More specifically, I could discriminate between directions in most ROIs for combined allocentric translations and rotations but could not discriminate between directions in combined clockwise and counterclockwise rotations in any ROIs.

During the test phase, for purely allocentric future movements, I could discriminate between directions in most ROIs for allocentric translations, in some ROIs for allocentric clockwise rotations and counterclockwise rotations. For purely egocentric future movements, I could only discriminate between directions in some ROIs for combined egocentric translations and rotations, and most ROIs for egocentric rotations. The results indicates that some regions (all subcortical ROIs: thalamus, hippocampus, caudate, putamen, pallidum, amygdala, nucleus accumbens, and auditory cortex) may no longer keep a representation of future egocentric translations in the test phase. The classification accuracy for combined egocentric translations and rotations was positively correlated with navigation performance, indicating that egocentric information may have been converted into actionable trajectories.

For classification of movements that may involve both reference frames, I could discriminate between directions in most ROIs for combined allocentric translations and rotations and in all ROIs for combined clockwise and counterclockwise rotations. This classification accuracy for combined allocentric translations and rotations was negatively correlated with navigation performance, which may suggest that the interaction between two reference frames is behavior-dependent.

3.3.4 What about the past?

For both exploration and test phases, past movements could be discriminated from signals in the stationary period, supporting previous studies about the past cognitive map (Wilson &

McNaughton, 1994). The allocentric reference frame was weakly observed during exploration, but was more strongly observed during the test. The egocentric reference frame was observed during both the exploration and test.

During the exploration phase, for purely allocentric past movements, I could discriminate between directions in some ROIs for rotations (clockwise or counterclockwise separately), but not in any ROIs for translations. For purely egocentric past movements, I could discriminate between directions in all ROIs for combined egocentric translations and rotations, and in most ROIs for egocentric rotations. For movements that could be classified with both reference frames, I could discriminate between directions in all ROIs for combined allocentric translations and rotations, but not in any ROIs in combined clockwise and counterclockwise rotations. The classification accuracy for combined egocentric translations and rotations was positively correlated with navigation performance, indicating that egocentric information may have been converted into actionable trajectories.

During the test phase, for purely allocentric past movements, I could discriminate between directions in some ROIs for translations, all ROIs for clockwise rotations, and some ROIs for counterclockwise rotations. For purely egocentric past movements, I could discriminate between directions in some ROIs for combined egocentric translations and rotations, and most ROIs for egocentric rotations. This indicates that some regions (all subcortical ROIs: thalamus, hippocampus, caudate, putamen, pallidum, amygdala, nucleus accumbens, and auditory cortex) may no longer keep representations of past egocentric translational movements in the test phase, especially that the pallidum no longer keep representation of both past egocentric translations and rotations in the test phase. For movements that could be classified with both reference frames, I could discriminate between directions in all ROIs for combined allocentric translations and rotations and in all ROIs for combined clockwise and counterclockwise rotations. Since the classification accuracy for combined allocentric translations and rotations was negatively correlated with navigation performance, it may

suggest that the interaction between two reference frames is behavior-dependent.

3.3.5 Common direction signals in the exploration phase and individual signals in the test phase

Across all analyses, I observed no individual differences during the exploration phase. I speculate three possible explanations. First, head and travel direction signals may still be emerging when people navigate the novel environment, thus the signal was still behavior-independent. Second, more specific to fMRI scanning, the brain may still be updating the head direction network in matching the expected sensory feedback to the actual sensory feedback (with only visual input in fMRI) in active motion (Brooks, Carriot, & Cullen, 2015; Cullen & Taube, 2017). Third, an additional strategy - *landmarks* (which could be categorized as a subtype of egocentric strategy because of the visual information about their relationship to the navigator) may actually be mainly utilized during the exploration phase for learning the environment. This might be possible because in our task (see Figure 3.1), there were four pictures hanging in the major hallways to guide directions. Whether there were individual differences in representing landmarks during explortion is beyond the scope for this study, but will be worth looking at for future research.

In contrast, I observed individual differences in different ROIs during the test phase. More specifically, for the present cognitive map, negative correlations between classification accuracy and navigation performance were observed in purely allocentric representations (allocentric stationary facing directions), purely egocentric representations (egocentric rotations), and the interaction between the two reference frames (combined clockwise and counterclockwise rotations). For the future cognitive map, negative correlations between classification accuracy and navigation performance were observed in egocentric rotations (for discriminating between left and right rotations), and interactions between the two reference frames (combined allocentric translational and rotational directions). For the past cognitive map,

negative correlations between classification accuracy and navigation performance were observed in allocentric translations, egocentric rotations, and interactions between the two reference frames (combined allocentric translational and rotational directions). Interestingly, for both past and future cognitive maps, positive correlations between classification accuracy and navigation performance were observed in a purely egocentric representation: the combined egocentric translations and rotations. This indicates that good navigators have signals that relate to egocentric movements, suggesting that they have converted this information into actionable trajectories, particularly in the past and future.

3.4 Conclusion

In this study, I observed widely distributed and dynamic representations of head and travel direction signals in the human brain when people actively navigate a complex, naturalistic environment. My results suggested dynamic involvement of egocentric and allocentric reference frames in directional representations during active navigation, possibly supporting flexible navigation. Further, the model detects the representation of multiple cognitive maps that has direction information for past, present, and future. Interestingly, I observed individual differences in the test phase, but not the environmental learning phase. Notably, during the test phase, good navigators have signals that relate to egocentric movements, suggesting that they have converted this information into actionable trajectories, particularly when considering their previous and upcoming movements. Together, these findings bring a more complete and nuanced understanding of how people learn new environments and use that knowledge to successfully navigate.

3.5 STAR Methods

3.5.1 Key resources table

REAGENT or RESOURCE	SOURCE	IDENTIFIER
Deposited Data		
Raw data	This paper	
Schaefer cortical atlas	(Schaefer et al., 2018)	https://github.com/ThomasYeoLab/CBIG/tree/master/stable_projects/brain_parcellation/Schaefer2018_LocalGlobal
Harvard-Oxford subcortical atlas	(Desikan et al., 2006; Frazier et al., 2005; Goldstein et al., 2007; Makris et al., 2006)	https://identifiers.org/neurovault.image:1700
NiBetaSeries	(J. Kent & Herholz, 2019)	https://nibetaseries.readthedocs.io/
Software and Algorithms		
RStudio 1.4		https://www.rstudio.com/
Python 3.0		https://www.python.org/
fMRIPrep	(Esteban, Blair, et al., 2018; Esteban, Markiewicz, et al., 2018)	https://fmriprep.org/
NiBetaSeries	(J. Kent & Herholz, 2019)	https://nibetaseries.readthedocs.io/
nilearn	(Abraham et al., 2014)	https://nilearn.github.io/
Scikit-learn	(Pedregosa et al., 2011)	https://scikit-learn.org/
NiBabel	(Brett et al., 2020)	https://nipy.org/nibabel/
NLTools		https://nltools.org/

3.5.2 Subject details

113 participants were recruited through previous studies, campus flyers, or word of mouth. Participants were pre-screened for neurological disease, psychotropic medication, and MRI safety compliance. Fifteen of those recruited failed to complete the experiment. Of these, five participants failed to schedule/show up the scan portion of the experiment, one subject was discarded due to technical issues, and nine subjects could not complete the study due to motion sickness or problems being in the MRI machine (e.g. claustrophobia). Thus, the final analyzed dataset consisted of 98 participants (45 females, 53 males; age 18-37, mean = 20.70, s.d = 3.15; two participants' behavioral data lacked one test phase block due to technical error during data collection).

3.5.3 Methods Details

Virtual environments and navigation interface

The desktop virtual maze environment (Figure 3.1A) was adapted from tasks the lab has used previously (Chrastil & Warren, 2013, 2014, 2015) and was designed to produce a wide range of performance. The environment consisted of several main hallways with branch alcoves containing nine target objects. Paintings on the walls of hallways served as landmarks to aid in orientation. Participants pressed arrow keys to move around the environment, with translations fixed at 1.0 m/s (virtual meters/second) and rotation speed fixed at 90° per second. Movement was gated such that the button press at each choice point caused visual movement to the next choice point. This was achieved by recording videos of the movement between locations. The correct video would play based on the person's location, facing direction, and the choice they made (left turn, right turn, or straight). A static image of each choice point was created by taking the first image of each video and adding the arrows of the potential choices in Photoshop (Adobe). The maze was created in Blender and rendered in Unity. The lab recorded videos from Unity and presented the experiment using E-Prime

(Psychology Software Tools) software.

Behavioral task

The Maze Learning Task was designed to assess the ability to learn the graph structure of an environment—the paths and connections between locations (Chrastil & Warren, 2014, 2015). A video example of a test trial is available online at https://www.youtube.com/watch?v=LMsGpo2Ss7M.

Exploration phase Participants navigated the virtual environment for 16 minutes, during two 8-minute fMRI scan runs, using a button box to make right or left turns or straight movement (Figure 3.1A and 3.1B). All participants were instructed to find all of the objects and learn their locations. Four different start locations were used; the start location was counterbalanced for each participant for each of the two runs.

Test phase Acquired spatial knowledge was tested on each trial by starting participants at one object in the maze, and then directing them to travel, via the shortest route, to another object using the hallways of the maze. Participants then used the button box to move through the maze like they did in the exploration phase, pressing a button when they thought they reached the target object. Feedback was minimized by changing all of the objects in the maze (including the start and target objects) into red spheres during test (Figure 3.1A and Figure 3.1C), although the landmark paintings in the hallway remained. The participant could be instructed either to "Start at the spaceship, go to the clock", or to "Go to the clock, start at the spaceship" and were informed of the subtle differences in wording prior to starting the trials. The start and target objects were each displayed for between 3-5 seconds, with the specific timing drawn from a random distribution in the range. This task tests graph knowledge (Chrastil & Warren, 2014, 2015) because it requires knowing the connections of the hallways to reach the target without necessarily knowing the metric distances and angles between locations. Trials had a 45 second time limit. When the

participant made a selection or when time expired, a 6-second (with random jitter) inter-trial interval began.

Procedure One day prior to imaging, participants were greeted in the lab and were given information about the study. They signed consent forms indicating their consent to participate in the study and completed several paper and pencil spatial abilities tasks.

The following day at the scanner, participants were given instructions about how to use the controller and given a short practice in a different environment to show them how the movement worked. They were instructed to find all the objects and learn their locations.

Participants changed into scrubs and were shown the scanning equipment. After aligning the participant in the scanner and ensuring their comfort, including giving them earplugs and cushions, the scan session began. The first set of anatomical scans was collected (see Image Acquisition), then the experimental task began.

Participants completed two 8-minute scan runs where they were free to explore the maze. At the end of the first run, participants were informed of how many objects they located and how many were left undiscovered.

After the learning phase, participants were given instructions for the test trials. They completed 6 blocks consisting of 8 trials each (total = 48 trials). With nine objects in the maze, a full permutation of all start and target pairs yielded 72 possible trials. However, due to time constraints, a subset of 48 trials was used for each participant. Three lists of trials were used, each with 2/3 of the possible trials. Each participant followed one of the lists. The trial list was presented in random order for each participant.

Navigation metrics

Accuracy Subjects were scored by their proportion of correct trials. Trials were considered "correct" if the participant ended at the target object, regardless of whether they pressed the "selection" button or whether they ran out of time when just reaching the target. Proportion correct scores ranged from around chance performance (chance is defined as .111, or ending at 1 out of the 9 possible target objects) to perfect. Very few participants were correct on every trial (n=4).

Allocentric stationary facing directions Based on each subject's individual behavioral travel trajectory, I constructed design matrices for subjects' stationary facing directions. There were 4 stationary facing directions: experiencing standing still at an intersection, *facing north, south, east or west*. Notice that the directions were arbitrarily defined, but different labels should not affect our analyses. Because subjects were freely moving in the maze in both the learning and test phases, I did not expect any two subjects would share the same trajectory. Therefore, I constructed one design matrix for the exploration phase (i.e., learning phase) and one design matrix for the test phase separately for each subject. [2]

Allocentric translations Based on each subject's individual behavioral travel trajectory, I constructed design matrices for subjects' translations. There were 4 translations: *moving toward the north, south, east or west directions*. More specifically, I constructed one design matrix for the exploration phase (i.e., learning phase) and one design matrix for the test phase separately for each subject. [3]

[2] I did not construct a design matrix for egocentric stationary facing directions or egocentric translations because there was only one egocentric stationary facing direction (facing forward) and one egocentric translations direction (moving forward). Also, because the maze environment is largely grid-based, almost all of the turns were 90°, so I did not analyze the very few 180° turning events (i.e., south to north, east to west, typically at dead ends) in the analyses.

[3] See footnote 2

Allocentric rotations Based on each subject's individual behavioral travel trajectory, I constructed design matrices for subjects' allocentric rotations. There were 8 allocentric rotations: *turning from north to east, east to south, south to west, west to north, north to west, west to south, south to east, and east to north*[4]. More specifically, I constructed one design matrix for the exploration phase (i.e., learning phase) and one design matrix for the test phase separately for each subject.

Egocentric rotations Based on each subject's individual behavioral travel trajectory, I constructed design matrices for subjects' egocentric rotations. There were 2 egocentric rotations: *turning left (counterclockwise) and turning right (clockwise).* More specifically, I constructed one design matrix for the exploration phase (i.e., learning phase) and one design matrix for the test phase separately for each subject.

Allocentric future movements Based on each subject's individual behavioral travel trajectory, I constructed design matrices for subjects' allocentric future movements during the decision making stage (i.e., when subjects were standing at an intersection deciding where to go next). There were 12 allocentric future movements: *moving straight north, south, east, west, or turning from north to east, east to south, south to west, west to north, north to west, west to south, south to east, and east to north*[5]. More specifically, I constructed one design matrix for the exploration phase (i.e., learning phase) and one design matrix for the test phase separately for each subject.

Egocentric future movements Based on each subject's individual behavioral travel trajectory, I constructed design matrices for subjects' egocentric future movements (i.e., when subjects were standing at an intersection deciding where to go next). There were 3 egocentric future movements: *moving forward, turning left (counterclockwise), or turning right (clockwise).* More specifically, I constructed one design matrix for the exploration phase (i.e.,

[4]See footnote 2
[5]See footnote 2

learning phase) and one design matrix for the test phase separately for each subject.

Allocentric past movements Based on each subject's individual behavioral travel trajectory, I constructed design matrices for subjects' allocentric past movementss during the decision making stage (i.e., when subjects were standing at an intersection deciding where to go next right after finishing the past movement). There were 12 allocentric past movementss: *moving north, south, east, west, or turning from north to east, east to south, south to west, west to north, north to west, west to south, south to east, and east to north*[6]. More specifically, I constructed one design matrix for the exploration phase (i.e., learning phase) and one design matrix for the test phase separately for each subject.

Egocentric past movements Based on each subject's individual behavioral travel trajectory, I constructed design matrices for subjects' egocentric past movementss (i.e., when subjects were standing at an intersection deciding where to go next, right after finishing a past movement). There were 3 egocentric past movementss: *moving forward, turning left, or turning right*. More specifically, I constructed one design matrix for the exploration phase (i.e., learning phase) and one design matrix for the test phase separately for each subject.

fMRI acquisition

MRI imaging was conducted on a 3.0T Siemens Prisma magnetic resonance imaging system at the UC Santa Barbara Brain Imaging Center using a 64-channel head coil. At the beginning of the scan session, approximately twenty minutes of anatomical scans were acquired, including a magnetization-prepared, rapid-acquisition gradient-echo (MPRAGE) T1 weighted sequence image (TR = 2500ms, TE = 2.2ms, 7° flip angle, FOV 256mm × 256mm, voxel size 0.9mm × 0.9mm × 0.9mm), field maps, and one scan of diffusion weighted images. A 7-minute task-free resting state functional scan was also acquired. Following this, two 8-minute task-based functional scans of the exploration phase of the maze task and six sets of

[6]See footnote 2

task-based functional scans were acquired for the testing phase of the maze task; this section lasted approximately 40-50 minutes. After the task, another twenty minutes of anatomical scans were collected, including a second set of diffusion weighted images, and several T2 weighted images. The functional images analyzed here were obtained as part of the larger study consisting of both fMRI and anatomical images; the anatomical portion (i.e., diffusion images and T2) and resting state data are not analyzed or reported here.

fMRI preprocessing

Results included in this manuscript come from preprocessing performed using *fMRIPrep* 1.5.10 (RRID:SCR_016216, Esteban, Blair, et al., 2018; Esteban, Markiewicz, et al., 2018), which is based on *Nipype* 1.4.2 (RRID:SCR_002502, K. Gorgolewski et al., 2011; K. J. Gorgolewski et al., 2018).

Anatomical data preprocessing The T1-weighted (T1w) image was corrected for intensity non-uniformity (INU) with `N4BiasFieldCorrection` (Tustison et al., 2010), distributed with ANTs 2.2.0 (Avants, Epstein, Grossman, & Gee, 2008, RRID:SCR_004757), and used as T1w-reference throughout the workflow. The T1w-reference was then skull-stripped with a *Nipype* implementation of the `antsBrainExtraction.sh` workflow (from ANTs), using OASIS30ANTs as target template. Brain tissue segmentation of cerebrospinal fluid (CSF), white-matter (WM) and gray-matter (GM) was performed on the brain-extracted T1w using `fast`
(FSL 5.0.9, RRID:SCR_002823, Y. Zhang, Brady, & Smith, 2001). Brain surfaces were reconstructed using `recon-all` (FreeSurfer 6.0.1, RRID:SCR_001847, Dale, Fischl, & Sereno, 1999), and the brain mask estimated previously was refined with a custom variation of the method to reconcile ANTs-derived and FreeSurfer-derived segmentations of the cortical gray-matter of Mindboggle (RRID:SCR_002438, Klein et al., 2017). Volume-based spatial normalization to one standard space (MNI152NLin2009cAsym) was performed through nonlinear

registration with `antsRegistration` (ANTs 2.2.0), using brain-extracted versions of both T1w reference and the T1w template. The following template was selected for spatial normalization: *ICBM 152 Nonlinear Asymmetrical template version 2009c* (RRID:SCR_008796, Fonov, Evans, McKinstry, Almli, & Collins, 2009, TemplateFlow ID:MNI152NLin2009cAsym).

Functional data preprocessing For each of the 9 BOLD runs found per subject (across all tasks and sessions), the following preprocessing was performed. First, a reference volume and its skull-stripped version were generated using a custom methodology of *fMRIPrep*. A B0-nonuniformity map (or fieldmap) was estimated based on a phase-difference map calculated with a dual-echo GRE (gradient-recall echo) sequence, processed with a custom workflow of SDCFlows inspired by the epidewarp.fsl script and further improvements in HCP Pipelines (Glasser et al., 2013). The fieldmap was then co-registered to the target EPI (echo-planar imaging) reference run and converted to a displacements field map (amenable to registration tools such as ANTs) with FSL's fugue and other SDCflows tools. Based on the estimated susceptibility distortion, a corrected EPI (echo-planar imaging) reference was calculated for a more accurate co-registration with the anatomical reference. The BOLD reference was then co-registered to the T1w reference using `bbregister` (FreeSurfer) which implements boundary-based registration (Greve & Fischl, 2009). Co-registration was configured with six degrees of freedom. Head-motion parameters with respect to the BOLD reference (transformation matrices, and six corresponding rotation and translation parameters) are estimated before any spatiotemporal filtering using `mcflirt` (FSL 5.0.9, Jenkinson, Bannister, Brady, & Smith, 2002). The BOLD time-series (including slice-timing correction when applied) were resampled onto their original, native space by applying the transforms to correct for head-motion. These resampled BOLD time-series will be referred to as *preprocessed BOLD in original space*, or just *preprocessed BOLD*. BOLD runs were slice-time corrected using 3dTshift from AFNI 20160207 (Cox & Hyde, 1997, RRID:SCR_005927). The BOLD time-series, were resampled to surfaces on the following spaces: fsaverage5. The BOLD time-series

(including slice-timing correction when applied) were resampled onto their original, native space by applying a single, composite transform to correct for head-motion and susceptibility distortions. These resampled BOLD time-series will be referred to as preprocessed BOLD in original space, or just preprocessed BOLD. The BOLD time-series were resampled into standard space, generating a preprocessed BOLD run in *MNI152NLin2009cAsym space*. First, a reference volume and its skull-stripped version were generated using a custom methodology of *fMRIPrep*. Several confounding time-series were calculated based on the *preprocessed BOLD*: framewise displacement (FD), DVARS and three region-wise global signals. FD and DVARS are calculated for each functional run, both using their implementations in *Nipype* (following the definitions by Power et al., 2014). The three global signals are extracted within the CSF, the WM, and the whole-brain masks. Additionally, a set of physiological regressors were extracted to allow for component-based noise correction (*CompCor*, Behzadi, Restom, Liau, & Liu, 2007). Principal components are estimated after high-pass filtering the *preprocessed BOLD* time-series (using a discrete cosine filter with 128s cut-off) for the two *CompCor* variants: temporal (tCompCor) and anatomical (aCompCor). tCompCor components are then calculated from the top 5% variable voxels within a mask covering the subcortical regions. This subcortical mask is obtained by heavily eroding the brain mask, which ensures it does not include cortical GM regions. For aCompCor, components are calculated within the intersection of the aforementioned mask and the union of CSF and WM masks calculated in T1w space, after their projection to the native space of each functional run (using the inverse BOLD-to-T1w transformation). Components are also calculated separately within the WM and CSF masks. For each CompCor decomposition, the k components with the largest singular values are retained, such that the retained components' time series are sufficient to explain 50 percent of variance across the nuisance mask (CSF, WM, combined, or temporal). The remaining components are dropped from consideration. The head-motion estimates calculated in the correction step were also placed within the corresponding confounds file. The confound time series derived from head motion

estimates and global signals were expanded with the inclusion of temporal derivatives and quadratic terms for each (Satterthwaite et al., 2013). Frames that exceeded a threshold of 0.5 mm FD or 1.5 standardised DVARS were annotated as motion outliers. All resamplings can be performed with *a single interpolation step* by composing all the pertinent transformations (i.e. head-motion transform matrices, susceptibility distortion correction when available, and co-registrations to anatomical and output spaces). Gridded (volumetric) resamplings were performed using `antsApplyTransforms` (ANTs), configured with Lanczos interpolation to minimize the smoothing effects of other kernels (Lanczos, 1964). Non-gridded (surface) resamplings were performed using `mri_vol2surf` (FreeSurfer).

Many internal operations of *fMRIPrep* use *Nilearn* 0.6.2
(Abraham et al., 2014, RRID:SCR_001362), mostly within the functional processing workflow. For more details of the pipeline, see the section corresponding to workflows in *fMRIPrep*'s documentation.

3.5.4 Beta series correlation analysis

Functional connectivity analyses were conducted using the beta series correlation analysis method (Rissman, Gazzaley, & D'Esposito, 2004), which has been used for previous navigation studies (T. I. Brown, Ross, Tobyne, & Stern, 2012; Sherrill et al., 2015a). The beta series correlation method utilizes the univariate fMRI data analysis so that parameter estimates (i.e., beta weights), reflecting the magnitude of the task-related blood oxygen level dependent (BOLD) responses are estimated for each trial. Therefore, the beta series correlation analysis requires that the individual trials of events examined in the functional connectivity analysis be modeled separately. The beta series correlation functional connectivity analysis method relies on the assumption that the degree of similarity (correlation strength) between the fluctuations of parameter estimates across trials extracted from regions of interest serves as a metric of the functional interaction between the regions (Rissman et al., 2004).

It is worth noting that, because all participants were allowed to freely move in the virtual environment during both exploration and test phases, the type of behavior (moving or stationary, facing which direction) at different time points will be different. Therefore, I did not create design matrix before the experiment, but constructed a design matrix for each trial of each participant separately based on their behavioral data. The individualized design matrices were then implemented for beta series analyses.

Results included in this manuscript come from modeling performed using *NiBetaSeries* 0.6.0 (J. D. Kent & Herholz, 2018), which is based on *Nipype* 1.4.2 (K. Gorgolewski et al., 2011; K. J. Gorgolewski et al., 2018).

Beta Series Modeling

In addition to condition regressors, csf, white_matter, global_signal, trans_x, trans_y, trans_z, rot_x, rot_y, rot_z, framewise_displacement, motion_outlier* [7] and a high-pass filter of 0.0078125 Hz (implemented using a cosine drift model) were included in the model. AR(1) prewhitening was applied in each model to account for temporal autocorrelation.

After fitting the model, the parameter estimate (i.e., beta) map associated with the target trial's regressor was retained and concatenated into a 4D image with all other trials from the same condition [8], resulting in a set of N 4D images where N refers to the number of conditions in the task. The number of volumes in each 4D image represents the number of trials in that condition.

[7] 'global_signal' refers to global signal processing. This confounder was included as suggested by (Ciric et al., 2017); 'trans_x, trans_y, trans_z, rot_x, rot_y, rot_z' refers to six degrees of head motion. Framewise displacement is a measurement of head motion from one voxel to the next. This confounder was included as it was shown to improve performance in groupwise analyses(Yan et al., 2013); Motion outlier is a type of volume censoring that discards problematic time points (* refers to wildcard matching of all motion outliers for each subject). These confounders were included as it was shown to be effective in reducing motion-related artefact (Parkes, Fulcher, Yücel, & Fornito, 2018)

[8] The same condition here means the same type of event. For example, in generating betaseries for stationary facing directions (north, east, south, west), all "north" event-related images will be concatenated as one 4D image for each run in each subject.

Software Dependencies

Additional libraries used in the NiBetaSeries workflow include *Pybids* 0.9.5 (Yarkoni et al., 2019), *Niworkflows* 1.0.4, *Nibabel* 3.1.0, *Pandas* 0.24.2 (McKinney, 2010), and *Numpy* 1.20.3 (Oliphant, 2006; Van Der Walt, Colbert, & Varoquaux, 2011).

3.5.5 ROI analyses

My principle fMRI analyses were conducted using targeted *a priori* regions of interest (ROIs) (see Fig. 3.2). Previous studies strongly suggest task-evoked directional activation in thalamus (Shine et al., 2016), retrosplenial cortex (Chrastil, Sherrill, Hasselmo, & Stern, 2016; Koch et al., 2020; Nau et al., 2020; Shine et al., 2016), precuneus (Baumann et al., 2010; Shine et al., 2016), extrastriate cortex (Sherrill et al., 2015b), and early visual cortex (Koch et al., 2020; Nau et al., 2020; Stringer, Michaelos, Tsyboulski, Lindo, & Pachitariu, 2021). Because navigation function has been found to be centered around the hippocampus (Chrastil et al., 2016; OKeefe & Nadel, 1978), I also selected the hippocampus as an ROI, along with the amygdala in the limbic system. Because I also investigated directional encoding for allocentric compared to egocentric frames of reference, I included basal ganglia regions, which are found to be important for navigation with egocentric strategy (Berke et al., 2009; Geerts et al., 2020; Hartley et al., 2003) and with decision making (Ding & Gold, 2013; Doll & Frank, 2009; Hikosaka, Ghazizadeh, Griggs, & Amita, 2018) (i.e., caudate, putamen, pallidum, and nucleus accumbens). I selected auditory cortex as a reference area. I did not include entorhinal cortex because segmenting entorhinal cortex requires expertise in manual segmentation and a high-resolution image of the medial temporal lobe.

All cortical ROIs (including retrosplenial cortex, precuneus, extrastriate cortex, and early visual cortex) were generated for each participant's brain in the 521MNI space based on the Schaefer 100 regions atlas (`https://github.com/ThomasYeoLab/CBIG/tree/master/stable_projects/brain_parcellation/Schaefer2018_LocalGlobal`)(Schaefer et al., 2018).

All subcortical ROIs (including thalamus, hippcampus, caudate, putamen, pallidum, amygdala, and nucleus accumbens) were generated for each participant's brain in the 521MNI space based on the Harvard-Oxford subcortical probabilistic atlas with 25% threshold (`https://identifiers.org/neurovault.image:1700`)(Desikan et al., 2006; Frazier et al., 2005; Goldstein et al., 2007; Makris et al., 2006). All ROIs included bilateral regions [9].

3.5.6 Multivariate pattern analysis

To derive an index of trial-wise directional representation in eight different directional behaviors (see Navigation metrics; e.g., north, east, south, west for stationary facing direction), I computed category-selective pattern using multivariate pattern analyses (MVPA). Under the assumption that each person has a unique cognitive map, I conducted MVPA for each participant, with separate exploration (i.e., learning) and test phases. Because I was interested in head direction under both egocentric and allocentric frames of reference, I focused on activity in 11 ROIs (see ROI analyses; with auditory cortex being the additioanl reference region). MVPA was performaned using nilearn (`https://nilearn.github.io/`), Scikit-learn (`https://scikit-learn.org/`), NLTools (`https://nltools.org/`) packages, and Python scripts.

The multi-class classification was performed using a gaussian-kernelized support vector machine (SVM) with nested cross-validation under L2 regularization, based on a one-versus-one classifier. For a better estimate of the generalization performance, I used a 3-fold cross validation to evaluate the combination of two parameters: gaussian kernel width and regularization penalization parameter (see Equation 3.3 and Equation 3.2). The data were first shuffled and then randomly split into 3 sets. For each parameter setting (grid search among 6 values (i.e., 0.001, 0.01, 0.1, 1, 10, 100) for each parameter, respectively), 3 accuracy values were computed, one for each split in the cross-validation. Then the parameter setting with the

[9]For this manuscript version, I only include left precuneus (all other ROIs are bilateral). Due to wide distribution of head and travel direction representation observed in the result, there may not be big difference if right precuneus is counted. I will include right precuneus for future analyses and updates.

highest mean validation accuracy was chosen. The 3-fold inner cross-validation was nested under a 10-fold outer cross-validation, where the dataset was first shuffled and then randomly split into 10 sets. The decoder was trained on 9 of the sets, and the performance was tested on the final set. This was done 10 times in a rotating fashion, so that each set was tested once. The performance on all test sets was generally averaged together to determine the overall performance (see Equation 3.1 and Equation 3.2). The performance was measured by accuracy.

The calculation follows the equations below:

$$CV(\hat{f}) = \frac{1}{N}\sum_{i=1}^{N} L(y_i, \hat{f}^{-k(i)}(x_i)) \tag{3.1}$$

$$f(x) = \sum_{i=1}^{S} \alpha_i k(x_i, x) + b \tag{3.2}$$

$$k(x_i, x_j) = e^{-\gamma||x_i - x_j||^2} \tag{3.3}$$

(3.1) Cross-validation function. CV is the accuracy. N refers to the number of folds. $K : \{1, \cdots, N\}$. L refers to loss function. $\hat{f}$ refers to the predicted label (e.g., north), calculated by equation (3.2). y_i refers to actual labels (e.g., north). x_i refers to neural signal (i.e., beta signal of each event). $N = 10$.

(3.2) Kernel Support Vector Machine (SVM) function. x_i refers to support vectors. S refers

to the number of support vector. α_i refers to coefficient. b is the parameter learned in the training phase. k is the kernel function, calculated by equation (3.3).

(3.3) Gaussian radial basis function. x_i, x_j are data points. $||x_i - x_j||^2$ denotes Euclidean distance. γ is the parameter that controls the width of the Gaussian kernel.

ROI masks were created using the Harvard-Oxford subcortical atlas and the Schaefer cortical atlas (see ROI analyses) and then applied to betaseries from the whole brain voxels (see Beta series correlation analysis) for each event type. To improve classification accuracy, I conducted a within-run mean-centering method for trial specific estimates (Lee & Kable, 2018) (i.e., subtracting each voxel's run-level mean across trials of all types within each run) with the exception of using default scaling for analyses that does not have all event types within each run (the test phase of the allocentric rotation, allocentric past direction, allocentric future direction analyses).

The theoretical baseline was established using $1/N$ (N denotes the number of categories). More specifically, for classification of stationary facing direction, chance was set at .250; for translations direction was .250; for allocentric rotation was .125; for egocentric rotation was .500; for allocentric future movements was .083; for egocentric future movements was .333; for allocentric past movements was .083; for egocentric past movements was .333. The empirical baseline was established using the same analyses pipeline described above with a meta permutation-based test (take the average of 98 tests with label shuffles) for each ROI.

3.5.7 Quantification and Statistical Analyses

A one-sample t test was conducted for group classification accuracy compared with theoretical baseline and empirical baseline, for each ROI, at exploration and test phases, respectively (with FDR correction for multiple comparison(Benjamini, Heller, & Yekutieli, 2009; Benjaminit & Hochberg, 1995; Yekutieli & Benjamini, 1999)). I also conducted Pearson cor-

relation between behavioral performance accuracy and the classification accuracy for each ROI at exploration and test phases, respectively (with FDR correction for multiple comparisons(Benjamini et al., 2009; Benjaminit & Hochberg, 1995; Yekutieli & Benjamini, 1999)). All statistical analyses were conducted in RStudio.

Chapter 4

A Neural Model of Travel Direction

4.1 Introduction

Imagine walking to your car in a large parking lot, returning to your cabin after a long hike, or heading to a classroom on campus. In all these scenarios, the ability to keep track of where you are while moving in space is the key to successfully reaching your destination. Although completing these daily life tasks may feel intuitive, massive and complex computations are going on in our brain to constantly update our position and direction while we are navigating. This process is called *path integration* (Byrne, Becker, & Burgess, 2007; Gallistel, 1990; OKeefe & Nadel, 1978).

How does our brain support path integration? Over the past few decades, neuroscientists have found partial answers to this question by discovering cells in the brain that support the coding of position and direction during path integration. These findings include place cells - discovered in the hippocampus - that are tuned to an animal's location in an environment (O'Keefe & Dostrovsky, 1971) and head direction cells - discovered throughout the limbic system and beyond - that are tuned to the direction an animal is facing (called both *head direction* or *facing direction*) (Ranck Jr, 1984; Taube et al., 1990a, 1990b).

However, the facing direction does not always align with the *travel direction* - the direction of one's body movement. A familiar example is that when we are walking, we constantly move our head to pay attention to our surroundings while keeping our travel direction. The misaligned head and travel direction is also commonly seen in animals. For example, a rat's head direction and travel direction may be different from each other during foraging behaviors. A *Drosophila* may walk or fly sideways (e.g., due to wind), in which case head direction and travel direction are orthogonal to one another. Such misalignment between movement trajectory and head orientation is important because travel direction, compared with head direction, is more vital to forming our travel trajectory over time [1].

[1]Travel trajectory is derived from time and velocity. Velocity in turn is composed of speed and travel direction, which is the direction of one's body movement.

Because the role of travel direction has largely been ignored in previous research, it is an open question as to whether travel direction is supported by brain signals that are separate from those supporting head direction. Direct evidence of travel direction cells comes from studies on insects. A recent *Drosophila* study reported that allocentric travel direction was tracked by hΔB cells in the fan-shaped body of the *Drosophila* brain (i.e., central complex), which is separate from EPG cells - head direction cells in the central complex - that were tuned to head direction in the *Drosophila* brain (Lyu et al., 2021). The same study also demonstrated that the hΔB signals might be built from a vector computation between egocentric motion inputs and allocentric head direction signals with perturbation studies. In rodent studies, researchers have only reported head direction cells (Jacob et al., 2017; Olson et al., 2017; Raudies et al., 2015) or place cells (Huxter et al., 2008) that conjunctively fire toward travel direction features. These conjunctive cells were found within and around the medial temporal lobe including the medial entorhinal cortex (Raudies et al., 2015), dysgranular retrosplenial cortex (Jacob et al., 2017), subiculum (Olson et al., 2017), and hippocampus (Huxter et al., 2008). Further, mixed relationships were found between firing patterns of these cells and environmental features: some firing patterns depends on landmarks (Jacob et al., 2017) or axes (Olson et al., 2017) in an environment, while others could be observed in an open arena (Huxter et al., 2008; Raudies et al., 2015).

In humans, a recent study reported motion aftereffects of travel direction in a series of psychophysics studies where travel direction was dissociated from head direction (see Chapter 2 for more details). The study suggested behavioral signatures of travel direction signals in humans that is independent of head direction.

Though we observe direct evidence of travel direction signals in animals, it is not clear how travel direction signals are represented in the human brain. We do not yet have a direct answer to this question, but we may gain some clues from previous fMRI studies that investigated related brain signals. Previous fMRI studies that looked at head direction signals

reported multiple brain regions that represent the head direction, which include in the thalamus, presubiculum, subiculum, and retrosplenial cortex (Cullen & Taube, 2017; Ranck Jr, 1984; Taube et al., 1990a, 1990b). In humans, head direction signals have been observed in the thalamus (Shine et al., 2016), retrosplenial cortex (Koch et al., 2020; Marchette et al., 2014; Nau et al., 2020; Shine et al., 2016), precuneus (Baumann et al., 2010; Shine et al., 2016), presubiculum (Vass & Epstein, 2013), extrastriate cortex (Sherrill et al., 2015a), and early visual cortex (Koch et al., 2020; Nau et al., 2020). Because head and travel directions have been conflated in previous studies, some of the findings on head direction signals may actually represent or include travel direction signals. A recent study took a step further and looked at head and travel direction during active navigation in a complex, naturalistic environment. The study reported an even more distributed brain regions, including hippocampus and striatum in addition to the regions reported before (see Chapter 3 for more details). Additionally, the study reported dynamic head and travel direction representations that differed during learning and testing. The study also reported predictions of future movement directions while people were stationary, planning for the next step, which could be regarded as more direct evidence for travel direction representations in the human brain.

Overall, previous fMRI studies revealed a widely distributed head and travel direction network in the human brain. Although fMRI signals only suggest neural activities at the meso-level (i.e., the level of group of neural populations), the widely distributed network for directional representation in the human brain aligns with cellular-level recordings of head direction cells in the rodents. Rodent studies determined that head direction cells were distributed throughout the limbic system and beyond (Chen et al., 1994; Cho & Sharp, 2001; Leutgeb, Ragozzino, & Mizumori, 2000; Mizumori & Williams, 1993; Ranck Jr, 1984; Sharp, Tinkelman, & Cho, 2001; Taube, 1995; Taube & Bassett, 2003; Taube et al., 1990a; Wiener, 1993). In addition, the dynamic directional representation in the human brain aligns with the dynamic involvement of reciprocal circuits for vestibular signals (Taube & Bassett, 2003) that are essential for generating head direction signals in the rodent brain. The dynamic

directional representation in the human brain also aligns with the recurrent circuit dynamics in the central complex of the *Drosophila* brain that enables locomotion, head direction coding, and flexible navigation behavior over time (Hulse et al., 2021). Therefore, I argue that if travel direction is represented by an independent system in the human brain, travel direction signals might be represented via a recurrently-connected network that is separate from the head direction network.

Although it is not clear how exactly the implementation between the travel direction and head direction differs in the brain, I could start with simulating travel direction system independently. This implementation is conducted by simulating the generation of a travel direction effect, that does not involve head direction, from a study (Cheng, Ling, Stern, Huang, & Chrastil, *in prep*) (also see Chapter 2) with a recurrently-connected artificial neural network. That study serves as a good starting point for understanding the travel direction system in the human brain for several reasons: 1) the study dissociated travel direction from head direction, 2) the environment (a virtual hallway) and stimuli (optic flow) were simple, and 3) most importantly, the adaptation effect observed for travel direction a behavioral signature of neural response toward stimuli was robust and unique. Based on previous literature, head direction cells do not show adaptation over time in rodents (Taube, 1998; Taube & Bassett, 2003), which suggests the adaptation effect observed for travel direction may demonstrate a property of travel direction cells that differs from that of head direction cells.

To build a biologically-plausible neural network for travel direction, I simulated the travel direction system in the human brain with an echo state network. An echo state network (ESN) is a type of reservoir computing where a recurrent neural network (RNN, or reservoir) is generated randomly with only the readout from the reservoir being trained (Jaeger, 2007, 2010; Lukoševičius, 2012). ESNs have been shown to have good performance in simulating a wide range of tasks (Ilies et al., 2007; Lukoševičius, Jaeger, & Schrauwen, 2012; Verstraeten,

Schrauwen, & Stroobandt, 2006; Zou, Hwu, Krichmar, & Neftci, 2020) including neural circuits in the brain (Dominey & Ramus, 2010). Thus, ESN is a good option for modeling the travel direction system.

Therefore, I hypothesize that an echo state network is sufficient to simulate the motion aftereffect of travel direction.

4.2 Previous Models

Previous computational models for simulating head direction cells were commonly based on different variations of the continous ring attractor model (Redish, Elga, & Touretzky, 1996; Skaggs, Knierim, Kudrimoti, & McNaughton, 1995; K. Zhang, 1996). In a classic continuous ring attractor model, the model consists of four layers: the excitatory head direction cells that provide excitatory input to other nearby head direction cells, and provide inhibitory input to distant head direction cells. This inhibition of head direction cells is implemented via the two AV-by-HD (angular velocity by head direction) inhibitory cell layers. There may also one layer of head direction inhibitory cells that are reciprocally connected to excitatory head direction cells to form the ring attractor. There are two angular velocity (AV) cells: one that fires for a clockwise turning velocity, the other fires for at counterclockwise turning velocity.

Although previous studies that modelled conjunctive cells that code both head direction and travel direction in the rodent brain also utilized variations of attractor models (Page & Jeffery, 2018; Raudies et al., 2015), a continous ring attractor model may not be a good candidate for simulating the travel direction in the current study for several reasons. First, in our study, there are no angular velocities for travel direction because travel direction only changes on a linear trajectory. All rotations that flip head direction in the experiments are rotations in place about the navigator's own axis, but an angular velocity for travel direction

requires a radius. Second, the movement speed in our study is randomly sampled but is constant for each phase within each trial. Thus, it is also difficult to directly utilize the ring attractor model to simulate momentary translational displacement due to no translational acceleration. Third, each back and forth movement in the study indicates a 180° sudden change of travel direction, which does not support the "continuous" element in a classic continuous ring attractor model (Hopfield, 1984; Redish et al., 1996; Skaggs et al., 1995; K. Zhang, 1996). Therefore, I utilized an alternative model to simulate travel direction (see details below).

4.3 The Proposed Model

Studies in humans have shown motion aftereffects of travel direction (see Chapter 2). Briefly, when people experienced consistent self-motion toward a particular movement direction over time (referred to as the adaptation direction), their reported rate of moving toward the adapted direction during the test phase was higher than usual. Modeling possible biological processes underlying the travel aftereffect raises two challenges. First, both the adaptation phase that generates the aftereffect and the test phase that measures the aftereffect are dynamic patterns that appear in time sequences. Second, the travel aftereffect is a high-level motion aftereffect that is induced by high-level cognitive regions beyond early visual cortex. How firing patterns of neurons in those brain areas change during adaptation process is unclear.

To solve these challenges, I propose to model travel aftereffects using an echo state network. The echo state network is a type of recurrent neural network that has been found to show good performance in simulating biological processes that changes with time (Jaeger, 2007; Schubert & Gros, 2021) and has been used to simulate brain circuits (Dominey & Ramus, 2010).

The core component of the model is an echo state network (ESN), which is a large, random, recurrently connected network (aka. A "reservoir"). Input signals to the ESN creates high-dimensional collection of non-linearly transformed neural activation. These activations will then be combined to yield a desired output signal (Jaeger, Lukoševičius, Popovici, & Siewert, 2007).

Here is a description of the input and output signals for the model. The model first learns adaptation during the adaptation phase, and then make predictions during the test phase. During the adaptation phase, the control input for the adapt phase is switched on while the control input for the test phase is switched off. Vice versa during the test phase. In the adaptation phase, the model learns the adaptation or no-adapt information through adaptation or no-adapt (i.e., control) inputs. The adaptation input is a time series of travel velocity (direction + speed) toward a particular direction (i.e., adapted direction). For example, an adaptation input of "10, 10, 10, $\cdots$, 10, 10, 10" means constantly traveling toward the sun direction in 10 virtual units/s; an adaptation input of "-10, -10, -10, $\cdots$, -10, -10, -10" means constantly traveling toward the moon direction (a cardinal direction opposite to the sun direction) in 10 virtual units/s. The control input is a time series of travel velocity with 0 speed. For example, a control input will look like "0, 0, 0, $\cdots$, 0, 0, 0", which means static. The test phase starts immediately after both adaptation and no-adapt (i.e., control) inputs in the adaptation phase. In the test phase, the model learns the local travel velocity sequence and predicts the global travel direction. For example, a test input of "10, -10, 10, $\cdots$, -10, -10, -10" means traveling in a sequence of "sun direction, moon direction, sun direction, $\cdots$, moon direction, moon direction, moon direction" in 10 virtual units/s. The model produces two sequences of travel direction predictions from spontaneous neural activations and uses an offline one-shot learning: one sequence is produced through the sun report neuron while the other is produced through the moon report neuron. Prediction sequences for both the sun and the moon output neurons are composed of "0s" and "1s", which may look like "1, 0, 0, $\cdots$, 1, 1". The two sequences are then converted into one final

report indicating the global travel direction (i.e., "sun" or "moon"). Figure 4.1 depicts the proposed model.

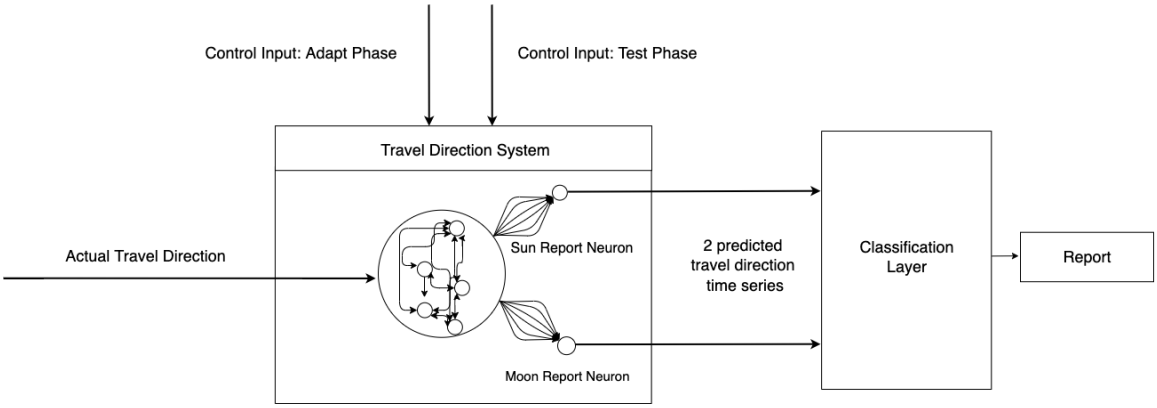

Figure 4.1: The proposed model for generating travel direction estimates in the motion adaptation task. An echo state network receives travel direction information from optic flow during the task. The echo state network contains one switch input, indicating whether it is the adaption or test phase. There are two output units in the readout layer, one for the sun report, the other one for the moon report. The synaptic connections between the two output neurons and the recurrent network (or called the output weight matrices) are modified during learning. The two reported time series then go through a classification layer to generate a final report at a behavioral level.

Neurons in the ESN follow the dynamics proposed in (Jaeger, 2007; Lukoševičius, 2012) with leaky-integrated discrete-time continuous-value units. Here are the RNN updates the equations:

$$\tilde{x}_n = tanh(W^{in}[1; u_{n1}S_n; u_{n2}] + Wx_{n-1}) \tag{4.1}$$

$$x_n = (1-\alpha)x_{n-1} + \alpha\tilde{x}_n \tag{4.2}$$

where x_n denotes a vector of reservoir neuron activation at time n. Similarly, x_{n-1} denotes a vector of reservoir neuron activation at time n-1. $\tilde{x}_n$ is the update of x_n at time step n. α is the speed of the reservoir update dynamics (*aka* leaking rate). *tanh* is a sigmoid activation function that is applied element-wise. $u1_n$ represents a vector of adaptation input neuron

activation at time n. $u2_n$ represents a vector of test input neuron activation at time n. S_n is a weight vector that could be applied element-wise for each adaptation time step input. $[\cdot;\cdot;\cdot]$ denotes a vertical matrix concatenation. W_{in} is the input weight matrix. W is the recurrent weight matrix. [2]

In the behavioral experiment, the sun and moon locations were infinitely far at the two ends of the hallway, representing cardinal directions. The linear readout layer is defined as Equation (4.5) for the sun readout neuron and Equation (4.6) for the moon readout neuron.

$$y1_n = W_1^{out}[1; u1_n S_n; u2_n; x_n] \tag{4.5}$$

$$y2_n = W_2^{out}[1; u1_n S_n; u2_n; x_n] \tag{4.6}$$

W_1^{out} is the output weight matrix for the sun report neuron, solved by Equation (4.7). W_2^{out} is the output weight matrix for the moon report neuron, solved by Equation (4.8). $y1_n$ is the network output for the sun report neuron at each time step. $y2_n$ is the network output for the moon report neuron at each time step. $[\cdot;\cdot;\cdot;\cdot]$ denotes a vertical matrix concatenation.

First, during the training session, the two output neurons' weight matrices could be expressed and solved via the following two linear equations, separately:

[2]The reservoir update dynamics can also be described in continuous time as an Ordinary Differential Equation:

$$\dot{x} = -x + tanh(W^{in}[1; u_{n1} S_n; u_{n2}] + Wx) \tag{4.3}$$

$$\frac{\delta x}{\delta t} = \frac{x(n+1) - x(n)}{\delta t} \approx \dot{x} \tag{4.4}$$

when α is taking the place of sampling interval δt, it can be considered as resampling two consecutive time steps in the discrete realization. Thus, yields Equation (4.1) and (4.2).

$$W_1^{out} = \arg\min_{W_1^{out}} \frac{1}{N_{y1}} \sum_{i=1}^{N_{y1}} (\sum_{n=1}^{T} (y1_{i_n} - y1_{i_n}^{target1})^2 + \beta ||W_1 i^{out}||^2) \tag{4.7}$$

$$W_2^{out} = \arg\min_{W_2^{out}} \frac{1}{N_{y2}} \sum_{i=1}^{N_{y2}} (\sum_{n=1}^{T} (y2_{i_n} - y2_{i_n}^{target2})^2 + \beta ||W_2 i^{out}||^2) \tag{4.8}$$

The two equations are basically minimizing RMSE via a matrix multiplication between the concatenated input and recurrent neuron activation matrix and the output neuron report (with ridge regression). Each report during the training session is first processed through one-hot encoding to fit the two report dimensions. For example, if in one trial, people report traveling in the sun direction, the sun report neuron will get an output value of 1, while the moon report neuron will get an output value of 0.

In the above equations, W_1^{out} is the output weight matrix for the sun report neuron. W_2^{out} is the output weight matrix for the moon report neuron. $y1^{target1}$ is the target output for the sun report neuron. $y2^{target2}$ is the target output for the moon report neuron. N_{y1} is the dimension for the output sun report neuron (i.e., number of trials in the training session). N_{y2} is the dimension for the output moon report neuron (i.e., number of trials in the training session). β is the regularization coefficient for ridge regression, which is set to 10^{-8}. $n = 1, ..., T$ is the discrete time (including both the adaptation and test phases) and T is the number of of data points in the training dataset (i.e., 70 data points - 60 points for the adaptation and then 10 for the test - for an initial trial, and 20 data point - 10 points for the adaptation and then 10 for the test - for a top-up trial). $W_1 i^{out}$ is the ith row of W_1^{out}. $||\cdot||$ represents the Euclidean norm. $\beta||W_2 i^{out}||^2$ is an L2 regularization term that was applied to prevent overfitting.

After output neurons' weight matrices are generated in the training phase, the model could then generate report predictions. Within each trial during the testing phase, the two output

neurons will yield two time series outputs based on the time series input of each trial. Based on the following equations:

$$\sum y1 = \frac{1}{|\tau|}\sum_{n\in\tau} y1_n = \frac{1}{|\tau|}\sum_{n\in\tau} W_1^{out}[1; u1_n S_n; u2_n; x_n] = W_1^{out}\frac{1}{|\tau|}\sum_{n\in\tau}[1; u1_n S_n; u2_n; x_n] \tag{4.9}$$

$$\sum y2 = \frac{1}{|\tau|}\sum_{n\in\tau} y2_n = \frac{1}{|\tau|}\sum_{n\in\tau} W_2^{out}[1; u1_n S_n; u2_n; x_n] = W_2^{out}\frac{1}{|\tau|}\sum_{n\in\tau}[1; u1_n S_n; u2_n; x_n] \tag{4.10}$$

where τ integration interval. In this study, it refers to the length of the whole sequence$[u1_n; u2_n]$: 70 for the initial trial and 20 for a top-up trial. $\sum y1$ is a shorthand notation for $y1_n$ averaged over time τ. $\sum y2$ is a shorthand notation for $y2_n$ averaged over time τ. yk_n refers to the kth dimension of y_n produced from $[u1_n; u2_n]$. In this study, k here has two dimensions each corresponds to a report class: one for the moon and one for the sun.

Finally, the task is to classify separate time series for each trial. After the predicted time series for each output neuron is generated, a binary classification will then be applied to the two time-averaged activations via argmax to decide the final report - either moving more toward the sun or moving more toward the moon - based on Equation (4.11) proposed in Lukoševičius (2012). As follows:

$$class([u1_n; u2_n]) = \arg\max_k(\frac{1}{|\tau|}\sum_{n\in\tau} yk_n) = \arg\max_k((\sum(y)_k) \tag{4.11}$$

where $class([u1_n; u2_n])$ refers to the class (i.e., the sun or the moon direction) that is predicted based on single sequence $[u1_n; u2_n]$.

4.4 Experiments and Results

4.4.1 Summary of the Behavioral Study

I tested the proposed model on data from Experiments 1 - 3 in the behavioral study of Chapter 2. In Experiment 1, I adopted a visual motion adaptation paradigm to probe for selectivity of travel direction (see Figure 4.2). In the experiment, people were first adapted to visual self-motion in one direction in a virtual hallway, either towards a sun or a moon. The head direction was reversed occasionally to be dissociated from the travel direction [3], while travel direction during the model performance was measured by first calculating the adaptation phase remained constant in one direction. Changing head direction precluded optic flow from contributing to any observed adaptation effects. Then people were tested with a series of visual back and forth movements, towards and away from the initial travel direction. The head direction also reversed occasionally during the test phase as well. At the end of each test trial, subjects were asked to report their net travel direction; this allowed for the measurement of psychometric functions for perceived travel direction. There was also a control condition where the viewer was stationary during the adaptation phase. The test phase of the control condition was the same as in the adaptation condition. Notably, the adaptation phase has multiple duration. The adaptation phase in the initial trial of each block is a long-term duration (60s for Experiment 1 and 2; with variations for Experiment 3). This long-term adaptation gives people sufficient exposure to the stimulus that sets up the adaptation state. The adaptation phase starting from the second trial to the last trial of each block has a shorter-term adaptation duration (10s for Experiment 1 and 2; with variations for Experiment 3). These shorter-term adaptation phases are called "top-up" adaptation, which means maintaining or bringing back the adaptation state sets up in the initial adaptation, after each test phase, by re-adapting with a shorter duration. This multiple adaptation duration setting has been utilized and proved to be effective in many

[3] note that in the current model we only kept the local travel direction as input

previous psychophysical studies (e.g., Bratch, Chen, Engel, and Kersten (2021); Curran, Clifford, and Benton (2006); Mei, Dong, and Bao (2017)).

I compared the adaptation condition with the no-adaptation control, and found a difference between people's reports of the net change of travel direction in the adaptation condition and in the control condition. The results indicated a motion aftereffect of travel direction, suggesting that travel direction is a fundamental component of human navigation. Interestingly, subjects had a higher frequency of reporting net travel *towards* the adapted direction, indicating that the aftereffect is opposite to the traditional motion aftereffect.

In Experiment 2, head direction was changed to be perpendicular to travel direction (see Appendix Figure B.5). The results replicated those found in Experiment 1, indicating that the travel aftereffect is not driven by response biases or approaching effects. In Experiment 3, four adaptation time lengths were implemented (same procedure as Experiment 1. see Figure 4.2). The results replicated the primary results from Experiment 1 and Experiment 2, while also suggesting that the magnitude of the travel motion aftereffect scales with adaptation time. For more details, see Chapter 2.

4.4.2 The Computational Model

I test the proposed travel direction adaptation model on three motion adaptation tasks. First, I compare the estimated travel aftereffects of the model with experimental data from a study on humans, along with a series of perturbation studies. Second, I compare the proposed model and an alternative model that differs in adaptation weights on the same experimental data, along with a series of perturbation studies. Third, I compare the generalizability of the proposed model and an alternative model that differs in adaptation weights on a new experimental data. All experimental data come from the study in Chapter2.

In all the experiments, the echo state network (ESN) has 2 inputs, 100 reservoir neurons,

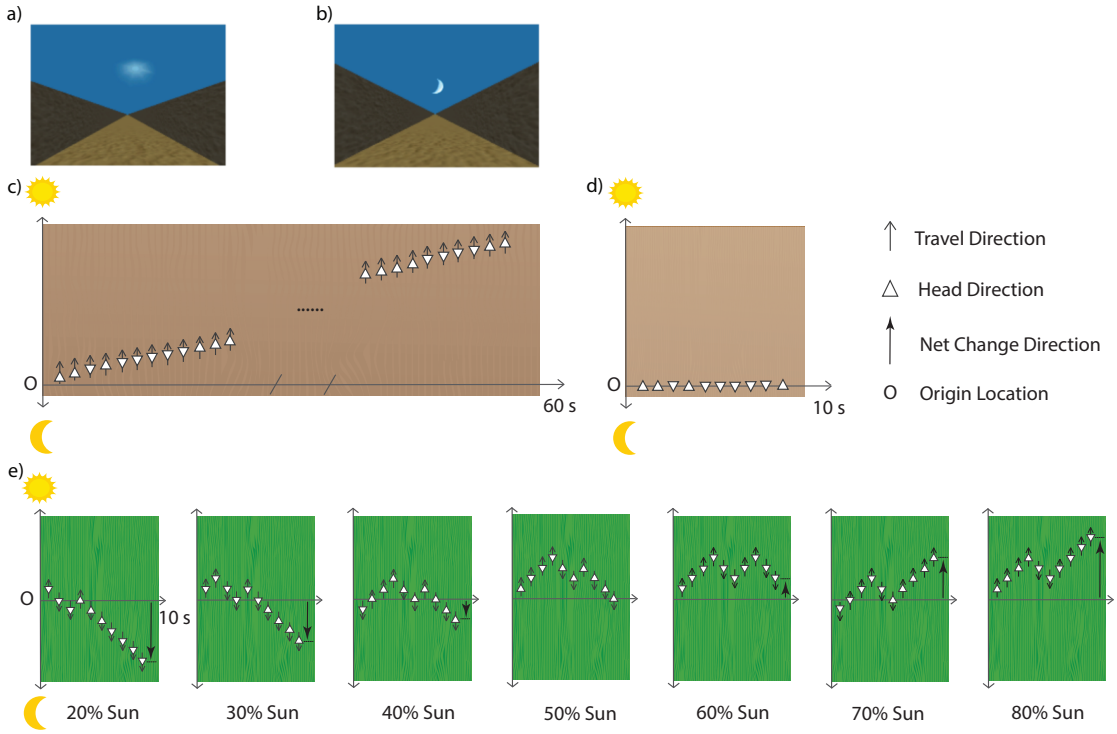

Figure 4.2: Experiment 1. Hallway during the adaptation phase, facing the a) sun or b) moon direction. Note that in the virtual environment, both the sun and the moon were rendered to move with the viewer at a constant distance; the size of the moon and the sun did not change with self-motion and participants could not evaluate distance change based on perceptual changes in either the sun or the moon. The extreme length of the hallway and random textures also precluded using changes in the hallway itself for location cues. The ground for the hallways turned green during the test phase to provide a visual cue for when to start tracking movement direction. c) The 60-second adaptation phase for the sun group. During the adaptation phase, visual movement traveled toward the sun while the facing direction occasionally changed. Half the participants were adapted to a similar moon condition, with travel direction toward the moon. d) The 10-second initial phase for the control session, which was the same for both the sun and moon groups. There was no visual travel, but the facing direction randomly changed. e) The test phase, which was the same for all sessions in all conditions. Visual movement traveled back-and-forth between the sun and the moon during a 10-second interval. Participants were asked to decide whether the total movement was more toward the sun or more toward the moon in that interval. The facing direction randomly changed during the test phase. Here, we show one example from each of the seven test phase conditions of the percent of net movement toward the adaptation direction (20%, 30%, 40%, 50%, 60%, 70%, 80%).

and 2 output neurons. The 100 recurrent neurons received travel direction information through the 2 input neurons: one neuron represents the travel direction in the adaptation phase, while the other represents the travel direction in the test phase. Input weights were

randomly drawn from a Gaussian distribution with a mean of 0. The standard deviation was $0.5/N_{ext}$ for input weights. This weight setting has been used in a previous study (Zou et al., 2020) to be small enough that it will not generate bias on particular portion of the connection but still ensure randomness. The input weight matrix has 100×103 dimensions.

The 2 input neurons were fully connected to 100 recurrent neurons. All recurrent neurons were fully connected with one another. Recurrent weights were randomly drawn from a Gaussian distribution with a mean of 0. The standard deviation was $0.05/N_{in}$ for recurrent weights. This weight setting has been shown in a previous study (Zou et al., 2020) to be small enough that it will not generating bias on particular portion of the connection but still ensure randomness. It is sparse enough that it could enable fast reservoir updates (Lukoševičius, 2012). The spectral radius of the recurrent matrix $\rho(W) \approx 0.005$, which is smaller than 1 and thus ensures the echo state property (Jaeger, 2010; Lukoševičius, 2012). The recurrent weight matrix has 100×100 dimensions. The recurrent layer was then fully connected with 2 neurons in the output layer. The 2 output neurons control the report for the sun direction and the moon direction, separately. For the leaky integrator, the leaking rate is set to 0.3.

For the adaptation weight, if a trial is the initial trial of a block, then each time step takes the same single weight (i.e., weight = 1) as a regular un-adapted time step; if a trial is not the initial trial of a block (called a top-up trial), extra weight (i.e., weight = 6) will be given. In theory, this weight setting fits the assumption that the adaptation time of the top-up trials can be much shorter than the initial trial, but still yields the same adaptation effect as the initial trial (e.g., Bratch et al. (2021); Curran et al. (2006); Mei et al. (2017)). In the behavioral experiment, the top-up trial was set to be six times shorter than the initial trial, so the weight for each top-up time step is 6. In computational theory, according to the description about regression weighting in (Lukoševičius, 2012), the 6 times extra weight for top-up trials is another way of saying that each top-up time step is equivalent to 6 regular time steps. This adaptation weight setting is implemented in the first task. Further

discussion on how such weight setting works in practice will be explored and tested in the second and the third tasks.

In each experiment, I applied 1,000 sampling cycles of Monte Carlo simulations[4]. Within each sampling cycle, I randomly sampled 20% of the trials (e.g., approximately 1,970 trials in Experiment 1) under each actual movement proportion toward the sun direction. Then for each simulation, data were randomly split into two sets, with 80% trials (e.g., approximately 1,570 trials in Experiment 1) used for training and 20% trials (e.g., approximately 390 trials in Experiment 1) used for testing.

The model will make one prediction of travel direction report (i.e., the sun or the moon direction) for each testing trial. The result of the reported rate in the experiment was then calculated by the following equation:

$$P_{ijkl} = \frac{1}{S} \sum_{n \in S} \frac{(N_{ijkl})_n}{(T_{ijkl})_n} \tag{4.12}$$

i refers to the actual percentage of moving toward the sun direction where $i = 20\%, 30\%, 40\%, 50\%, 60\%, 70\%, 80\%$ in Experiment 1 and 2 and $i = 30\%, 50\%, 70\%$ in Experiment 3. j refers to the experimental condition where $j = 1, 2$ that each refers to either the adaptation session or the control session. k refers to the adaptation group k where $k = 1, 2$ that each refers to either the sun adaptation group or the moon adaptation group in Experiment 1, or $k = 1$ that only refers to the sun adaptation group in Experiment 2 and 3. l refers to the adaptation duration where $l = 60$ in Experiment 1 and 2, or $l = 18, 36, 54, 72$ in Experiment 3. P_{ijk} refers to the reported rate of moving toward the sun direction, which is categorized by the actual percentage of moving toward the sun direction i, the experimental condition j, the adaptation group k, the adaptation duration l. S refers to the total number of sampling

[4]The Monte Carlo Simulation here could also be regarded as echo state network cross-validation.

cycles, which is 1000 in all experiments. n refers to the order of sampling cycle, where $n = 1, \cdots, S$. N refers to the total number of reports toward the sun under the actual percentage of movement toward the sun i, the experimental condition j, the adaptation group k, and the adaptation duration l, within sampling cycle n. T refers to the total number of trials under the actual percentage of movement toward the sun i, the experimental condition j, the adaptation group k, and the adaptation duration l, within sampling cycle n.

The model performance was measured by first calculating the classification accuracy (1 or 0) for each trial, and then calculating the mean accuracy across all trials that were separated by actual percentage of movements and adaptation conditions.

The Python code used in experiments will be available on GitHub.

4.4.3 Data Preprocessing

For the input data, I used the raw travel direction data used to generate optic flow in the original experiments in Chapter 2. All empirical data used for the original experiment were used here. Raw data also underwent the same preprocessing steps as the original experiment, such that trials with reaction times above or below three standard deviations were removed. Since in the original experiment, movement speed was randomly drawn from a uniform distribution between 10 - 15 virtual unit/s for each phase (the adaptation or test phase) of each trial, I went through the same process to include randomly generated speeds for each input data. In Experiment 1, I clustered trials from all actual movement proportions (20% - 80%), all sessions (the adaptation session and the control session), all adaptation groups (the sun adaptation group and the moon adaptation group) across all subjects (60 people) as input data. A similar input data generation process was used for all perturbation studies and follow up simulations for Experiment 2 and Experiment 3.

4.4.4 Experiment 1 - The Original Model

As described in Section 4.4.2, in Experiment 1, I trained an RNN on 80% of the experimental data to predict reported rate on the rest 20% of the data, and the results were averaged across 1,000 samples. Consistent with the behavioral study, the model predicted aftereffects of travel direction. More specifically, the model predicts a higher frequency of reporting travel toward the adapted direction compared to a no-adapt control - an aftereffect that runs contrary to low-level motion aftereffects, which aligns with the behavioral study (see Figure 4.3a). The model performance also reflects task difficulty in that the prediction accuracy decreases with the actual percentage of movement toward the sun getting closer to 50% (see Figure 4.3b). This pattern is similar to the patterns of reaction times observed in the behavioral study, that people responded slower as the actual percentage of movement toward the sun getting closer to 50%, which also reflects task difficulty.

In addition, I separated results based on the sun or moon adaptation group (see Figure 4.4). In the behavioral study, half of the subjects were randomly assigned to adapt to the sun direction, while the rest were assigned to adapt to the moon direction. Similar patterns of results were observed in the separated adaptation groups as in the combined data. The predicted travel direction seem to be modulated by reference points (i.e., sun or moon) such that slightly stronger aftereffects were seen in the sun group (see Figure 4.4a) than in the moon group (see Figure 4.4c), which also aligns with findings in the behavioral experiment.

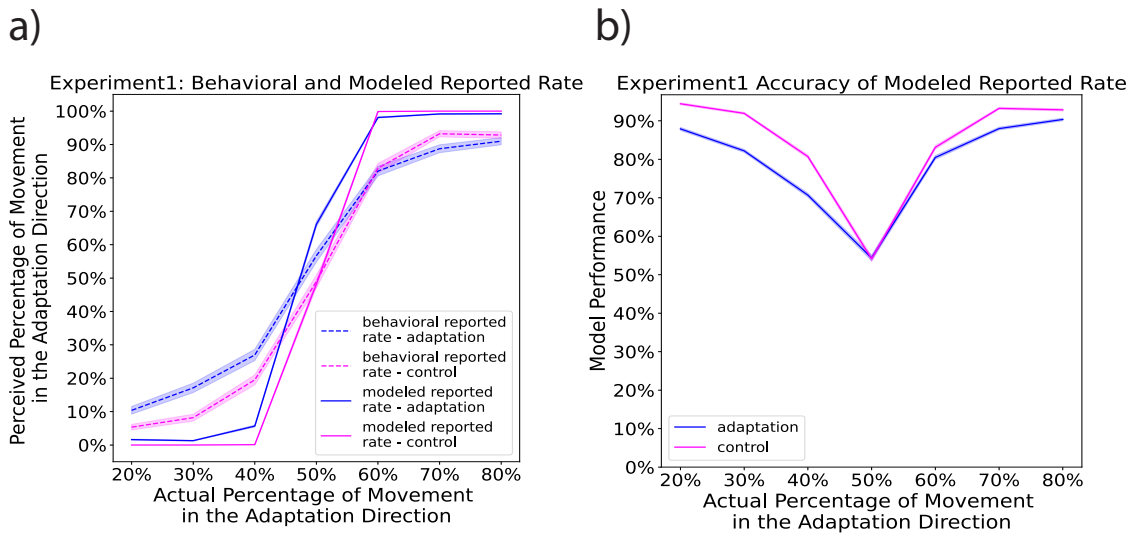

Figure 4.3: Experiment 1 The Modeled and Behavioral Reported Rates: a) The modeled reported rate compared with the behavioral reported rate (60 subjects). Similar to the behavioral data, for the modeled data, the adaptation condition showed significantly higher reported percentages than the corresponding control conditions at 20%, 30%, 40%, and 50%, supporting the aftereffect (all $ps < 0.001$). This result suggests an aftereffect in the same direction of travel. Solid lines indicate the grand average value for the modeled reported rate, while dashed lines indicate the grand average for the behavioral reported rate. The shaded areas indicate 95% confidence interval of the mean. b) Accuracy of the modeled reported rate (averaged trial-based classification accuracy across all simulations). The prediction accuracy decreased as the actual percentage of movement in the adaptation direction gets closer to 50%, which aligns with the task difficulty levels. The task gets more difficult as the actual percentage of movement in the adaptation direction gets closer to 50%. The shaded areas indicate 95% confidence interval of the mean.

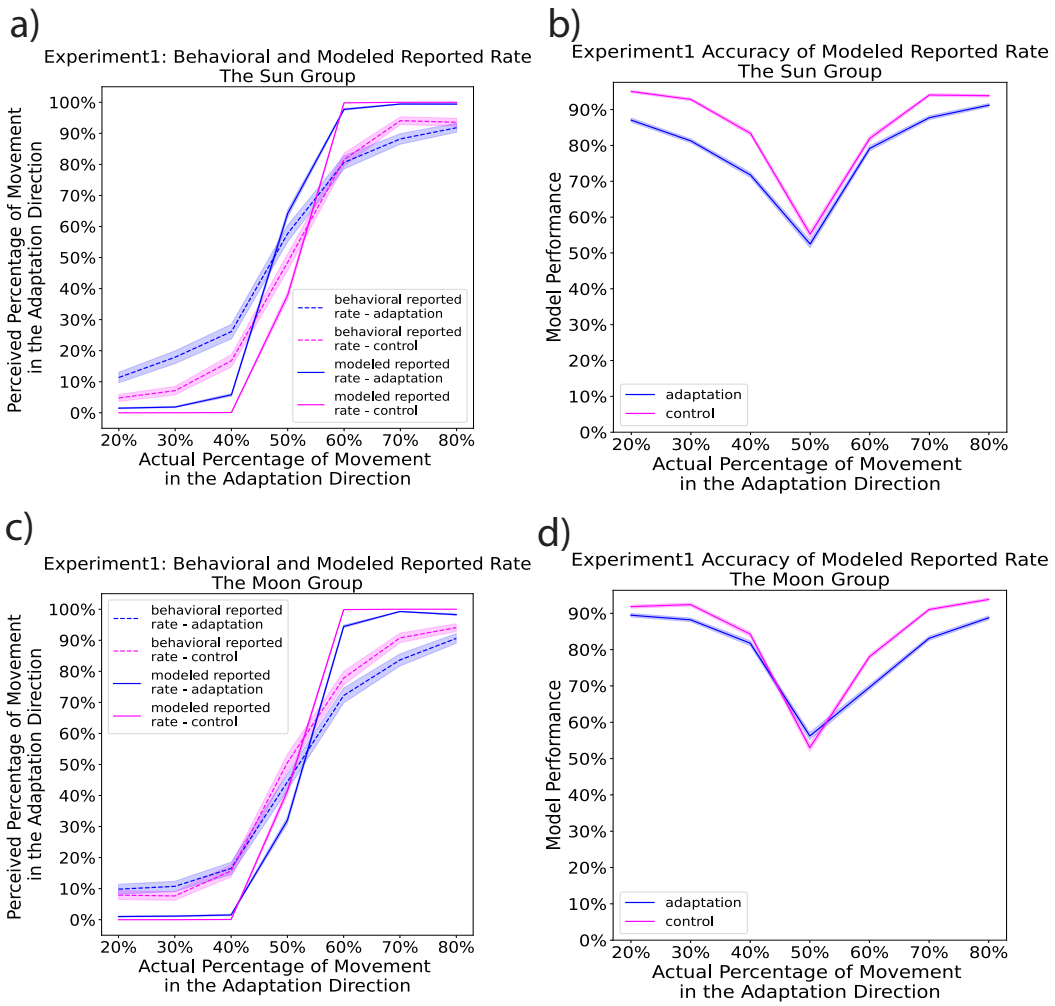

Figure 4.4: Experiment 1 The Modeled and Behavioral Reported Rates Separated by Adaptation Groups: a) The modeled reported rate compared with the behavioral reported rate for the sun group (30 subjects). Similar to the behavioral data, for the predicted data, the adaptation condition showed significantly higher reported percentages than the corresponding control conditions at 20%, 30%, 40%, and 50%, supporting the aftereffect (all $ps < 0.001$). This result suggests an aftereffect in the same direction as the travel adaptation. Solid lines indicate the grand average value for the modeled reported rate, while dashed lines indicate the grand average for the behavioral reported rate. The shaded areas indicate 95% confidence interval of the mean. b) Accuracy of the modeled reported rate for the sun group (averaged trial-based classification accuracy across all simulations). The prediction accuracy decreased as the actual percentage of movement in the adaptation direction gets closer to 50%, which aligns with the task difficulty levels. The task gets more difficult as the actual percentage of movement in the adaptation direction gets closer to 50%. The shaded areas indicate 95% confidence interval of the mean. c) similar to a), The modeled reported rate compared with the behavioral reported rate for the moon group (30 subjects). d) similar to b), Accuracy of the modeled reported rate for the moon group (averaged trial-based classification accuracy across all simulations).

Next, I tested the model with a series of perturbation studies (see Figure 4.5 and Figure 4.6). The difference between the modeled reported rate between the intact model and the perturbed model were measured by calculating the normalized difference (i.e., the Z score) in modeled reported rate at each actual percentage of movement based on the following equation:

$$Z_i = \frac{\bar{f}_i - \bar{y}_i}{\sqrt{{\sigma_{f_i}}^2 + {\sigma_{y_i}}^2}} \tag{4.13}$$

where Z represents the normalized difference (i.e., the Z score) between the modeled reported rate distribution predicted by the intact model and the perturbed model. i refers to the actual percentage of moving toward the sun direction where $i = 20\%, 30\%, 40\%, 50\%, 60\%, 70\%, 80\%$ in Experiment 1 and 2 and $i = 30\%, 50\%, 70\%$ in Experiment 3. $\bar{f}$ refers to the mean reported rate predicted by the perturbed model, which is calculated by Equation (4.14). $\bar{y}$ refers to the mean reported rate predicted by the intact model, which is calculated by Equation (4.15). σ_f is the standard error of the reported rate predicted by the perturbed model, which is calculated by Equation (4.16). σ_y is the standard error of the reported rate predicted by the intact model, which is calculated by Equation (4.17).

$$\bar{f}_i = \frac{1}{S} \sum_{n \in S} (f_i)_n \tag{4.14}$$

$$\bar{y}_i = \frac{1}{S} \sum_{n \in S} (y_i)_n \tag{4.15}$$

where $\bar{f}$ refers to the mean reported rate predicted by the perturbed model. f refers to the reported rate predicted by the perturbed model. $\bar{y}$ refers to the mean reported rate

predicted by the intact model. y refers to the reported rate predicted by the intact model. i refers to the actual percentage of moving toward the sun direction where $i = 20\%, 30\%, 40\%, 50\%, 60\%, 70\%, 80\%$ in Experiment 1 and 2 and $i = 30\%, 50\%, 70\%$ in Experiment 3. S refers to the total number of sampling cycles, which is 1000 in all experiments. n refers to the order of sampling cycle, where $n = 1, \cdots, S$.

$$\sigma_{f_i} = \frac{1}{S}\sqrt{\sum_{n \in S}((f_i - \frac{1}{S}\sum_{n \in S}(f_i)_n)^2)_n} \tag{4.16}$$

$$\sigma_{y_i} = \frac{1}{S}\sqrt{\sum_{n \in S}((y_i - \frac{1}{S}\sum_{n \in S}(y_i)_n)^2)_n} \tag{4.17}$$

where σ_f is the standard error of the reported rate predicted by the perturbed model. f refers to the reported rate predicted by the perturbed model. σ_y is the standard error of the reported rate predicted by the intact model. y refers to the reported rate predicted by the intact model. i refers to the actual percentage of moving toward the sun direction where $i = 20\%, 30\%, 40\%, 50\%, 60\%, 70\%, 80\%$ in Experiment 1 and 2 and $i = 30\%, 50\%, 70\%$ in Experiment 3. S refers to the total number of sampling cycles, which is 1000 in all experiments. n refers to the order of sampling cycle, where $n = 1, \cdots, S$.

In Experiment 1.1, the adaptation phase was not given any input. The result shows no change of prediction for trials in the control sessions, but trials in the adaptation sessions shifted towards the control line (see Figure 4.5a and Figure 4.6a). This result supports the idea that the aftereffect (i.e., the difference between the control session line and the adaptation session line in the figure) was indeed induced by the adaptation phase.

In Experiment 1.2, the test phase was not given any input. The result shows chance level (50%) prediction at every actual percentage of movement, indicating that the model is indeed making predictions based on the test phase, not the adaptation phase (see Figure 4.5b and

Figure 4.6b).

In Experiment 1.3, time steps in the test phase were shuffled. The result shows no change in the prediction, suggesting that there was no time-dependency for particular time steps in the test phase that affect the travel direction prediction (see Figure 4.5c and Figure 4.6c). This result also aligns with the empirical results of no primacy effects and no recency effects in the behavioral study (see Chapter 2 for details).

In Experiment 1.4 - 1.8, different parts of the model weights were shuffled separately (i.e., input neuron weights, reservoir neuron weights, the sun output neuron weights, the moon output neuron weights, and both the sun and the moon output neuron weights), all leading to predictions that dropped to chance levels (see Figure 4.5d-h and Figure 4.6d-h). These results further support that it is the neural network that simulates the dynamic of travel direction in the study. Perturbation results separated by the adaptation group showed similar patterns as observed in the combined results (see Appendix Figure B.1 - B.4).

Data from Experiments 2 and 3 were used to train two additional separate RNNs. The model and perturbation study findings from Experiment 1 were replicated for Experiment 2 (see Appendix Figure B.6-B.8) and Experiment 3 (see Appendix Figure B.9-B.17).

However, one qualitative difference between the behavioral results and model predictions was observed in Experiment 3. Although the model trained with Experiment 3 data qualitatively reproduced the results that the travel aftereffects (i.e., the difference between the control line and the adaptation line) scale with adaptation time (see Appendix Figure B.9), the difference seemed to come from a difference among the modelled reported rate for control sessions in the 36s, 54s, and 72s conditions (see Figure 4.7g). In contrast, in the empirical behavioral experiment, the difference arose mainly from adaptation lines. This difference makes us speculate on the extent to which the model trained on Experiment 3 really captured the real adaptation dynamics in the adaptation trials.

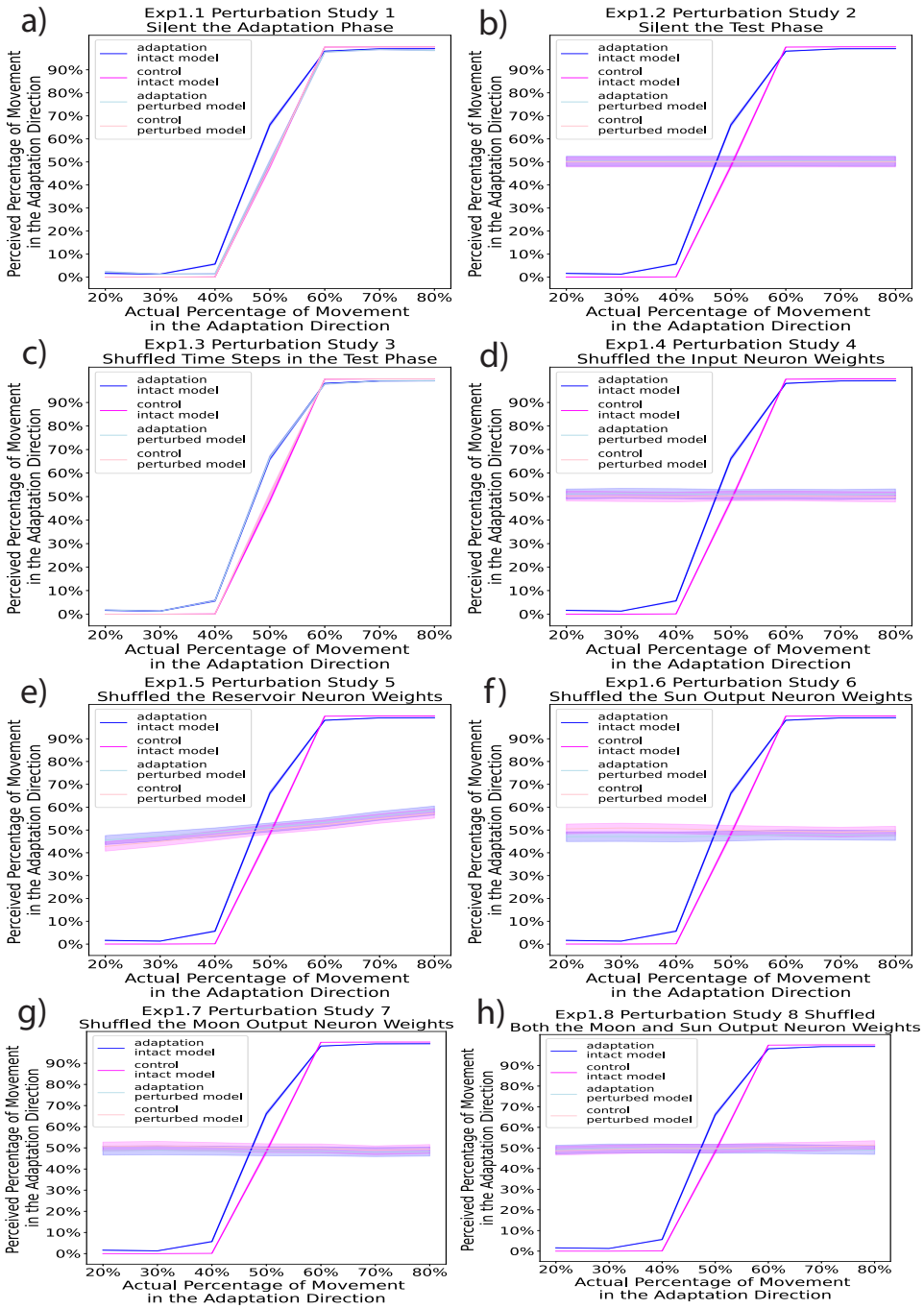

Figure 4.5: Experiment 1 modeled reported rates predicted by the perturbed model and the intact model: a) Perturbation study 1 - silencing the adaptation phase b) Perturbation study 2 - silencing the test phase c) Perturbation study 3 - shuffled time steps in the test phase b) Perturbation study 4 - shuffled the input neuron weights b) Perturbation study 5 - shuffled the reservoir neuron weights b) Perturbation study 6 - shuffled the sun output neuron weights b) Perturbation study 7 - shuffled the moon output neuron weights b) Perturbation study 8 - shuffled both the sun and moon output neuron weights

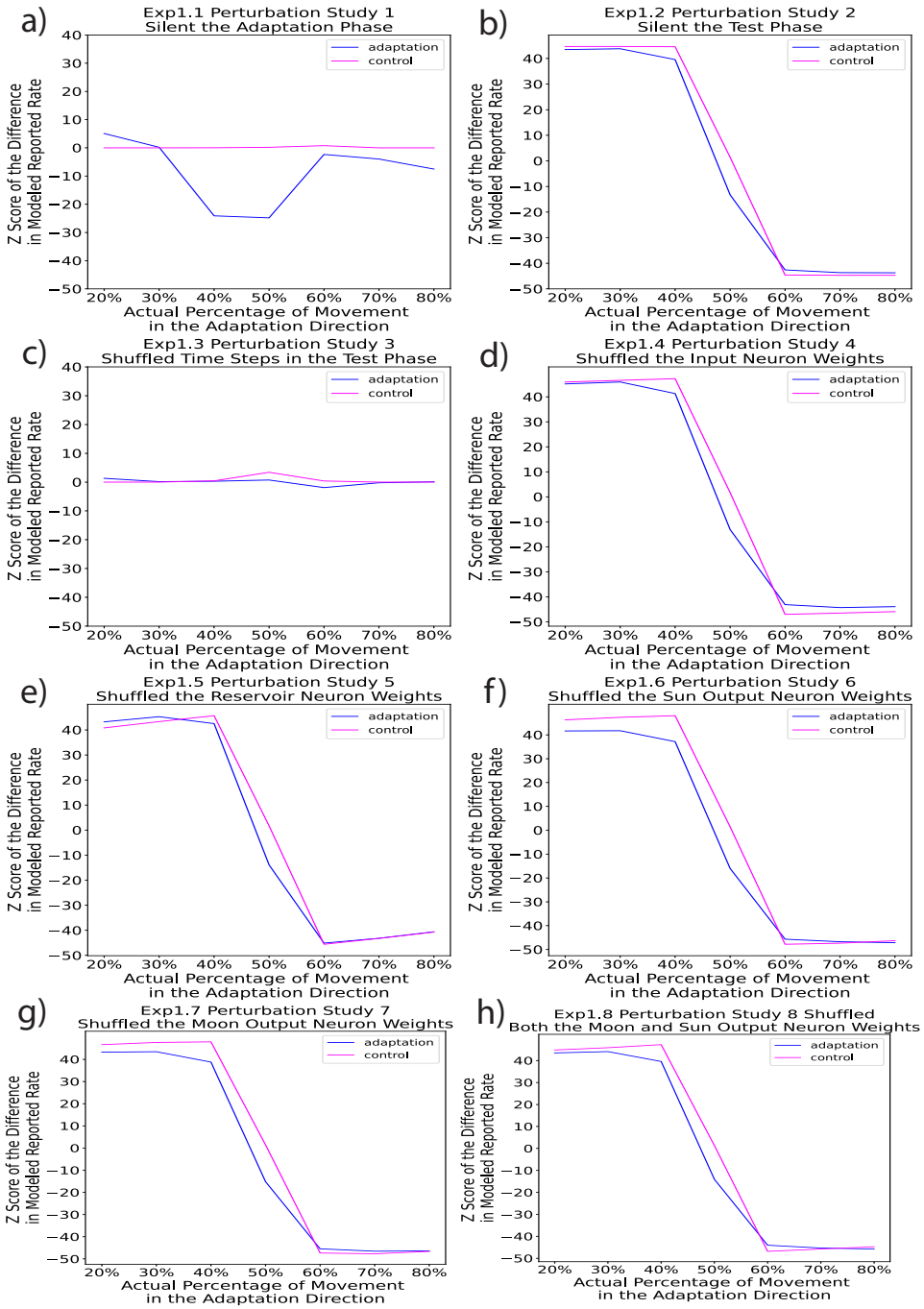

Figure 4.6: Experiment 1 normalized difference in modeled reported rate between the perturbed model and the intact model: a) Perturbation study 1 - silencing the adaptation phase b) Perturbation study 2 - silencing the test phase c) Perturbation study 3 - shuffled time steps in the test phase b) Perturbation study 4 - shuffled the input neuron weights b) Perturbation study 5 - shuffled the reservoir neuron weights b) Perturbation study 6 - shuffled the sun output neuron weights b) Perturbation study 7 - shuffled the moon output neuron weights b) Perturbation study 8 - shuffled both the sun and moon output neuron weights

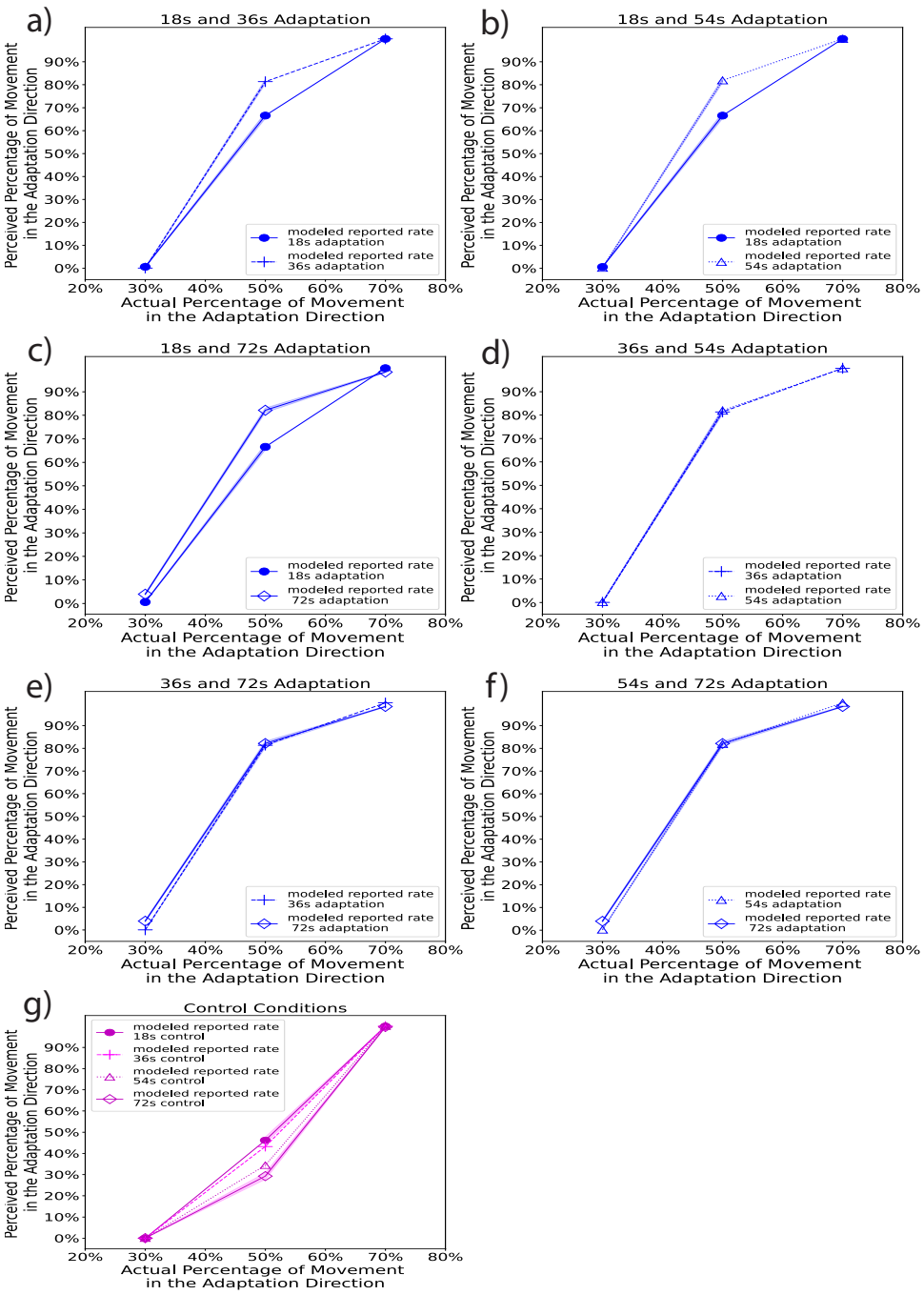

Figure 4.7: Experiment 3 The Pairwise Comparison of Modeled Reported Rates Separated by Experimental Conditions (n = 28): a) The modeled reported rates for the 18s and 36s adaptation conditions. b) The modeled reported rates for the 18s and 54s adaptation conditions. c) The modeled reported rates for the 18s and 72s adaptation conditions. d) The modeled reported rates for the 36s and 54s adaptation conditions. e) The modeled reported rates for the 36s and 72s adaptation conditions. f) The modeled reported rates for the 54s and 72s adaptation conditions. g) The modeled reported rates for all four control conditions.

4.4.5 Experiment 1 - An Alternative Model

One remaining question which has also been mentioned in the Section 4.4.2 is the weight setting for time steps in the adaptation phase. In the original proposed model, if a trial was the initial trial of a block, then each time step took the same single weight (i.e., weight = 1); if a trial was not the initial trial of a block (i.e., a top-up trial), extra weight (i.e., weight = 6) was given. This setting fits the psychology theory in the original behavioral experiment design under the assumption that the adaptation effect of top-up trials can be much shorter than the initial trial while still yielding the same adaptation effect as the initial trial (e.g., Bratch et al. (2021); Curran et al. (2006); Mei et al. (2017)). In the behavioral experiment, the top-up trial was set to be six times shorter than the initial trial, so the weight for each top-up time step was 6.

Although such weight setting worked when applied and tested in Experiments 1 - 3, I wondered whether the ESN was able to learn the relationships between initial adaptation and the top-up adaptation on its own without the additional information of extra weight. To test this hypothesis, I propose an alternative model that to large extent is the same as the original model with the only difference being all weights in the adaptation phase are set to be single weight no matter its an initial trial or a top-up trial. In other words, for the alternative model, $S_n = 1$ in Equation 4.1, 4.2, 4.5, 4.6, 4.9, 4.10.

The result shows that the RNN trained on Experiment 1 data with a single adaptation weight across the board (see Figure 4.8) reached almost the same performance as the RNN trained on Experiment 1 data with extra top-up adaptation weight. The alternative had similar results to the original model in Experiment 1 (see Figure 4.3) and in the perturbation studies (see Figure 4.9 and Figure 4.10). These findings suggest that the RNN is able to consider both the initial adaptation trial and the top-up adaptation trial similarly, although they differ in duration. When separated by adaptation groups (sun or moon), the result predicted by the alternative model was also very similar to the prediction from the original model (see

Appendix Figure B.18).

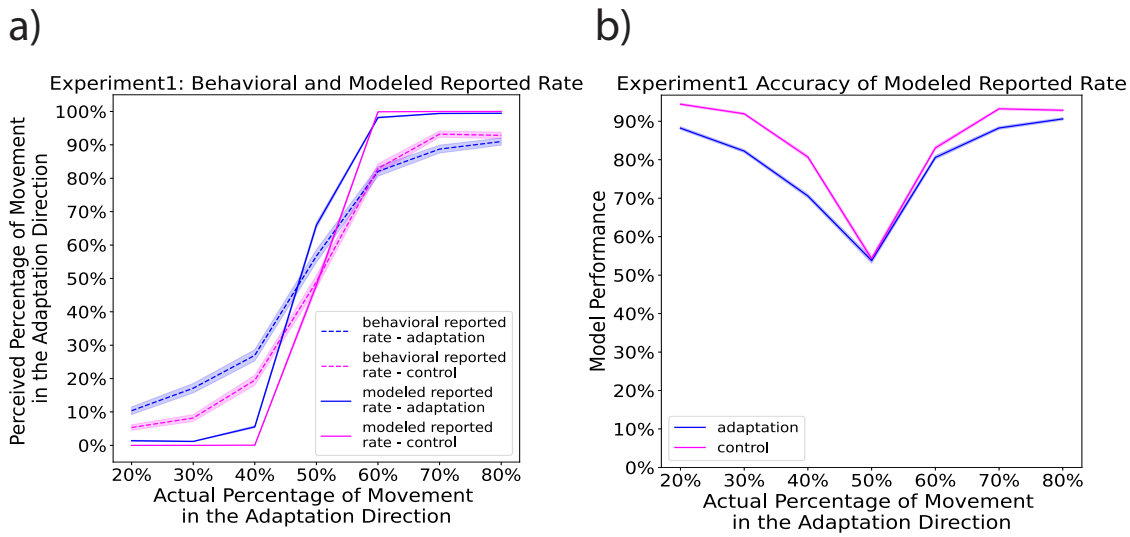

Figure 4.8: Experiment 1 The Behavioral Reported Rate and the Modeled Reported Rate with Single Weight Applied Across the Board: a) The modeled reported rate compared with the behavioral reported rate (60 subjects). Similar to the behavioral data, for the modeled data, the adaptation condition showed significantly higher reported percentages than the corresponding control conditions at 20%, 30%, 40%, and 50%, supporting the aftereffect (all $ps < 0.001$). This result suggests an aftereffect in the same direction of travel. Solid lines indicate the grand average value for the modeled reported rate, while dashed lines indicate the grand average for the behavioral reported rate. The shaded areas indicate 95% confidence interval of the mean. b) Accuracy of the modeled reported rate (averaged trial-based classification accuracy across all simulations). The prediction accuracy decreased as the actual percentage of movement in the adaptation direction gets closer to 50%, which aligns with the task difficulty levels. The task gets more difficult as the actual percentage of movement in the adaptation direction gets closer to 50%. The shaded areas indicate 95% confidence interval of the mean.

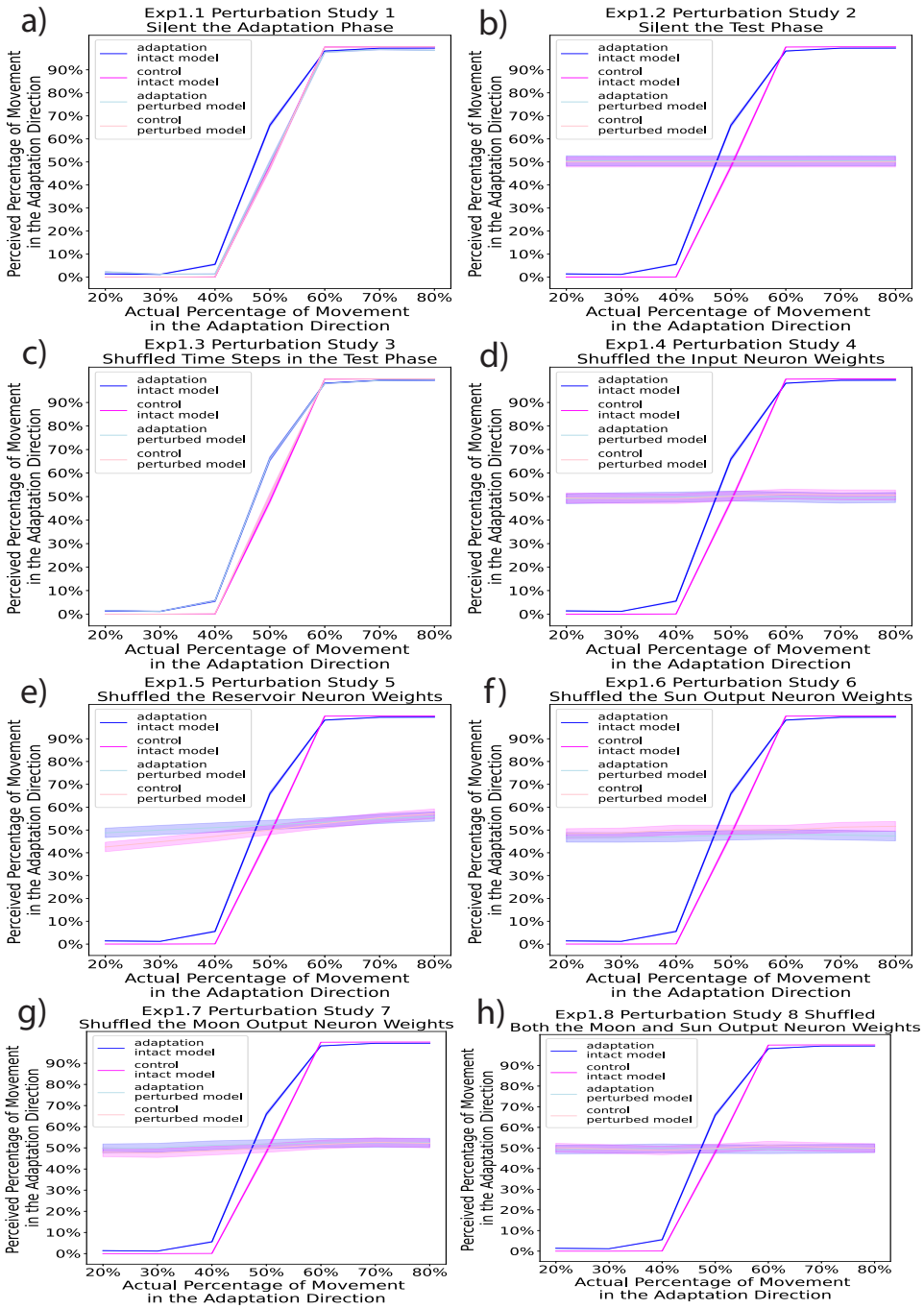

Figure 4.9: Experiment 1 reported rates predicted by the perturbed alternative model and the intact alternative model: a) Perturbation study 1 - silencing the adaptation phase b) Perturbation study 2 - silencing the test phase c) Perturbation study 3 - shuffled time steps in the test phase b) Perturbation study 4 - shuffled the input neuron weights b) Perturbation study 5 - shuffled the reservoir neuron weights b) Perturbation study 6 - shuffled the sun output neuron weights b) Perturbation study 7 - shuffled the moon output neuron weights b) Perturbation study 8 - shuffled both the sun and moon output neuron weights

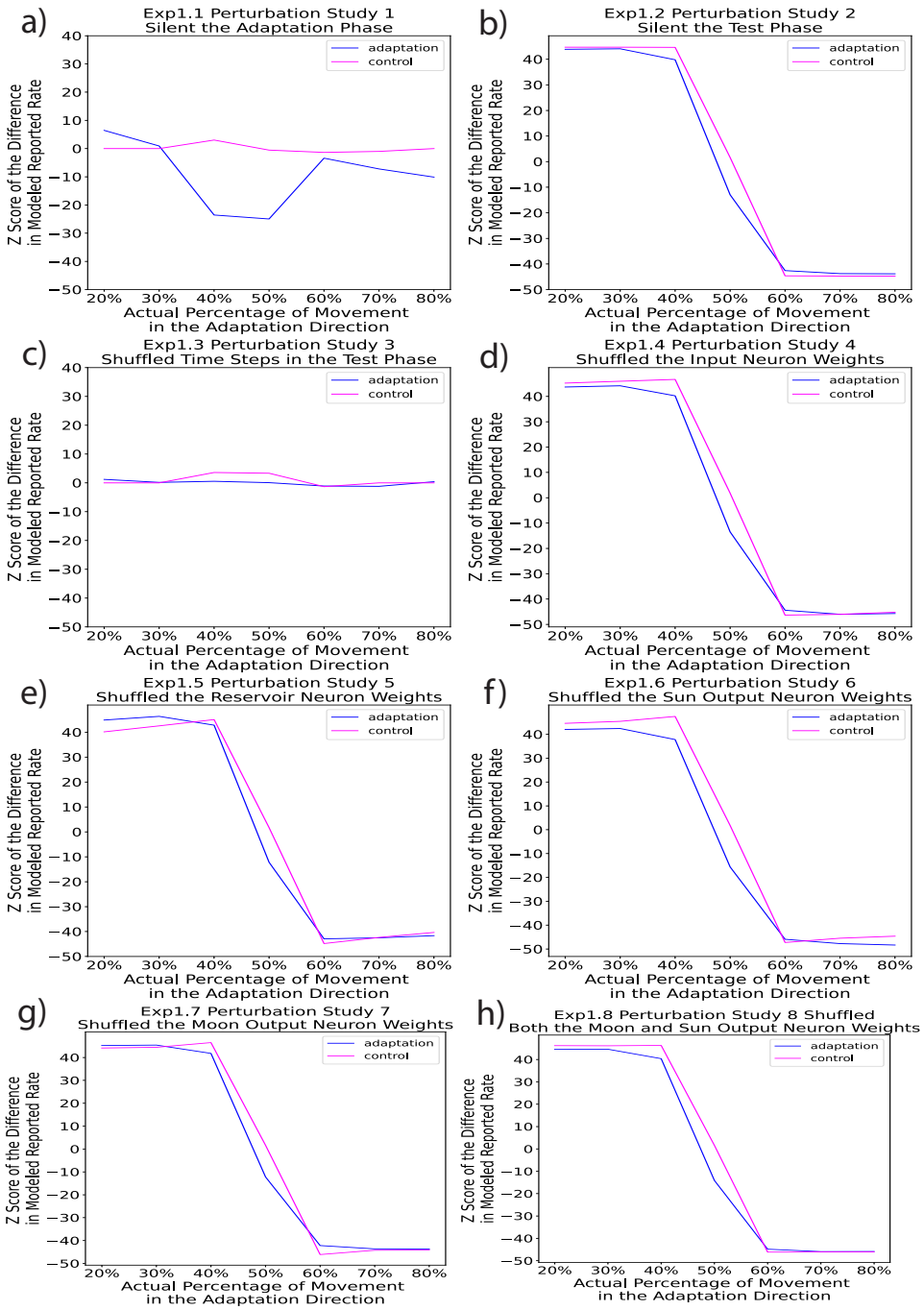

Figure 4.10: Experiment 1 normalized difference in modeled reported rate between the perturbed alternative model and the intact alternative model: a) Perturbation study 1 - silencing the adaptation phase b) Perturbation study 2 - silencing the test phase c) Perturbation study 3 - shuffled time steps in the test phase b) Perturbation study 4 - shuffled the input neuron weights b) Perturbation study 5 - shuffled the reservoir neuron weights b) Perturbation study 6 - shuffled the sun output neuron weights b) Perturbation study 7 - shuffled the moon output neuron weights b) Perturbation study 8 - shuffled both the sun and moon output neuron weights

4.4.6 Comparison Between the Two Models: Predictions on Experiment 3

Although the original model and the alternative model reached similar performance when trained and tested with data from Experiment 1 as well as in a series of perturbation studies, I wondered whether the two models differ in generalizability. In other words, I expect the two models may differ in making predictions based on a data set that has not been included in the training - data from Experiment 3. Experiment 1 and Experiment 3 are common in the task environment and the way that the head direction and travel direction is dissociated, with 2 important differences. The first difference is that Experiment 3 has more variation in the adaptation duration in the adaptation phase: there are 4 adaptation durations (18s, 36, 54s, and 72s for the initial adaptation; 3s, 6s, 9s, and 12s for the corresponding top-up adaptation) in Experiment 3 while Experiment 1 only has 1 adpatation duration (60s for the initial adaptation and 10s for the top-up adaptation). The second difference is that Experiment 3 has fewer actual percentages of movement toward the sun direction in the test phase: there are 3 percentages (30$, 50%, 70%) in Experiment 3 while Experiment 1 has 7 percentages (ranges from 20% - 80% with 10% interval). Note that the time duration during the test phase was constant (10s) in both experiments.

I hypothesize that the alternative model will have better performance in making predictions on Experiment 3 than the original model. This is because the alternative model is trained with less information about adaptation time, it might be more versatile in predicting data that varies in adaptation time.

To test this hypothesis, I trained the two models on data from Experiment 1 and then tested them with data from Experiment 3. The model training process was the same as described in Section 4.4.2. Final results were averaged from 1000 sampling cycles. Each sampling cycle includes 2 separate samples, one is the training sample from Experiment 1, the other is the testing sample from Experiment 3. During training, 20% of the data from Experiment 1 was

randomly sampled and 80% of those sampled data were used. During testing, 20% of the data from Experiment 3 was randomly sampled and 20% of those sampled data were used for testing.

The original model was built by giving extra weights to top-up trials and the alternative model was built with only single weight for all trials. First, I tested whether the original model could predict Experiment 3. I processed the input data under the same hypothesis that each time step in top-up trials were be given 6 times extra weights than initial trials to emphasis its importance for both the training and the testing data set. The result shows that the original model could not make predictions in Experiment 3 (see Figure 4.11 and Figure 4.12). This result suggests that although in theory, a time step during the top-up adaptation carries as much or more information about travel direction than a time step during the initial adaptation, such importance could not simply be quantified by giving it extra weights. Further, the results showed that the original model could not predict both the adaptation condition and the control condition. This may suggest that there are common mechanisms for coding travel directions that are shared between the adaptation and the control condition. This common mechanism may not be learned when a model is built based on extra weights on the top-up trials.

Next, I tested whether the alternative model that was only built from giving single weight to all adaptation time steps could predict Experiment 3. Consistent with my hypothesis, the result shows that the alternative model could predict the travel aftereffect for 54s and 72s adaptation trials - the adaptation time that are close to the 60s adaptation in the training data set - but could not predict travel aftereffects for trials with the 18s and 36s adaptation duration (see Figure 4.13). It is worth noting that behavioral results for 18s adaptation in Experiment 3 was quite weak, such that the difference between the adaptation and the control conditions was almost undistinguishable. Therefore, not predicting travel aftereffects on 18s adaptation trials is actually preferable, as there may not be much travel adaptation

happening in 18s adaptation. However, the model's prediction for the 36s adaptation trial was different from the behavioral data, which may indicate a lower bound for the alternative model's ability to capture travel adaptation.

Although the alternative model could not predict travel aftereffects for all adaptation durations in Experiment 3, it predicted pairwise differences between adaptation conditions (see Figure 4.13). Interestingly, this prediction about the relationship between adaptation conditions was even more accurate than the prediction from the original model that was both trained and tested by Experiment3 (see Figure 4.7). The original model that is trained and tested using data from Experiment 3 with extra weights given to top-up trial predicted the relationship between different adaptation conditions: the magnitude of motion aftereffect that scaled with adaptation duration (see Figure 4.7a-f). However, the difference in aftereffect (i.e., difference in the reported rate between the adaptation condition and the control condition) was mainly due to variations in control conditions (see Figure 4.7g) but not variations in adaptation conditions (see Figure 4.7a-f). Such a difference is suspicious because there was no actual "adaptation" for control conditions in different adaptation duration blocks. In the "adaptation" phase of control conditions, the screen was static with no travel. For example, trials in the 18s control condition had 18s static duration during the "adaptation" phase and trials in the 36s control condition had 36s static duration during the "adaptation" phase. Although control conditions differ in static time durations, it should not make any difference in the reported rate. Therefore, it's possible that the extra weight added to top-up trials was actually forcing the model to learn "pseudo" travel adaptation from control conditions. More specifically, adding extra weights to time steps during "top-up" trials does not help the RNN to pick up "adaptation" information from adaptation trials, but instead let it misrecognise regular control trials as "adaptation" trials that were adapted to a different direction from the actual travel aftereffect.

To prevent the possibility that the difference between the original and the alternative models

in predicting Experiment 3 did not come from differences in the testing data, I conducted additional model comparisons by testing the original model using testing data processed with a single weight and testing the alternative model using testing data processed with extra weights in top-up trials. Results were consistent with the previous findings. More specifically, the original model could not predict Experiment 3 when top-up trials in the testing data were given a single weight (See Figure 4.15 and Figure 4.16). The alternative model could predict trials in control conditions with 54s and 72s adaptation duration, but could not predict trials in any of the adaptation conditions (See Figure 4.17 and Figure 4.18). This is preferabe because control trials does not have adaptation, so predictions on control trials in the alternative model were not affected by extra adaptation weights.

Taken together, results in model comparison reveal that the RNN is able to learn the relationship between initial adaptation trials and top-up adaptation trials even when no additional information about the difference between the two adaptation trials was externally provided. The importance of each time step in top-up trials could not be simply quantified with extra weights. Further, learning the relationship between initial adaptation trials and the top-up adaptation trials seems to be essential in making travel aftereffect predictions.

Experiment 1 The Modeled and Behavioral Reported Rates:

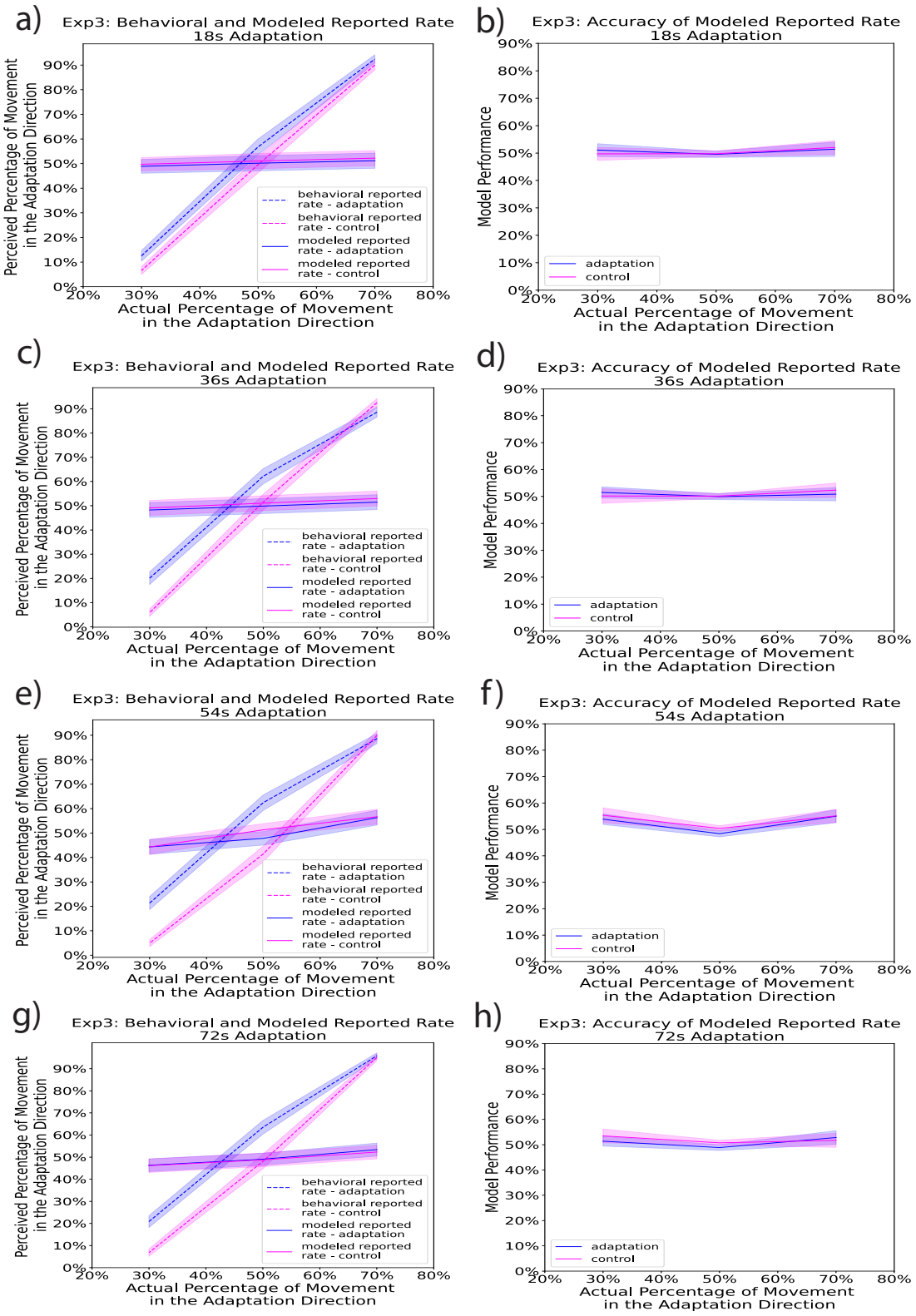

Figure 4.11: Experiment 3 The Modeled and Behavioral Reported Rates Separated by Adaptation Time Periods. The model was built from Experiment 1 with extra weights and predicted Experiment 3 with extra weights.

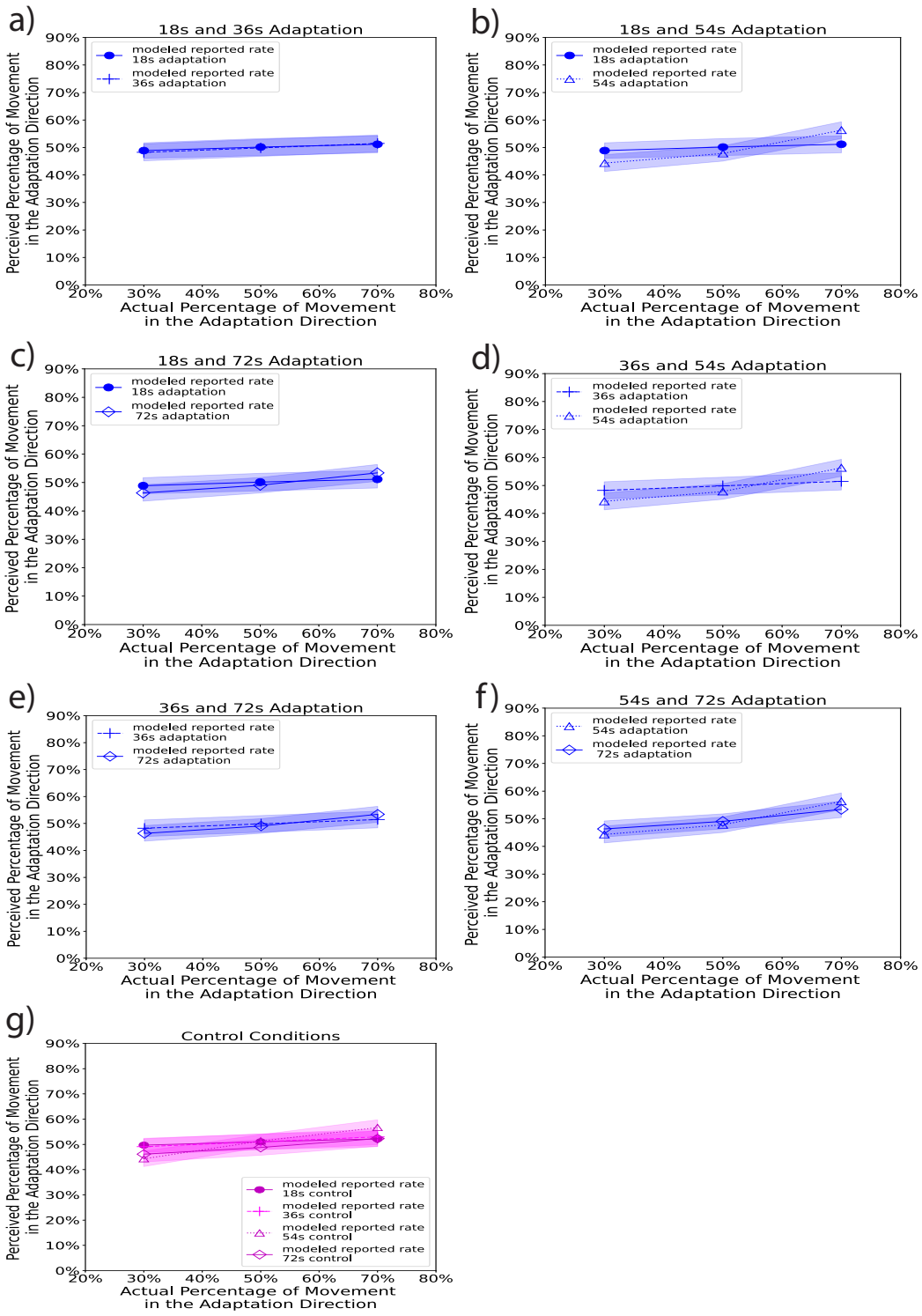

Figure 4.12: Experiment 3 The Modeled and Behavioral Reported Rates Separated by Experimental Conditions. The model was built from Experiment 1 with extra weights and predicted Experiment 3 with extra weights.

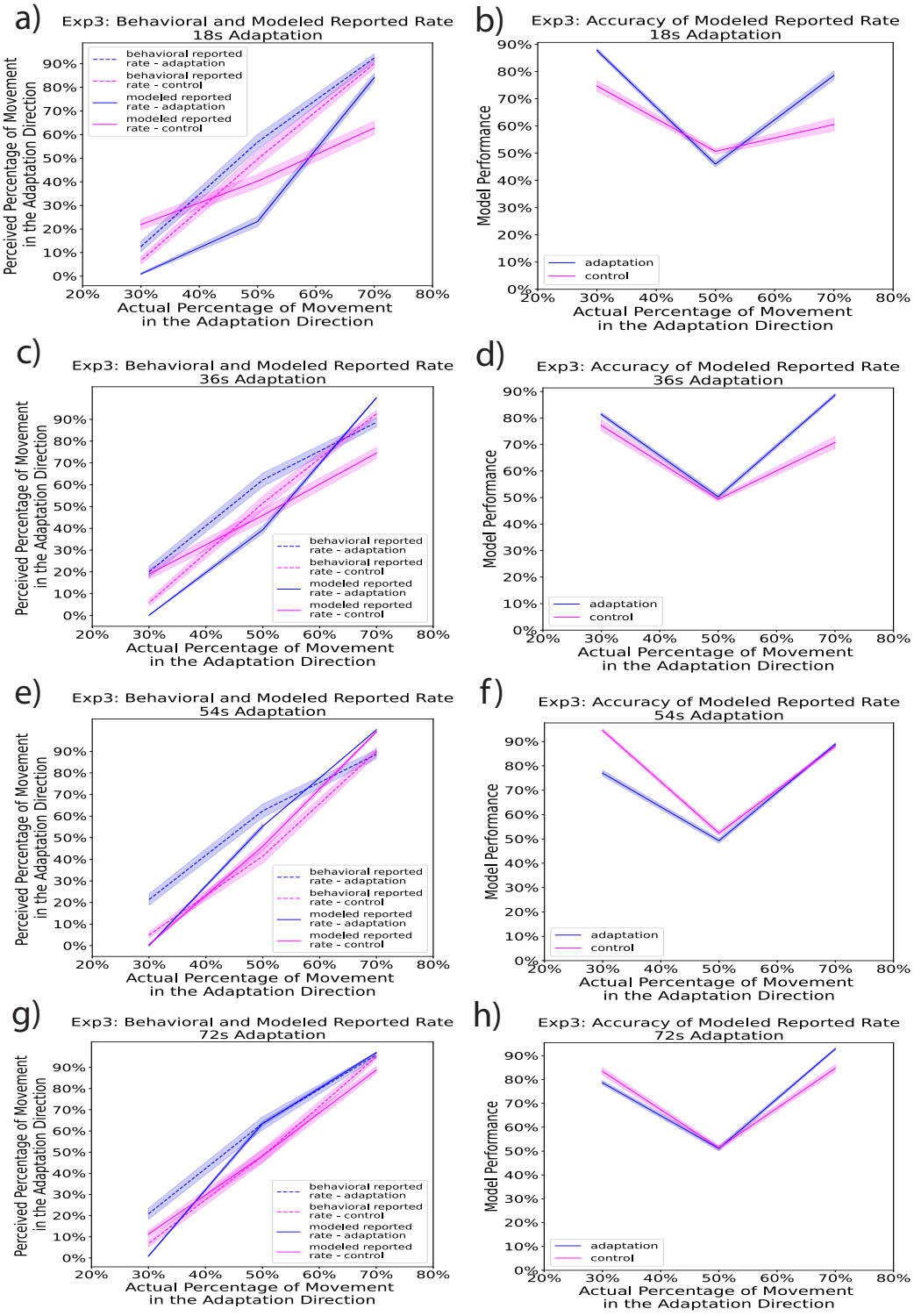

Figure 4.13: Experiment 3 The Modeled and Behavioral Reported Rates Separated by Adaptation Time Periods. The model was built from Experiment 1 with a single weight and predicted Experiment 3 with a single weight.

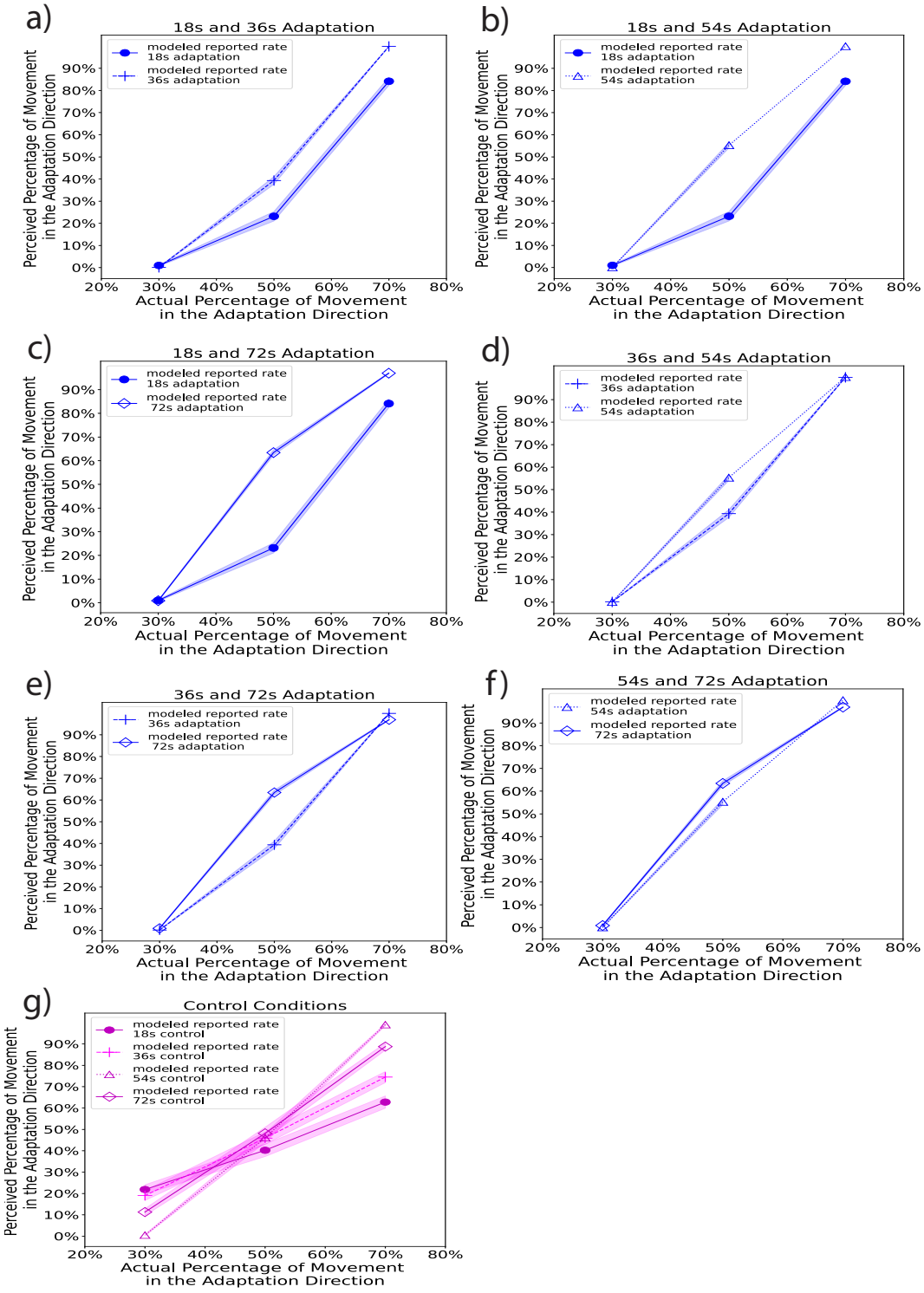

Figure 4.14: Experiment 3 The Modeled and Behavioral Reported Rates Separated by Experimental Conditions. The model was built from Experiment 1 with a single weight and predicted Experiment 3 with a single weight.

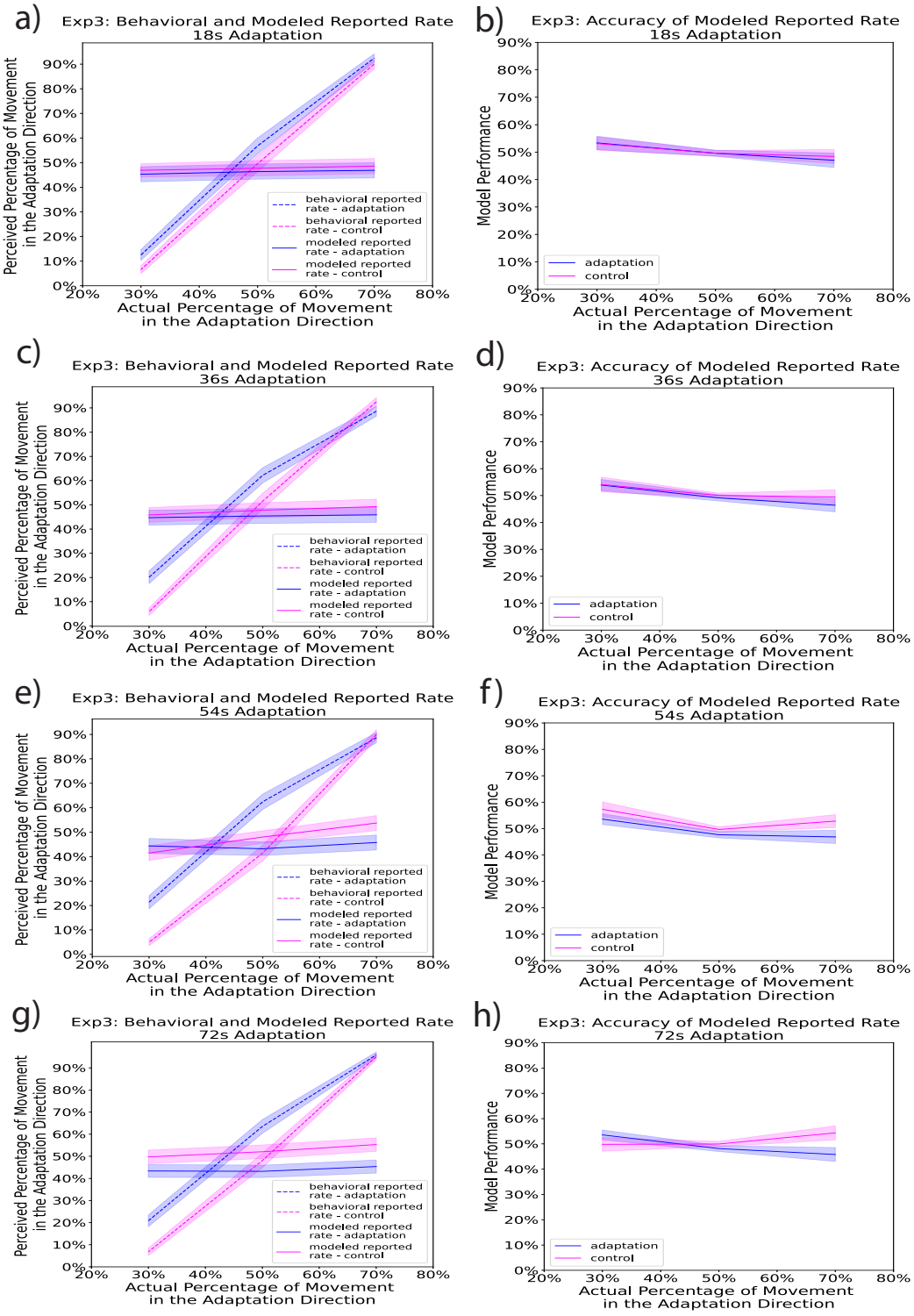

Figure 4.15: Experiment 3 The Modeled and Behavioral Reported Rates Separated by Adaptation Time Periods. The model was built from Experiment 1 with extra weights and predicted Experiment 3 with a single weight.

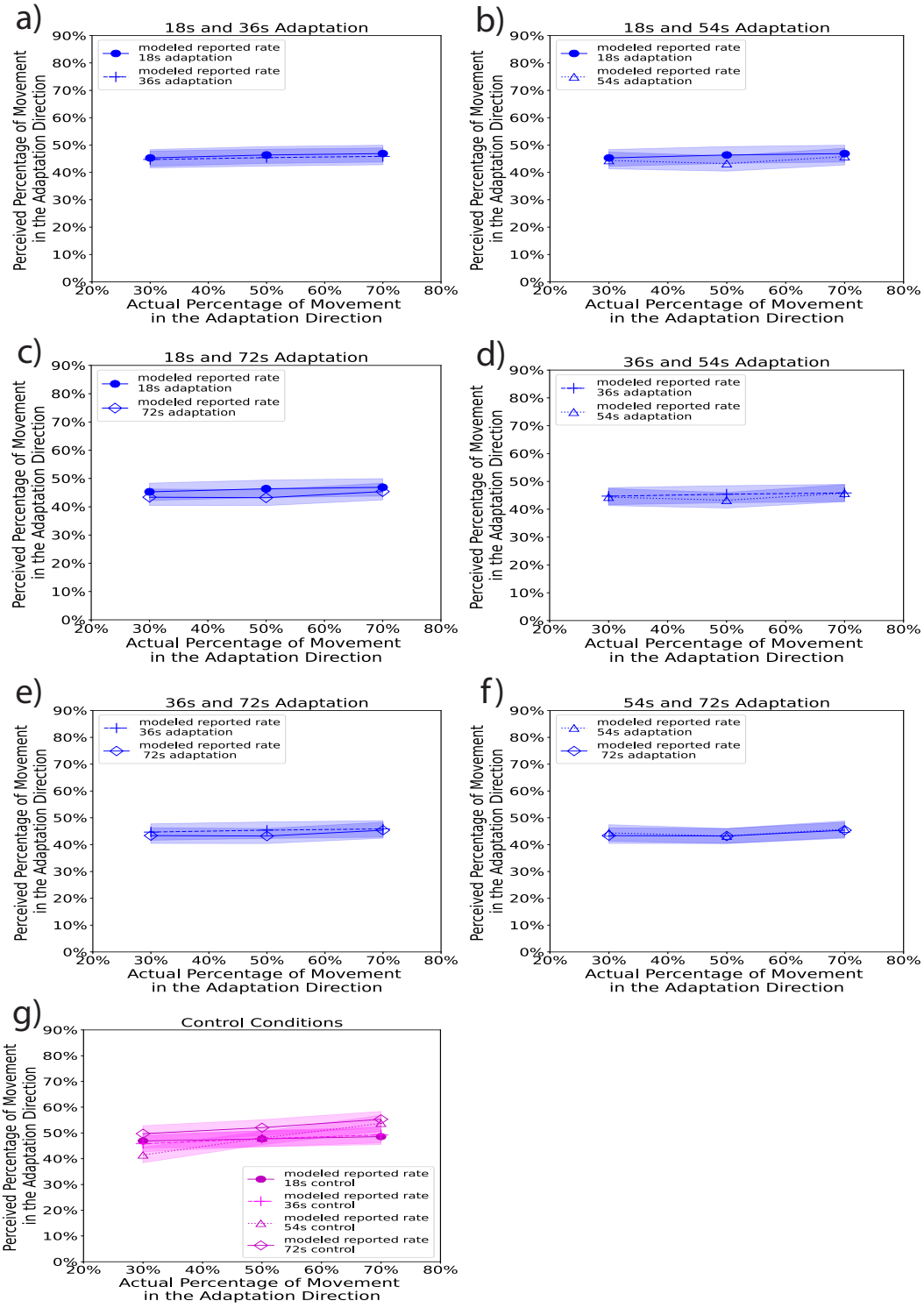

Figure 4.16: Experiment 3 The Modeled and Behavioral Reported Rates Separated by Experimental Conditions. The model was built from Experiment 1 with extra weights and predicted Experiment 3 with a single weight.

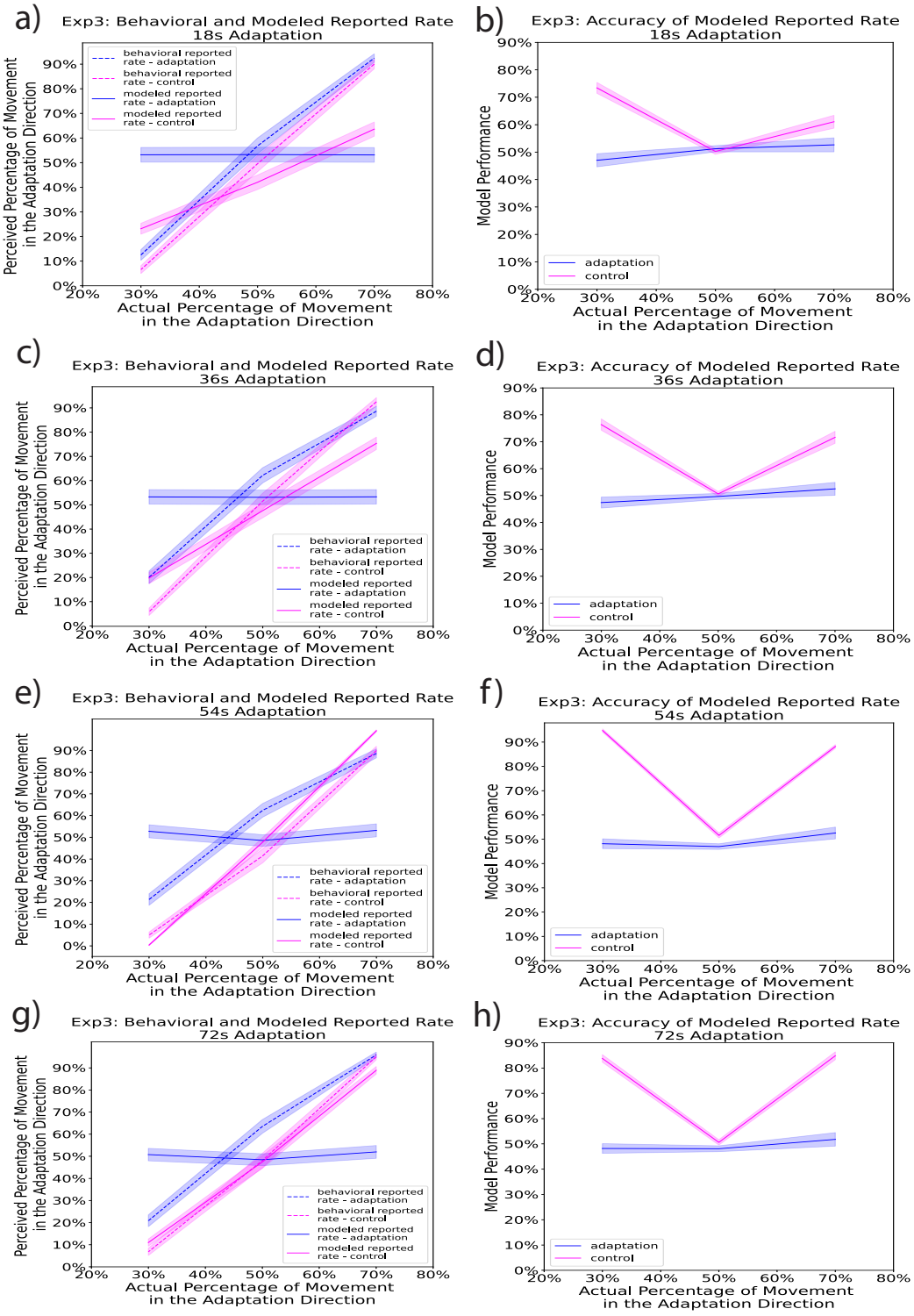

Figure 4.17: Experiment 3 The Modeled and Behavioral Reported Rates Separated by Adaptation Time Periods. The model was built from Experiment 1 with a single weight and predicted Experiment 3 with extra weights.

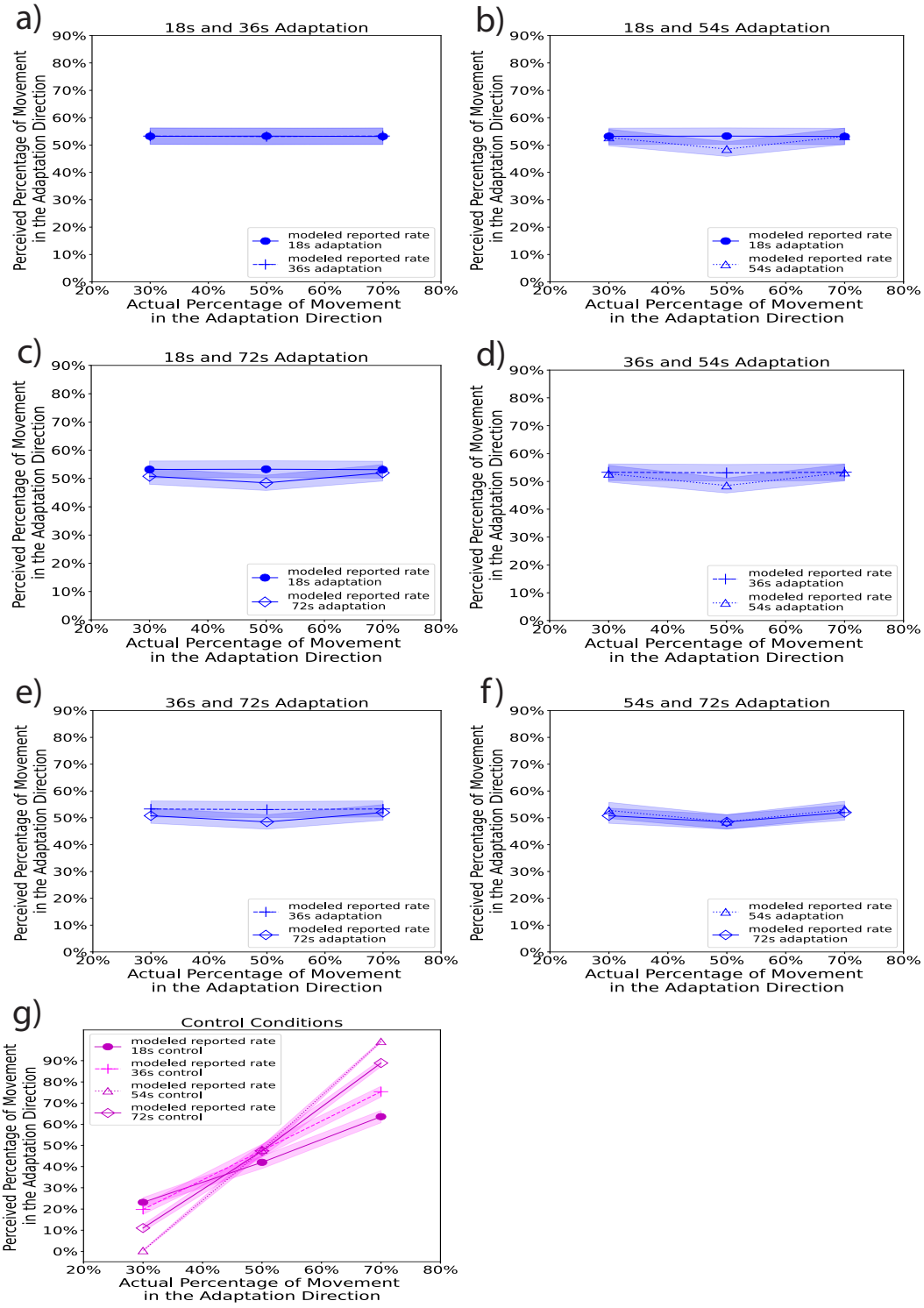

Figure 4.18: Experiment 3 The Modeled and Behavioral Reported Rates Separated by Experimental Conditions. The model was built from Experiment 1 with a single weight and predicted Experiment 3 with extra weights.

4.5 Discussion

In this study, I present a biologically plausible computational model of travel direction in humans. The model implements motion adaptation paradigms using an RNN and is able to simulate experimental findings by showing separate trajectories for the experimental adaptation condition and the control condition. The model also qualitatively reproduces the experimentally observed modulation of reference points and adaptation duration on the magnitude of travel aftereffects. Furthermore, the model could learn the relationship between different adaptation time durations and could be generalized in predicting new data set. As far as I know, this is the first neural network model of travel direction in humans. It demonstrates that an echo state network is sufficient to simulate the motion aftereffect of travel direction.

To determine where in the human brain the recurrent neural network for travel direction might be mapped, I cross-referenced relevant head and travel direction findings across insect, rodent, and human brain research.

4.5.1 The Pure Travel Direction Signal in the *Drosophila* Central Complex

By far the most direct evidence of a pure allocentric travel direction signal comes from the *Drosophila* brain (*aka.*, central complex) where head direction and travel direction were separately represented both structurally and functionally (Lyu et al., 2021). In the *Drosophila* central complex, allocentric travel direction was represented via hΔB cells which are located in the fan-shaped body (Lyu et al., 2021; Scheffer et al., 2020) while allocentric head direction was represented via EPG neurons which are located in the ellipsoid body and protocerebral bridge (Giraldo et al., 2018; Green et al., 2017; Kim, Rouault, Druckmann, & Jayaraman, 2017; Seelig & Jayaraman, 2015; Turner-Evans et al., 2017). A vector computation might take place in the central complex. That computation transforms allocentric head direction

signals into allocentric travel direction signals, with additional input from PFN_d and PFN_v cells (i.e., that represents egocentric travel direction signals) (Lyu et al., 2021; Wolff, Iyer, & Rubin, 2015). Although there is no direct evidence of such vector computation measured in the central complex, it is supported both structurally, mathematically, and through perturbation studies (Lyu et al., 2021). The vector computation theory suggests a possible relationship between head direction signals and travel direction signals which may generalize to the mammalian brain.

With regard to the travel direction system in the brain, if the vector computation theory sheds lights on the first half of the story on how the allocentric travel direction signal is generated, the current study focuses on the latter half of the story. That is to say, it focuses on how purely local allocentric travel direction signals accumulate overtime to form a global allocentric travel direction signal. Therefore, the next step is to seek evidence for areas that code pure allocentric travel direction, store accumulated allocentric travel direction information, as well as give rise to final report of travel direction. These areas may correspond to our recurrent neural network. If such evidence were to emerge regarding these areas, we will be in a better position to map the dynamic of the recurrent neural network to the human brain. Thus, we could better understand how the brain forms a travel trajectory over time.

4.5.2 Mixed Selectivity for Travel Direction Signals in the Rodent Brain

More direct evidence of travel direction signals in the mammalian brain comes from rodents. Two studies have reported conjunctive cells that code both travel direction and head direction using environments with boundaries (i.e., these neurons fire toward mixed travel direction signals), similar to the current study. One study reported bidirectional head direction cells in the dysgranular retrosplenial cortex. These cells have two opposing tuning curves that fire

at two opposite directions in compartmental environments (Jacob et al., 2017). However, the directional tuning of bi-directional head direction cells depends on landmarks and only functions in a compartmentalized environment; the directional tuning would be lost once the navigator enters into an open field.

These characteristics suggest that bi-directional head direction cells may only represent egocentric travel direction. The egocentric signal can be a major input to generate allocentric travel direction according to the vector computation theory, but it plays a minimal role in our recurrent neural network.

A similar interpretation could also be applied to the other study that reported axis-tuned neurons in the subiculum (Olson et al., 2017). The axis-tuned neurons also have two opposing tuning curves that fire at head directions 180° apart in a multi-path environment. Just like the bi-directional head direction cells in dysgranular retrosplenial cortex, directional tuning of axis-tuned neurons also relies on particular local environmental features (i.e., axis in the maze) and disappear after moving to an open arena. Such characteristics suggest that axis-tuned neurons may also represent egocentric travel direction. If we were to apply the same interpretation, this would lead us to believe that these cells are not included in our recurrent neural network. In addition, another study reported conjunctive cells in the medial entorhinal cortex that code both head direction and travel direction in an open arena, but no cells that purely code travel direction in the same brain region (Raudies et al., 2015). This suggests that medial entorhinal cortex could be a region where the vector computation that generates allocentric travel direction could take place. Overall, rodent studies only provide evidence for input signals that may generate allocentric travel direction, not representing the pure allocentric travel direction.

4.5.3 Travel Direction Signals in Humans

Studies in the human brain on directional representations were mainly based on fMRI signals. Although fMRI studies provide less direct neural evidence compared with animal research, they still provide useful information on human orientation signals. A recent fMRI study reported a widely distributed network for the head and travel directions when people actively navigated a dynamic and naturalistic environment (see Chapter 3). In the study, researchers reported representations for future and past travel directions when people were stationary, facing a particular direction that may or may not align with the future or past movements. These results support that travel direction could be represented in the human brain, independent of head direction. The brain regions that support future and past travel direction representations were reported in widely distributed brain areas including thalamus, retrosplenial cortex, precuneus, visual cortex, hippocampus, and striatum.

In addition, there is some evidence supporting the involvement of the hippocampus in the recurrent neural network of travel direction. First, conjunctive cells in the hippocampus have been reported in the rodent brain that code both present location and predict future travel direction (Huxter et al., 2008). Second, in Experiment 1, different magnitudes of travel aftereffects were observed in groups adapting to different reference points (i.e., the sun and the moon). Previous studies reported that the receptive field of place cells in the hippocampus could be modulated by different reference points Acharya, Aghajan, Vuong, Moore, and Mehta (2016); Jercog et al. (2019); Markus et al. (1995); Rubin, Yartsev, and Ulanovsky (2014). Thus, the magnitude of the difference in travel aftereffects toward different reference points could be a modulated through the hippocampus.

Regardless of whether there are particular cells in the human brain that code travel direction, this study provides a biologically plausible explanation for how travel direction might be represented in the human brain. The model demonstrates that the travel direction could be represented through dynamics in a recurrent neural network that is composed of simple

leaky integrator neurons and is independent of head direction.

4.5.4 Future Directions

Future research on the computational model of travel direction could look at how the head direction and travel direction systems differ in directional representation, as well as incorporating representations of other basic spatial signals (e.g., place cells, grid cells and speed cells) in explaining more complex human navigation behaviors.

4.6 Conclusion

I introduced a model of the human travel direction system using an RNN that receives local travel direction inputs and generates global travel direction reports. When a particular travel direction was adapted through extended movement in that direction, the model is able to qualitatively reproduce motion aftereffects of travel direction; these aftereffects mirror the results observed in the behavioral experiment. Further, the model could be generalized to predict travel aftereffects in new data set. Model comparison also suggests that the relationship between the initial adaptation and the top-up adaptation might be essential in generating travel aftereffects. As far as I know, this is the first computational model that simulates travel aftereffects in the human brain. This biologically plausible model provides a new way of representing travel direction in humans.

Chapter 5

Conclusions

Spatial navigation is not possible without knowing where our body is moving toward. Understanding how travel direction the direction of ones body movement - is represented in the human brain is key to understanding human spatial navigation. This dissertation sets out to understand the representation of travel direction in the internal orientation system of human navigation. Nevertheless, there is one additional layer of complexity to this question: travel direction is often assumed to be redundant with head direction, such that the two directions are usually conflated. Detecting travel direction out of the clouds of head direction information is a challenging question. Complicated questions such as this usually cannot be solved with one approach. Therefore, this dissertation investigates travel direction in human navigation by integrating psychophysics, neuroimaging, and computational modeling approaches. This final chapter will first review contributions of this dissertation, and then discuss directions for future research.

5.1 Contributions

Since travel direction has largely been ignored in the field of spatial navigation, my first step was to understand whether travel direction is a fundamental component in the internal orientation system of human navigation. In the first study (Chapter 2), I employed a motion adaptation paradigm from visual neuroscience designed to preclude the contribution of head direction. I found high-level aftereffects of perceived travel direction, indicating that travel direction is a fundamental component of human navigation. Interestingly, I discovered a higher frequency of reporting perceived travel toward the adapted direction compared to a no-adapt control an aftereffect that runs contrary to low-level motion aftereffects. This travel aftereffect was maintained after controlling for possible response biases and approaching effects, and it scaled with adaptation duration. These findings represent the first evidence for a pure travel direction signal in humans, independent of head direction.

While I found evidence that supports a pure travel direction signal in humans, where travel

direction is represented in the human brain is still not clear. In the second study (Chapter 3), I explored brain regions where travel direction might be represented when people actively navigate a complex, naturalistic environment during fMRI scanning. The study provides two threads of information about travel direction representations. The first thread comes from the movement (translating or rotating) period when peoples head and travel directions were aligned. I found widely distributed brain areas that represent head and travel directions, which provides a large array of candidate brain regions for coding the present travel direction. These regions include thalamus, retrosplenial cortex, precuneus, visual cortex, hippocampus, and striatum. The second thread comes from the stationary period when people were facing a particular direction, while planning for the next movement. In this period, head direction and travel direction could be dissociated because directions of peoples future movement or past movement do not always align with their present facing direction. I decoded both future and past travel directions from the stationary period in multiple brain regions. These regions include thalamus, retrosplenial cortex, precuneus, visual cortex, hippocampus, and striatum. These findings bring a more complete and nuanced understanding of where travel direction information is represented in the human brain.

Based on the first two studies, the third study (Chapter 4) continues to explore how travel direction might be represented in the human brain. In the third study, I built a biologically plausible computational model to simulate the unique motion aftereffect of travel direction observed in the first study using the same motion adaptation task. The model used a recurrent neural network (RNN) that receives local travel direction inputs and generates global travel direction reports. When a particular travel direction was adapted through extended movement in that direction, the model is able to qualitatively reproduce motion aftereffects of travel direction; these aftereffects mirror the results observed in the behavioral experiment. Further, the model could be generalized to predict travel aftereffects in a new data set. Model comparison suggests that the relationship between the initial adaptation and the top-up adaptation might be essential to generating travel aftereffects. This study

provides a new way of representing travel direction in humans.

The key findings in these chapters contribute a body of knowledge about travel direction across several different aspects. These aspects include different environments (a simple environment in studies 1 and 3 vs. a complex environment in the study 2), different types of spatial learning (passive navigation in studies 1 and 3 vs. goal-directed active navigation in the study 2), as well as different temporal domains (the present directional representation in studies 1 and 3 vs. past, present, and future directional representations in the study 2).Although each chapter took a very different approach (i.e., psychophysics, neuroimaging, and computational modeling), from their own scales they all shed light on the core question regarding the representation of travel direction in humans. At a behavioral level, study 1 provides evidence of what is the role of travel direction in the internal orientation system of human navigation. At a meso-level (i.e., the level of groups of neural populations), study 2 features a distributed travel and head direction system in discriminating directions in a complex navigation task, suggesting where in the human brain travel directions could be represented. Connecting the behavior and the neuronal levels, study 3 continues exploring travel direction by demonstrating how the travel direction system might work in the human brain using a computational neuroscience model. When combined, each approach provides an additional level of understanding regarding travel direction at a different scale.

5.2 Future Directions

Here, I laid out several research questions that evolved from the presented work and how I think these questions could be studied.

Question 1: How does the travel direction network coordinate with representations of other spatial information in the human brain to support flexible navigation?

Although travel direction is essential to forming the travel trajectory, there are many other fundamental spatial signals (e.g., the head direction, location, metric, boundary, and speed, etc.) that are crucial to human navigation. Only by understanding how travel direction systems work in concert with neural systems that represent other fundamental spatial information in the human brain can we eventually illustrate the intricacies of complex human navigation behaviors.

Leveraging the advantages of multidisciplinary approaches would be key to answering this big question because complicated questions cannot be solved with approaches from only one discipline. This dissertation demonstrates an example of studying complicated questions in neuroscience with integrated approaches. For example, study 1 suggests a pure signal for travel direction in humans by providing empirical evidence using an approach from cognitive psychology. The research was then further consolidated with computational insights from study 3, which demonstrates how this pure signal of travel direction might be represented in the human brain using an approach from computational neuroscience. Study 2 informs study 3 that a recurrent neural network is biologically plausible because head and travel directions are represented in the human brain via a widely distributed network. But how could study 3 support study 2? Perhaps integrating the current travel direction model with a head direction model and models of other spatial signals could be one future direction. That way, we could provide a more considerable understanding of flexible human navigation in complex environments.

Question 2: If the head and travel direction are so widely represented in the human brain, why do people still get lost?

Study 2 revealed widely distributed brain areas that represent head and travel directions in the human brain when actively navigating a complex environment. If many brain areas could play the role of internal compasses simultaneously during active navigation, then why is navigation ability so susceptible to normal aging and many neurological disorders (e.g., Alzheimers diseases, Parkinsons disease, and Huntingtons disease, etc.)? There might be various possible answers, but here is one of my hypotheses: although there seems to be sufficient sense of direction information represented in the human brain, utilizing the information for actual navigation might require an interpreter. In other words, we may have complete cognitive maps in our mind, but not every human brain knows how to read it; those who could not read the map or read it in a wrong way get lost. According to this hypothesis, the next step would be searching for brain areas that function as a readout layer of those senses of direction information. A combination of neuropsychology findings in patient studies, TMS approach in healthy populations, and perturbation studies from computational models could be an integrated approach to test this hypothesis.

Question 3: Can we add a developmental perspective to understand how representations of head direction and travel direction differ in humans?

Humans physical development follows an up to down order: a newborn will first be able to move their head while lying on their back, and then be able to move their body (Shelov & American Academy of Pediatrics., 1993). From *Drosophila* research, we learned that head direction signals are very likely to be a major input for generating allocentric travel direction in the central complex (i.e., the *Drosophila* brain) (Lyu et al., 2021). Findings in navigation circuits of the *Drosophila* central complex have been informative to and align with the functional organization of the navigation system in the mammalian brain. For example, the structure organization of the ellipsoid body in the *Drosophila* central complex - where head-direction-like cells (or EPG neurons) were discovered (Green et al., 2017) - matches the functional organization of head direction cells in the rodent brain (i.e., continuous ring

attractor model (Redish et al., 1996; Skaggs et al., 1995; K. Zhang, 1996)). Therefore, the combined findings that 1) head direction signals may generate allocentric travel direction signals in *Drosophila* and 2) that the head movement is developed prior to the body movement in humans may suggest that head direction signals emerge earlier than travel direction signals in the human brain. More future research will be needed to test the hypothesis.

Studying the question about the emergence of head and travel direction signals in humans could be useful for designing navigation systems in intelligent agents such as robots. Many robots are designed with dissociated head and travel direction systems to enable flexible activities (e.g., BB2, Toyota HSR., etc.). Robots acquire cognitive abilities gradually through trial and error. Studying how head and travel direction signals emerge in humans may help with designing more energy efficient robots, such as spontaneously generating travel direction from the head direction system.

5.3 Concluding Remarks

Taken together, the current study only takes a first step in understanding the travel direction system of human navigation. The research findings open many new questions regarding the role of travel direction in human development as well as in the entire navigation system. Much more research needs to be done in the future so that we could bring different pieces together to solve the puzzle of how humans navigate as well as how people get lost.

Eventually, I would like people to continue to move around and explore the environment, but also know how to return home.

References

Abraham, A., Pedregosa, F., Eickenberg, M., Gervais, P., Mueller, A., Kossaifi, J., ... Varoquaux, G. (2014, 2). Machine learning for neuroimaging with scikit-learn. *Frontiers in Neuroinformatics*, *8*(FEB), 14. Retrieved from `www.frontiersin.org` doi: 10.3389/fninf.2014.00014

Acharya, L., Aghajan, Z. M., Vuong, C., Moore, J. J., & Mehta, M. R. (2016). Causal influence of visual cues on hippocampal directional selectivity. *Cell*, *164*(1-2), 197–207.

Anstis, S. (1995). Aftereffects from jogging. *Experimental Brain Research*, *103*(3), 476–478.

Anstis, S., Verstraten, F. A. J., & Mather, G. (1998). The motion aftereffect. *Trends in cognitive sciences*, *2*(3), 111–117.

Antal, A., Varga, E. T., Nitsche, M. A., Chadaide, Z., Paulus, W., Kovács, G., & Vidnyánszky, Z. (2004). Direct current stimulation over MT+/V5 modulates motion aftereffect in humans. *Neuroreport*, *15*(16), 2491–2494.

Arleo, A., Déjean, C., Allegraud, P., Khamassi, M., Zugaro, M. B., & Wiener, S. I. (2013, 10). Optic Flow Stimuli Update Anterodorsal Thalamus Head Direction Neuronal Activity in Rats. *Journal of Neuroscience*, *33*(42), 16790–16795. Retrieved from `https://www.jneurosci.org/content/33/42/16790https://www.jneurosci.org/content/33/42/16790.abstract` doi: 10.1523/JNEUROSCI.2698-13.2013

Ashida, H., & Osaka, N. (1994). Difference of spatial frequency selectivity between static and flicker motion aftereffects. *Perception*, *23*(11), 1313–1320.

Avants, B. B., Epstein, C. L., Grossman, M., & Gee, J. C. (2008, 2). Symmetric diffeomorphic image registration with cross-correlation: evaluating automated labeling of elderly and neurodegenerative brain. *Medical image analysis*, *12*(1), 26–41. Retrieved from `https://pubmed.ncbi.nlm.nih.gov/17659998/` doi: 10.1016/J.MEDIA.2007.06.004

Bach, M., & Ullrich, D. (1994). Motion adaptation governs the shape of motion-evoked cortical potentials. *Vision Research*, *34*(12), 1541–1547.

Bai, J., He, X., Jiang, Y., Zhang, T., & Bao, M. (2020). Rotating One's Head Modulates the Perceived Velocity of Motion Aftereffect. *Multisensory Research*, *33*(2), 189–212. doi: 10.1163/22134808-20191477

Barlow, H. B. (1990). A theory about the functional role and synaptic mechanism of visual after-effects. *Vision: Coding and efficiency*, *363375*.

Barlow, H. B., & Hill, R. M. (1963). Selective sensitivity to direction of movement in ganglion cells of the rabbit retina. *Science*, *139*(3553), 412.

Baumann, O., Chan, E., & Mattingley, J. B. (2010). Dissociable neural circuits for encoding and retrieval of object locations during active navigation in humans. *Neuroimage*, *49*(3), 2816–2825. Retrieved from https://pubmed.ncbi.nlm.nih.gov/19837178/

Behzadi, Y., Restom, K., Liau, J., & Liu, T. T. (2007). A component based noise correction method (CompCor) for BOLD and perfusion based fMRI. *NeuroImage*, *37*(1), 90–101. Retrieved from http://www.sciencedirect.com/science/article/pii/S1053811907003837 doi: 10.1016/j.neuroimage.2007.04.042

Benjamini, Y., Heller, R., & Yekutieli, D. (2009, 11). Selective inference in complex research. *Philosophical Transactions of the Royal Society A: Mathematical, Physical and Engineering Sciences*, *367*(1906), 4255–4271. Retrieved from https://royalsocietypublishing.org/doi/full/10.1098/rsta.2009.0127 doi: 10.1098/RSTA.2009.0127

Benjaminit, Y., & Hochberg, Y. (1995, 1). Controlling the False Discovery Rate: A Practical and Powerful Approach to Multiple Testing. *Journal of the Royal Statistical Society: Series B (Methodological)*, *57*(1), 289–300. Retrieved from https://onlinelibrary.wiley.com/doi/full/10.1111/j.2517-6161.1995.tb02031.xhttps://onlinelibrary.wiley.com/doi/abs/10.1111/j.2517-6161.1995.tb02031.xhttps://rss.onlinelibrary.wiley.com/doi/10.1111/j.2517-6161.1995.tb02031.x doi: 10.1111/J.2517-6161.1995.TB02031.X

Berke, J. D., Breck, J. T., & Eichenbaum, H. (2009, 3). Striatal Versus Hippocampal Representations During Win-Stay Maze Performance. *Journal of Neurophysiology*, *101*(3), 1575. Retrieved from /pmc/articles/PMC2666400//pmc/articles/PMC2666400/?report=abstracthttps://www.ncbi.nlm.nih.gov/pmc/articles/PMC2666400/ doi: 10.1152/JN.91106.2008

Bex, P. J., Metha, A. B., & Makous, W. (1999). Enhanced motion aftereffect for complex motions. *Vision Research*, *39*(13), 2229–2238.

Blair, H. T., & Sharp, P. E. (1996). Visual and vestibular influences on head-direction cells in the anterior thalamus of the rat. *Behavioral neuroscience*, *110*(4), 643–660. Retrieved from https://pubmed.ncbi.nlm.nih.gov/8864258/ doi: 10.1037//0735-7044.110.4.643

Bratch, A., Chen, Y., Engel, S. A., & Kersten, D. J. (2021, 5). Visual adaptation selective for individual limbs reveals hierarchical human body representation. *Journal of Vision*, *21*(5), 18–18. Retrieved from https://doi.org/10.1167/jov.21.5.18. doi: 10.1167/JOV.21.5.18

Brett, M., Markiewicz, C. J., Hanke, M., Côté, M.-A., Cipollini, B., McCarthy, P., ... freec84 (2020, 11). *nipy/nibabel: 3.2.1.* Retrieved from https://zenodo.org/record/4295521 doi: 10.5281/ZENODO.4295521

Brooks, J. X., Carriot, J., & Cullen, K. E. (2015, 8). Learning to expect the unexpected: rapid updating in primate cerebellum during voluntary self-motion. *Nature Neuroscience 2015 18:9*, *18*(9), 1310–1317. Retrieved from https://www.nature.com/articles/nn.4077 doi: 10.1038/nn.4077

Brown, S. P., & Masland, R. H. (2001). Spatial scale and cellular substrate of contrast adaptation by retinal ganglion cells. *Nature neuroscience*, *4*(1), 44–51.

Brown, T. I., Carr, V. A., LaRocque, K. F., Favila, S. E., Gordon, A. M., Bowles, B., ... Wagner, A. D. (2016). Prospective representation of navigational goals

in the human hippocampus. *Science*, *352*(6291), 1323–1326. Retrieved from http://www.sciencemag.org/cgi/doi/10.1126/science.aaf0784 doi: 10.1126/science.aaf0784

Brown, T. I., Ross, R. S., Tobyne, S. M., & Stern, C. E. (2012, 4). Cooperative interactions between hippocampal and striatal systems support flexible navigation. *NeuroImage*, *60*(2), 1316–1330. Retrieved from http://www.povray.org/ doi: 10.1016/J.NEUROIMAGE.2012.01.046

Byrne, P., Becker, S., & Burgess, N. (2007). Remembering the past and imagining the future: a neural model of spatial memory and imagery. *Psychological review*, *114*(2), 340–375. Retrieved from http://www.pubmedcentral.nih.gov/articlerender.fcgi?artid=2678675&tool=pmcentrez&rendertype=abstract doi: 10.1037/0033-295X.114.2.340.Remembering

Cardin, V., Hemsworth, L., & Smith, A. T. (2012). Adaptation to heading direction dissociates the roles of human MST and V6 in the processing of optic flow. *Journal of Neurophysiology*, *108*(3), 794–801. doi: 10.1152/jn.00002.2012

Chen, L. L., Lin, L.-H., Green, E. J., Barnes, C. A., & McNaughton, B. L. (1994). Head-direction cells in the rat posterior cortex. *Experimental brain research*, *101*(1), 8–23.

Cho, J., & Sharp, P. E. (2001). Head direction, place, and movement correlates for cells in the rat retrosplenial cortex. *Behavioral neuroscience*, *115*(1), 3.

Chrastil, E. R. (2013). Neural evidence supports a novel framework for spatial navigation. *Psychonomic bulletin & review*, *20*(2), 208–27. Retrieved from http://www.ncbi.nlm.nih.gov/pubmed/23229443%5Cnhttp://link.springer.com/10.3758/s13423-012-0351-6 doi: 10.3758/s13423-012-0351-6

Chrastil, E. R., Nicora, G. L., & Huang, A. (2019). Vision and proprioception make equal contributions to path integration in a novel homing task. *Cognition*, *192*, 103998. Retrieved from https://faculty.sites.uci.edu/spatialneuro/files/2020/08/rbecca-paper-1.pdf

Chrastil, E. R., Sherrill, K. R., Hasselmo, M. E., & Stern, C. E. (2016). Which Way and How Far ? Tracking of Translation and Rotation Information for Human Path Integration. *Human Brain Mapping*, *3655*(March), 3636–3655. doi: 10.1002/hbm.23265

Chrastil, E. R., & Warren, W. H. (2013). Active and Passive Spatial Learning in Human Navigation : Acquisition of Survey Knowledge. *Journal of Experimental Psychology: Learning Memory and Cognition*, *39*(5), 1520–1537. doi: 10.1037/a0032382

Chrastil, E. R., & Warren, W. H. (2014). From Cognitive Maps to Cognitive Graphs. *PLoS One*, *9*(11). doi: 10.1371/journal.pone.0112544

Chrastil, E. R., & Warren, W. H. (2015, 7). Active and passive spatial learning in human navigation: acquisition of graph knowledge. *Journal of experimental psychology. Learning, memory, and cognition*, *41*(4), 1162–1178. Retrieved from https://pubmed.ncbi.nlm.nih.gov/25419818/ doi: 10.1037/XLM0000082

Ciric, R., Wolf, D. H., Power, J. D., Roalf, D. R., Baum, G. L., Ruparel, K., ... others (2017). Benchmarking of participant-level confound regression strategies for the control of motion artifact in studies of functional connectivity. *Neuroimage*, *154*, 174–187.

Clark, B. J., & Harvey, R. E. (2016, 9). Do the anterior and lateral thalamic nuclei make distinct contributions to spatial representation and memory? *Neurobiology of learning and memory*, *133*, 69–78. Retrieved from https://pubmed.ncbi.nlm.nih.gov/

27266961/ doi: 10.1016/J.NLM.2016.06.002

Cox, R. W., & Hyde, J. S. (1997). Software tools for analysis and visualization of fMRI data. *NMR in Biomedicine*, *10*(4-5), 171–178. doi: 10.1002/(SICI)1099-1492(199706/08)10:4/5⟨171::AID-NBM453⟩3.0.CO;2-L

Culham, J. C., Nishida, S., Ledgeway, T., Cavanagh, P., von Grünau, M. W., Kwas, M., & Raymond, J. (1998). Higher order effects. In *The motion aftereffect: A modern perspective* (pp. 85–124). MIT Press Cambridge, MA.

Culham, J. C., Verstraten, F. A. J., Ashida, H., & Cavanagh, P. (2000). Independent aftereffects of attention and motion. *Neuron*, *28*(2), 607–615. Retrieved from https://www.sciencedirect.com/science/article/pii/S0896627300001379

Cullen, K. E. (2011, 8). The neural encoding of self-motion. *Current Opinion in Neurobiology*, *21*(4), 587–595. doi: 10.1016/J.CONB.2011.05.022

Cullen, K. E. (2012, 3). The vestibular system: multimodal integration and encoding of self-motion for motor control. *Trends in neurosciences*, *35*(3), 185. Retrieved from /pmc/articles/PMC4000483//pmc/articles/PMC4000483/?report=abstracthttps://www.ncbi.nlm.nih.gov/pmc/articles/PMC4000483/ doi: 10.1016/J.TINS.2011.12.001

Cullen, K. E., & Taube, J. S. (2017). Our sense of direction: progress, controversies and challenges. *Nature neuroscience*, *20*(11), 1465–1473. Retrieved from https://pubmed.ncbi.nlm.nih.gov/29073639/ doi: 10.1038/NN.4658

Curran, W., Clifford, C. W., & Benton, C. P. (2006, 11). The direction aftereffect is driven by adaptation of local motion detectors. *Vision Research*, *46*(25), 4270–4278. doi: 10.1016/J.VISRES.2006.08.026

Dale, A. M., Fischl, B., & Sereno, M. I. (1999). Cortical Surface-Based Analysis: I. Segmentation and Surface Reconstruction. *NeuroImage*, *9*(2), 179–194. Retrieved from http://www.sciencedirect.com/science/article/pii/S1053811998903950 doi: 10.1006/nimg.1998.0395

Desikan, R. S., Ségonne, F., Fischl, B., Quinn, B. T., Dickerson, B. C., Blacker, D., ... others (2006). An automated labeling system for subdividing the human cerebral cortex on MRI scans into gyral based regions of interest. *Neuroimage*, *31*(3), 968–980.

Ding, L., & Gold, J. I. (2013, 8). The Basal Ganglias Contributions to Perceptual Decision Making. *Neuron*, *79*(4), 640–649. doi: 10.1016/J.NEURON.2013.07.042

Doeller, C. F., King, J. A., & Burgess, N. (2008). Parallel striatal and hippocampal systems for landmarks and boundaries in spatial memory. *Proceedings of the National Academy of Sciences*, *105*(15), 5915–5920. Retrieved from http://www.pnas.org/cgi/doi/10.1073/pnas.0801489105 doi: 10.1073/pnas.0801489105

Doll, B. B., & Frank, M. J. (2009, 1). The basal ganglia in reward and decision making: computational models and empirical studies. *Handbook of Reward and Decision Making*, 399–425. doi: 10.1016/B978-0-12-374620-7.00019-4

Dominey, P. F., & Ramus, F. (2010). Neural network processing of natural language: I. Sensitivity to serial, temporal and abstract structure of language in the infant. *http://dx.doi.org/10.1080/016909600386129*, *15*(1), 87–127. Retrieved from https://www.tandfonline.com/doi/abs/10.1080/016909600386129 doi: 10.1080/016909600386129

Dragoi, G., & Tonegawa, S. (2011, 1). Preplay of future place cell sequences by hippocampal

cellular assemblies. *Nature*, *469*(7330), 397–401. Retrieved from https://pubmed.ncbi.nlm.nih.gov/21179088/ doi: 10.1038/NATURE09633

Dubé, S., & Von Grünau, M. (1992). Comparing local and remote motion aftereffects. *Spatial vision*, *6*(4), 303–314.

Durgin, F. H., & Pelah, A. (1999). Visuomotor adaptation without vision? *Experimental Brain Research*, *127*(1), 12–18.

Earhart, G. M., Melvill Jones, G., Horak, F. B., Block, E. W., Weber, K. D., & Fletcher, W. A. (2001). Forward versus backward walking: transfer of podokinetic adaptation. *Journal of Neurophysiology*, *86*(4), 1666–1670.

Ekstrom, a. D., Kahana, M. J., Caplan, J. B., Fields, T. a., Isham, E. a., Newman, E. L., & Fried, I. (2003). Cellular networks underlying human spatial navigation. *Nature*, *425*(6954), 184–188. Retrieved from http://www.ncbi.nlm.nih.gov/entrez/query.fcgi?cmd=Retrieve&db=PubMed&dopt=Citation&list_uids=12968182 doi: 10.1038/nature01955.1.

Erdfelder, E., Faul, F., & Buchner, A. (1996). GPOWER: A general power analysis program. *Behavior research methods, instruments, & computers*, *28*(1), 1–11.

Esteban, O., Blair, R., Markiewicz, C. J., Berleant, S. L., Moodie, C., Ma, F., ... Gorgolewski, K. J. (2018). fMRIPrep. *Software*. doi: 10.5281/zenodo.852659

Esteban, O., Markiewicz, C. J., Blair, R. W., Moodie, C. A., Isik, A. I., Erramuzpe, A., ... Gorgolewski, K. J. (2018, 12). fMRIPrep: a robust preprocessing pipeline for functional MRI. *Nature Methods 2018 16:1*, *16*(1), 111–116. Retrieved from https://www.nature.com/articles/s41592-018-0235-4 doi: 10.1038/s41592-018-0235-4

Fang, F., & He, S. (2005, 3). Viewer-Centered Object Representation in the Human Visual System Revealed by Viewpoint Aftereffects. *Neuron*, *45*(5), 793–800. Retrieved from http://www.cell.com/article/S0896627305000759/fulltexthttp://www.cell.com/article/S0896627305000759/abstracthttps://www.cell.com/neuron/abstract/S0896-6273(05)00075-9 doi: 10.1016/J.NEURON.2005.01.037

Fang, F., Murray, S. O., Kersten, D., & He, S. (2005). Orientation-tuned fMRI adaptation in human visual cortex. *Journal of Neurophysiology*, *94*(6), 4188–4195.

Fonov, V. S., Evans, A. C., McKinstry, R. C., Almli, C. R., & Collins, D. L. (2009). Unbiased nonlinear average age-appropriate brain templates from birth to adulthood. *NeuroImage*, *47, Supplement 1*, S102. doi: 10.1016/S1053-8119(09)70884-5

Frank, L. M., Brown, E. N., & Wilson, M. (2000). Trajectory encoding in the hippocampus and entorhinal cortex. *Neuron*, *27*(1), 169–178.

Frazier, J. A., Chiu, S., Breeze, J. L., Makris, N., Lange, N., Kennedy, D. N., ... others (2005). Structural brain magnetic resonance imaging of limbic and thalamic volumes in pediatric bipolar disorder. *American Journal of Psychiatry*, *162*(7), 1256–1265.

Fyhn, M., Molden, S., Witter, M. P., Moser, E. I., & Moser, M. B. (2004, 8). Spatial representation in the entorhinal cortex. *Science*, *305*(5688), 1258–1264. Retrieved from https://www.science.org/doi/full/10.1126/science.1099901 doi: 10.1126/SCIENCE.1099901/SUPPL{_}FILE/FYNH.SOM.PDF

Gallistel, C. (1990). *The organization of learning*. MIT Press.

Geerts, J. P., Chersi, F., Stachenfeld, K. L., & Burgess, N. (2020). A general model of hippocampal and dorsal striatal learning and decision making. *Proceedings of the National Academy of Sciences*. Retrieved from https://www.pnas.org/doi/10.1073/

pnas.2007981117
Giraldo, Y. M., Leitch, K. J., Ros, I. G., Warren, T. L., Weir, P. T., & Dickinson, M. H. (2018, 9). Sun Navigation Requires Compass Neurons in Drosophila. *Current Biology*, *28*(17), 2845. Retrieved from /pmc/articles/PMC7301569//pmc/articles/PMC7301569/?report=abstracthttps://www.ncbi.nlm.nih.gov/pmc/articles/PMC7301569/ doi: 10.1016/J.CUB.2018.07.002
Giudice, N. A. (2018). Navigating without Vision: Principles of Blind Spatial Cognition. In *Handbook of behavioral&cognitive geogrphy.*
Glasser, M. F., Sotiropoulos, S. N., Wilson, J. A., Coalson, T. S., Fischl, B., Andersson, J. L., ... Jenkinson, M. (2013). The minimal preprocessing pipelines for the Human Connectome Project. *NeuroImage*, *80*, 105–124. Retrieved from http://www.sciencedirect.com/science/article/pii/S1053811913005053 doi: 10.1016/j.neuroimage.2013.04.127
Goldstein, J. M., Seidman, L. J., Makris, N., Ahern, T., OBrien, L. M., Caviness Jr, V. S., ... Tsuang, M. T. (2007). Hypothalamic abnormalities in schizophrenia: sex effects and genetic vulnerability. *Biological psychiatry*, *61*(8), 935–945.
Gordon, C. R., Fletcher, W. A., Jones, G. M., & Block, E. W. (1995). Adaptive plasticity in the control of locomotor trajectory. *Experimental Brain Research*, *102*(3), 540–545.
Gorgolewski, K., Burns, C. D., Madison, C., Clark, D., Halchenko, Y. O., Waskom, M. L., & Ghosh, S. (2011). Nipype: a flexible, lightweight and extensible neuroimaging data processing framework in Python. *Frontiers in Neuroinformatics*, *5*, 13. doi: 10.3389/fninf.2011.00013
Gorgolewski, K. J., Esteban, O., Markiewicz, C. J., Ziegler, E., Ellis, D. G., Notter, M. P., ... Ghosh, S. (2018). Nipype. *Software*. doi: 10.5281/zenodo.596855
Green, J., Adachi, A., Shah, K. K., Hirokawa, J. D., Magani, P. S., & Maimon, G. (2017). A neural circuit architecture for angular integration in Drosophila. *Nature*, *546*(7656), 101–106. doi: 10.1038/nature22343
Greve, D. N., & Fischl, B. (2009). Accurate and robust brain image alignment using boundary-based registration. *NeuroImage*, *48*(1), 63–72. doi: 10.1016/j.neuroimage.2009.06.060
Grill-Spector, K., & Malach, R. (2001). fMR-adaptation: a tool for studying the functional properties of human cortical neurons. *Acta psychologica*, *107*(1-3), 293–321.
Guldin, W. O., & Grüsser, O. J. (1998, 6). Is there a vestibular cortex? *Trends in neurosciences*, *21*(6), 254–259. Retrieved from https://pubmed.ncbi.nlm.nih.gov/9641538/ doi: 10.1016/S0166-2236(97)01211-3
Hafting, T., Fyhn, M., Molden, S., Moser, M.-B., & Moser, E. I. (2005). Microstructure of a spatial map in the entorhinal cortex. *Nature*, *436*(7052), 801–806.
Hartley, T., Maguire, E. A., Spiers, H. J., & Burgess, N. (2003). The well-worn route and the path less traveled: Distinct neural bases of route following and wayfinding in humans. *Neuron*, *37*(5), 877–888. doi: 10.1016/S0896-6273(03)00095-3
Hassabis, D., Chu, C., Rees, G., Weiskopf, N., Molyneux, P. D., & Maguire, E. A. (2009). Decoding neuronal ensembles in the human hippocampus. *Current Biology*, *19*(7), 546–554.
Hikosaka, O., Ghazizadeh, A., Griggs, W., & Amita, H. (2018, 3). Parallel basal ganglia circuits for decision making. *Journal of Neural Transmission*, *125*(3), 515–529. Retrieved

from https://link.springer.com/article/10.1007/s00702-017-1691-1 doi: 10.1007/S00702-017-1691-1/FIGURES/6

Hiris, E., & Blake, R. (1992). Another perspective on the visual motion aftereffect. *Proceedings of the National Academy of Sciences*, *89*(19), 9025–9028.

Hopfield, J. J. (1984). Neurons with graded response have collective computational properties like those of two-state neurons. *Proceedings of the National Academy of Sciences of the United States of America*, *81*(10 I), 3088–3092. Retrieved from https://www.pnas.org doi: 10.1073/PNAS.81.10.3088

Hulse, B. K., Haberkern, H., Franconville, R., Turner-Evans, D. B., Takemura, S. Y., Wolff, T., ... Jayaraman, V. (2021, 10). A connectome of the drosophila central complex reveals network motifs suitable for flexible navigation and context-dependent action selection. *eLife*, *10*. doi: 10.7554/ELIFE.66039

Huxter, J. R., Senior, T. J., Allen, K., & Csicsvari, J. (2008, 4). Theta phasespecific codes for two-dimensional position, trajectory and heading in the hippocampus. *Nature Neuroscience 2008 11:5*, *11*(5), 587–594. Retrieved from https://www.nature.com/articles/nn.2106 doi: 10.1038/nn.2106

Ilies, I., Jaeger, H., Kosuchinas, O., Rincon, M., Sak, V., & Vaškevičius, N. (2007). *Stepping forward through echoes of the past: forecasting with Echo State Networks* (Tech. Rep.). Retrieved from http://www.neural-forecasting-competition.com/downloads/NN3/methods/27-NN3 doi: 10.1016/j.neunet.2007.04.001

Jacob, P. Y., Casali, G., Spieser, L., Page, H., Overington, D., & Jeffery, K. (2017). An independent, landmark-dominated head-direction signal in dysgranular retrosplenial cortex. *Nature Neuroscience*, *20*(2), 173–175. doi: 10.1038/nn.4465

Jacobs, J., Weidemann, C. T., Miller, J. F., Solway, A., Burke, J. F., Wei, X. X., ... Kahana, M. J. (2013, 8). Direct recordings of grid-like neuronal activity in human spatial navigation. *Nature Neuroscience 2013 16:9*, *16*(9), 1188–1190. Retrieved from https://www.nature.com/articles/nn.3466 doi: 10.1038/nn.3466

Jaeger, H. (2007). *Echo state network* (Vol. 2) (No. 9). Scholarpedia. doi: 10.4249/SCHOLARPEDIA.2330

Jaeger, H. (2010). *The "echo state" approach to analysing and training recurrent neural networks - with an Erratum note* (Tech. Rep.). Fraunhofer Institute for Autonomous Intelligent Systems. Retrieved from https://www.ai.rug.nl/minds/uploads/EchoStatesTechRep.pdf

Jaeger, H., Lukoševičius, M., Popovici, D., & Siewert, U. (2007, 4). Optimization and applications of echo state networks with leaky- integrator neurons. *Neural Networks*, *20*(3), 335–352. doi: 10.1016/J.NEUNET.2007.04.016

Jenkinson, M., Bannister, P., Brady, M., & Smith, S. (2002). Improved Optimization for the Robust and Accurate Linear Registration and Motion Correction of Brain Images. *NeuroImage*, *17*(2), 825–841. Retrieved from http://www.sciencedirect.com/science/article/pii/S1053811902911328 doi: 10.1006/nimg.2002.1132

Jercog, P. E., Ahmadian, Y., Woodruff, C., Deb-Sen, R., Abbott, L. F., & Kandel, E. R. (2019). Heading direction with respect to a reference point modulates place-cell activity. *Nature Communications*, *10*(1), 1–8. Retrieved from http://dx.doi.org/10.1038/s41467-019-10139-7 doi: 10.1038/s41467-019-10139-7

Johnson, A., & Redish, A. D. (2007, 11). Neural Ensembles in CA3 Transiently En-

code Paths Forward of the Animal at a Decision Point. *Journal of Neuroscience*, *27*(45), 12176–12189. Retrieved from https://www.jneurosci.org/content/27/45/12176https://www.jneurosci.org/content/27/45/12176.abstract doi: 10.1523/JNEUROSCI.3761-07.2007

Kent, J., & Herholz, P. (2019, 9). NiBetaSeries: task related correlations in fMRI. *Journal of Open Source Software*, *4*(41), 1295. Retrieved from https://joss.theoj.org/papers/10.21105/joss.01295 doi: 10.21105/joss.01295

Kent, J. D., & Herholz, P. (2018). NiBetaSeries. *Software*. doi: 10.5281/zenodo.1342291

Kim, S. S., Rouault, H., Druckmann, S., & Jayaraman, V. (2017, 5). Ring attractor dynamics in the Drosophila central brain. *Science (New York, N.Y.)*, *356*(6340), 849–853. Retrieved from https://pubmed.ncbi.nlm.nih.gov/28473639/ doi: 10.1126/SCIENCE.AAL4835

Klein, A., Ghosh, S. S., Bao, F. S., Giard, J., Häme, Y., Stavsky, E., ... Keshavan, A. (2017). Mindboggling morphometry of human brains. *PLOS Computational Biology*, *13*(2), e1005350. Retrieved from http://journals.plos.org/ploscompbiol/article?id=10.1371/journal.pcbi.1005350 doi: 10.1371/journal.pcbi.1005350

Koch, C., Li, S.-C., Polk, T. A., & Schuck, N. W. (2020). Effects of aging on encoding of walking direction in the human brain. *Neuropsychologia*, *141*, 107379.

Kohn, A., & Movshon, J. (2003, 8). Neuronal Adaptation to Visual Motion in Area MT of the Macaque. *Neuron*, *39*(4), 681–691. Retrieved from https://linkinghub.elsevier.com/retrieve/pii/S0896627303004380 doi: 10.1016/S0896-6273(03)00438-0

Lanczos, C. (1964). Evaluation of Noisy Data. *Journal of the Society for Industrial and Applied Mathematics Series B Numerical Analysis*, *1*(1), 76–85. Retrieved from http://epubs.siam.org/doi/10.1137/0701007 doi: 10.1137/0701007

Lee, S., & Kable, J. W. (2018, 11). Simple but robust improvement in multivoxel pattern classification. *PLOS ONE*, *13*(11), e0207083. Retrieved from https://journals.plos.org/plosone/article?id=10.1371/journal.pone.0207083 doi: 10.1371/JOURNAL.PONE.0207083

Leopold, D. A., Rhodes, G., Müller, K. M., & Jeffery, L. (2005, 5). The dynamics of visual adaptation to faces. *Proceedings. Biological sciences*, *272*(1566), 897–904. Retrieved from https://pubmed.ncbi.nlm.nih.gov/16024343/ doi: 10.1098/RSPB.2004.3022

Leutgeb, S., Ragozzino, K. E., & Mizumori, S. J. (2000, 9). Convergence of head direction and place information in the CA1 region of hippocampus. *Neuroscience*, *100*(1), 11–19. Retrieved from https://pubmed.ncbi.nlm.nih.gov/10996454/ doi: 10.1016/S0306-4522(00)00258-X

Lisberger, S. G., & Movshon, J. A. (1999). Visual motion analysis for pursuit eye movements in area MT of macaque monkeys. *Journal of Neuroscience*, *19*(6), 2224–2246.

Loomis, J. M., Klatzky, R. L., Golledge, R. G., Cicinelli, J. G., Pellegrino, J. W., & Fry, P. A. (1993). Nonvisual navigation by blind and sighted: assessment of path integration ability. *Journal of experimental psychology. General*, *122*(1), 73–91. doi: 10.1037/0096-3445.122.1.73

Lukoševičius, M. (2012). A Practical Guide to Applying Echo State Networks. In G. Montavon, G. B. Orr, & K.-R. Müller (Eds.), *Neural networks: Tricks of the trade, reloaded.* Springer.

Lukoševičius, M., Jaeger, H., & Schrauwen, B. (2012, 11). Reservoir Computing Trends. *KI - Kunstliche Intelligenz*, *26*(4), 365–371. Retrieved from https://link.springer.com/article/10.1007/s13218-012-0204-5 doi: 10.1007/S13218-012-0204-5/FIGURES/1

Lyu, C., Abbott, L. F., & Maimon, G. (2021). Building an allocentric travelling direction signal via vector computation. *Nature*, *601*(January). doi: 10.1038/s41586-021-04067-0

Maffei, L., Fiorentini, A., & Bisti, S. (1973). Neural correlate of perceptual adaptation to gratings. *Science*, *182*(4116), 1036–1038.

Makris, N., Goldstein, J. M., Kennedy, D., Hodge, S. M., Caviness, V. S., Faraone, S. V., ... Seidman, L. J. (2006). Decreased volume of left and total anterior insular lobule in schizophrenia. *Schizophrenia research*, *83*(2-3), 155–171.

Marchette, S. A., Vass, L. K., Ryan, J., & Epstein, R. A. (2014). Anchoring the neural compass: coding of local spatial reference frames in human medial parietal lobe. *Nature Neuroscience*, *17*(11), 1598–1606. Retrieved from http://www.nature.com/doifinder/10.1038/nn.3834 doi: 10.1038/nn.3834

Markus, E. J., Qin, Y.-L., Leonard, B., Skaggs, W. E., McNaughton, B. L., & Barnes, C. A. (1995). Interactions between location and task affect the spatial and directional firing of hippocampal neurons. *Journal of Neuroscience*, *15*(11), 7079–7094.

Mather, G., Pavan, A., Campana, G., & Casco, C. (2008). The motion aftereffect reloaded. *Trends in Cognitive Sciences*, *12*(12), 481–487. doi: 10.1016/j.tics.2008.09.002

Mather, G. E., Verstraten, F. E., & Anstis, S. E. (1998). *The motion aftereffect: A modern perspective.* The MIT Press.

McKinney, W. (2010). Data structures for statistical computing in python. In *Proceedings of the 9th python in science conference* (Vol. 445, pp. 51–56).

Medrea, I., & Cullen, K. E. (2013, 12). Multisensory integration in early vestibular processing in mice: The encoding of passive vs. active motion. *Journal of Neurophysiology*, *110*(12), 2704–2717. Retrieved from https://journals.physiology.org/doi/full/10.1152/jn.01037.2012 doi: 10.1152/JN.01037.2012/ASSET/IMAGES/LARGE/Z9K0241322310009.JPEG

Mei, G., Dong, X., & Bao, M. (2017, 1). The timescale of adaptation at early and mid-level stages of visual processing. *Journal of Vision*, *17*(1), 1–1. doi: 10.1167/17.1.1

Miller, E. K., Gochin, P. M., & Gross, C. G. (1991). Habituation-like decrease in the responses of neurons in inferior temporal cortex of the macaque. *Visual neuroscience*, *7*(4), 357–362.

Mizumori, S. J., & Williams, J. D. (1993). Directionally selective mnemonic properties of neurons in the lateral dorsal nucleus of the thalamus of rats. *The Journal of neuroscience : the official journal of the Society for Neuroscience*, *13*(9), 4015–4028. Retrieved from https://pubmed.ncbi.nlm.nih.gov/8366357/ doi: 10.1523/JNEUROSCI.13-09-04015.1993

Mood, A. M., Graybill, F. A., & Boes, D. C. (1974). *Introduction to the Theory of Statistics* (3rd ed.). Boston: McGraw Hill.

Moser, E. I., Moser, M. B., & McNaughton, B. L. (2017, 11). Spatial representation in the hippocampal formation: a history. *Nature Neuroscience 2017 20:11*, *20*(11), 1448–1464. Retrieved from https://www.nature.com/articles/nn.4653 doi: 10.1038/

nn.4653
Mulavara, A. P., Feiveson, A. H., Fiedler, J., Cohen, H., Peters, B. T., Miller, C., ... Bloomberg, J. J. (2010). Locomotor function after long-duration space flight: effects and motor learning during recovery. *Experimental brain research*, *202*(3), 649–659.
Nau, M., Schröder, T. N., Frey, M., & Doeller, C. F. (2020). Behavior-dependent directional tuning in the human visual-navigation network. *Nature communications*, *11*(1), 1–13. Retrieved from https://www.nature.com/articles/s41467-020-17000-2
Nishida, S., & Sato, T. (1995). Motion aftereffect with flickering test patterns reveals higher stages of motion processing. *Vision research*, *35*(4), 477–490.
O'Keefe, J. (1976, 1). Place units in the hippocampus of the freely moving rat. *Experimental Neurology*, *51*(1), 78–109. doi: 10.1016/0014-4886(76)90055-8
O'Keefe, J., & Dostrovsky, J. (1971). The hippocampus as a spatial map. Preliminary evidence from unit activity in the freely-moving rat. *Brain Research*, *34*(1). doi: 10.1016/0006-8993(71)90358-1
Oliphant, T. E. (2006). *A guide to NumPy* (Vol. 1). Trelgol Publishing USA.
Olson, J. M., Tongprasearth, K., & Nitz, D. A. (2017, 2). Subiculum neurons map the current axis of travel. *Nature neuroscience*, *20*(2), 170–172. Retrieved from https://pubmed.ncbi.nlm.nih.gov/27991899/ doi: 10.1038/NN.4464
OKeefe, J., & Nadel, L. (1978). *The Hippocampus as a Cognitive Map*. doi: 10.1017/CBO9781107415324.004
Page, H. J., & Jeffery, K. J. (2018). Landmark-based updating of the head direction system by retrosplenial cortex: A computational model. *Frontiers in Cellular Neuroscience*, *12*(July), 1–17. doi: 10.3389/fncel.2018.00191
Parkes, L., Fulcher, B., Yücel, M., & Fornito, A. (2018). An evaluation of the efficacy, reliability, and sensitivity of motion correction strategies for resting-state functional MRI. *Neuroimage*, *171*, 415–436.
Pedregosa, F., Michel, V., Varoquaux, G., Thirion, B., Dubourg, V., Passos, A., ... Duchesnay, . (2011). *Scikit-learn: Machine Learning in Python* (Vol. 12; Tech. Rep. No. 85). Retrieved from http://scikit-learn.sourceforge.net.
Power, J. D., Mitra, A., Laumann, T. O., Snyder, A. Z., Schlaggar, B. L., & Petersen, S. E. (2014). Methods to detect, characterize, and remove motion artifact in resting state fMRI. *NeuroImage*, *84*(Supplement C), 320–341. Retrieved from http://www.sciencedirect.com/science/article/pii/S1053811913009117 doi: 10.1016/j.neuroimage.2013.08.048
Prins, N., & Kingdom, F. A. A. (2018, 7). Applying the Model-Comparison Approach to Test Specific Research Hypotheses in Psychophysical Research Using the Palamedes Toolbox. *Frontiers in Psychology*, *9*, 1250. Retrieved from https://www.frontiersin.org/article/10.3389/fpsyg.2018.01250/full doi: 10.3389/fpsyg.2018.01250
Quirk, G. J., Muller, R. U., Kubie, J. L., & Ranck, J. B. (1992). The positional firing properties of medial entorhinal neurons: description and comparison with hippocampal place cells. *Journal of Neuroscience*, *12*(5), 1945–1963.
Ranck Jr, J. B. (1984). Head direction cells in the deep layer of dorsal presubiculum in freely moving rats. In *Society of neuroscience abstract* (Vol. 10, p. 599).
Raudies, F., Brandon, M. P., Chapman, G. W., & Hasselmo, M. E. (2015, 9). Head direction is coded more strongly than movement direction in a population of entorhinal neurons.

Brain Research, *1621*(3), 355–367. Retrieved from https://linkinghub.elsevier.com/retrieve/pii/S0006899314014759 doi: 10.1016/j.brainres.2014.10.053

Redish, A. D., Elga, A. N., & Touretzky, D. S. (1996). A coupled attractor model of the rodent head direction system. *Network: Computation in Neural Systems*, *7*(4), 671–685.

Rissman, J., Gazzaley, A., & D'Esposito, M. (2004). Measuring functional connectivity during distinct stages of a cognitive task. *Neuroimage*, *23*(2), 752–763.

Robertson, R. G., Rolls, E. T., Georges-François, P., & Panzeri, S. (1999). Head Direction Cells in the Primate Pre-Subiculum. *Hippocampus*, *9*(3), 206–19. doi: 10.1002/(SICI)1098-1063(1999)9:3

Rubin, A., Yartsev, M. M., & Ulanovsky, N. (2014). Encoding of head direction by hippocampal place cells in bats. *Journal of Neuroscience*, *34*(3), 1067–1080.

Satterthwaite, T. D., Elliott, M. A., Gerraty, R. T., Ruparel, K., Loughead, J., Calkins, M. E., ... Wolf, D. H. (2013). An improved framework for confound regression and filtering for control of motion artifact in the preprocessing of resting-state functional connectivity data. *NeuroImage*, *64*(1), 240–256. Retrieved from http://linkinghub.elsevier.com/retrieve/pii/S1053811912008609 doi: 10.1016/j.neuroimage.2012.08.052

Schaefer, A., Kong, R., Gordon, E. M., Laumann, T. O., Zuo, X.-N., Holmes, A. J., ... Yeo, B. T. T. (2018). Local-global parcellation of the human cerebral cortex from intrinsic functional connectivity MRI. *Cerebral cortex*, *28*(9), 3095–3114.

Scheffer, L. K., Xu, C. S., Januszewski, M., Lu, Z., Takemura, S. Y., Hayworth, K. J., ... Plaza, S. M. (2020, 9). A connectome and analysis of the adult drosophila central brain. *eLife*, *9*, 1–74. doi: 10.7554/ELIFE.57443

Schubert, F., & Gros, C. (2021, 2). Local Homeostatic Regulation of the Spectral Radius of Echo-State Networks. *Frontiers in Computational Neuroscience*, *15*, 12. doi: 10.3389/FNCOM.2021.587721/BIBTEX

Seelig, J. D., & Jayaraman, V. (2015). Neural dynamics for landmark orientation and angular path integration. *Nature*, *521*(7551), 186–191. doi: 10.1038/nature14446

Sharp, P. E., Tinkelman, A., & Cho, J. (2001). Angular velocity and head direction signals recorded from the dorsal tegmental nucleus of gudden in the rat: Implications for path integration in the head direction cell circuit. *Behavioral Neuroscience*, *115*(3), 571–588. Retrieved from /record/2001-07029-004 doi: 10.1037/0735-7044.115.3.571

Shelov, S. P., & American Academy of Pediatrics. (1993). Caring for your baby and young child : birth to age 5. , 676.

Sherrill, K. R., Chrastil, E. R., Ross, R. S., Erdem, M., Hasselmo, M. E., & Stern, C. E. (2015b). NeuroImage Functional connections between optic flow areas and navigationally responsive brain regions during goal-directed navigation. *NeuroImage*, *118*, 386–396. doi: 10.1016/j.neuroimage.2015.06.009

Sherrill, K. R., Chrastil, E. R., Ross, R. S., Erdem, U. M., Hasselmo, M. E., & Stern, C. E. (2015a, 9). Functional connections between optic flow areas and navigationally responsive brain regions during goal-directed navigation. *NeuroImage*, *118*, 386–396. Retrieved from https://linkinghub.elsevier.com/retrieve/pii/S1053811915004851 doi: 10.1016/j.neuroimage.2015.06.009

Shine, J. P., Valdés-Herrera, J. P., Hegarty, M., & Wolbers, T. (2016, 6). The Hu-

man Retrosplenial Cortex and Thalamus Code Head Direction in a Global Reference Frame. *The Journal of Neuroscience*, *36*(24), 6371–6381. Retrieved from http://www.jneurosci.org/lookup/doi/10.1523/JNEUROSCI.1268-15.2016 doi: 10.1523/JNEUROSCI.1268-15.2016

Skaggs, W. E., Knierim, J. J., Kudrimoti, H. S., & McNaughton, B. L. (1995). A model of the neural basis of the rat's sense of direction. In *Advances in neural information processing systems* (Vol. 7, pp. 173–180). Adv Neural Inf Process Syst. Retrieved from https://pubmed.ncbi.nlm.nih.gov/11539168/

Spiers, H. J., & Gilbert, S. J. (2015, 3). Solving the detour problem in navigation: A model of prefrontal and hippocampal interactions. *Frontiers in Human Neuroscience*, *9*(MAR), 125. doi: 10.3389/FNHUM.2015.00125/BIBTEX

Stone, T., Webb, B., Adden, A., Weddig, N. B., Honkanen, A., Templin, R., ... Heinze, S. (2017, 10). An Anatomically Constrained Model for Path Integration in the Bee Brain. *Current Biology*, *27*(20), 3069–3085. doi: 10.1016/J.CUB.2017.08.052

Stringer, C., Michaelos, M., Tsyboulski, D., Lindo, S. E., & Pachitariu, M. (2021, 5). High-precision coding in visual cortex. *Cell*, *184*(10), 2767–2778. doi: 10.1016/J.CELL.2021.03.042

Sutherland, N. S. (1961). Figural after-effects and apparent size. *Quarterly Journal of Experimental Psychology*, *13*(4), 222–228.

Taube, J. S. (1995). Head direction cells recorded in the anterior thalamic nuclei of freely moving rats. *Journal of Neuroscience*, *15*(1), 70–86.

Taube, J. S. (1998). Head direction cells and the neurophysiological basis for a sense of direction. *Progress in Neurobiology*, *55*(3), 225–256. doi: 10.1016/S0301-0082(98)00004-5

Taube, J. S., & Bassett, J. P. (2003). Persistent Neural Activity in Head Direction Cells. *Cerebral Cortex*, *13*(11), 1162–1172. doi: 10.1093/cercor/bhg102

Taube, J. S., Muller, R. U., & Ranck, J. B. (1990a). Head-direction cells recorded from the postsubiculum in freely moving rats. I. Description and quantitative analysis. *Journal of Neuroscience*, *10*(2), 420–435. doi: 10.1523/jneurosci.10-02-00420.1990

Taube, J. S., Muller, R. U., & Ranck, J. B. (1990b). Head-direction cells recorded from the postsubiculum in freely moving rats. II. Effects of environmental manipulations. *Journal of Neuroscience*, *10*(2), 436–447.

Tolman, E. C. (1948, 7). Cognitive maps in rats and men. *Psychological Review*, *55*(4), 189–208. Retrieved from /record/1949-00103-001 doi: 10.1037/H0061626

Turner-Evans, D., Wegener, S., Rouault, H., Franconville, R., Wolff, T., Seelig, J. D., ... Jayaraman, V. (2017, 5). Angular velocity integration in a fly heading circuit. *eLife*, *6*. doi: 10.7554/ELIFE.23496

Tustison, N. J., Avants, B. B., Cook, P. A., Zheng, Y., Egan, A., Yushkevich, P. A., & Gee, J. C. (2010). N4ITK: Improved N3 Bias Correction. *IEEE Transactions on Medical Imaging*, *29*(6), 1310–1320. doi: 10.1109/TMI.2010.2046908

Van Der Walt, S., Colbert, S. C., & Varoquaux, G. (2011). The NumPy array: a structure for efficient numerical computation. *Computing in Science & Engineering*, *13*(2), 22.

Vass, L. K., & Epstein, R. A. (2013, 4). Abstract Representations of Location and Facing Direction in the Human Brain. *Journal of Neuroscience*, *33*(14), 6133–6142. Retrieved from https://www.jneurosci.org/content/33/14/6133https://

www.jneurosci.org/content/33/14/6133.abstract doi: 10.1523/JNEUROSCI.3873-12.2013

Vautin, R. G., & Berkley, M. A. (1977). Responses of single cells in cat visual cortex to prolonged stimulus movement: neural correlates of visual aftereffects. *Journal of Neurophysiology*, *40*(5), 1051–1065. doi: 10.1152/JN.1977.40.5.1051

Verstraeten, D., Schrauwen, B., & Stroobandt, D. (2006). Reservoir-based techniques for speech recognition. In *Ieee international conference on neural networks - conference proceedings* (pp. 1050–1053). Institute of Electrical and Electronics Engineers Inc. doi: 10.1109/IJCNN.2006.246804

Verstraten, F. A. J., Van Der Smagt, M. J., & Van De Grind, W. A. (1998). Aftereffect of high-speed motion. *Perception*, *27*(9), 1055–1066.

Von Grünau, M. W. (1986). A motion aftereffect for long-range troboscopic apparent motion. *Perception & Psychophysics*, *40*(1), 31–38.

Weber, K. D., Fletcher, W. A., Gordon, C. R., Jones, G. M., & Block, E. W. (1998). Motor learning in the podokinetic system and its role in spatial orientation during locomotion. *Experimental brain research*, *120*(3), 377–385.

Weisberg, S. M., & Newcombe, N. S. (2016). How do (some) people make a cognitive map? Routes, places, and working memory. *Journal of Experimental Psychology: Learning, Memory, and Cognition*, *42*(5), 768.

Weisberg, S. M., Schinazi, V. R., Newcombe, N. S., Shipley, T. F., & Epstein, R. A. (2014). Variations in cognitive maps: Understanding individual differences in navigation. *Journal of Experimental Psychology: Learning Memory and Cognition*, *40*(3), 669–682. doi: 10.1037/a0035261

Wiener, S. I. (1993). Spatial and behavioral correlates of striatal neurons in rats performing a self-initiated navigation task. *The Journal of neuroscience : the official journal of the Society for Neuroscience*, *13*(9), 3802–3817. Retrieved from https://pubmed.ncbi.nlm.nih.gov/8366346/ doi: 10.1523/JNEUROSCI.13-09-03802.1993

Wikenheiser, A. M., & Redish, A. D. (2015, 2). Hippocampal theta sequences reflect current goals. *Nature neuroscience*, *18*(2), 289–294. Retrieved from https://pubmed.ncbi.nlm.nih.gov/25559082/ doi: 10.1038/NN.3909

Wilson, M. A., & McNaughton, B. L. (1994). Reactivation of Hippocampal Ensemble Memories During Sleep. *Science*, *265*(5172), 676–679. Retrieved from https://www.science.org/doi/abs/10.1126/science.8036517 doi: 10.1126/SCIENCE.8036517

Wolbers, T., & Hegarty, M. (2010). What determines our navigational abilities? *Trends in Cognitive Sciences*, *14*(3), 138–146. doi: 10.1016/j.tics.2010.01.001

Wolff, T., Iyer, N. A., & Rubin, G. M. (2015, 5). Neuroarchitecture and neuroanatomy of the Drosophila central complex: A GAL4-based dissection of protocerebral bridge neurons and circuits. *The Journal of comparative neurology*, *523*(7), 997–1037. Retrieved from https://pubmed.ncbi.nlm.nih.gov/25380328/ doi: 10.1002/CNE.23705

Yan, C.-G., Cheung, B., Kelly, C., Colcombe, S., Craddock, R. C., Di Martino, A., ... Milham, M. P. (2013). A comprehensive assessment of regional variation in the impact of head micromovements on functional connectomics. *Neuroimage*, *76*, 183–201.

Yarkoni, T., Markiewicz, C. J., de la Vega, A., Gorgolewski, K. J., Salo, T., Halchenko, Y. O., ... Blair, R. (2019). PyBIDS: Python tools for BIDS datasets. *Journal of Open Source Software*, *4*(40). doi: 10.21105/joss.01294

Yekutieli, D., & Benjamini, Y. (1999, 12). Resampling-based false discovery rate controlling multiple test procedures for correlated test statistics. *Journal of Statistical Planning and Inference*, *82*(1-2), 171–196. doi: 10.1016/S0378-3758(99)00041-5

Yoder, R. M., & Taube, J. S. (2014, 4). The vestibular contribution to the head direction signal and navigation. *Frontiers in Integrative Neuroscience*, *8*(APR). Retrieved from /pmc/articles/PMC4001061//pmc/articles/PMC4001061/?report=abstracthttps://www.ncbi.nlm.nih.gov/pmc/articles/PMC4001061/ doi: 10.3389/FNINT.2014.00032

Zhang, K. (1996). Representation of spatial orientation by the intrinsic dynamics of the head-direction cell ensemble: a theory. *Journal of Neuroscience*, *16*(6), 2112–2126.

Zhang, Y., Brady, M., & Smith, S. (2001). Segmentation of brain MR images through a hidden Markov random field model and the expectation-maximization algorithm. *IEEE Transactions on Medical Imaging*, *20*(1), 45–57. doi: 10.1109/42.906424

Zou, X., Hwu, T., Krichmar, J., & Neftci, E. (2020). Terrain classification with a reservoir-based network of spiking neurons. In *Proceedings - ieee international symposium on circuits and systems* (Vol. 2020-October). Institute of Electrical and Electronics Engineers Inc. doi: 10.1109/ISCAS45731.2020.9180740/VIDEO

Appendix A

Chapter 2: (Don't) Look Where You're Going: Evidence for a Travel Direction Signal in Humans that is Independent of Head Direction

A.1 Experiment 1: Raw Data

A.1.1 Reaction Time

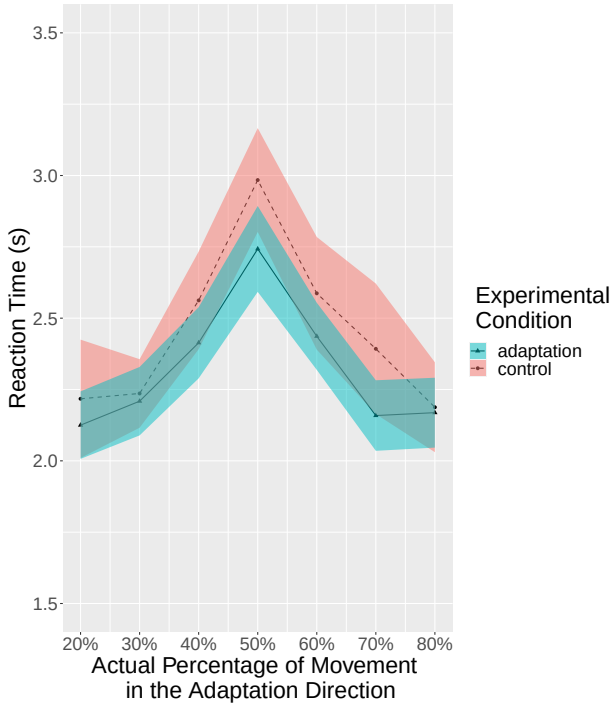

Figure A.1: Experiment 1: Reaction times of all subjects(n=60). The reaction time increased as the actual percentage approached 50%. Solid lines indicate the grand average value, and the shaded area indicate 1 standard error of means.

A.1.2 Reported Rate Table

Condition	20%		30%		40%		50%		60%		70%		80%	
	M	*SE*	*M*	*SE*	*M*	*SE*	*M*	*SE*	*M*	*SE*	*M*	*SE*	*M*	*SE*
Adaptation	10%	2%	17%	3%	27%	3%	57%	2%	82%	2%	89%	2%	91%	2%
Control	5%	1%	8%	1%	20%	2%	49%	2%	82%	2%	93%	1%	92%	2%
Significance	0.023*		0.002**		0.013*		0.006**		0.822		0.028*		0.440	

*$p < .05$. **$p < .01$., Tukey correction.

Table A.1: Experiment 1: Average perceived percentage of movement in the adaptation direction and standard error of the adaptation and the control conditions for all subjects (n = 60), by level of actual percentage of movement in the adaptation direction.

A.1.3 Individual Psychometric Functions

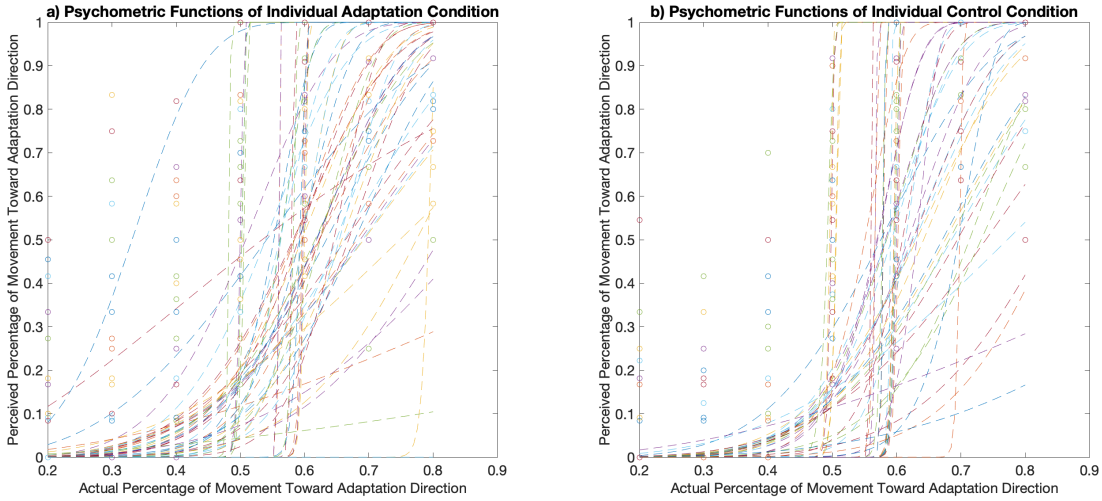

Figure A.2: Experiment 1: Psychometric functions of all observers' data (n = 60) a) Adaptation condition. b) Control condition.

A.2 Experiment 1: Separate Results for Sun and Moon Groups

A.2.1 ANOVA

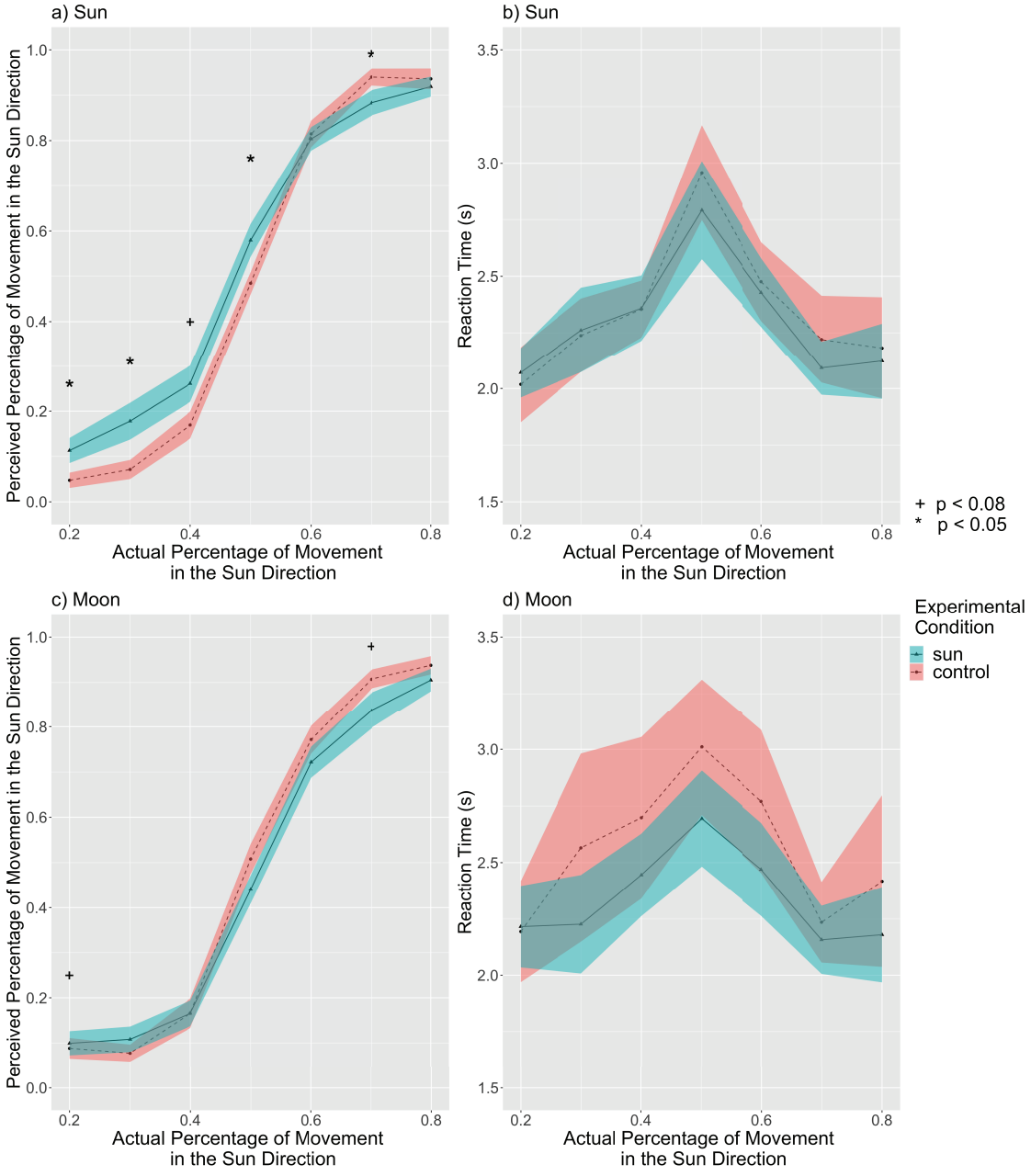

Figure A.3: The perceived percentage of movement in the sun direction compared with the actual percentage for all subjects. a) The Reported Rate of the sun group. The sun adaptation condition had an overall higher reported percentage than the control condition. This result suggests an aftereffect in the same direction of travel ($p = 0.012$). The adaptation condition showed higher reported percentages than corresponding control conditions at 20%, 30%, 40%, and 50%, supporting this aftereffect. This result also suggests an aftereffect in the same direction of travel. There was also a significant interaction between condition and the actual percentage. b) Reaction times of the sun group. The reaction time increased as the actual percentage approached 50%. c) The Reported Rate of the moon group. The moon adaptation had a marginally lower reported percentage overall than the control condition ($p = 0.051$). This result suggests an aftereffect in the same direction of travel. The adaptation condition showed marginally lower reported percentages than corresponding control conditions at the 50% and 70%, supporting this aftereffect. d) The reaction time of the moon group. The reaction time increased as the actual percentage got closer to 50%. Solid lines indicate the grand average value, and the shaded area indicate 1 standard error of means. $^{+}$ $p < 0.08$; * $p < 0.05$, Tukey correction.

A.2.2 Reported Rate Tables

The Sun Group

Condition	20%		30%		40%		50%		60%		70%		80%	
	M	*SE*	*M*	*SE*	*M*	*SE*	*M*	*SE*	*M*	*SE*	*M*	*SE*	*M*	*SE*
Adaptation	11%	3%	18%	4%	26%	4%	58%	4%	80%	3%	88%	3%	92%	2%
Control	5%	2%	7%	2%	17%	3%	48%	2%	81%	3%	94%	2%	94%	2%
Significance	0.032*		0.016*		0.053^{+}		0.017*		0.716		0.030*		0.526	

$+p < .08$. $*p < .05$., Tukey correction.

Table A.2: Experiment 1: Average perceived percentage of movement in the sun direction and standard error of the adaptation and the control conditions for the sun adaptation group subjects (n = 30), by level of actual percentage of movement in the adaptation direction.

The Moon Group

Condition	20%		30%		40%		50%		60%		70%		80%	
	M	*SE*	*M*	*SE*	*M*	*SE*	*M*	*SE*	*M*	*SE*	*M*	*SE*	*M*	*SE*
Adaptation	10%	3%	11%	3%	17%	3%	44%	3%	72%	3%	84%	4%	91%	3%
Control	9%	2%	8%	2%	17%	3%	51%	3%	77%	3%	91%	2%	94%	2%
Significance	0.066^{+}		0.315		0.997		0.132		0.120		0.060^{+}		0.295	

$+p < .08$., Tukey correction.

Table A.3: Experiment 1: Average perceived percentage of movement in the sun direction and standard error of the adaptation and the control conditions for the moon adaptation group subjects (n = 30), by level of actual percentage of movement in the adaptation direction.

A.3 Experiment 1: Serial Position Effects for Sun and Moon Adaptation Groups

In order to determine if any portion of the 10-second test phase contributed to the Reported Rate, we tested for a serial position effect. A serial position effect occurs when people tend to remember the first items (the *primacy effect*) or the last items (the *recency effect*) best in a list. In this case, if there is a serial position effect for movements within the 10-second test trial, people's performance could be influenced by the movement towards the sun in the first few seconds (primacy effect) or the last few seconds (recency effect) of movement. For example, if by chance the last 3 seconds of movement in the 10-second test phase was in the sun direction, perhaps people would be more inclined to select "sun", even if the overall movement was more toward the moon. If people's judgements were based on only a portion of the test trial, then the actual percentage of the 10-second trial was not fully used for judgements. Therefore, we first recalculated the "actual percentage" assuming people only

made judgements based on the first 1 - 9 seconds or the last 1- 9 seconds separately and then conducted the same analysis protocol used in the full 10-second test trials to see if the adaptation effect would be found in certain partial movement steps.

For convenience, in both groups, "percentage" refers to the percentage of movement in the sun direction.

A.3.1 Primacy Effects

We first calculated the actual movement percentage of each of the 9 possible first time steps (i.e., 1 s, 1 s - 2 s, 1 s - 3 s, 1 s - 4 s, 1 s - 5 s, 1 s - 6 s, 1 s - 7 s, 1 s - 8 s, and 1 s - 9 s). Next, we conducted the 2-way experimental condition actual percentage within-subjects repeated measures ANOVA and then Tukey HSD paired t-tests for adaptation trials and control trials within each actual percentage in each of the 9 first time steps. Note that the possible actual percentages vary in different time steps. For perceived percentage, results in both the sun group (see Figure A.4a) and the moon group (see Figure A.4b) revealed "opposite aftereffects" that adaptation increased the Reported Rate in the same direction, which is similar to the previous full 10-second results. Also similar to previous results, reaction time in both the sun group (see Figure A.5a) and the moon group (see Figure A.5b) did not have any differences between the adaptation condition and the control condition. Therefore, no primacy effect was found to affect the results in either the sun group or the moon group.

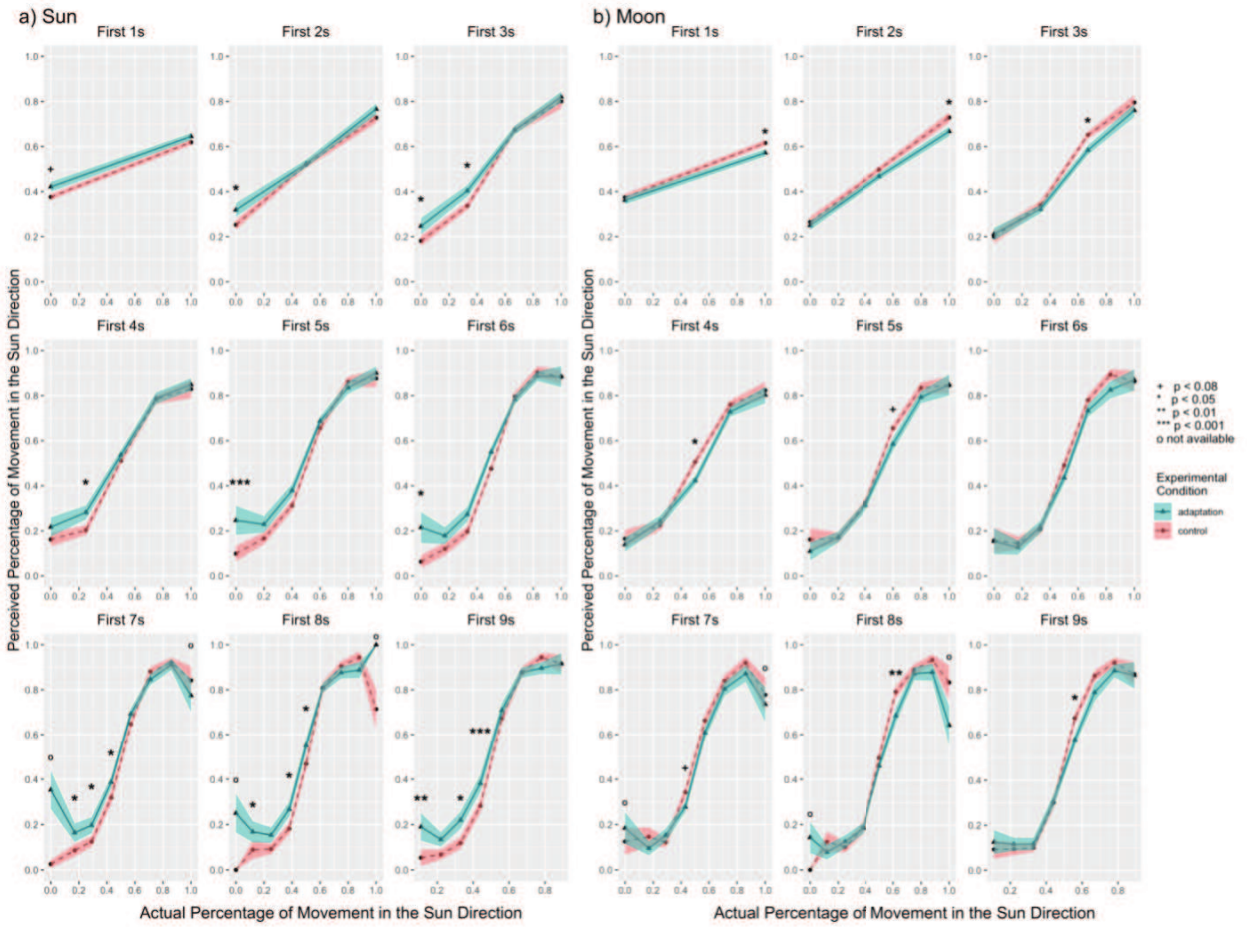

Figure A.4: Experiment 1: We looked for primacy effects by examining the reported percentage of the first 1 - 9 seconds of travel. a) The sun group. Adaptation toward the sun direction increased the perceived percentage of movement in the sun direction, similar to the full 10-second trial. b) The moon group. Adaptation toward the moon direction decreased the perceived percentage of movement in the sun direction, i.e., increased perceived percentage of movement in the moon direction, similar to the full 10-second trial. Solid lines indicate the grand average value, and the shaded area indicate 1 standard error of means. $^{+}$ $p < 0.08$; * $p < 0.05$; ** $p < 0.01$; *** $p < 0.001$; o not enough data for analysis under the corresponding condition, Tukey correction.

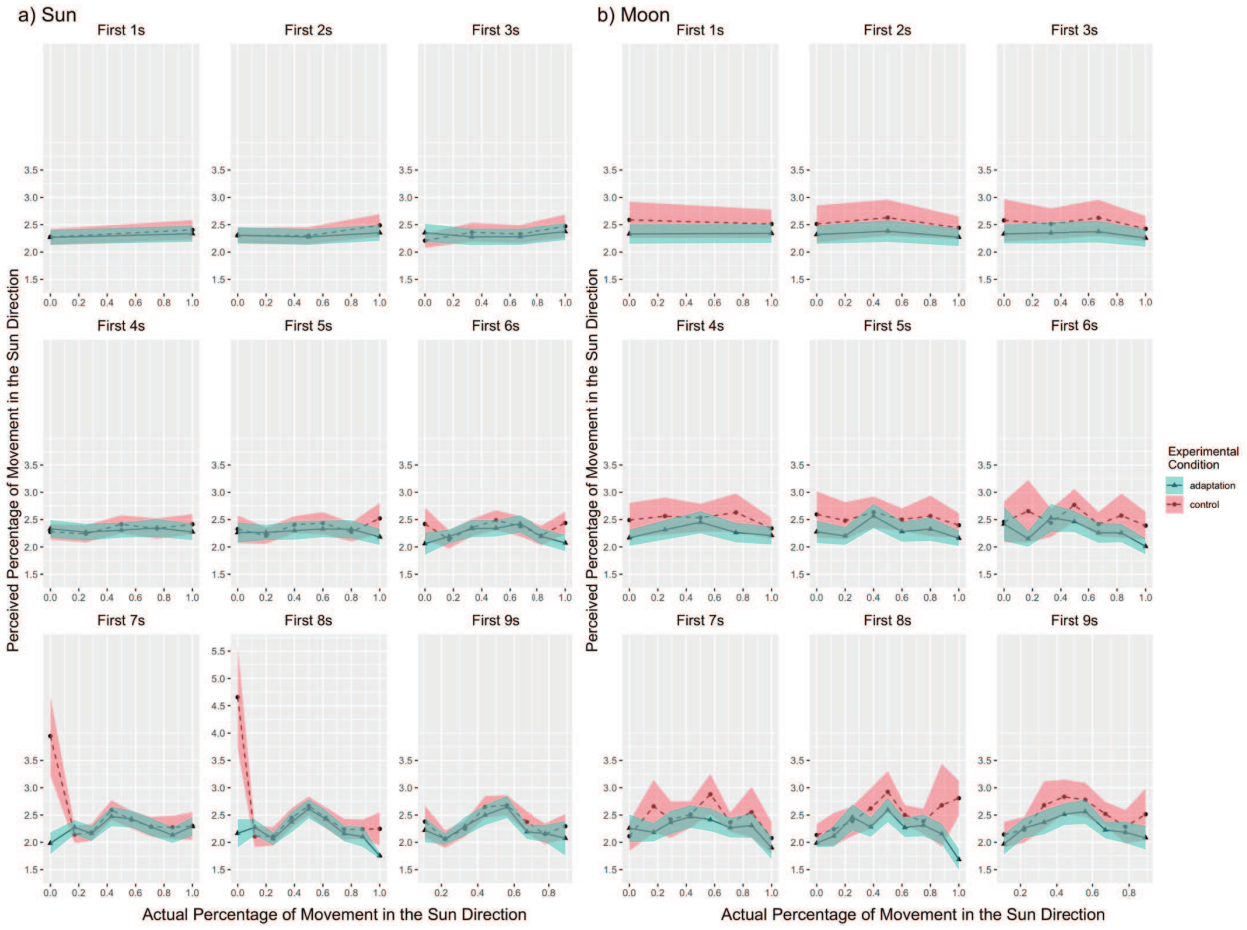

Figure A.5: Experiment 1: We looked for primacy effects by examining the reaction time of the first 1 - 9 seconds of travel. a) The sun group. We did not observe any differences between the adaptation condition and the control condition. b) The moon group. We did not observe any differences between the adaptation condition and the control condition. Solid lines indicate the grand average value, and the shaded area indicate 1 standard error of means.

A.3.2 Recency Effects

We first calculated the actual movement percentage of each of the 9 possible last time steps (i.e., 10 s, 9 s - 10 s, 8 s - 10 s, 7 s - 10 s, 6 s - 10s, 5 s - 10 s, 4 s - 10 s, 3 s - 10 s, and 2 s - 10 s). Next, we conducted the 2-way experimental condition actual percentage within-subjects repeated measures ANOVA and then Tukey HSD paired t-tests for adaptation trials and control trials within each actual percentage in each of the 9 last time steps. Note that the possible actual percentages vary in different time steps. The results of the perceived percentage in both the sun group (see Figure A.6a) and the moon group (see Figure A.6b) showed similar "opposite aftereffects" as found in the full 10-second trial analyses. Also similar to previous analyses, the results of reaction time in both the sun group and the moon group did not show any differences between the adaptation condition and the control condition. Therefore, no recency effect was found to affect the results in either the sun group (see Figure A.7a) or the moon group (see Figure A.7b). The lack of primacy or recency effects suggests that people used the entire test phase to make their judgments.

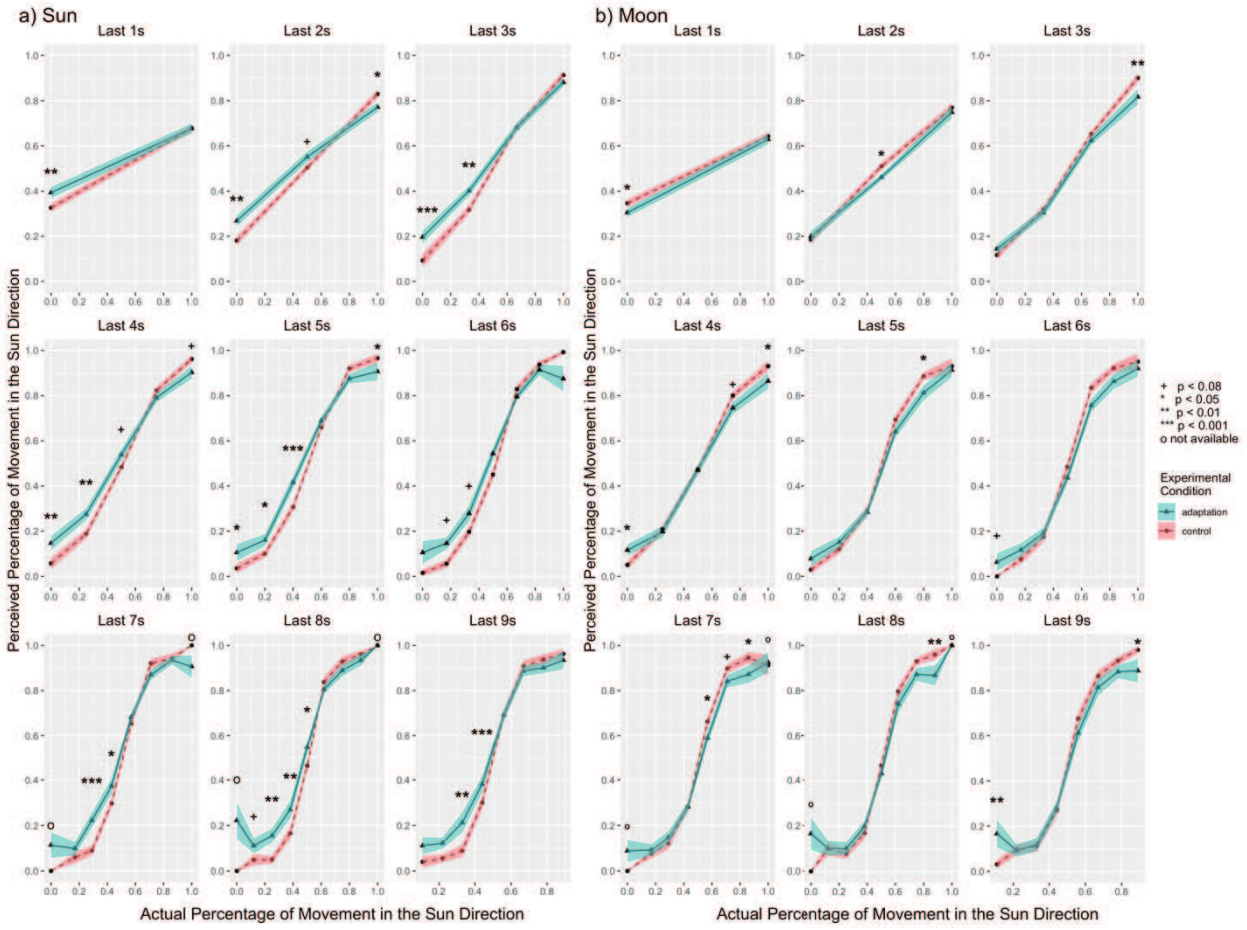

Figure A.6: Experiment 1: We looked for recency effects by examining the reported percentage of the last 1 - 9 seconds of travel. a) The sun group. Adaptation toward the sun direction increased the perceived percentage of movement in the sun direction, similar to the full 10-second trial. b) The moon group. Adaptation toward the moon direction decreased the perceived percentage of movement in the sun direction, i.e., increased perceived percentage of movement in the moon direction, similar to the full 10-second trial. Solid lines indicate the grand average value, and the shaded area indicate 1 standard error of means. $^{+}$ $p < 0.08$; * $p < 0.05$; ** $p < 0.01$; *** $p < 0.001$; o not enough data for analysis under the corresponding condition, Tukey correction.

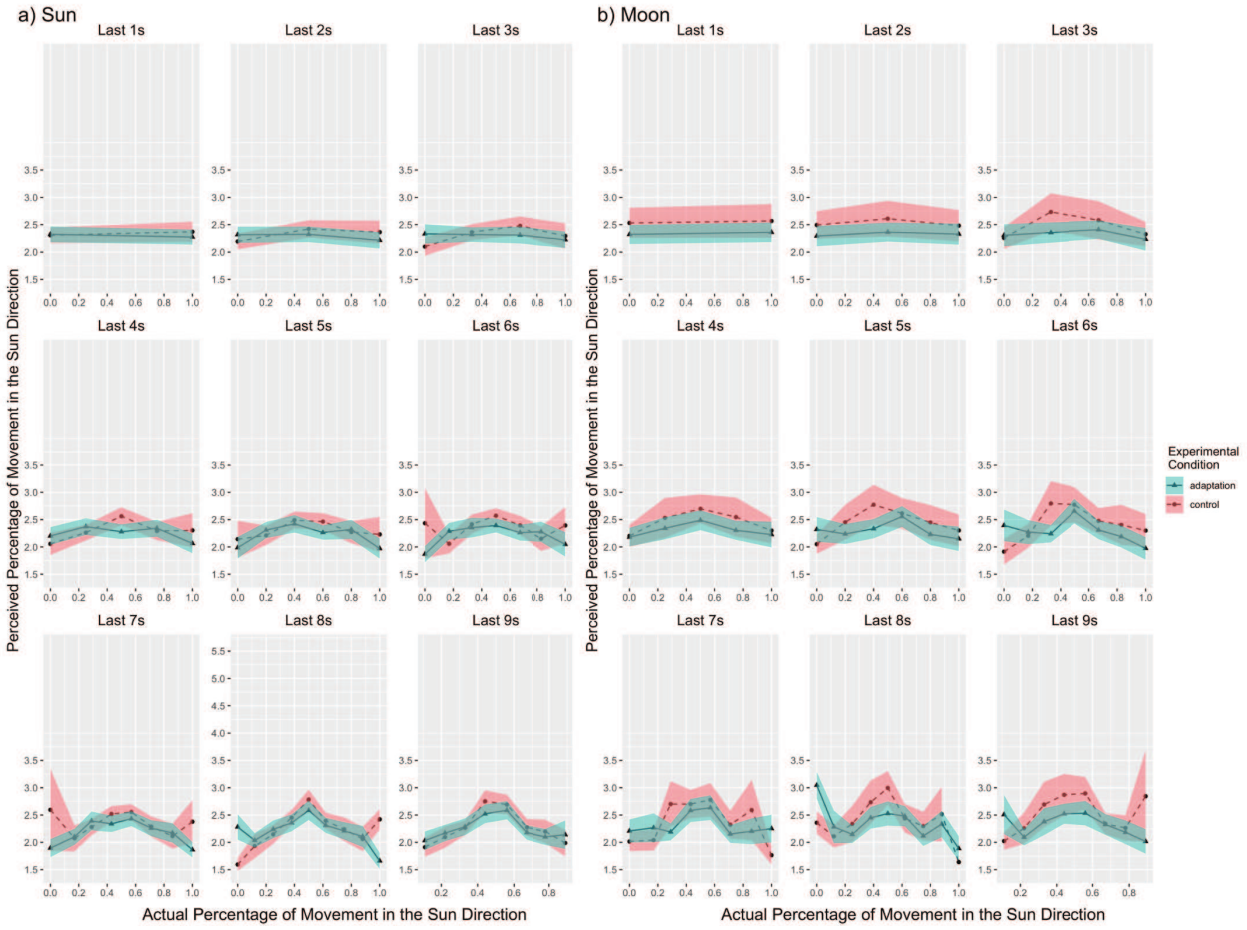

Figure A.7: Experiment 1: We looked for recency effects by examining the reaction time of the first 1 - 9 seconds of travel. a) The sun group. We did not observe any differences between the adaptation condition and the control condition. b) The moon group. We did not observe any differences between the adaptation condition and the control condition. Solid lines indicate the grand average value, and the shaded area indicate 1 standard error of means.

A.4 Experiment 1: Initial Trial Results for Sun and Moon Adaptation Groups

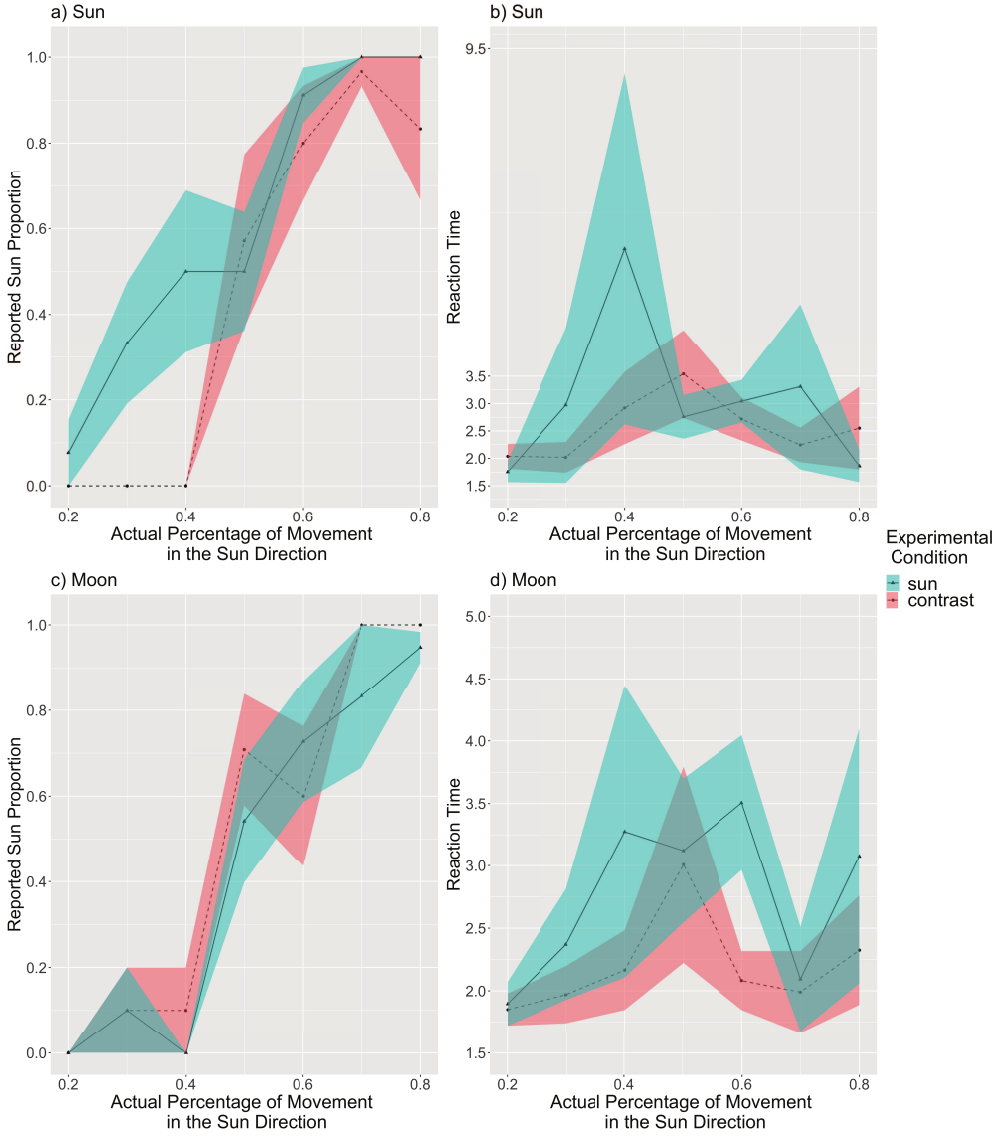

Figure A.8: The perceived percentage of movement in the sun direction compared with the actual percentage for all initial trials. a) The Reported Rate of the sun group. The sun adaptation condition showed a tendency of overall higher reported percentage than the control condition. b) Reaction times of the sun group. No difference were observed in reaction time between the two conditions. c) The Reported Rate of the moon group. The moon adaptation showed a tendency of lower reported percentage overall than the control condition. d) The reaction time of the moon group. Reaction times of the sun group. No difference were observed in reaction time between the two conditions. Solid lines indicate the grand average value, and the shaded area indicate 1 standard error of means. No inferential statistical analyses was conducted due to not enough initial trials.

A.5 Experiment 1: Filtered Data

A.5.1 ANOVA

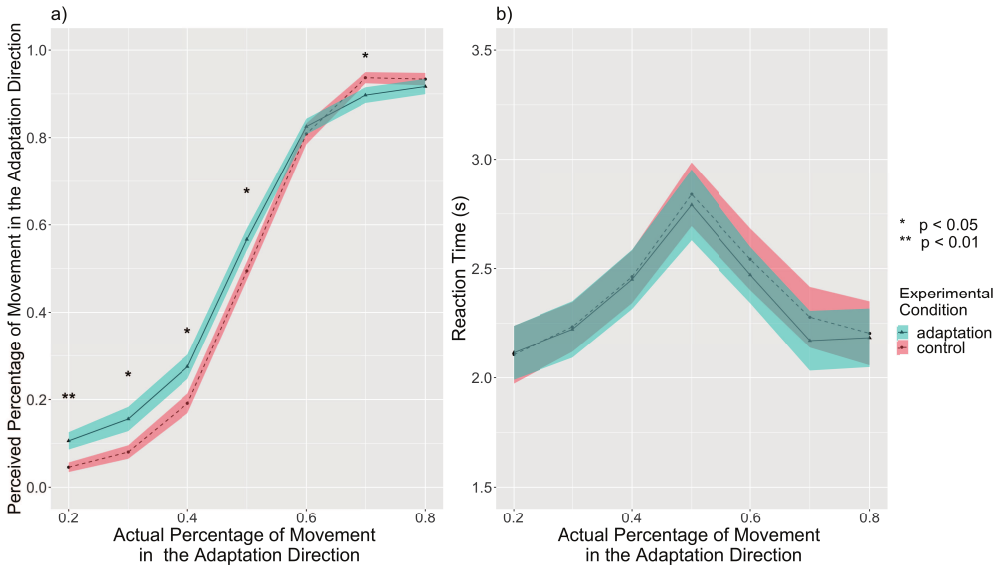

Figure A.9: Experiment 1: The perceived percentage of movement in the adaptation direction compared with the actual percentage for filtered subjects (n = 51). a) The Reported Rate of filtered subjects. The adaptation condition had an overall higher reported percentage than the control condition ($p = 0.002$). The adaptation condition showed higher reported percentages than corresponding control conditions at 20%, 30%, 40%, and 50%, supporting the aftereffect. This result suggests an aftereffect in the same direction of travel. There was also a significant interaction between condition and the actual percentage. b) Reaction times of filtered subjects. The reaction time increased as the actual percentage approached 50%. Solid lines indicate the grand average value, and the shaded area indicate 1 standard error of means. * $p < 0.05$; ** $p < 0.01$, Tukey correction.

A.5.2 Reported Rate Table

Condition	20%		30%		40%		50%		60%		70%		80%	
	M	*SE*	*M*	*SE*	*M*	*SE*	*M*	*SE*	*M*	*SE*	*M*	*SE*	*M*	*SE*
Adaptation	11%	2%	16%	3%	28%	3%	57%	2%	83%	2%	90%	2%	92%	2%
Control	5%	1%	8%	2%	19%	2%	49%	2%	81%	2%	93%	1%	94%	1%
Significance	0.007**		0.012*		0.010*		0.031*		0.509		0.049*		0.378	

*$p < .05$. **$p < .01$., Tukey correction.

Table A.4: Experiment 1: Average perceived percentage of movement in the adaptation direction and standard error of the adaptation and the control conditions for filtered subjects (n = 51), by level of actual percentage of movement in the adaptation direction.

A.5.3 Individual Psychometric Functions

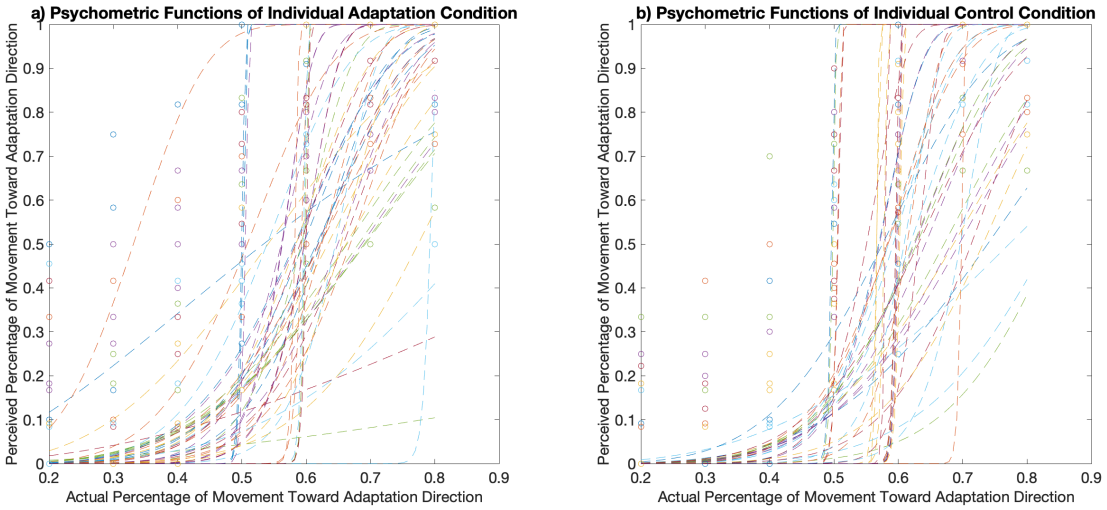

Figure A.10: Experiment 1: Psychometric functions of 51 observers' data a) Adaptation condition. b) Control condition.

A.5.4 Group Psychometric Functions

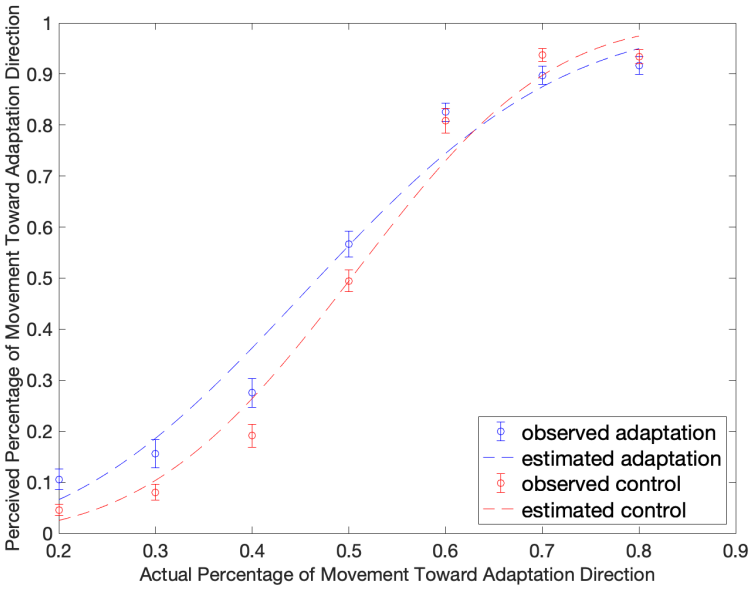

Figure A.11: Experiment 1: The average psychometric functions. Results were pooled across the 51 observers after filtering. The psychometric function (i.e., α) shifts toward a lower percentage of movement toward the adaptation condition compared to the control, but was not significant ($p = 0.185$). The psychometric function (i.e., β) became more flattened when adapted, indicating that observers' detectability of the difference between the two directions was decreased by adaptation ($p = 0.002$). Error bars indicate standard errors.

A.6 Experiment 1: Strategies

A.6.1 Task Difficulty

Raw Data

As for the rated difficulty of each condition, participants rated the adaptation session (overall $M = 3.42 \pm 0.19$; sun session $M = 3.53 \pm 0.28$; moon session $M = 3.30 \pm 0.26$) to be around the same difficulty as the control session (overall $M = 3.48 \pm 0.19$: sun session $M = 3.73 \pm 0.25$; moon session $M = 3.23 \pm 0.29$)($t(59) = 0.333$, $p = 0.740$, $Cohen's\, d = 0.045$, $95\%CI =$ [-0.221, 0.311], ns). For filtered data, the result shows the same pattern. See below for more details.

Filtered Data

As for the rated difficulty of each condition, participants rated the adaptation session (overall $M = 3.59 \pm 0.21$; sun session $M = 3.56 \pm 0.31$; moon session $M = 3.25 \pm 0.29$) to be around the same difficulty as the control session (overall $M = 3.41 \pm 0.21$: sun session $M = 3.74 \pm 0.27$; moon session $M = 3.42 \pm 0.35$)($t(50) = 0.802$, $p = 0.426$, $Cohen's\, d = 0.116$, $95\%CI =$ [-0.171, 0.403], ns).

A.6.2 Task Difficulty in Different Strategies.

Raw Data

For the task difficulty, we conducted an *experimental condition*(adaptation, control) *strategy*(counting strategies, focusing on part of the environment, unique strategies) mixed-subjects repeated measures ANOVA. We found a main effect of strategy where people who used unique strategies rated tasks being easier than people who used counting strategies ($p = 0.040$) and focused on a certain part of the environment ($p = 0.018$). For filtered data, the result shows the same pattern. See below for more details.

Filtered Data

Then we conducted the same ANOVA analyses on filtered data. We found a main effect of strategy ($F(2, 48) = 3.95$, $p = 0.026$, $\eta_p^2 = 0.141$, $95\%CI = [0.000, 0.315]$) where people who used unique strategies ($M = 2.17 \pm 0.27$) rated tasks being easier than people who used counting strategies ($M = 3.68 \pm 0.19$; $p = 0.023$) and focused on a certain part of the environment ($M = 3.68 \pm 0.30$;$p = 0.041$). There was no main effect of condition ($F(1, 48) = 0.02$, $p = 0.897$, $\eta_p^2 < 0.001$, $95\%CI = [0.000, 0.056]$, ns) or interaction between strategy and condition ($F(2, 48) = 1.53$, $p = 0.228$, $\eta_p^2 = 0.060$, $95\%CI = [0.000, 0.206]$, ns).

A.6.3 Reported Rate in Different Strategies.

Raw Data

For the perceived percentage, we conducted an *experimental condition*(adaptation, control) × *actual percentage*(20%, 30%, 40%, 50%, 60% ,70%, 80%) × *strategy*(counting strategies, focusing on part of the environment, unique strategies) mixed-subjects repeated measures ANOVA. There was no main effect of strategy ($F(2, 53) < 0.001$, $p = 0.398$, $\eta_p^2 < 0.001$, $95\%CI = [0.000, 0.000]$, ns), condition ($F(1, 53) = 2.62$, $p = 0.112$, $\eta_p^2 = 0.047$, $95\%CI = [0.000, 0.196]$, ns), or interaction between strategy and condition ($F(2, 53) = 0.87$, $p = 0.424$, $\eta_p^2 = 0.032$, $95\%CI = [0.000, 0.148]$, ns). As expected, there was also a main effect of the actual percentage ($F(2.08, 110.39) = 257.10$, $p < 0.001$, $\eta_p^2 = 0.829$, $95\%CI = [0.799, 0.852]$) that showed the perceived percentage increased with the actual percentage. We also found a marginally significant interaction between strategy and the actual percentage ($F(4.17, 110.39) = 2.34$, $p = 0.057$, $\eta_p^2 = 0.081$, $95\%CI = [0.007, 0.113]$). There was no interaction between condition and the actual percentage ($F(4.04, 214.16) = 1.47$, $p = 0.213$, $\eta_p^2 = 0.027$, $95\%CI = [0.000, 0.053]$, ns), or interaction among strategy, condition, and the actual percentage ($F(8.08, 214.16) = 1.34$, $p = 0.224$, $\eta_p^2 = 0.048$, $95\%CI = [0.000, 0.066]$, ns). Mixed-subjects repeated measures ANOVA on the filtered Reported Rate revealed the same pattern of results as the raw data except that there was no interaction between strategy and the actual percentage. For more details, see below.

Filtered Data

Then we conducted the same ANOVA analyses on filtered data. There was no main effect of strategy ($F(2, 44) = 0.02$, $p = 0.977$, $\eta_p^2 = 0.001$, $95\%CI = [0.000, 0.000]$, ns), condition ($F(1, 44) = 2.82$, $p = 0.100$, $\eta_p^2 = 0.060$, $95\%CI = [0.000, 0.234]$, ns), or interaction between strategy and condition ($F(2, 44) = 0.97$, $p = 0.386$, $\eta_p^2 = 0.042$, $95\%CI = [0.000, 0.182]$, ns). As expected, there was also a main effect of the actual percentage ($F(2.13, 93.83) =$

312.39, $p < 0.001$, $\eta_p^2 = 0.877$, $95\%CI = [0.852, 0.895]$) that showed the perceived percentage increased with the actual percentage. We found no interaction between strategy and the actual percentage ($F(4.27, 93.83) = 1.38$, $p = 0.244$, $\eta_p^2 = 0.059$, $95\%CI = [0.000, 0.109]$), between condition and the actual percentage ($F(3.76, 165.34) = 1.03$, $p = 0.393$, $\eta_p^2 = 0.023$, $95\%CI = [0.000, 0.047]$, ns), or among strategy, condition, and the actual percentage ($F(7.52, 165.34) = 1.71$, $p = 0.105$, $\eta_p^2 = 0.072$, $95\%CI = [0.000, 0.100]$, ns).

A.6.4 Reaction Time in Different Strategies

There were also no reaction time differences in strategies. For more details, see below.

Raw Data

For the reaction time, we conducted an *experimental condition*(adaptation, control) × *actual percentage*(20%, 30%, 40%, 50%, 60% ,70%, 80%) × *strategy*(counting strategies, focusing on part of the environment, unique strategies) mixed-subjects repeated measures ANOVA. There was no main effect of strategy ($F(2, 53) = 1.56$, $p = 0.220$, $\eta_p^2 = 0.056$, $95\%CI = [0.000, 0.192]$, ns), condition ($F(1, 53) = 2.49$, $p = 0.121$, $\eta_p^2 = 0.045$, $95\%CI = [0.000, 0.192]$, ns), or interaction between strategy and condition ($F(2, 53) = 4.37$, $p = 0.224$, $\eta_p^2 = 0.055$, $95\%CI = [0.000, 0.191]$, ns). As expected, there was a main effect of the actual percentage ($F(4.23, 223.96) = 7.34$, $p < 0.001$, $\eta_p^2 = 0.122$, $95\%CI = [0.051, 0.179]$) that showed the perceived percentage increased with the actual percentage. We found no interaction between strategy and the actual percentage ($F(8.45, 223.96) = 1.32$, $p = 0.229$, $\eta_p^2 = 0.048$, $95\%CI = [0.000, 0.089]$, ns), between condition and the actual percentage ($F(3.79, 200.86) = 0.41$, $p = 0.790$, $\eta_p^2 = 0.008$, $95\%CI = [0.000, 0.014]$, ns), or interaction among strategy, condition, and the actual percentage ($F(7.58, 200.86) = 0.66$, $p = 0.715$, $\eta_p^2 = 0.024$, $95\%CI = [0.000, 0.025]$, ns).

Filtered Data

Then we conducted the same ANOVA analyses on filtered data. There was no main effect of strategy ($F(2, 44) = 0.69$, $p = 0.506$, $\eta_p^2 = 0.030$, $95\%CI = [0.000, 0.157]$, ns), condition ($F(1, 44) = 2.98$, $p = 0.091$, $\eta_p^2 = 0.063$, $95\%CI = [0.000, 0.238]$, ns), or interaction between strategy and condition ($F(2, 44) = 1.60$, $p = 0.213$, $\eta_p^2 = 0.068$, $95\%CI = [0.000, 0.225]$, ns). As expected, there was a main effect of the actual percentage ($F(4.19, 184.32) = 7.40$, $p < 0.001$, $\eta_p^2 = 0.144$, $95\%CI = [0.061, 0.210]$) that showed the perceived percentage increased with the actual percentage. We found no interaction between strategy and the actual percentage ($F(8.38, 184.32) = 1.37$, $p = 0.208$, $\eta_p^2 = 0.059$, $95\%CI = [0.000, 0.108]$, ns), between condition and the actual percentage ($F(4.54, 199.65) = 0.31$, $p = 0.891$, $\eta_p^2 = 0.007$, $95\%CI = [0.000, 0.010]$, ns), or interaction among strategy, condition, and the actual percentage ($F(9.07, 199.65) = 0.56$, $p = 0.831$, $\eta_p^2 = 0.025$, $95\%CI = [0.000, 0.021]$, ns).

A.7 Experiment 2: Raw Data

A.7.1 Reaction Time

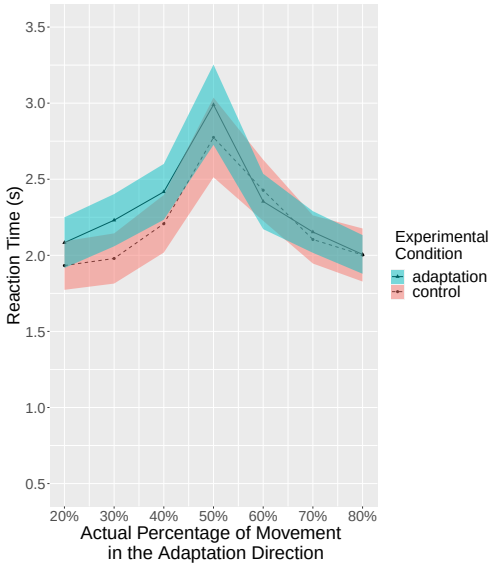

Figure A.12: Experiment 1: Reaction times of all subjects (n=30). The reaction time increased as the actual percentage approached 50%. Solid lines indicate the grand average value, and the shaded area indicate 1 standard error of means.

A.7.2 Reported Rate Table

Condition	20%		30%		40%		50%		60%		70%		80%	
	M	*SE*	*M*	*SE*	*M*	*SE*	*M*	*SE*	*M*	*SE*	*M*	*SE*	*M*	*SE*
Adaptation	13%	3%	16%	4%	28%	4%	57%	4%	81%	3%	88%	3%	89%	3%
Control	7%	2%	10%	2%	18%	3%	51%	3%	82%	3%	86%	3%	91%	2%
Significance	0.016*		0.192		0.027*		0.145		0.753		0.436		0.568	

*$p < .05$. , Tukey correction.

Table A.5: Experiment 2: Average perceived percentage of movement in the adaptation direction and standard error of the adaptation and the control conditions for all subjects (n = 30), by level of actual percentage of movement in the adaptation direction.

A.7.3 Individual Psychometric Functions

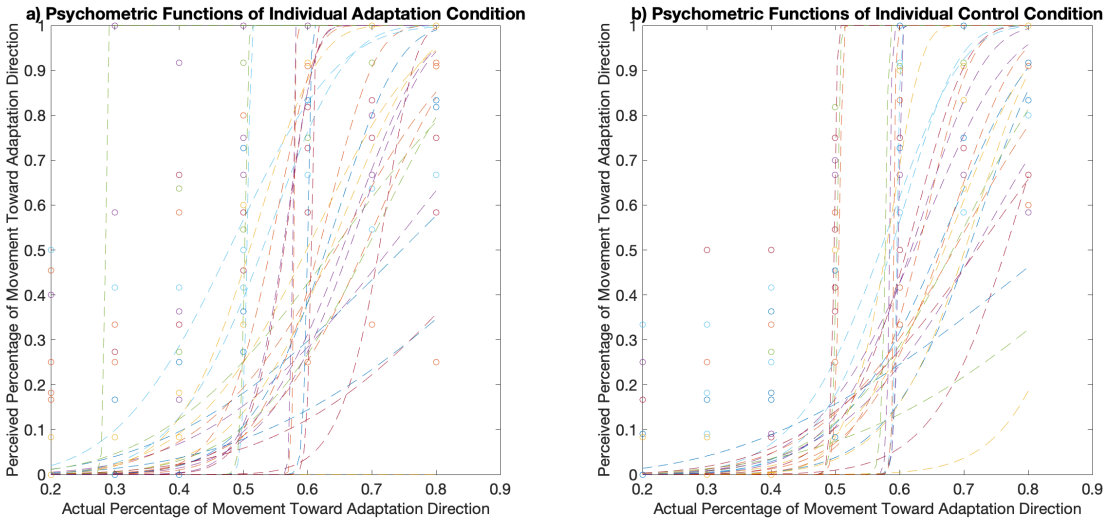

Figure A.13: Experiment 2: Psychometric functions of all observers' data (n = 30) a) Adaptation condition. b) Control condition.

A.8 Experiment 2: Filtered Data

A.8.1 ANOVA

A.8.2 Reported Rate Table

Condition	20%		30%		40%		50%		60%		70%		80%	
	M	*SE*	*M*	*SE*	*M*	*SE*	*M*	*SE*	*M*	*SE*	*M*	*SE*	*M*	*SE*
Adaptation	14%	4%	16%	4%	29%	4%	54%	4%	79%	2%	88%	3%	90%	3%
Control	6%	2%	11%	3%	20%	3%	51%	3%	83%	3%	85%	3%	92%	2%
Significance	0.008**		0.244		0.044*		0.364		0.295		0.162		0.513	

*$p < .05$. **$p < .01$., Tukey correction.

Table A.6: Experiment 2: Average perceived percentage of movement in the adaptation direction and standard error of the adaptation and the control conditions for filtered subjects (n = 23), by level of actual percentage of movement in the adaptation direction.

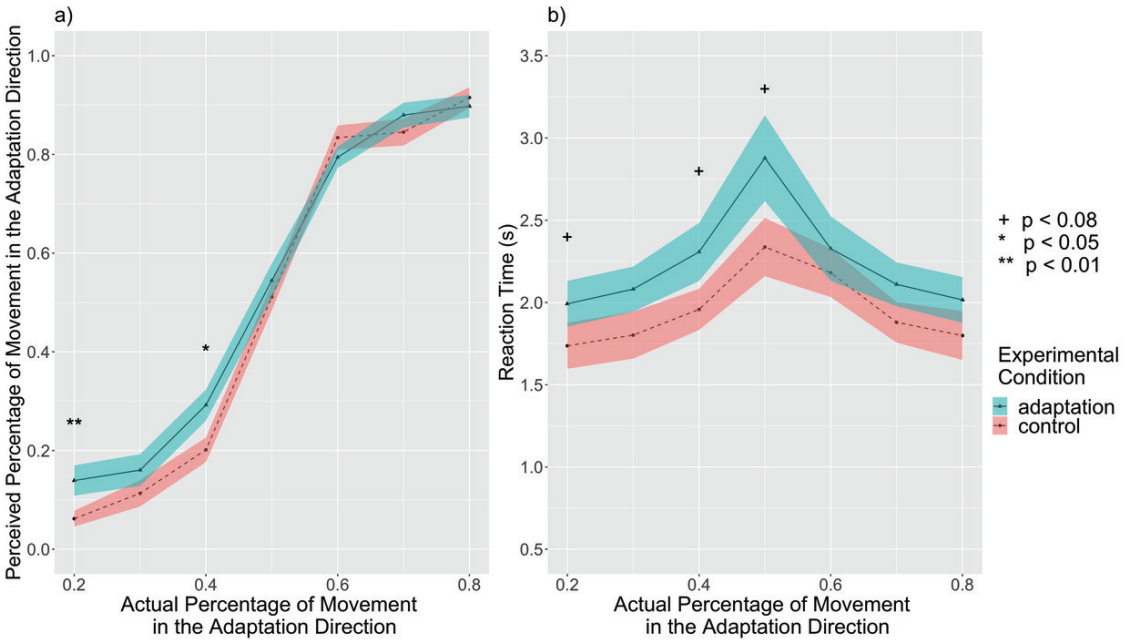

Figure A.14: figure

Experiment 2: The perceived percentage of movement in the adaptation direction compared with the actual percentage for filtered subjects (n = 23). a) The Reported Rate of filtered subjects. The adaptation condition had an overall marginally higher reported percentage than the control condition ($p = 0.078$). The adaptation condition showed higher reported percentages than corresponding control conditions at 20% and 40%, supporting the aftereffect. This result suggests an aftereffect in the same direction of travel. There was also a marginally significant interaction between condition and the actual percentage. b) Reaction times of filtered subjects. The reaction time increased as the actual percentage approached 50%. Solid lines indicate the grand average value, and the shaded area indicate 1 standard error of means. $^{+}$ p < 0.08; * p < 0.05; ** p < 0.01, Tukey correction.

A.8.3 Individual Psychometric Functions

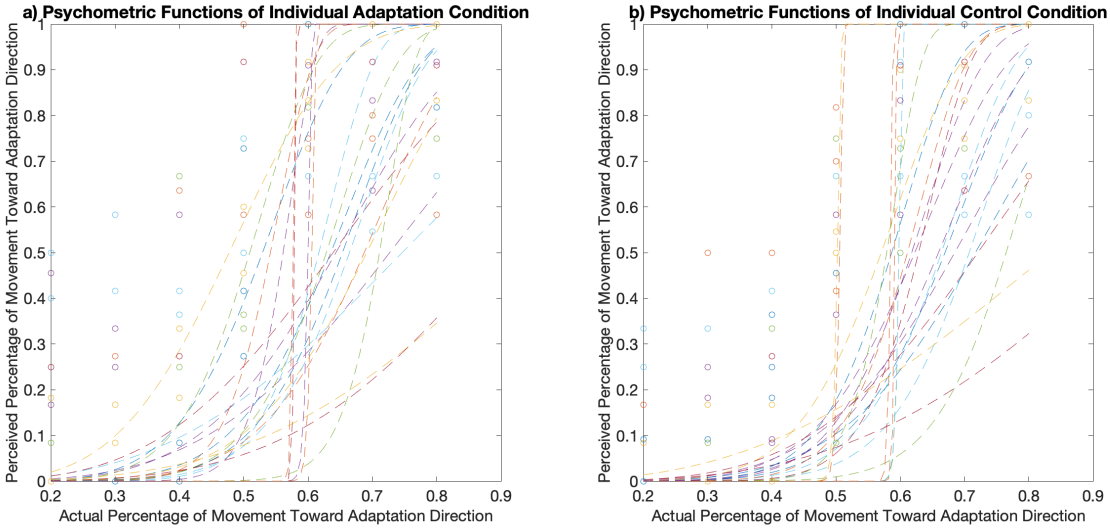

Figure A.15: Experiment 2: Psychometric functions of 23 observers' data a) Adaptation condition. b) Control condition.

A.8.4 Group Psychometric Functions

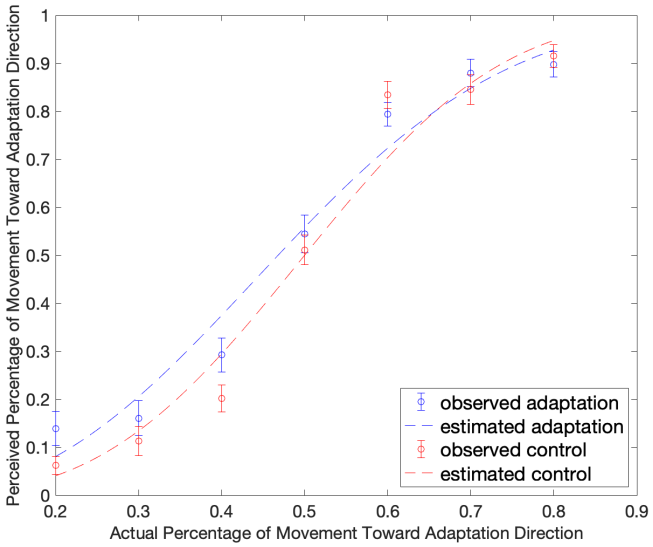

Figure A.16: Experiment 2: The average psychometric functions. Results were pooled across the 23 observers after filtering. The psychometric function (i.e., α) shifts toward a lower percentage of movement toward the adaptation condition compared to the control, but was not significant ($p = 0.728$). The psychometric function (i.e., β) indicates that observers' detectability of the difference between the two directions was decreased by adaptation but was not significant ($p = 0.152$). Error bars indicate standard errors.

A.9 Experiment 2: Strategies

A.9.1 Task Difficulty

Raw Data

As for the rated difficulty of each condition, participants rated the adaptation session ($M = 3.93 \pm 0.25$) to be more difficult than the control session ($M = 3.43 \pm 0.27$)($t(29)$ = -2.347, p = 0.026, $Cohen's\, d$ = -0.347, 95%CI = [-0.652, -0.042]). For filtered data, the result shows the same pattern. For more details, see below.

Filtered Data

Participants rated the adaptation session ($M = 4.00 \pm 0.30$) to be more difficult than the control session ($M = 3.30 \pm 0.32$)($t(22)$ = -2.82, p = 0.010, $Cohen's\, d$ = -0.463, 95%CI = [-0.811, -0.114]).

A.9.2 Task Difficulty in Different Strategies.

Raw Data

For the task difficulty, we conducted an *experimental condition*(adaptation, control) × *strategy*(counting strategies, focusing on part of the environment, unique strategies) mixed-subjects repeated measures ANOVA. There was no main effect of strategy ($F(2, 27) = 0.65$, $p = 0.529$, $\eta_p^2 = 0.046$, 95%$CI = [0.000, 0.229]$, ns). We found a main effect of condition ($F(1, 27) = 4.38$, $p = 0.046$, $\eta_p^2 = 0.140$, 95%$CI = [0.000, 0.385]$) where people rated adaptation sessions ($M = 3.93 \pm 0.25$) being more difficult than control sessions ($M = 3.43 \pm 0.27$). There was no interaction between strategy and condition ($F(2, 27) = 0.67$, $p = 0.518$, $\eta_p^2 = 0.048$, 95%$CI = [0.000, 0.232]$, ns).

Filtered Data

Then we conducted the same ANOVA analyses on filtered data. There was no main effect of strategy ($F(2, 20) = 1.53$, $p = 0.242$, $\eta_p^2 = 0.132$, $95\%CI = [0.000, 0.388]$, ns). We found a main effect of condition ($F(1, 20) = 6.41$, $p = 0.020$, $\eta_p^2 = 0.243$, $95\%CI = [0.005, 0.516]$) where people rated adaptation sessions ($M = 4.00 \pm 0.30$) being more difficult than control sessions ($M = 3.30 \pm 0.32$). There was no interaction between strategy and condition ($F(2, 20) = 1.11$, $p = 0.348$, $\eta_p^2 = 0.100$, $95\%CI = [0.000, 0.347]$, ns).

A.9.3 Reported Rate in Different Strategies

Raw Data

For the perceived percentage, we conducted an *experimental condition*(adaptation, control) × *actual percentage*(20%, 30%, 40%, 50%, 60% ,70%, 80%) × *strategy*(counting strategies, focusing on part of the environment, unique strategies) mixed-subjects repeated measures ANOVA. There was a main effect of strategy ($F(2, 27) = 8.79$, $p = 0.001$, $\eta_p^2 = 0.394$, $95\%CI = [0.097, 0.597]$) where people who focused on a certain part of the environment ($M = 0.578 \pm 0.037$) reported more toward adaptation direction than people using counting strategies ($M = 0.496 \pm 0.029$;$p = 0.003$) or unique strategies ($M = 0.487 \pm 0.029$;$p = 0.002$). There was no difference in Reported Rate between people who used counting strategies or unique strategies ($p = 0.886$).

There was also a main effect of condition ($F(1, 27) = 5.58$, $p = 0.026$, $\eta_p^2 = 0.171$, $95\%CI = [0.000, 0.418]$) where people reported more toward the adaptation direction in the adaptation session ($M = 0.532 \pm 0.025$) than in the control session ($M = 0.493 \pm 0.026$).

There was a marginally significant interaction between strategy and condition ($F(2, 27) = 3.10$, $p = 0.061$, $\eta_p^2 = 0.187$, $95\%CI = [0.000, 0.417]$). As expected, there was also a main effect of the actual percentage ($F(2.12, 57.37) = 214.78$, $p < 0.001$, $\eta_p^2 = 0.888$, $95\%CI = [0.859, 0.909]$) that showed the perceived percentage increased with the actual

percentage. There was no interaction between strategy and the actual percentage ($F(4.25, 57.37) = 1.33$, $p = 0.269$, $\eta_p^2 = 0.090$, $95\%CI = [0.000, 0.122]$, ns).

There was a significant interaction between condition and the actual percentage ($F(3.53, 95.40) = 3.23$, $p = 0.020$, $\eta_p^2 = 0.107$, $95\%CI = [0.012, 0.178]$). Tukey HSD analyses revealed that people reported more toward the adaptation direction in the adaptation session than in the condition session at 20% ($p = 0.003$), 40% ($p = 0.005$), 50% ($p = 0.031$), and marginally significant at 30% ($p = 0.070$).

There was a marginally significant interaction among strategy, condition, and the actual percentage ($F(7.07, 95.40) = 2.10$, $p = 0.050$, $\eta_p^2 = 0.135$, $95\%CI = [0.003, 0.185]$).

The filtered data had similar results; for more details, see below.

Filtered Data

Then we conducted the same ANOVA analyses on filtered data. There was a main effect of strategy ($F(2, 20) = 13.83$, $p < 0.001$, $\eta_p^2 = 0.580$, $95\%CI = [0.241, 0.747]$) where people who focused on a certain part of the environment ($M = 0.582 \pm 0.046$) reported more toward adaptation direction than people using counting strategies ($M = 0.497 \pm 0.029$;$p < 0.001$) or unique strategies ($M = 0.503 \pm 0.033$;$p < 0.001$). There was no difference in Reported Rate between people who used counting strategies or unique strategies ($p = 0.910$).

There was also a main effect of condition ($F(1, 27) = 5.58$, $p = 0.026$, $\eta_p^2 = 0.171$, $95\%CI = [0.000, 0.418]$) where people reported more toward the adaptation direction in the adaptation session ($M = 0.532 \pm 0.025$) than in the control session ($M = 0.493 \pm 0.026$).

There was no interaction between strategy and condition ($F(2, 20) = 2.03$, $p = 0.158$, $\eta_p^2 = 0.169$, $95\%CI = [0.000, 0.428]$, ns). As expected, there was also a main effect of the actual percentage ($F(2.30, 45.93) = 151.55$, $p < 0.001$, $\eta_p^2 = 0.883$, $95\%CI = [0.847, 0.908]$) that showed the perceived percentage increased with the actual percentage. There was no interaction between strategy and the actual percentage ($F(4.59, 45.93) = 1.24$, $p = 0.307$, $\eta_p^2 = 0.110$, $95\%CI = [0.000, 0.194]$, ns).

There was a significant interaction between condition and the actual percentage ($F(3.94, 78.80) = 4.90$, $p = 0.001$, $\eta_p^2 = 0.197$, $95\%CI = [0.056, 0.295]$). Tukey HSD analyses revealed that people reported more toward the adaptation direction in the adaptation session than in the condition session at 20% ($p < 0.001$) and 40% ($p = 0.004$), and marginally significant at 50% ($p = 0.073$).

There was a significant interaction among strategy, condition, and the actual percentage ($F(7.88, 78.80) = 3.21$, $p = 0.003$, $\eta_p^2 = 0.243$, $95\%CI = [0.060, 0.320]$). Tukey HSD analyses revealed that people who used strategy of focusing on part of the environment reported more toward the adaptation direction in the adaptation session than in the condition session at 20% ($p = 0.012$), 40% ($p = 0.021$), and marginally significant at 50% ($p = 0.072$). People who used unique strategies reported more toward the adaptation direction in the adaptation session than in the condition session at 20% ($p = 0.029$). At 40% actual percentage, people who focused on part of the environment reported more toward the adaptation direction in adaptation sessions than people with counting strategies in adaptation sessions ($p = 0.014$) and people with unique strategies in control sessions ($p = 0.018$). At 50% actual percentage, people who focused on part of the environment reported more toward the adaptation direction in adaptation sessions than people with unique strategies in both adaptation sessions ($p = 0.018$) and control sessions ($p = 0.042$), as well as people with counting strategies in both adaptation sessions ($p = 0.021$) and control sessions ($p = 0.017$).

A.9.4 Reaction Time in Different Strategies.

There were no reaction time differences in strategies. For more details, see below.

Raw Data

For the reaction time, we conducted an *experimental condition*(adaptation, control) × *actual percentage*(20%, 30%, 40%, 50%, 60% ,70%, 80%) × *strategy*(counting strategies, focusing on part of the environment, unique strategies) mixed-subjects repeated measures ANOVA.

There was no main effect of strategy ($F(2,\ 27) = 0.77$, $p = 0.472$, $\eta_p^2 = 0.054$, $95\%CI = [0.000, 0.244]$, ns), condition ($F(1,\ 27) = 0.44$, $p = 0.514$, $\eta_p^2 = 0.016$, $95\%CI = [0.000, 0.202]$, ns), or interaction between strategy and condition ($F(2,\ 27) = 0.59$, $p = 0.560$, $\eta_p^2 = 0.042$, $95\%CI = [0.000, 0.220]$, ns). As expected, there was a main effect of the actual percentage ($F(2.61,\ 70.40) = 14.51$, $p < 0.001$, $\eta_p^2 = 0.349$, $95\%CI = [0.221, 0.440]$) such that the reaction time increased with actual percentage, peaking at 50%. We found no interaction between strategy and the actual percentage ($F(5.21,\ 70.40) = 0.73$, $p = 0.608$, $\eta_p^2 = 0.051$, $95\%CI = [0.000, 0.058]$, ns), between condition and the actual percentage ($F(2.72,\ 73.32) = 1.02$, $p = 0.384$, $\eta_p^2 = 0.036$, $95\%CI = [0.000, 0.077]$, ns), or interaction among strategy, condition, and the actual percentage ($F(5.43,\ 73.32) = 1.66$, $p = 0.150$, $\eta_p^2 = 0.109$, $95\%CI = [0.000, 0.193]$, ns).

Filtered Data

Then we conducted the same ANOVA analyses on filtered data. We found a marginally significant main effect of strategy ($F(2,\ 20) = 2.68$, $p = 0.093$, $\eta_p^2 = 0.211$, $95\%CI = [0.000, 0.471]$). Tukey HSD analyses did not found difference in reaction time between people focusing on part of the environment ($M = 1.555 \pm 0.096s$) and people using counting strategies ($M = 2.348 \pm 0.072s$; $p = 0.089$), or people using unique strategies ($M = 1.986 \pm 0.081s$; $p = 0.513$). There was also no difference in reaction time between people using counting strategies and people using unique strategies ($p = 0.444$). We found a main effect of experimental condition ($F(1,\ 20) = 4.82$, $p = 0.040$, $\eta_p^2 = 0.194$, $95\%CI = [0.000, 0.474]$) where people responded slower in the adaptation session ($M = 2.244 \pm 0.077s$) than in the control session ($M = 1.956 \pm 0.063a$).

There was no interaction between strategy and condition ($F(2,\ 20) = 0.56$, $p = 0.580$, $\eta_p^2 = 0.053$, $95\%CI = [0.000, 0.271]$, ns). As expected, there was a main effect of the actual percentage ($F(2.43,\ 48.62) = 7.14$, $p = 0.001$, $\eta_p^2 = 0.263$, $95\%CI = [0.112, 0.366]$) such that the reaction time increased with actual percentage, peaking at 50%. We found no

interaction between strategy and the actual percentage ($F(4.86, 48.62) = 0.56$, $p = 0.729$, $\eta_p^2 = 0.053$, $95\%CI = [0.000, 0.046]$, ns), between condition and the actual percentage ($F(3.40, 68.05) = 0.90$, $p = 0.457$, $\eta_p^2 = 0.043$, $95\%CI = [0.000, 0.088]$, ns), or interaction among strategy, condition, and the actual percentage ($F(6.81, 68.05) = 1.16$, $p = 0.337$, $\eta_p^2 = 0.104$, $95\%CI = [0.000, 0.185]$, ns).

A.10 Experiment 3: Raw Data

A.10.1 Reported Rate by Control Conditions

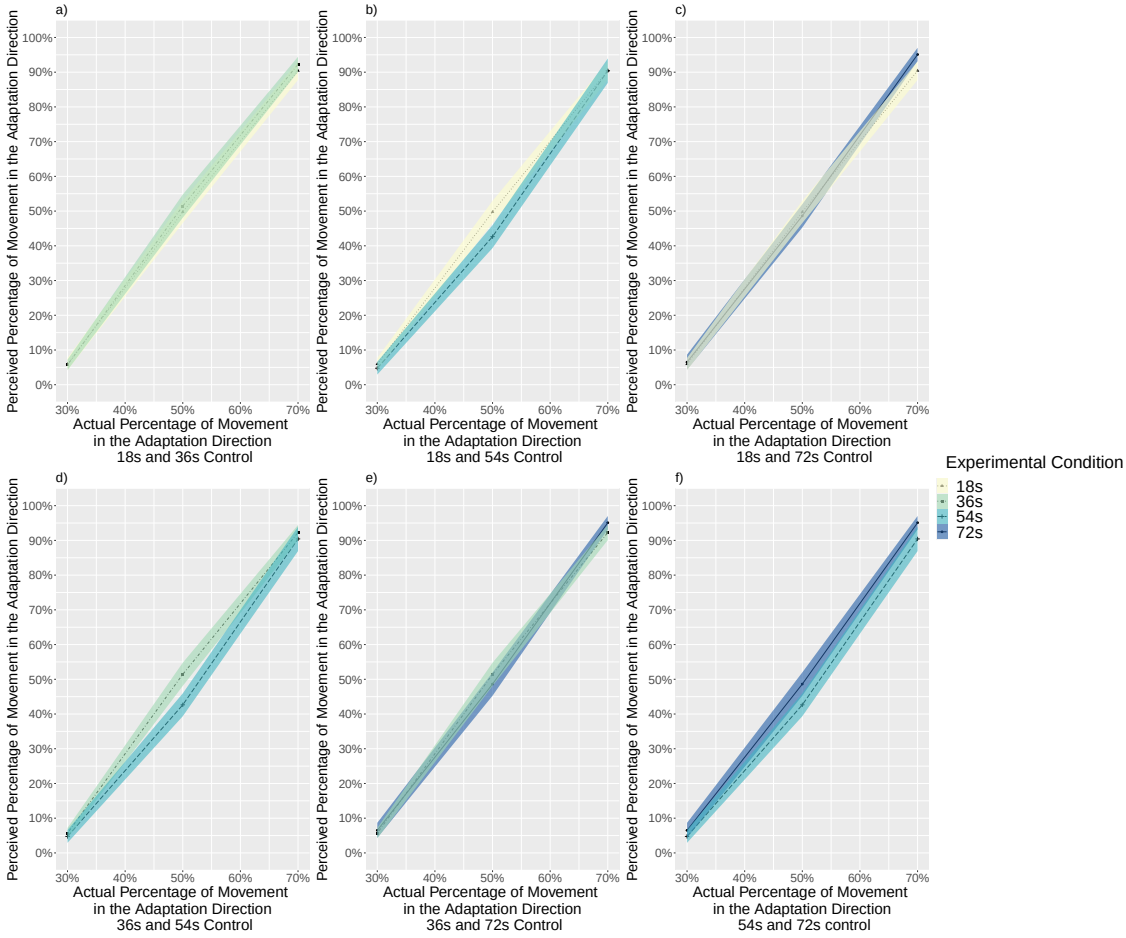

Figure A.17: Experiment 3: The perceived percentage of movement in the adaptation direction compared with the actual percentage for all subjects, separated by control conditions (n = 28). a) The Reported Rate for the 18s and 36s control conditions. b) The Reported Rate for the 18s and 54s control conditions. c) The Reported Rate for the 18s and 72s control conditions. d) The Reported Rate for the 36s and 54s control conditions. e) The Reported Rate for the 36s and 72s control conditions. f) The Reported Rate for the 54s and 72s control conditions. Solid lines indicate the grand average value, and the shaded area indicate 1 standard error of means. All results are reported with the Tukey correction for multiple comparisons.

A.10.2 Reported Rate Table

Cond.	18s			36s			54s			72s		
	30%	50%	70%	30%	50%	70%	30%	50%	70%	30%	50%	70%
%	*M(SE)*	*M(SE)*	*M(SE)*	*M(SE)*	*M(SE)*	*M(SE)*	*M(SE)*	*M(SE)*	*M(SE)*	*M(SE)*	*M(SE)*	*M(SE)*
Adapt	10(2)	56(4)	91(2)	17(5)	61(3)	88(3)	20(5)	64(4)	89(3)	19(6)	63(4)	96(2)
Control	6(2)	53(3)	92(2)	6(2)	52(4)	93(2)	6(2)	44(4)	92(3)	7(2)	49(3)	96(2)
Sig.	0.183	0.577	0.672	0.013*	0.048*	0.106	0.009**	0.001**	0.342	0.077+	0.027*	1.000

$+p < .08.$, $*p < .05.$, $**p < .01.$, Tukey correction.

Table A.7: Experiment 3: Average perceived percentage of movement in the adaptation direction and standard error of the adaptation and the control conditions for filtered subjects (n = 24), by adaptation time periods and level of actual percentage of movement in the adaptation direction.

A.10.3 Individual Psychometric Functions

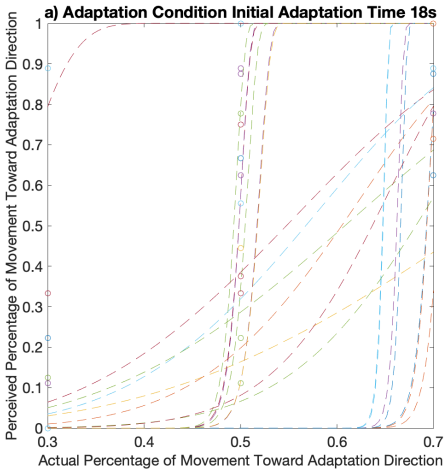

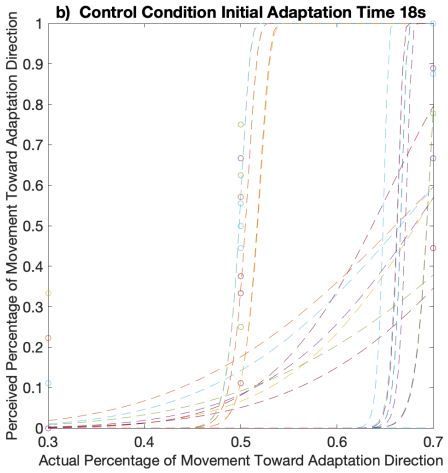

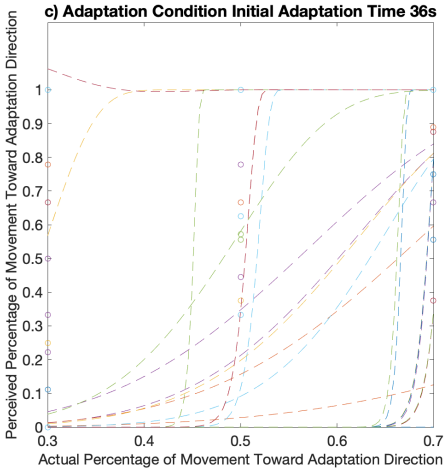

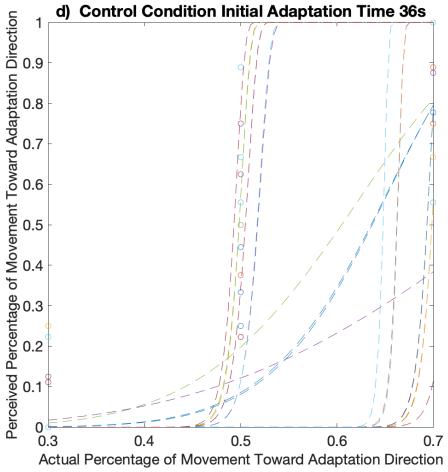

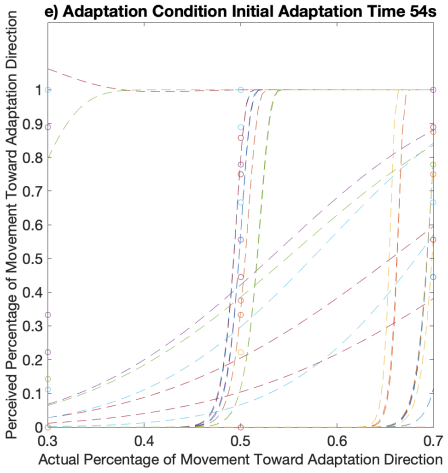

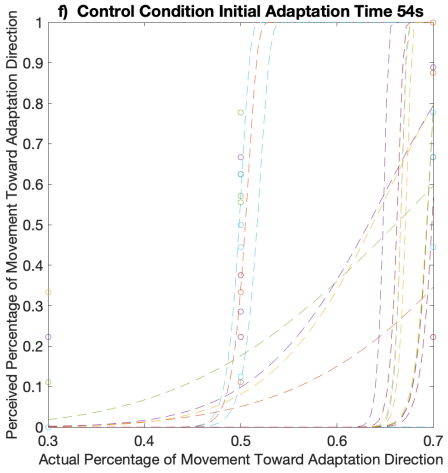

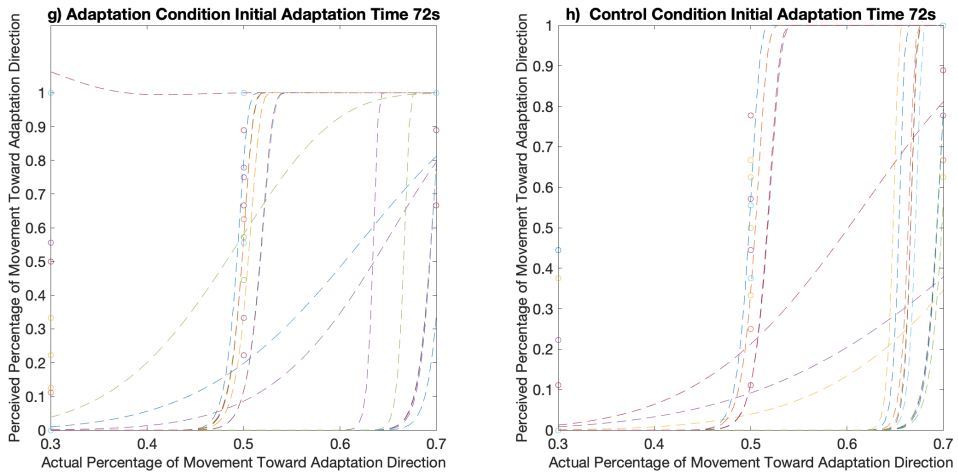

Figure A.18: Experiment 3: Psychometric functions of all observers' data (n = 28) a) Adaptation condition at 18s adaptation. b) Control condition at 18s adaptation. c) Adaptation condition at 36s adaptation. d) Control condition at 36s adaptation. e) Adaptation condition at 54s adaptation. f) Control condition at 54s adaptation. g) Adaptation condition at 72s adaptation. h) Control condition at 72s adaptation.

A.10.4 Reaction Times by Adaptation Time Periods

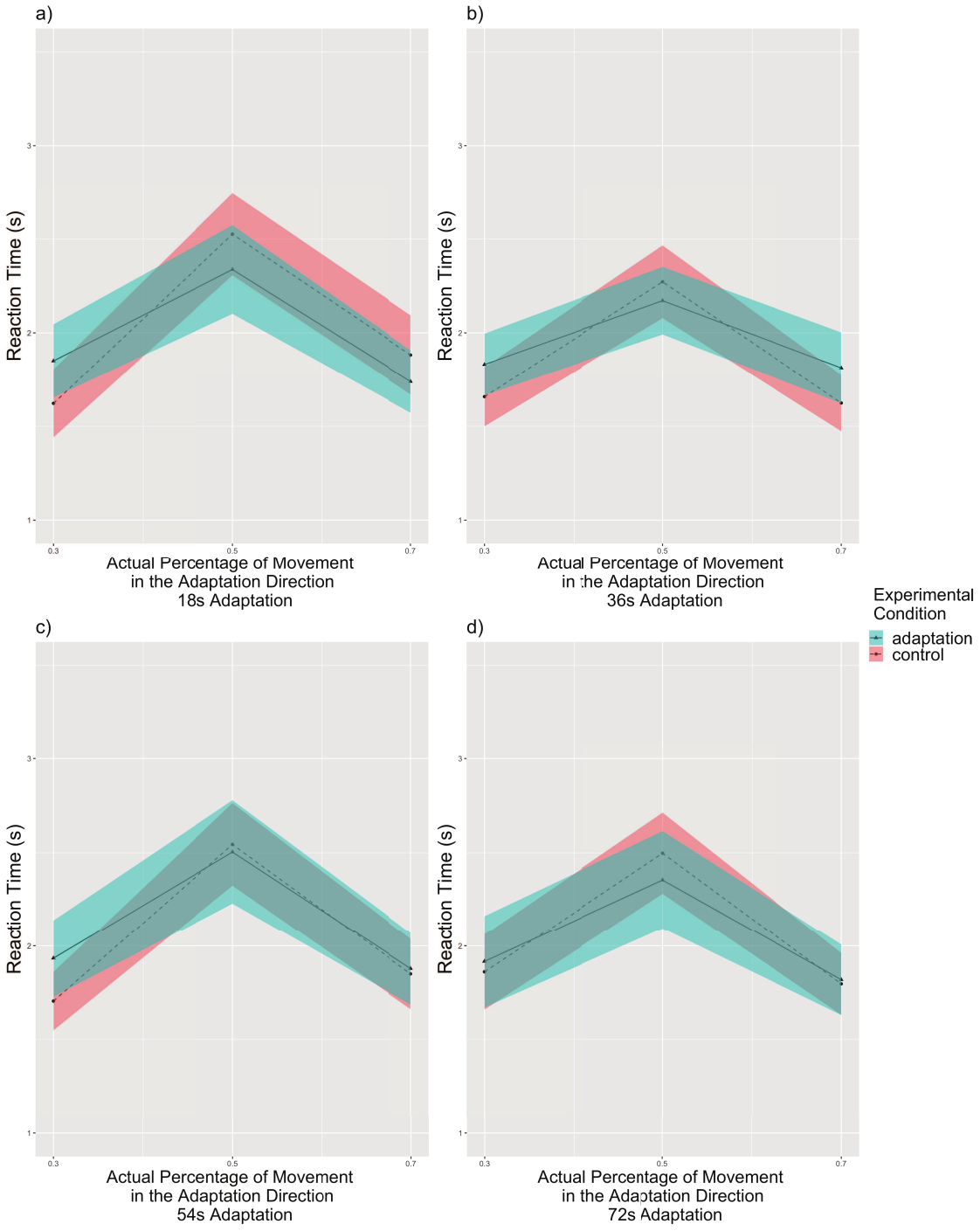

Figure A.19: Experiment 3: Reaction times compared with the actual percentage for all subjects, separated by adaptation time periods (n = 28). The reaction time increased as the actual percentage approached 50% in all adaptation time periods. a) Reaction times for 18s adaptation trials. b) Reaction times for 36s adaptation trials. c) Reaction times for 54s adaptation trials. d) Reaction times for 72s adaptation trials. Solid lines indicate the grand average value, and the shaded area indicate 1 standard error of means. Tukey correction.

A.10.5 Reaction Times by Experimental Conditions

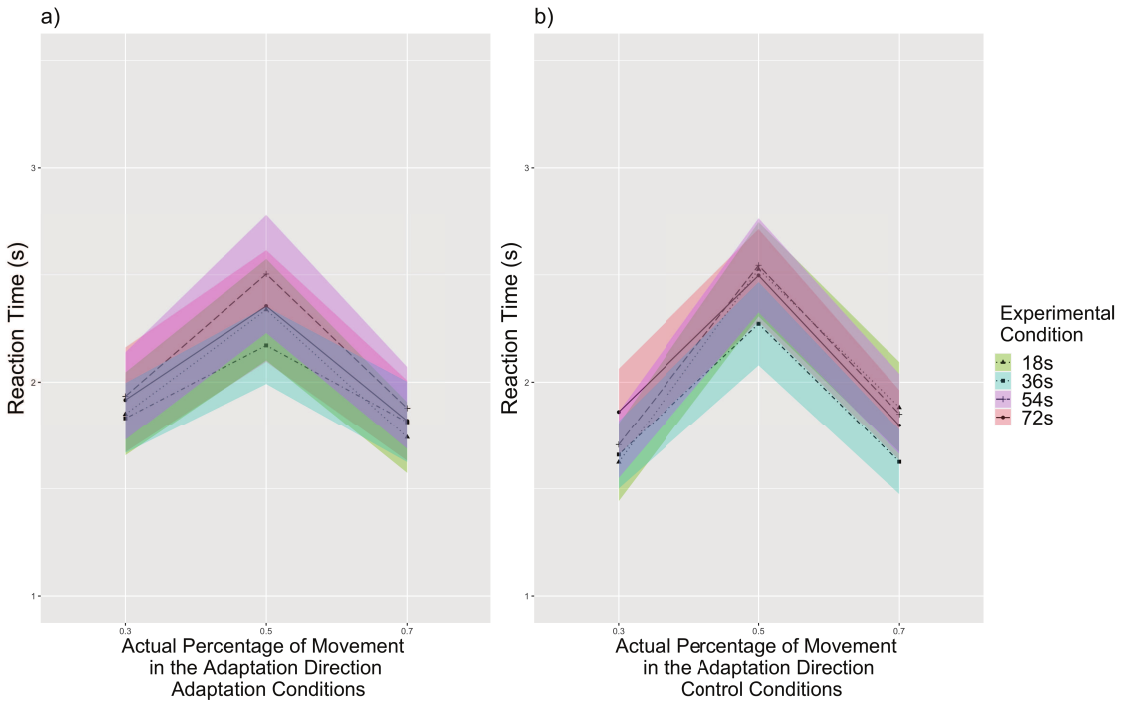

Figure A.20: Experiment 3: Reaction times compared with the actual percentage for all subjects, separated by experimental conditions (n = 28). The reaction time increased as the actual percentage approached 50% in both experimental conditions. a) Reaction times for adaptation condition. b) Reaction times for control condition. At 30%, people responded slightly slower to 72s adaptation trials than to 18s adaptation trials ($p = 0.054$). At 70%, people responded slightly slower to 54s adaptation trials than to 36s adaptation trials ($p = 0.074$). Solid lines indicate the grand average value, and the shaded area indicate 1 standard error of means. Tukey correction.

A.11 Experiment 3: Filtered Data

A.11.1 Reported Rate by Adaptation Time Periods

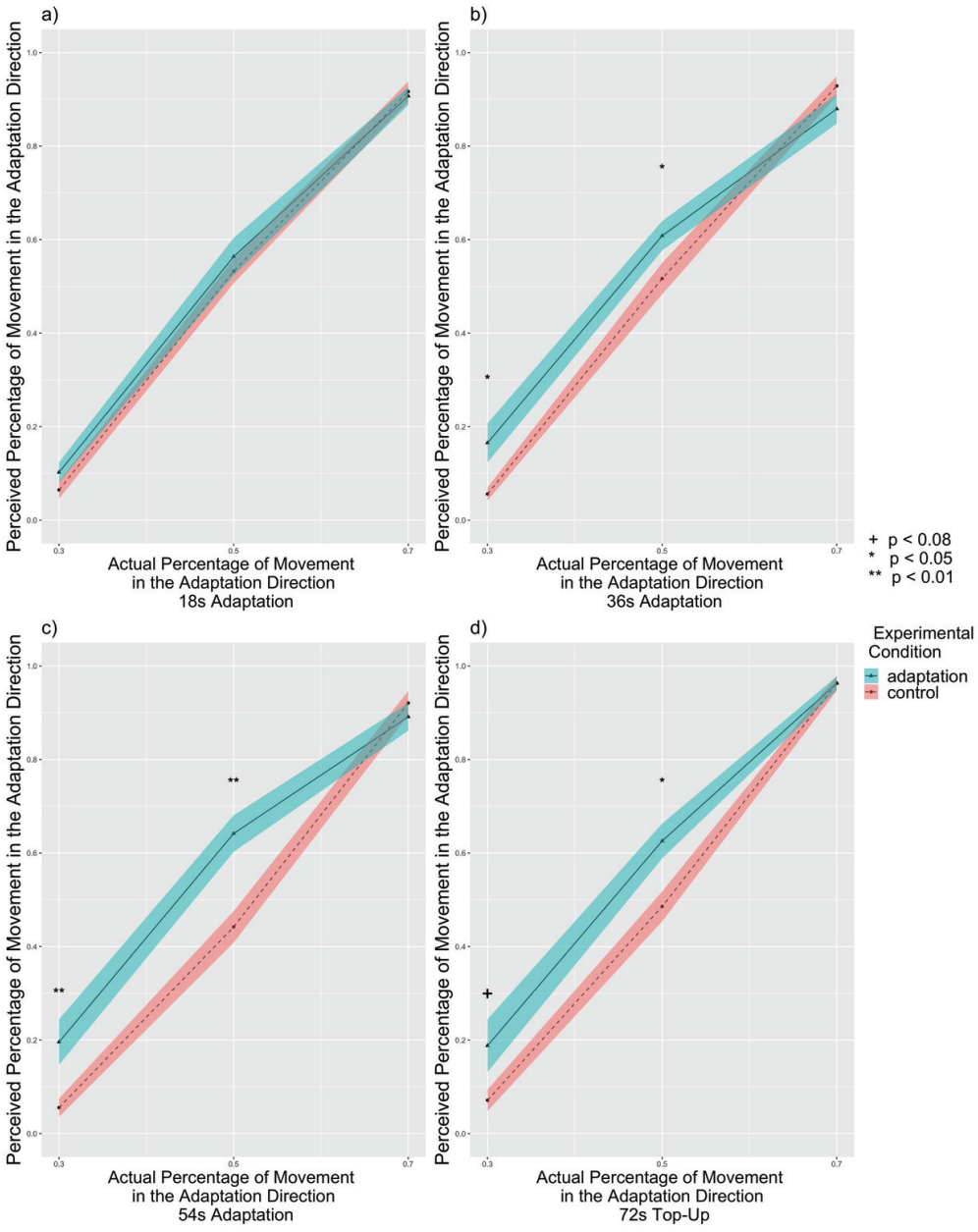

Figure A.21: Experiment 3: The perceived percentage of movement in the adaptation direction compared with the actual percentage for filtered subjects, separated by adaptation time periods (n = 24). a) The Reported Rate for 18s adaptation trials. The adaptation condition showed no difference from the control condition (p = 0.367). b) The Reported Rate for 36s adaptation trials. The adaptation condition showed slightly higher reported percentages than control conditions (p = 0.061) particularly at 30% (p = 0.013) and 50% (p = 0.048), supporting the aftereffect in the same direction of travel. c) The Reported Rate for 54s adaptation trials. The adaptation condition showed higher reported percentages than control conditions (p = 0.004) particularly at 30% (p = 0.009) and 50% (p = 0.001), supporting the aftereffect. d) The Reported Rate for 72s adaptation trials. The adaptation condition showed higher reported percentages than control conditions (p = 0.022) particularly at 30% (p = 0.076) and 50% (p = 0.027), supporting the aftereffect in the same direction of travel. Solid lines indicate the grand average value, and the shaded area indicate 1 standard error of means. + $p < 0.08$, * $p < 0.05$, ** $p < 0.01$, Tukey correction.

A.11.2 Reported Rate Table

Cond.	18s			36s			54s			72s		
	30%	50%	70%	30%	50%	70%	30%	50%	70%	30%	50%	70%
%	*M(SE)*	*M(SE)*	*M(SE)*	*M(SE)*	*M(SE)*	*M(SE)*	*M(SE)*	*M(SE)*	*M(SE)*	*M(SE)*	*M(SE)*	*M(SE)*
Adapt	12(3)	57(4)	92(2)	19(5)	61(3)	89(3)	20(5)	62(5)	90(3)	20(6)	62(4)	96(1)
Control	6(2)	50(3)	90(3)	6(2)	51(3)	92(2)	5(2)	43(3)	90(4)	6(2)	49(3)	95(2)
Sig.	0.112	0.149	0.673	0.015*	0.032	0.213	0.007**	0.001**	0.881	0.047*	0.031*	0.681

*$p < .05.$, **$p < .01.$, Tukey correction.

Table A.8: Experiment 3: Average perceived percentage of movement in the adaptation direction and standard error of the adaptation and the control conditions for all subjects (n = 28), by adaptation time periods and level of actual percentage of movement in the adaptation direction.

A.11.3 Individual Psychometric Functions

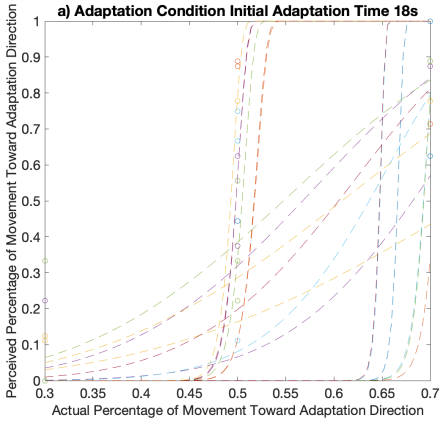

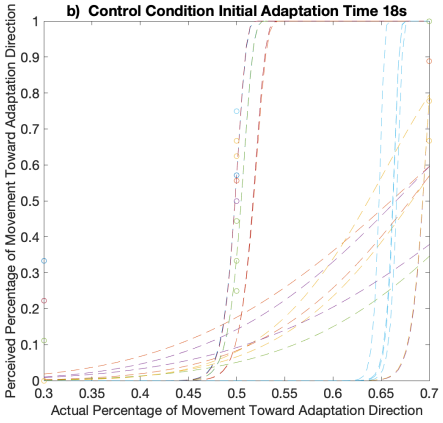

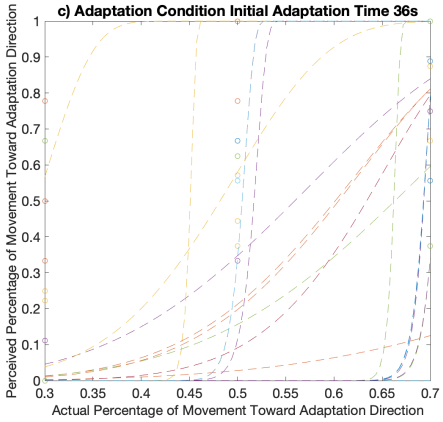

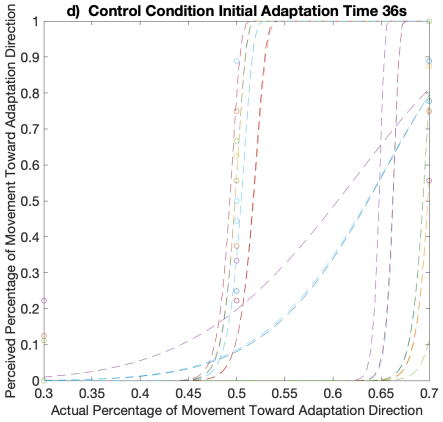

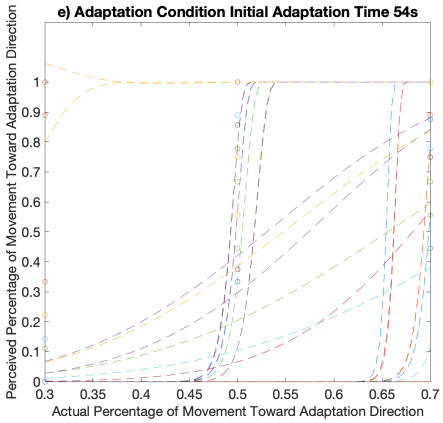

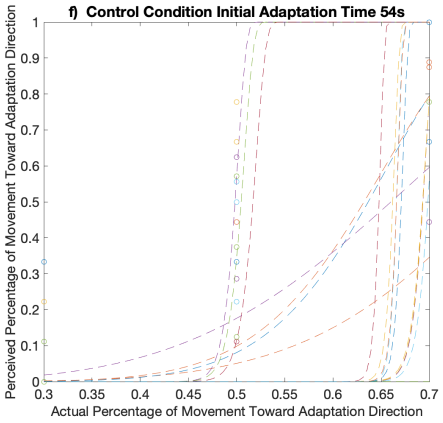

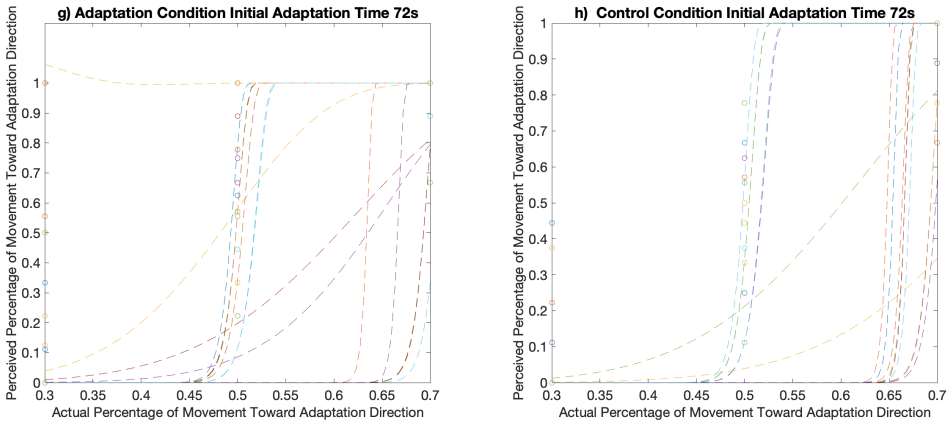

Figure A.22: Experiment 3: Psychometric functions of all observers' data (n = 24) a) Adaptation condition at 18s adaptation. b) Control condition at 18s adaptation. c) Adaptation condition at 36s adaptation. d) Control condition at 36s adaptation. e) Adaptation condition at 54s adaptation. f) Control condition at 54s adaptation. g) Adaptation condition at 72s adaptation. h) Control condition at 72s adaptation.

A.11.4 Group Psychometric Functions

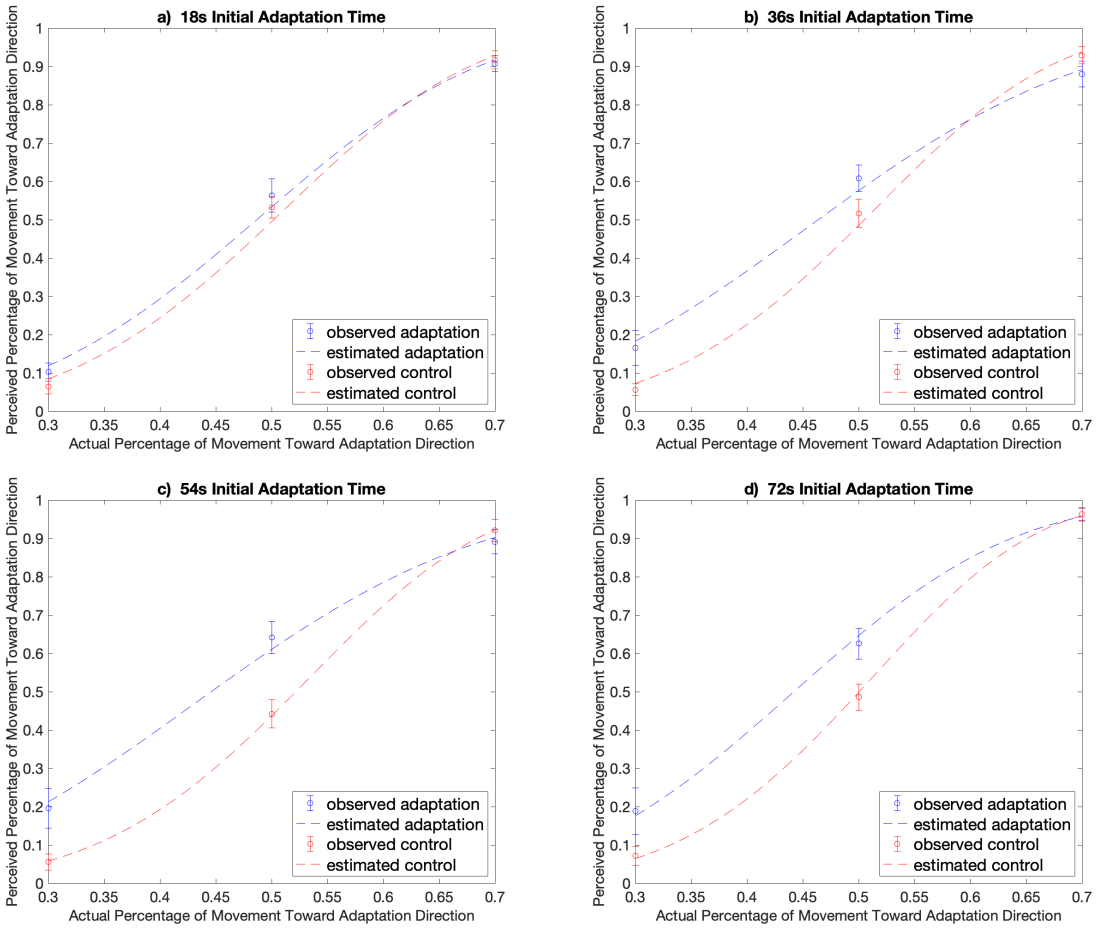

Figure A.23: Experiment 3: The average psychometric functions by adaptation time periods. Results were pooled across 24 observers. The psychometric function (i.e., α) shifts toward lower percentage of movement toward the adaptation direction when adapted but were not significant at 18s ($p = 0.836$), 36s ($p = 0.315$), 54s ($p = 0.898$), or 72s adaptation ($p = 0.103$) time periods. The psychometric function (i.e., β) indicates that observers' detectability of the difference between the two directions was decreased by adaptation but were not significant at 18s ($p = 0.495$) or 36s ($p = 0.081$) adaptation time periods, and was significant at 54s ($p = 0.036$) and 72s ($p = 0.033$) adaptation time periods. Error bars indicate standard errors.

A.11.5 Reaction Times by Adaptation Time Periods

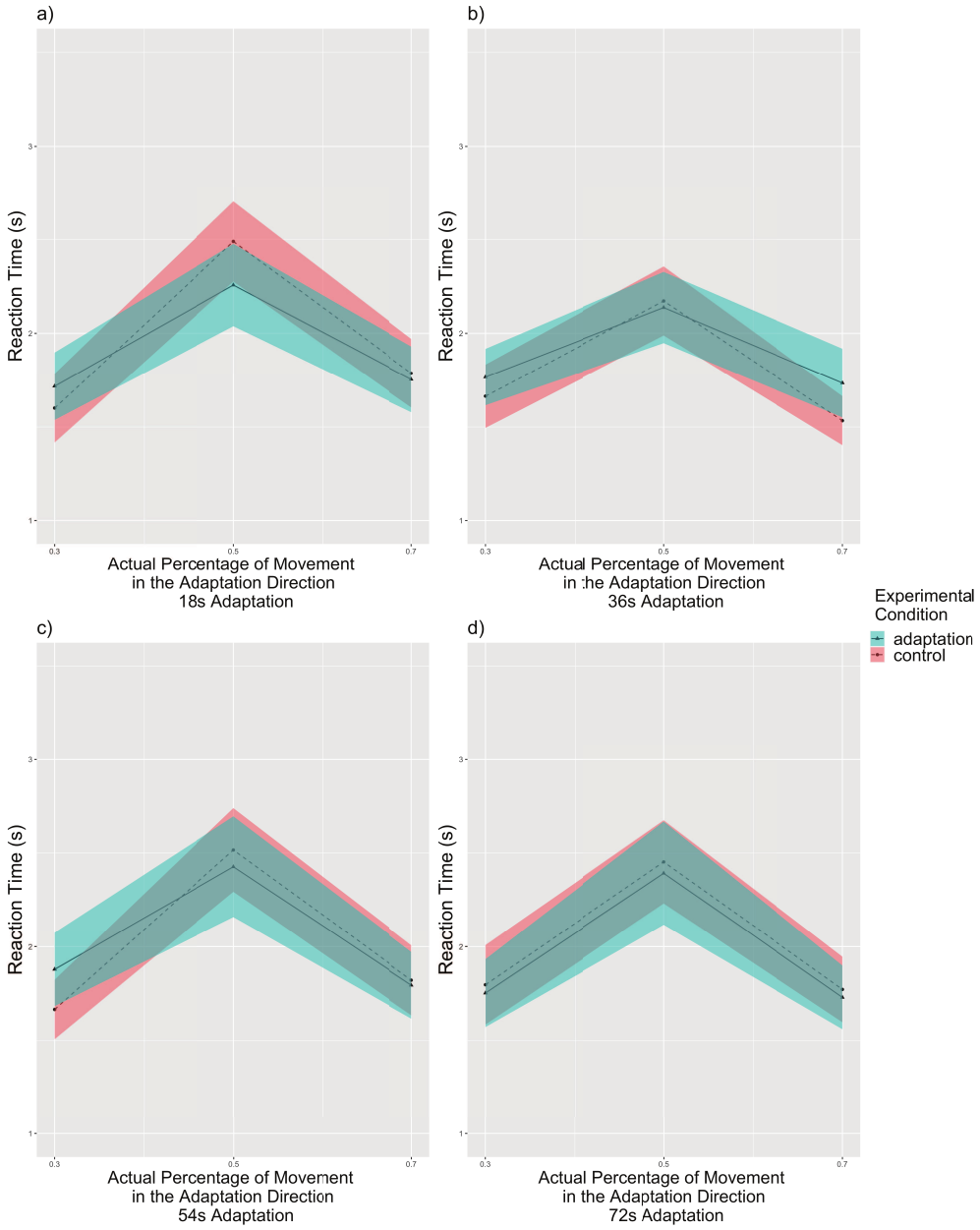

Figure A.24: Experiment 3: Reaction times compared with the actual percentage for filtered subjects, separated by adaptation time periods (n = 24). The reaction time increased as the actual percentage approached 50% in all adaptation time periods. a) Reaction times for 18s adaptation trials. b) Reaction times for 36s adaptation trials. c) Reaction times for 54s adaptation trials. d) Reaction times for 72s adaptation trials. Solid lines indicate the grand average value, and the shaded area indicate 1 standard error of means. Tukey correction.

A.11.6 Reported Rate by Experimental Conditions

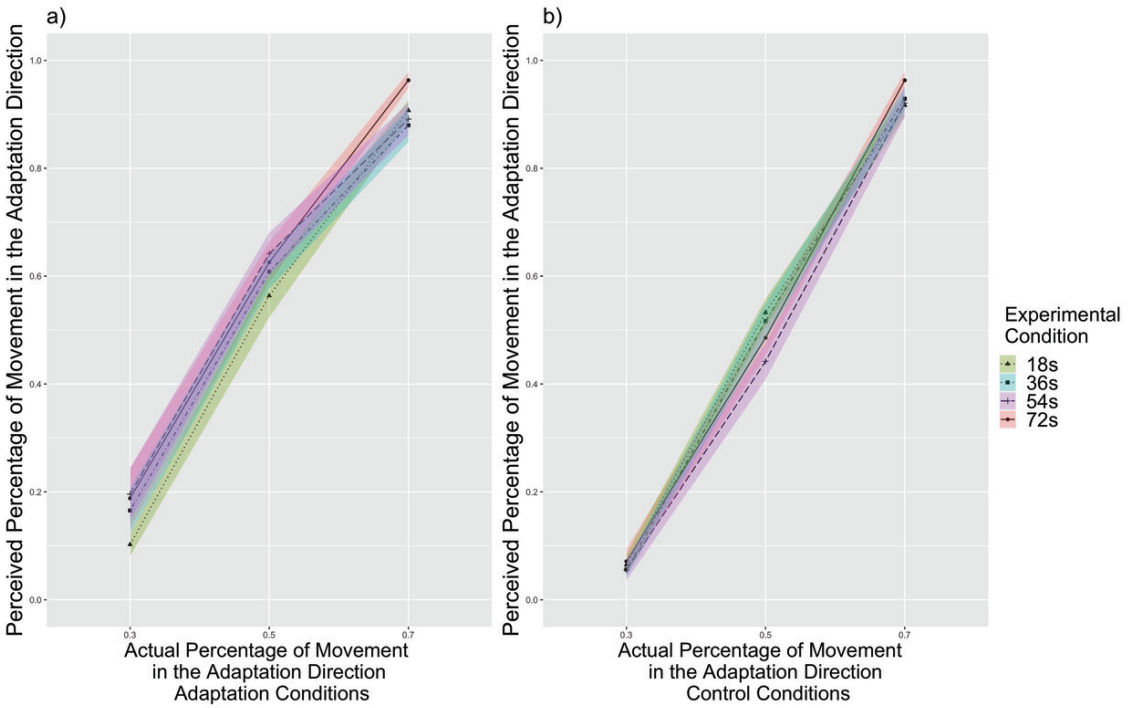

Figure A.25: Experiment 3: The perceived percentage of movement in the adaptation direction compared with the actual percentage for filtered subjects, separated by experimental conditions (n = 24). a) The Reported Rate for adaptation condition. At 70%, 72s adaptation trials had higher perceived percentage than 36s adaptation trials ($p = 0.014$) and slightly higher than 54s adaptation trials ($p = 0.053$), supporting that the aftereffect increased with adaptation time. The aftereffect is in the same direction of travel. b) The Reported Rate for control condition. There were no differences between trials with different adaptation time periods within any actual percentage. Tukey correction.

A.11.7 Reaction Times by Experimental Conditions

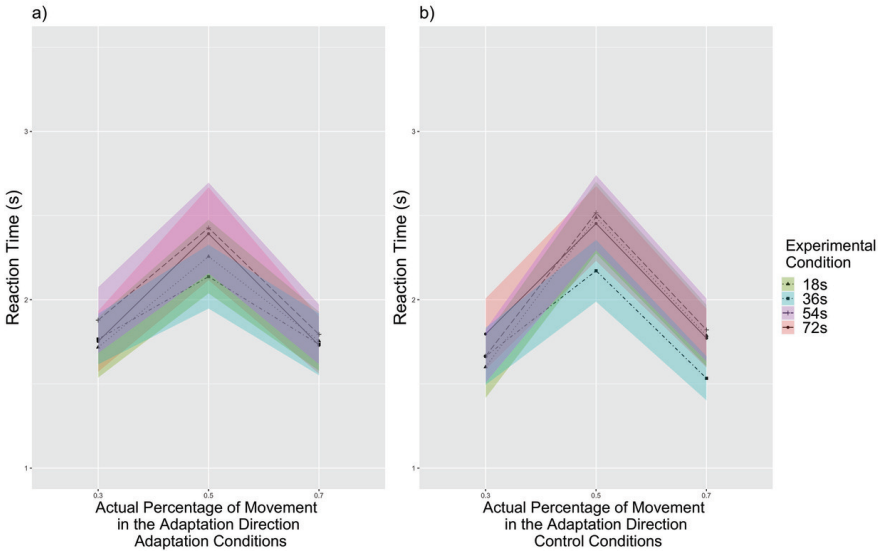

Figure A.26: Experiment 3: Reaction times compared with the actual percentage for filtered subjects, separated by experimental conditions (n = 24). The reaction time increased as the actual percentage approached 50% in both experimental conditions. a) Reaction times for adaptation condition. b) Reaction times for control condition. At 30%, people responded slightly slower to 72s adaptation trials than to 18s adaptation trials (p = 0.054). At 70%, people responded slower to 54s adaptation trials than to 36s adaptation trials (p = 0.034). Solid lines indicate the grand average value, and the shaded area indicate 1 standard error of means. Tukey correction.

A.12 Experiment 3: Strategies

A.12.1 Task Difficulty

Raw Data

For the task difficulty, we conducted an *experimental condition*(adaptation, control) × *strategy*(counting strategies, focusing on part of the environment, unique strategies) mixed-subjects repeated measures ANOVA. There was no main effect of strategy ($F(2,\ 25) = 0.32$, $p = 0.726$, $\eta_p^2 = 0.025$, $95\%CI = [0.000, 0.184]$, ns), no main effect of condition ($F(1,\ 25) = 1.15$, $p = 0.295$, $\eta_p^2 = 0.044$, $95\%CI = [0.000, 0.270]$, ns), or interaction between

strategy and condition ($F(2, 25) = 0.93$, $p = 0.409$, $\eta_p^2 = 0.069$, $95\%CI = [0.000, 0.277]$, ns). For filtered data, the result shows the same pattern. For more details, see below.

Filtered Data

As for the rated difficulty of each condition, participants rated the adaptation session ($M = 4.63 \pm 0.24$) to be around the same difficulty level as the control session ($M = 4.50 \pm 0.21$)($t(23)$ = -0.531, $p = 0.601$, $Cohen's\, d$ = -0.113, $95\%CI$ = [-0.544, -0.318], ns).

A.12.2 Task Difficulty in Different Strategies.

Raw Data

For the task difficulty, we conducted an *experimental condition*(adaptation, control) *strategy*(counting strategies, focusing on part of the environment, unique strategies) mixed-subjects repeated measures ANOVA. We found no main effect of experimental condition, no main effect of strategy, or interaction between experimental condition and strategies (all $p > 0.08$). For filtered data, the result shows the same pattern. For more details, see below.

Filtered Data

Then we conducted the same ANOVA analyses on filtered data. There was no main effect of strategy ($F(2, 21) = 1.05$, $p = 0.369$, $\eta_p^2 = 0.091$, $95\%CI = [0.000, 0.329]$, ns), no main effect of the experimental condition ($F(1, 21) = 1.25$, $p = 0.277$, $\eta_p^2 = 0.056$, $95\%CI = [0.000, 0.313]$, ns), and no interaction between strategy and condition ($F(2, 21) = 0.62$, $p = 0.547$, $\eta_p^2 = 0.056$, $95\%CI = [0.000, 0.272]$, ns).

A.12.3 Reported Rate in Different Strategies.

Raw Data

For the perceived percentage, we conducted an *experimental condition*(adaptation, control) $\times$ *actual percentage*(30%, 50%, 70%) *adaptation time periods* (18s, 36s, 54s, 72s) *strategy*(counting strategies, focusing on part of the environment, unique strategies) mixed-subjects repeated measures ANOVA. There was a main effect of condition ($F(1, 25) = 4.69$, $p = 0.040$, $\eta_p^2 = 0.129$, $95\%CI = [0.000, 0.383]$) where people reported more toward the adaptation direction in the adaptation session ($M = 0.566 \pm 0.020$) than in the control session ($M = 0.486 \pm 0.021$). As expected, there was also a main effect of the actual percentage ($F(1.37, 34.18) = 298.65$, $p < 0.001$, $\eta_p^2 = 0.920$, $95\%CI = [0.849, 0.951]$) that showed the perceived percentage increased with the actual percentage. There was a marginally significant interaction between the experimental condition and the actual percentage ($F(1.65, 41.22) = 2.99$, $p = 0.070$, $\eta_p^2 = 0.107$, $95\%CI = [0.000, 0.270]$). Because the interaction was only marginally significant, we did not conduct further post-hoc analyses.

There were no main effect of strategy ($F(2, 25) = 0.06$, $p = 0.946$, $\eta_p^2 = 0.004$, $95\%CI = [0.000, 0.060]$, ns), no main effect of adaptation time periods ($F(2.68, 66.89) = 0.72$, $p = 0.529$, $\eta_p^2 = 0.014$, $95\%CI = [0.000, 0.056]$, ns), no interaction between the strategy and the experimental condition ($F(2, 25) = 0.33$, $p = 0.725$, $\eta_p^2 = 0.020$, $95\%CI = [0.000, 0.167]$, ns), no interaction between the strategy and the actual percentage ($F(2.73, 34.18) = 2.50$, $p = 0.081$, $\eta_p^2 = 0.162$, $95\%CI = [0.000, 0.356]$, ns), no interaction between the strategy and adaptation time periods ($F(5.35, 66.89) = 0.64$, $p = 0.684$, $\eta_p^2 = 0.024$, $95\%CI = [0.000, 0.000]$, ns), no interaction between the actual percentage and adaptation time periods ($F(4.41, 110.33) = 1.33$, $p = 0.269$, $\eta_p^2 = 0.090$, $95\%CI = [0.000, 0.122]$, ns), no interaction between the experimental condition and adaptation time periods ($F(4.25, 57.37) = 0.66$, $p = 0.637$, $\eta_p^2 = 0.026$, $95\%CI = [0.000, 0.053]$, ns), no interaction among the strategy, the experimental condition, and the actual percentage ($F(3.30, 41.22) = 2.10$, $p = 0.050$, η_p^2

$= 0.103$, $95\%CI = [0.000, 0.234]$, ns), no interaction among the strategy, the experimental condition, and adaptation time periods ($F(4.77,\ 59.61) = 0.73$, $p = 0.601$, $\eta_p^2 = 0.055$, $95\%CI = [0.000, 0.112]$, ns), no interaction among the strategy, the actual percentage, and adaptation time periods ($F(8.83,\ 110.33) = 0.82$, $p = 0.594$, $\eta_p^2 = 0.062$, $95\%CI = [0.000, 0.074]$, ns), no interaction among the experimental condition, the actual percentage, and adaptation time periods ($F(4.13,\ 103.23) = 1.45$, $p = 0.223$, $\eta_p^2 = 0.055$, $95\%CI = [0.000, 0.106]$, ns), or interaction among the strategy, the experimental condition, the actual percentage, and adaptation time periods ($F(8.26,\ 103.23) = 1.18$, $p = 0.318$, $\eta_p^2 = 0.086$, $95\%CI = [0.000, 0.155]$, ns).

Filtered Data

For the perceived percentage, we conducted an *experimental condition*(adaptation, control) $\times$ *actual percentage*(30%, 50%, 70%) *adaptation time periods* (18s, 36s, 54s, 72s) *strategy*(counting strategies, focusing on part of the environment, unique strategies) mixed-subjects repeated measures ANOVA. There was a main effect of condition ($F(1,\ 21) = 4.66$, $p = 0.043$, $\eta_p^2 = 0.203$, $95\%CI = [0.000, 0.476]$) where people reported more toward the adaptation direction in the adaptation session ($M = 0.561 \pm 0.021$) than in the control session ($M = 0.496 \pm 0.022$). As expected, there was also a main effect of the actual percentage ($F(1.32,\ 27.71) = 281.68$, $p < 0.001$, $\eta_p^2 = 0.964$, $95\%CI = [0.927, 0.979]$) that showed the perceived percentage increased with the actual percentage. There was a significant interaction between the experimental condition and the actual percentage ($F(1.98,\ 41.56) = 4.57$, $p = 0.016$, $\eta_p^2 = 0.179$, $95\%CI = [0.007, 0.368]$). Tukey HSD post-hoc analyses revealed that people had increased Reported Rate in the adaptation condition than the control condition at 50% actual percentage ($p = 0.011$).

There were no main effect of strategy ($F(2,\ 21) = 0.14$, $p = 0.866$, $\eta_p^2 = 0.014$, $95\%CI = [0.000, 0.147]$, ns), no main effect of adaptation time periods ($F(2.63,\ 55.16) = 0.82$, $p = 0.474$, $\eta_p^2 = 0.037$, $95\%CI = [0.000, 0.169]$, ns), no interaction between the strategy and the

experimental condition ($F(2,\ 21) = 0.01$, $p = 0.993$, $\eta_p^2 < 0.001$, $95\%CI = [0.000, 0.000]$, ns), no interaction between the strategy and the actual percentage ($F(2.64,\ 27.71) = 1.58$, $p = 0.220$, $\eta_p^2 = 0.231$, $95\%CI = [0.000, 0.449]$, ns), no interaction between the strategy and adaptation time periods ($F(5.25,\ 55.16) = 0.77$, $p = 0.578$, $\eta_p^2 = 0.067$, $95\%CI = [0.000, 0.069]$, ns), no interaction between the actual percentage and adaptation time periods ($F(4.78,\ 100.36) = 0.71$, $p = 0.614$, $\eta_p^2 = 0.033$, $95\%CI = [0.000, 0.067]$, ns), no interaction between the experimental condition and adaptation time periods ($F(2.51,\ 52.76) = 1.84$, $p = 0.160$, $\eta_p^2 = 0.080$, $95\%CI = [0.000, 0.204]$, ns), no interaction among the strategy, the experimental condition, and the actual percentage ($F(3.96,\ 41.56) = 2.00$, $p = 0.113$, $\eta_p^2 = 0.160$, $95\%CI = [0.000, 0.320]$, ns), no interaction among the strategy, the experimental condition, and adaptation time periods ($F(5.02,\ 52.76) = 0.61$, $p = 0.690$, $\eta_p^2 = 0.055$, $95\%CI = [0.000, 0.112]$, ns), no interaction among the strategy, the actual percentage, and adaptation time periods ($F(9.56,\ 100.36) = 0.90$, $p = 0.535$, $\eta_p^2 = 0.079$, $95\%CI = [0.000, 0.098]$, ns), no interaction among the experimental condition, the actual percentage, and adaptation time periods ($F(3.81,\ 79.98) = 1.80$, $p = 0.140$, $\eta_p^2 = 0.079$, $95\%CI = [0.000, 0.146]$, ns), or interaction among the strategy, the experimental condition, the actual percentage, and adaptation time periods ($F(7.62,\ 79.98) = 1.20$, $p = 0.311$, $\eta_p^2 = 0.103$, $95\%CI = [0.000, 0.137]$, ns).

A.12.4 Reaction Time in Different Strategies.

There were also no reaction time differences in strategies. For more details, see below.

Raw Data

For the reaction time, we conducted an *experimental condition*(adaptation, control) × *actual percentage*(30%, 50%, 70%) *adaptation time periods* (18s, 36s, 54s, 72s) *strategy*(counting strategies, focusing on part of the environment, unique strategies) mixed-subjects repeated measures ANOVA. We only observed a main effect of the actual percentage ($F(1.29,\ 32.36) =$

37.87, $p < 0.001$, $\eta_p^2 = 0.087$, $95\%CI = [0.000, 0.305]$) such that the reaction time increased with actual percentage, peaking at 50%.

There were no effect of condition ($F(1,\ 25) = 0.26$, $p = 0.612$, $\eta_p^2 < 0.001$, $95\%CI = [0.000, 0.113]$, ns), no main effect of strategy ($F(2,\ 25) = 0.81$, $p = 0.455$, $\eta_p^2 = 0.061$, $95\%CI = [0.000, 0.264]$, ns), no main effect of adaptation time periods ($F(2.55,\ 63.65) = 1.52$, $p = 0.223$, $\eta_p^2 = 0.004$, $95\%CI = [0.000, 0.000]$, ns), no interaction between the experimental condition and the actual percentage ($F(1.79,\ 44.70) = 0.98$, $p = 0.374$, $\eta_p^2 = 0.038$, $95\%CI = [0.000, 0.164]$, ns), no interaction between the strategy and the experimental condition ($F(2,\ 25) = 0.11$, $p = 0.896$, $\eta_p^2 < 0.001$, $95\%CI = [0.000, 0.000]$, ns), no interaction between the strategy and the actual percentage ($F(2.59,\ 32.36) = 2.25$, $p = 0.109$, $\eta_p^2 = 0.011$, $95\%CI = [0.000, 0.000]$, ns), no interaction between the strategy and adaptation time periods ($F(5.09,\ 63.65) = 0.46$, $p = 0.809$, $\eta_p^2 = 0.002$, $95\%CI = [0.000, 0.000]$, ns), no interaction between the actual percentage and adaptation time periods ($F(4.18,\ 104.47) = 0.74$, $p = 0.573$, $\eta_p^2 = 0.029$, $95\%CI = [0.000, 0.060]$, ns), no interaction between the experimental condition and adaptation time periods ($F(2.71,\ 67.72) = 0.46$, $p = 0.691$, $\eta_p^2 = 0.018$, $95\%CI = [0.000, 0.079]$, ns), no interaction among the strategy, the experimental condition, and the actual percentage ($F(3.58,\ 44.70) = 0.75$, $p = 0.551$, $\eta_p^2 = 0.056$, $95\%CI = [0.000, 0.157]$, ns), no interaction among the strategy, the experimental condition, and adaptation time periods ($F(5.42,\ 67.72) = 1.11$, $p = 0.367$, $\eta_p^2 = 0.081$, $95\%CI = [0.000, 0.159]$, ns), no interaction among the strategy, the actual percentage, and adaptation time periods ($F(8.36,\ 104.47) = 0.59$, $p = 0.795$, $\eta_p^2 = 0.045$, $95\%CI = [0.000, 0.041]$, ns), no interaction among the experimental condition, the actual percentage, and adaptation time periods ($F(3.80,\ 94.98) = 0.73$, $p = 0.568$, $\eta_p^2 = 0.028$, $95\%CI = [0.000, 0.059]$, ns), or interaction among the strategy, the experimental condition, the actual percentage, and adaptation time periods ($F(7.60,\ 94.98) = 0.41$, $p = 0.907$, $\eta_p^2 = 0.032$, $95\%CI = [0.000, 0.010]$, ns).

Filtered Data

Then we conducted the same ANOVA analyses on filtered data. Again, we only observed a main effect of the actual percentage ($F(1.22, 25.52) = 36.42$, $p < 0.001$, $\eta_p^2 = 0.101$, $95\%CI = [0.000, 0.343]$) such that the reaction time increased with actual percentage, peaking at 50%. There were no effect of condition ($F(1,\ 21) = 0.15$, $p = 0.705$, $\eta_p^2 < 0.001$, $95\%CI = [0.000, 0.108]$, ns), no main effect of strategy ($F(2,\ 21) = 0.43$, $p = 0.655$, $\eta_p^2 = 0.040$, $95\%CI = [0.000, 0.238]$, ns), no main effect of adaptation time periods ($F(2.53,\ 53.17) = 1.80$, $p = 0.166$, $\eta_p^2 = 0.005$, $95\%CI = [0.000, 0.000]$, ns), no interaction between the experimental condition and the actual percentage ($F(1.71,\ 35.88) = 0.58$, $p = 0.539$, $\eta_p^2 = 0.027$, $95\%CI = [0.000, 0.152]$, ns), no interaction between the strategy and the experimental condition ($F(2,\ 21) = 0.24$, $p = 0.791$, $\eta_p^2 = 0.022$, $95\%CI = [0.000, 0.000]$, ns), no interaction between the strategy and the actual percentage ($F(2.43,\ 25.52) = 2.19$, $p = 0.124$, $\eta_p^2 = 0.013$, $95\%CI = [0.000, 0.000]$, ns), no interaction between the strategy and adaptation time periods ($F(5.06,\ 53.17) = 0.52$, $p = 0.761$, $\eta_p^2 = 0.003$, $95\%CI = [0.000, 0.000]$, ns), no interaction between the actual percentage and adaptation time periods ($F(4.19,\ 88.07) = 1.30$, $p = 0.275$, $\eta_p^2 = 0.058$, $95\%CI = [0.000, 0.114]$, ns), no interaction between the experimental condition and adaptation time periods ($F(2.75,\ 57.79) = 0.36$, $p = 0.768$, $\eta_p^2 = 0.017$, $95\%CI = [0.000, 0.194]$, ns), no interaction among the strategy, the experimental condition, and the actual percentage ($F(3.42,\ 35.88) = 0.58$, $p = 0.653$, $\eta_p^2 = 0.052$, $95\%CI = [0.000, 0.153]$, ns), no interaction among the strategy, the experimental condition, and adaptation time periods ($F(5.50,\ 57.79) = 1.18$, $p = 0.328$, $\eta_p^2 = 0.101$, $95\%CI = [0.000, 0.194]$, ns), no interaction among the strategy, the actual percentage, and adaptation time periods ($F(8.39,\ 88.07) = 1.01$, $p = 0.438$, $\eta_p^2 = 0.088$, $95\%CI = [0.000, 0.158]$, ns), no interaction among the experimental condition, the actual percentage, and adaptation time periods ($F(3.69,\ 77.59) = 0.74$, $p = 0.558$, $\eta_p^2 = 0.034$, $95\%CI = [0.000, 0.070]$, ns), or interaction among the strategy, the experimental condition, the actual percentage, and adaptation time periods ($F(7.39,\ 77.59) = 0.62$, $p = 0.750$, $\eta_p^2 = 0.055$, $95\%CI = [0.000, 0.054]$, ns).

A.13 Experiment 4: Methods

A.13.1 Participants, Stimuli, Task, Design, and Procedure

Similar to Experiment 2 and 3, we calculated a sample size of 24 for within-group comparison in Experiment 4 determined based on power analysis using G*Power software (http://www.gpower.hhu.de/)Erdfelder et al. (1996) based on the weakest effect size from Experiment 1. We recruited 37 participants for Experiment 3, which is more than adequate for the main objectives of this study. All participants were UCI students who participated in return for course credit or monetary incentive ($12/hour). Six participants were discarded for not completing both control and adaptation sessions ($n = 6$). The final pool consisted of 31 participants (15 males, 16 females). Ages of the remaining 31 participants ranged from 18 to 31 (mean 21.71). All participants signed an informed consent form in agreement with the UCI Institutional Review Board requirements in accordance with the Declaration of Helsinki.

The Stimuli, Task, Design, and Procedure are the same as Experiment 3. The only change was that in the adaptation session, a few (0 - 3) blocks were inadvertently randomly changed to adaptation to the moon direction. Regardless of whether the block was adapted to the sun or to the moon direction, within each block the initial trial and top-up trials all adapted to the same direction. Participants were not informed of this change in advance. Data from both directions were combined for analysis based on the adaptation direction.

A.13.2 Data Analysis

We first removed outlier trials that were 3 standard deviations above or below of the mean of each subject's reaction time. Approximately 1.88% of trials were removed: 1.70% trials were removed from the experimental session and 2.06% trials were removed from the control session. From the remaining trials for each participant, we calculated the reported percentage of movement toward the adaptation direction as well as mean reaction time for each

percentage level at each adaptation condition (the initial adaptation trial in each block were not included). We filtered 4 subjects' data based on the same criteria from Weibull model fit in Experiment 3. The rest of the data analyses were the same as Experiment.

Same as we have observed in Experiment 1, 2, and 3, people's report covered three main types of strategies in Experiment 4: counting strategies ($n = 18$), keeping focus on a certain part of the environment for distance estimation ($n = 4$), and a unique strategy ($n = 9$). For the filtered data, there were still subjects using counting ($n = 15$), focusing on a part of the environment ($n = 4$), and a unique strategy ($n = 8$). Again, we controlled for the influence of strategies by adding strategy as a factor in the above ANOVA analyses for Reported Rate and reaction time.

A.14 Experiment 4: Raw Data

A.14.1 Reported Rate by Adaptation Time Periods

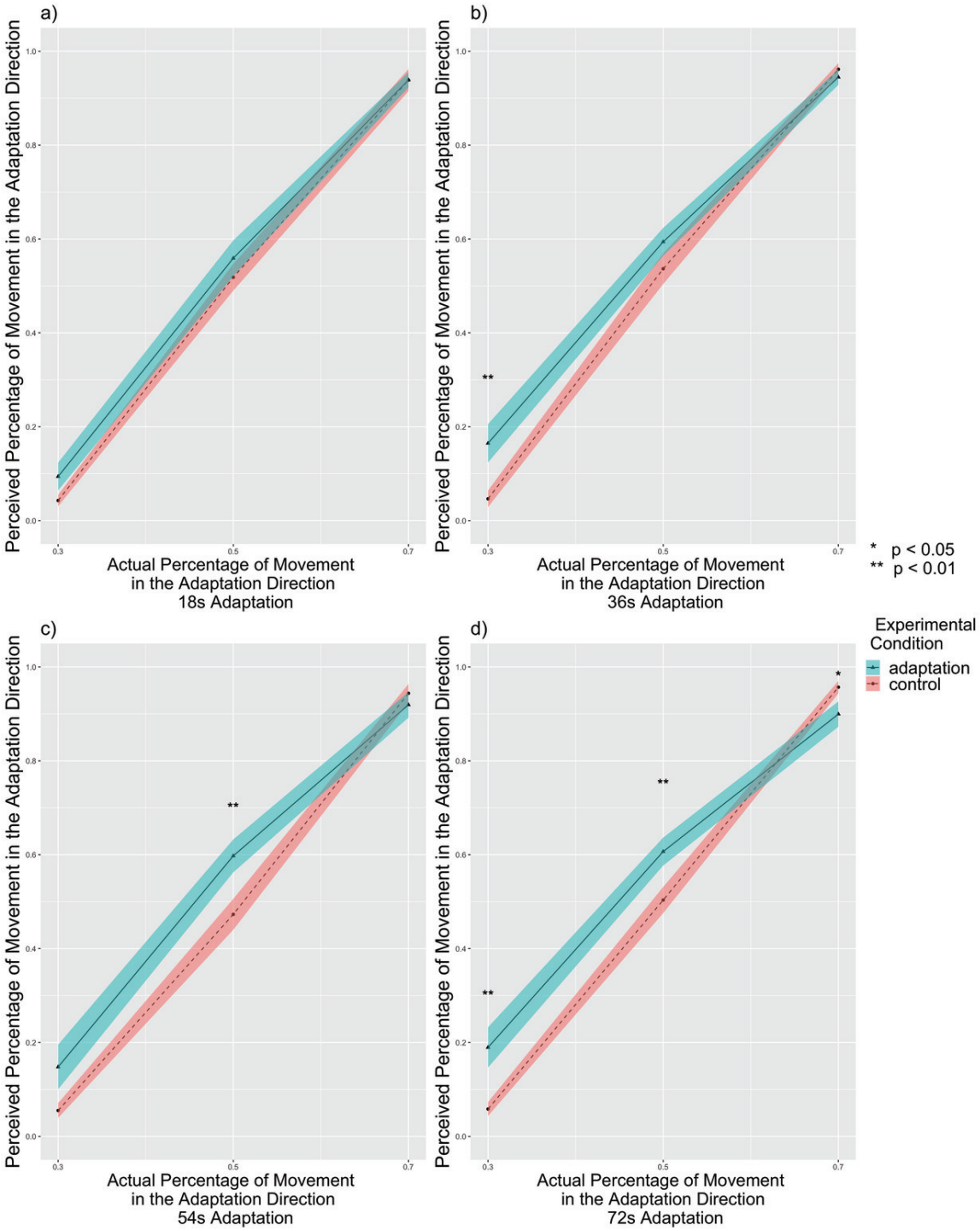

Figure A.27: Experiment 4: The perceived percentage of movement in the adaptation direction compared with the actual percentage for all subjects, separated by adaptation time periods (n = 31). a) The reported rate for 18s adaptation trials. The adaptation condition did not show different reported percentages from the control condition (p = 0.106). b) The reported rate for 36s adaptation trials. The adaptation condition showed higher reported percentages than control conditions (p = 0.015) particularly at 30% (p = 0.004), supporting the aftereffect in the same direction of travel. c) The reported rate for 54s adaptation trials. The adaptation condition showed higher reported percentages than control conditions (p = 0.021) particularly at 50% (p = 0.003), supporting the aftereffect. d) The reported rate for 72s adaptation trials. The adaptation condition showed higher reported percentages than control conditions (p = 0.019) particularly at 30% (p = 0.002) and 50% (p = 0.008), supporting the aftereffect in the same direction of travel. At 70%, the adaptation condition showed lower reported percentages than control conditions (p = 0.047). Solid lines indicate the grand average value, and the shaded area indicate 1 standard error of means. * p ¡ 0.05, ** p ¡ 0.01, Tukey correction.

A.14.2 Reported Rate by Experimental Conditions

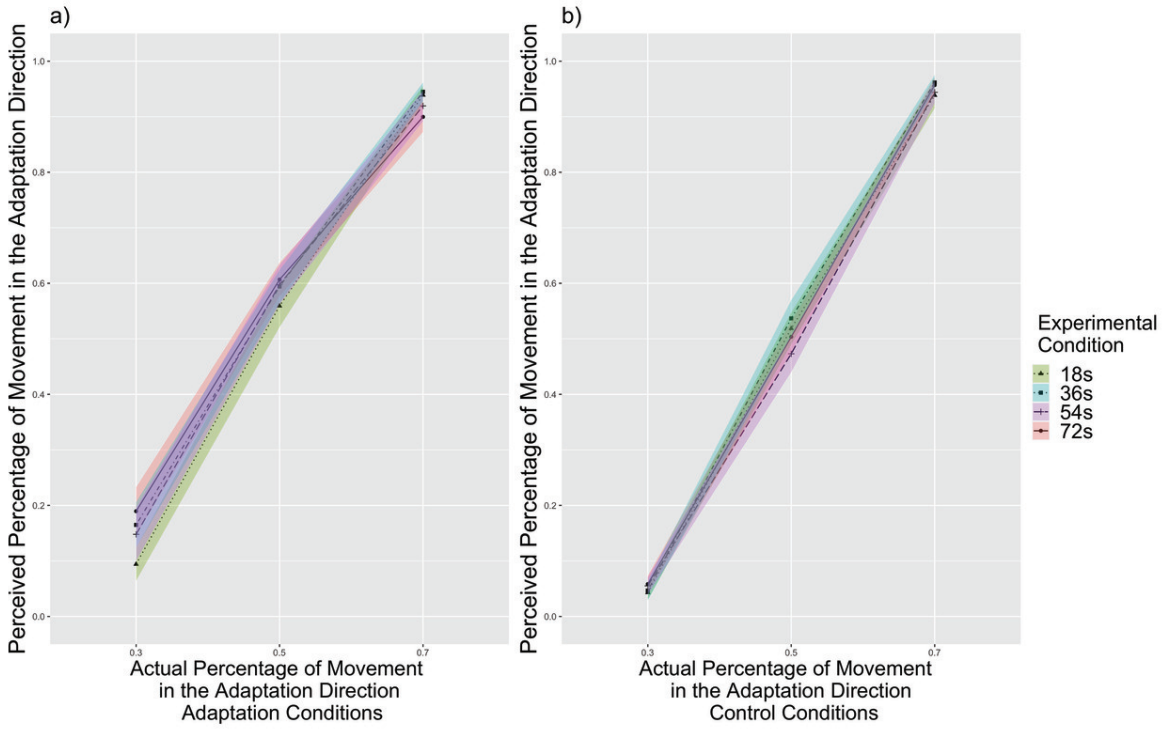

Figure A.28: Experiment 4: The perceived percentage of movement in the adaptation direction compared with the actual percentage for all subjects, separated by experimental conditions (n = 31). a) The reported rate for adaptation conditions. There were no differences between trials with different adaptation time periods within any actual percentage. b) The reported rate for control conditions. There were no differences between trials with different adaptation time periods within any actual percentage.

A.14.3 Reported Rate Table

Condition	18s			36s			54s			72s		
	30%	50%	70%	30%	50%	70%	30%	50%	70%	30%	50%	70%
%	*M(SE)*	*M(SE)*	*M(SE)*	*M(SE)*	*M(SE)*	*M(SE)*	*M(SE)*	*M(SE)*	*M(SE)*	*M(SE)*	*M(SE)*	*M(SE)*
Adapt	9(3)	56(4)	94(2)	16(4)	59(3)	94(2)	15(5)	60(4)	92(3)	19(4)	61(3)	90(3)
Control	4(1)	52(3)	94(2)	5(2)	54(3)	96(1)	6(2)	47(3)	94(2)	6(1)	50(3)	96(1)
Sig.	0.089	0.360	0.986	0.004**	0.250	0.331	0.085	0.003**	0.445	0.002**	0.008**	0.047*

*$p < .05.$, **$p < .01.$, Tukey correction.

Table A.9: Experiment 4: Average perceived percentage of movement in the adaptation direction and standard error of the adaptation and the control conditions for all subjects (n = 31), by adaptation time periods and level of actual percentage of movement in the adaptation direction.

A.14.4 Individual Psychometric Functions

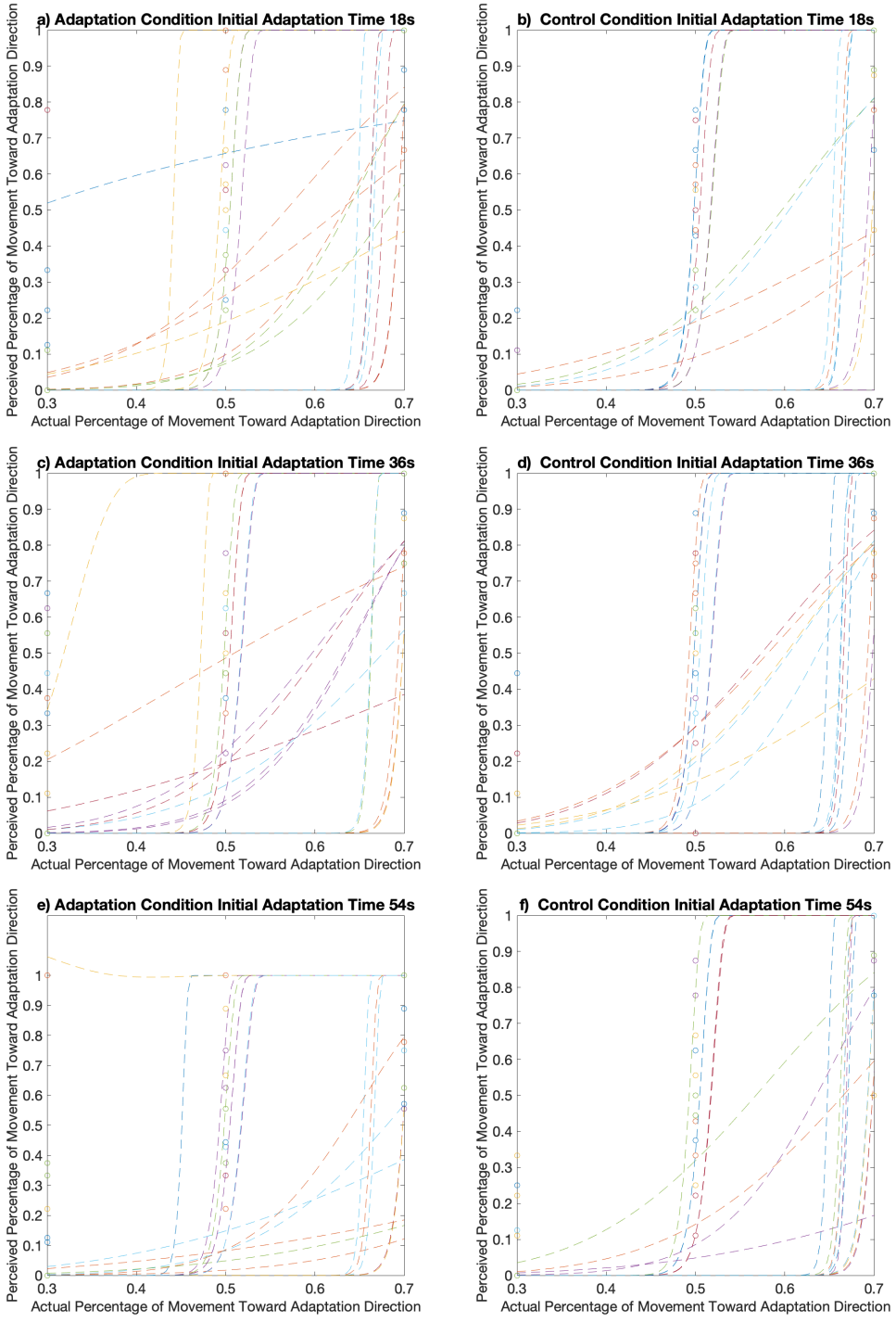

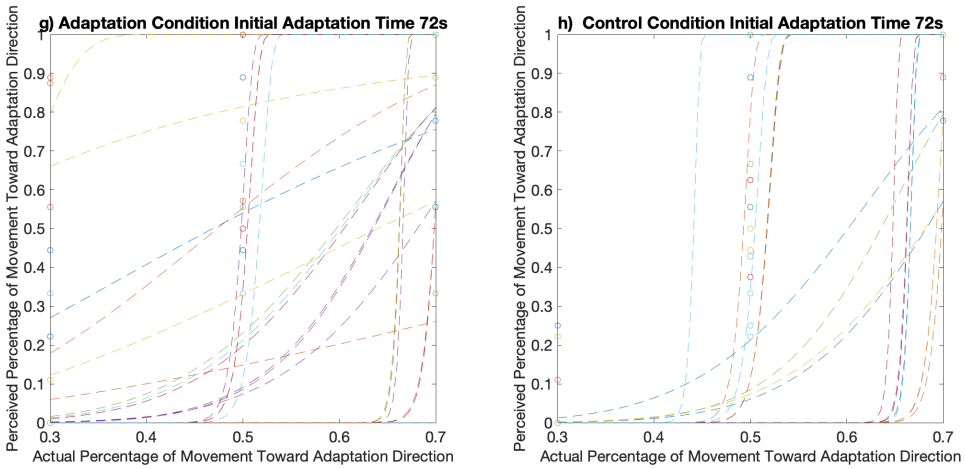

Figure A.29: Experiment 4: Psychometric functions of all observers' data (n = 31) a) Adaptation condition at 18s initial adaptation. b) Control condition at 18s initial adaptation. c) Adaptation condition at 36s initial adaptation. d) Control condition at 36s initial adaptation. e) Adaptation condition at 54s initial adaptation. f) Control condition at 54s initial adaptation. g) Adaptation condition at 72s initial adaptation. h) Control condition at 72s initial adaptation.

A.14.5 Group Psychometric Functions

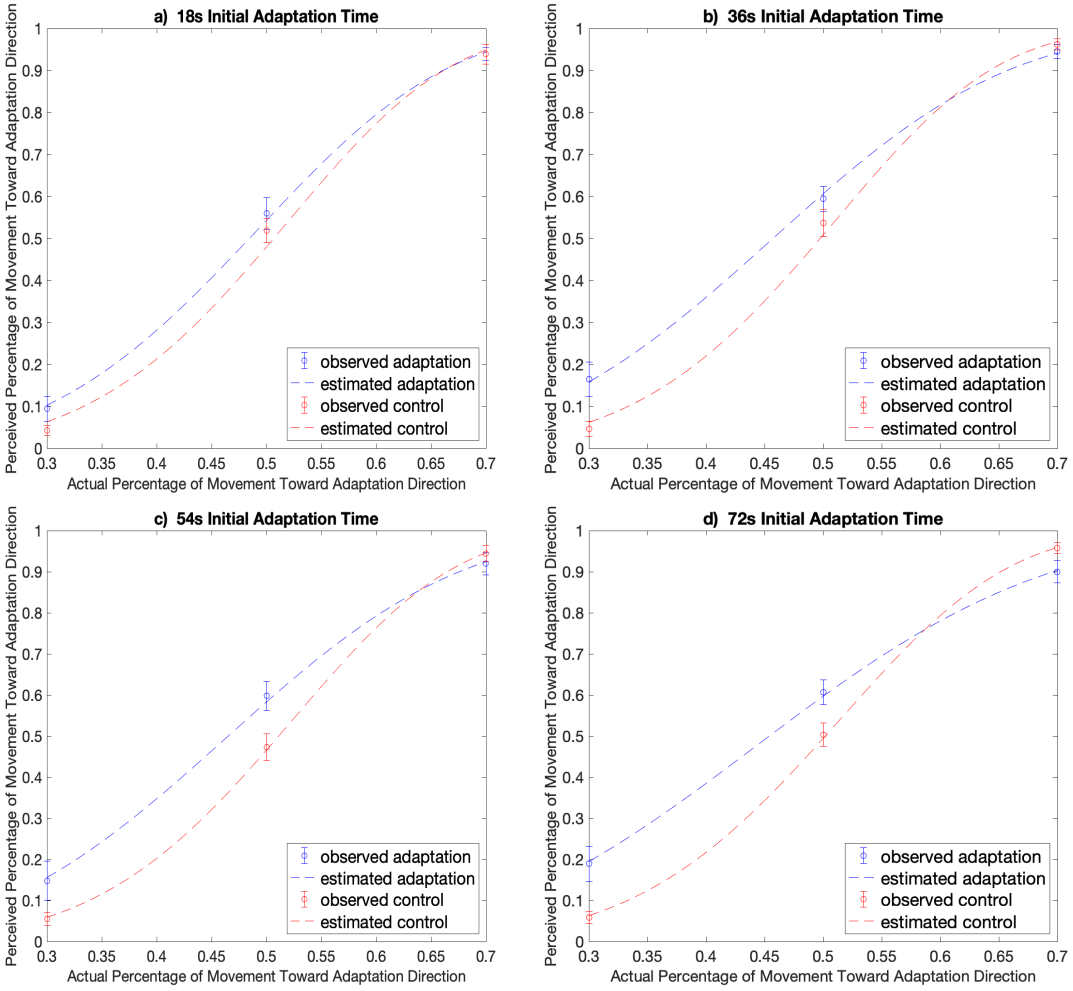

Figure A.30: Experiment 4: The average psychometric functions by adaptation time periods. Results were pooled across 31 observers. The psychometric function (i.e., α) shifts toward lower percentage of movement toward the adaptation direction when adapted at 72s adaptation time period ($p = 0.056$), but were not significant at 18s ($p = 0.315$), 36s ($p = 0.407$), or 54s ($p = 0.669$) adaptation time periods. The psychometric function (i.e., β) indicates that observers' detectability of the difference between the two directions was decreased by adaptation but were not significant at 18s ($p = 0.543$) or 36s ($p = 0.132$) adaptation time periods, and was significant at 54s ($p = 0.017$) adaptation time period and marginally significant at 72s ($p = 0.074$) adaptation time period. Error bars indicate standard errors.

A.14.6 Reaction Times by Adaptation Time Periods

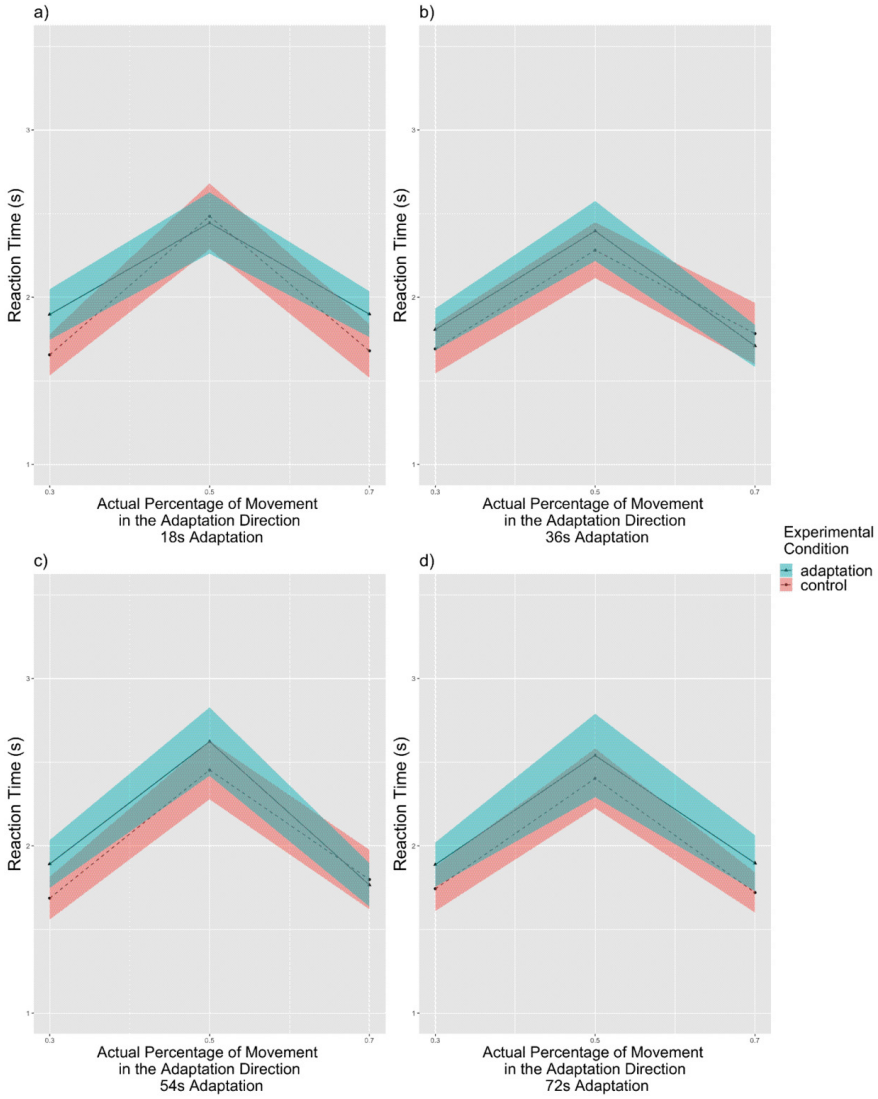

Figure A.31: Experiment 4: Reaction times compared with the actual percentage for all subjects, separated by adaptation time periods (n = 31). The reaction time increased as the actual percentage approached 50% in all adaptation time periods. a) Reaction times for 18s adaptation trials. b) Reaction times for 36s adaptation trials. c) Reaction times for 54s adaptation trials. d) Reaction times for 72s adaptation trials. Solid lines indicate the grand average value, and the shaded area indicate 1 standard error of means. Tukey correction.

A.14.7 Reaction Times by Experimental Conditions

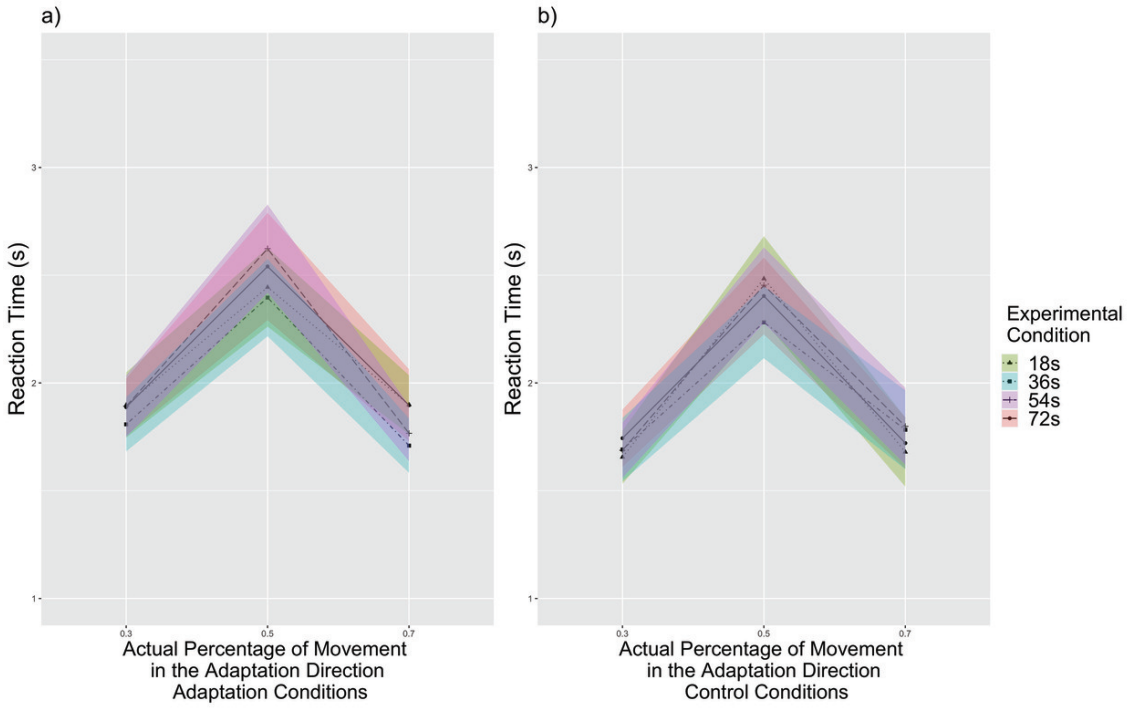

Figure A.32: Experiment 4: Reaction times compared with the actual percentage for all subjects, separated by experimental conditions (n = 31). The reaction time increased as the actual percentage approached 50% in both experimental conditions. a) Reaction times for adaptation conditions. b) Reaction times for control conditions. Solid lines indicate the grand average value, and the shaded area indicate 1 standard error of means.

A.15 Experiment 4: Filtered Data

A.15.1 Reported Rate by Adaptation Time Periods

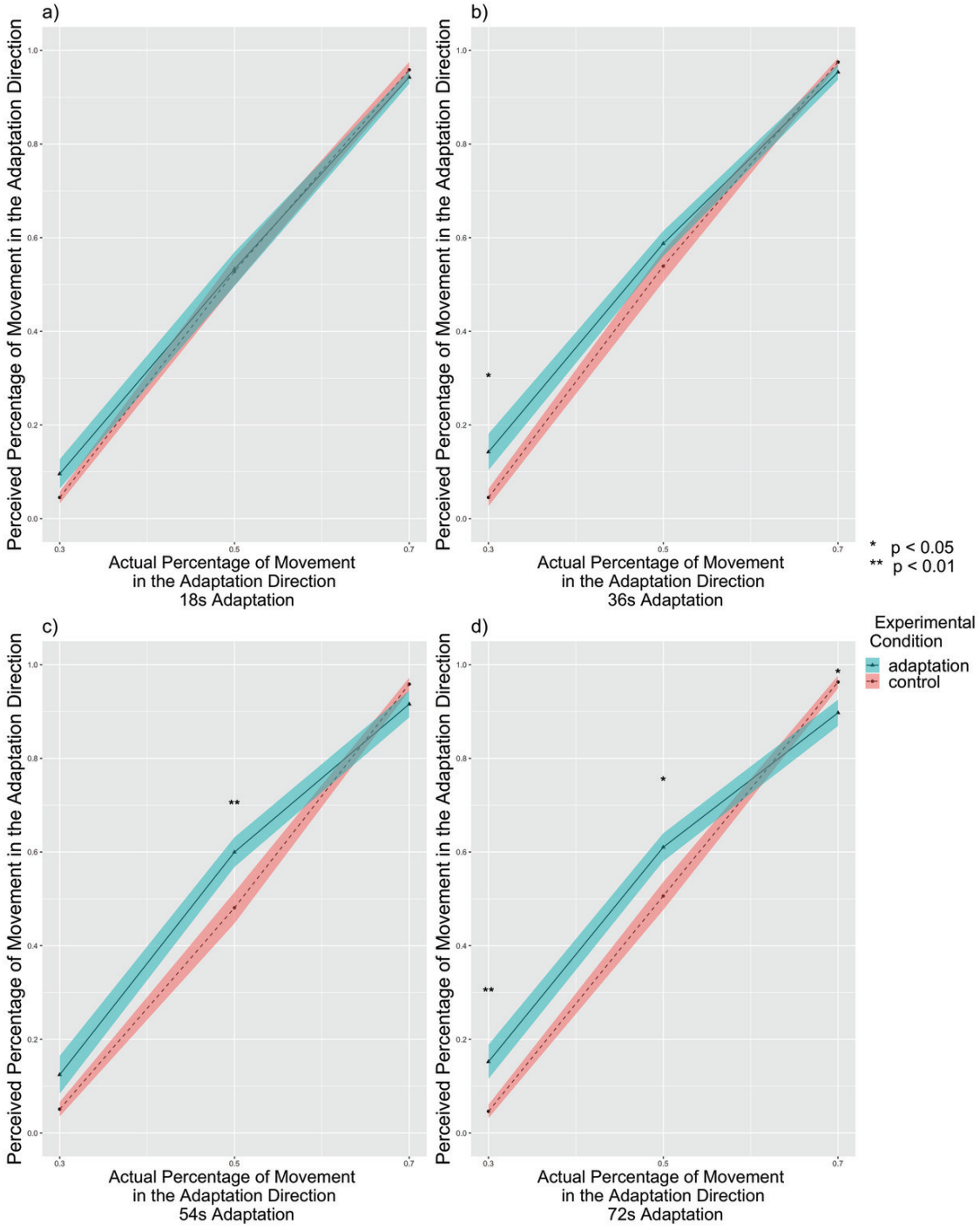

Figure A.33: Experiment 4: The perceived percentage of movement in the adaptation direction compared with the actual percentage for filtered subjects, separated by adaptation time periods (n = 27). a) The Reported Rate for 18s adaptation trials. The adaptation condition showed no difference from the control condition (p = 0.474). b) The Reported Rate for 36s adaptation trials. The adaptation condition showed higher reported percentages than control conditions (p = 0.029) particularly at 30% (p = 0.012), supporting the aftereffect in the same direction of travel. c) The Reported Rate for 54s adaptation trials. The adaptation condition showed higher reported percentages than control conditions (p = 0.043) particularly at 50% (p = 0.006), supporting the aftereffect. d) The Reported Rate for 72s adaptation trials. The adaptation condition showed slightly higher reported percentages than control conditions (p = 0.055) particularly at 30% (p = 0.004) and 50% (p = 0.015), supporting the aftereffect in the same direction of travel. Higher reported percentages was shown in the control condition than in the adaptation condition at 30% (p = 0.043) though. Solid lines indicate the grand average value, and the shaded area indicate 1 standard error of means. * $p < 0.05$, ** $p < 0.01$, Tukey correction.

A.15.2 Reported Rate by Experimental Conditions

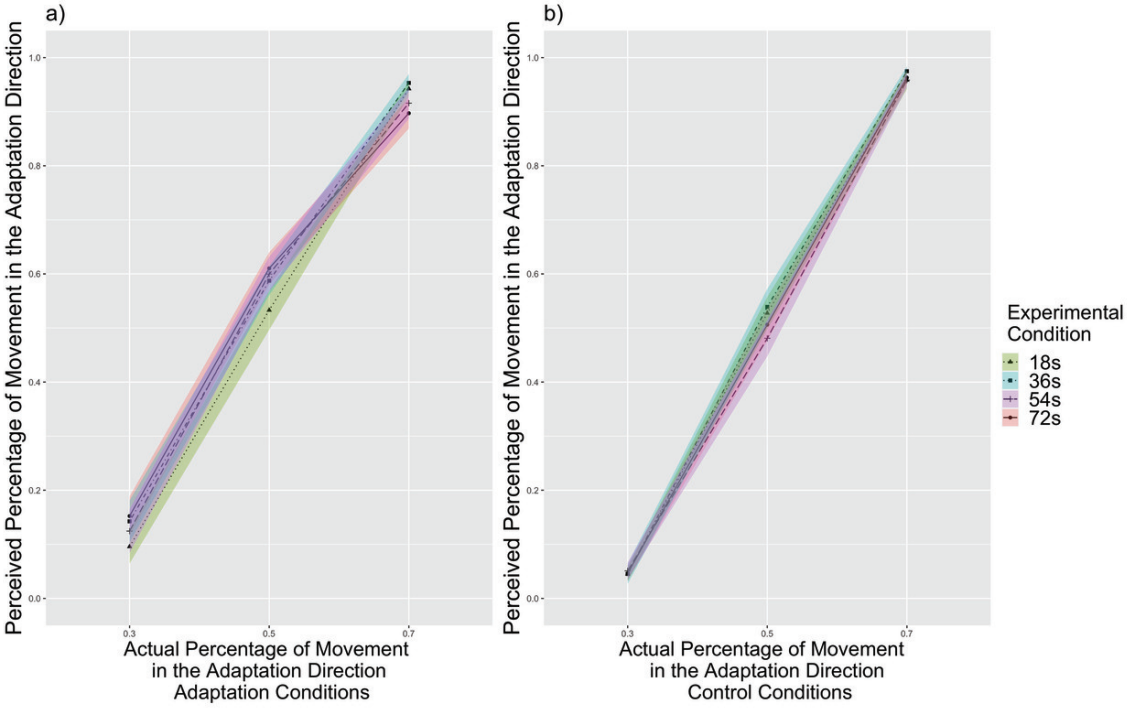

Figure A.34: Experiment 4: The perceived percentage of movement in the adaptation direction compared with the actual percentage for filtered subjects, separated by experimental conditions (n = 27). a) The Reported Rate for adaptation conditions. At 70%, 72s adaptation trials had slightly higher perceived percentage than 36s adaptation trials (p = 0.058), supporting that the aftereffect increased with adaptation time. The aftereffect is in the same direction of travel. b) The Reported Rate for control conditions. There were no differences between trials with different adaptation time periods within any actual percentage. Tukey correction.

A.15.3 Reported Rate Table

Condition	18s			36s			54s			72s		
	30%	50%	70%	30%	50%	70%	30%	50%	70%	30%	50%	70%
%	*M(SE)*	*M(SE)*	*M(SE)*	*M(SE)*	*M(SE)*	*M(SE)*	*M(SE)*	*M(SE)*	*M(SE)*	*M(SE)*	*M(SE)*	*M(SE)*
Adapt	10(3)	53(4)	94(1)	14(4)	59(3)	95(2)	12(4)	60(3)	92(3)	15(4)	61(3)	90(3)
Control	5(1)	53(3)	96(2)	5(2)	54(4)	97(1)	5(2)	48(4)	96(1)	5(2)	51(3)	96(1)
Sig.	0.135	0.906	0.397	0.012*	0.331	0.249	0.133	0.006**	0.171	0.004**	0.015*	0.043

*$p < .05.$, **$p < .01.$, Tukey correction.

Table A.10: Experiment 4: Average perceived percentage of movement in the adaptation direction and standard error of the adaptation and the control conditions for filtered subjects (n = 27), by adaptation time periods and level of actual percentage of movement in the adaptation direction.

A.15.4 Individual Psychometric Functions

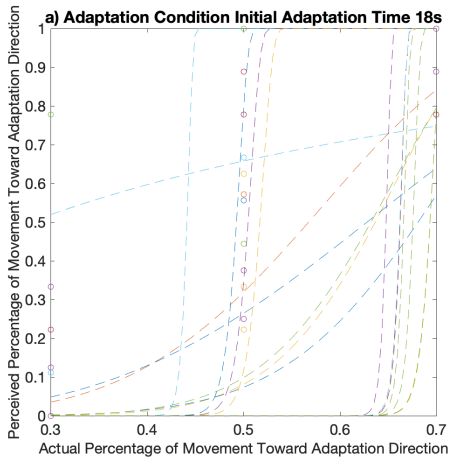

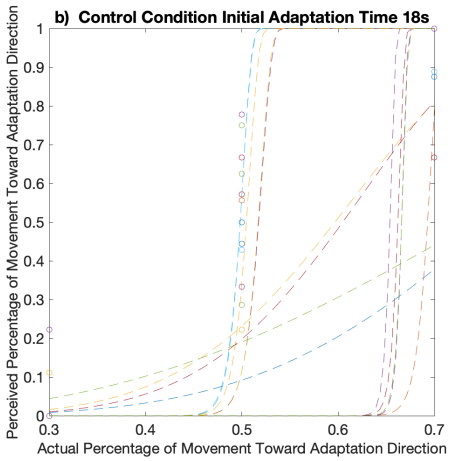

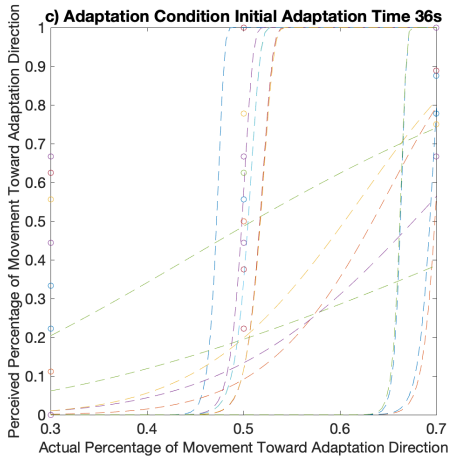

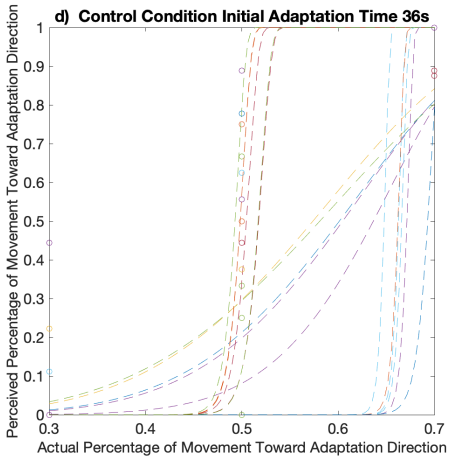

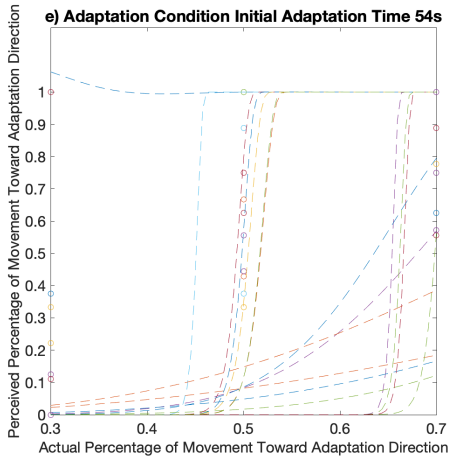

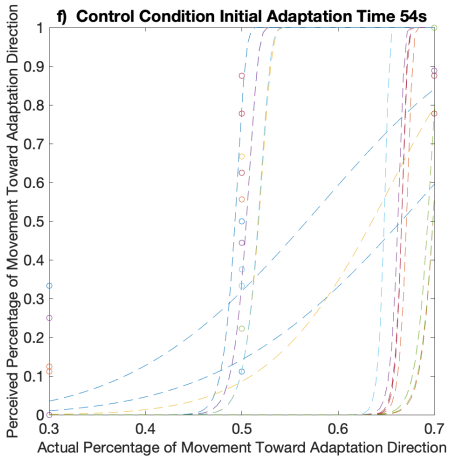

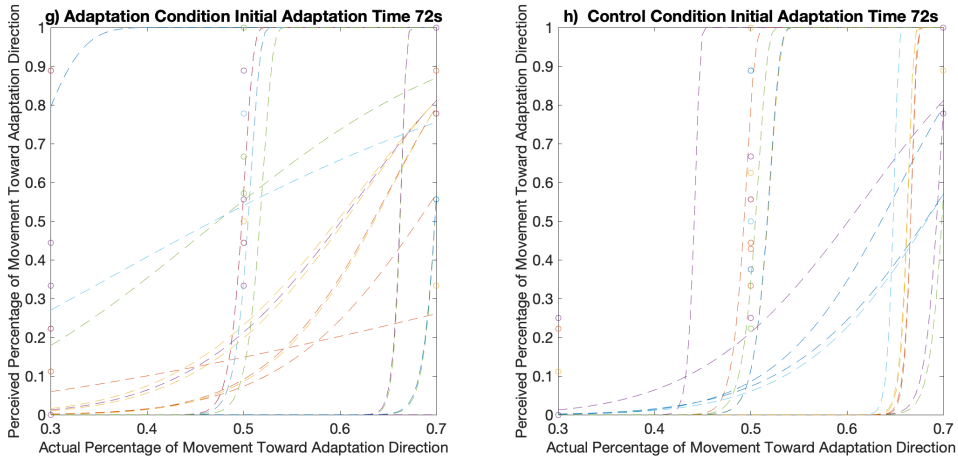

Figure A.35: Experiment 4: Psychometric functions of filtered data (n = 27) a) Adaptation condition at 18s adaptation. b) Control condition at 18s adaptation. c) Adaptation condition at 36s adaptation. d) Control condition at 36s adaptation. e) Adaptation condition at 54s adaptation. f) Control condition at 54s adaptation. g) Adaptation condition at 72s adaptation. h) Control condition at 72s adaptation.

A.15.5 Group Psychometric Functions

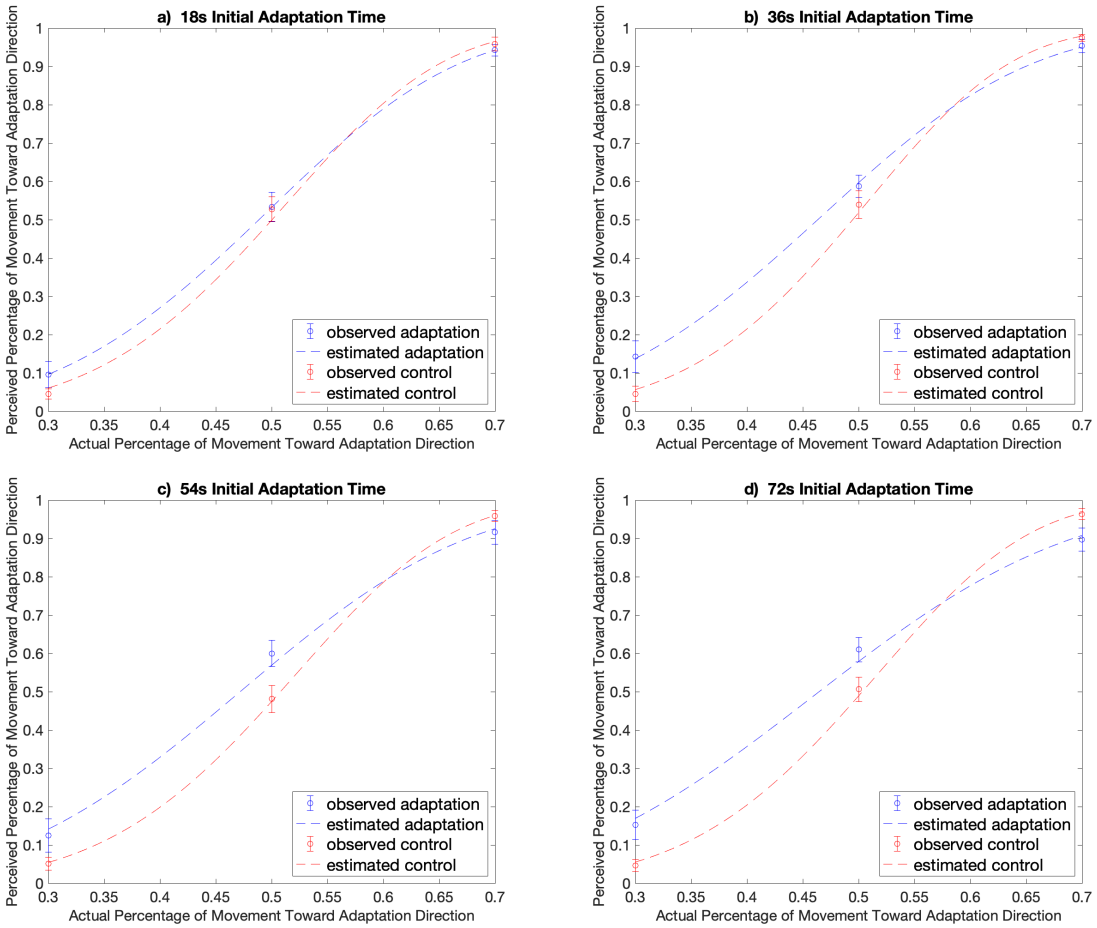

Figure A.36: Experiment 4: The average psychometric functions by adaptation time periods. Results were pooled across 27 observers. The psychometric function (i.e., α) shifts toward lower percentage of movement toward the adaptation direction when adapted but were not significant at 18s ($p = 0.676$), 36s ($p = 0.768$), 54s ($p = 0.880$), or 72s adaptation ($p = 0.314$) time periods. The psychometric function (i.e., β) indicates that observers' detectability of the difference between the two directions was decreased by adaptation but were not significant at 18s ($p = 0.822$) or 36s ($p = 0.211$) adaptation time periods, and were significant at 9s ($p = 0.046$) and 12s ($p = 0.004$) adaptation time periods. Error bars indicate standard errors.

A.15.6 Reaction Times by Adaptation Time Periods

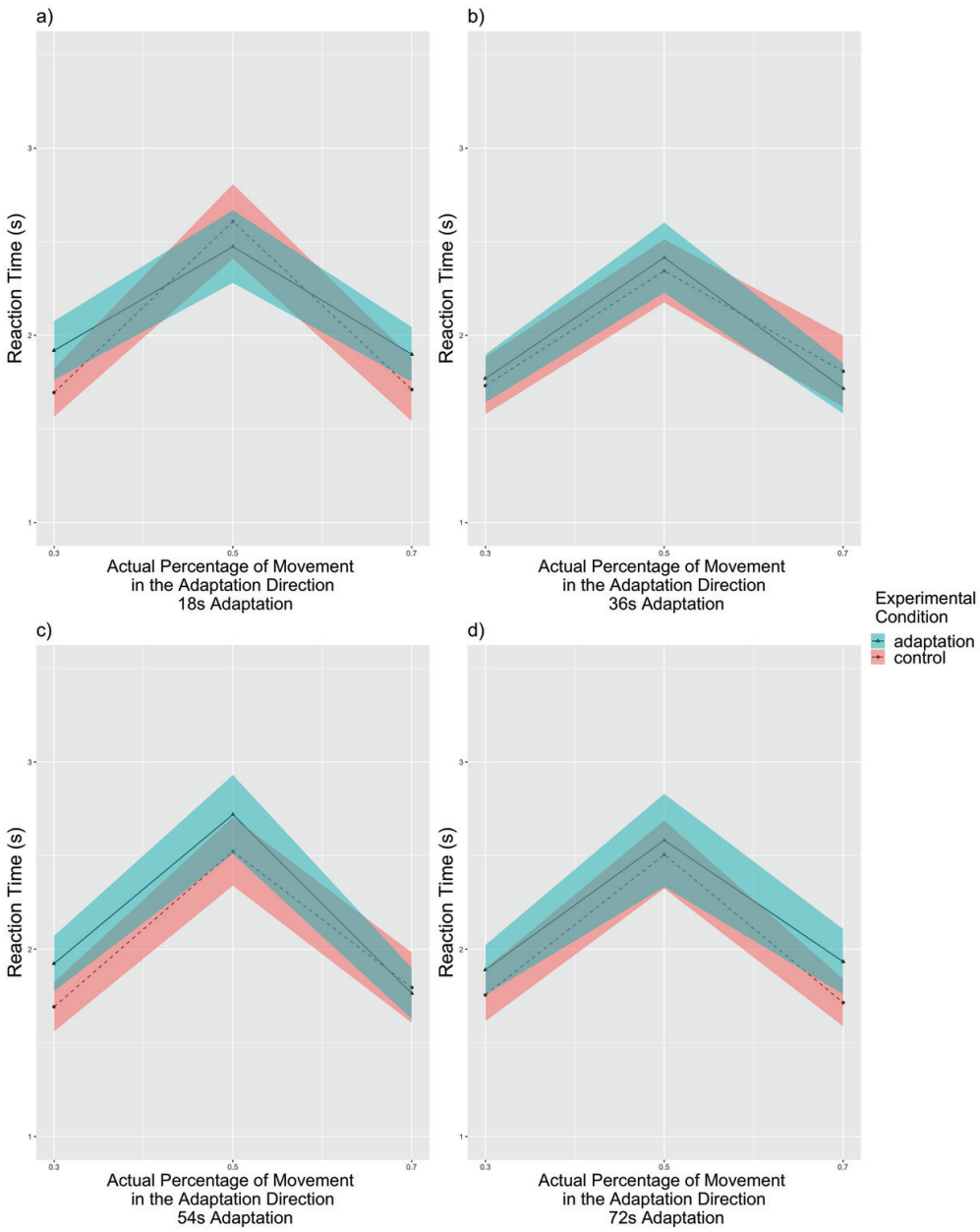

Figure A.37: Experiment 4: Reaction times compared with the actual percentage for filtered subjects, separated by adaptation time periods (n = 27). The reaction time increased as the actual percentage approached 50% in all adaptation time periods. a) Reaction times for 18s adaptation trials. b) Reaction times for 36s adaptation trials. c) Reaction times for 54s adaptation trials. d) Reaction times for 72s adaptation trials. Solid lines indicate the grand average value, and the shaded area indicate 1 standard error of means. Tukey correction.

A.15.7 Reaction Times by Experimental Conditions

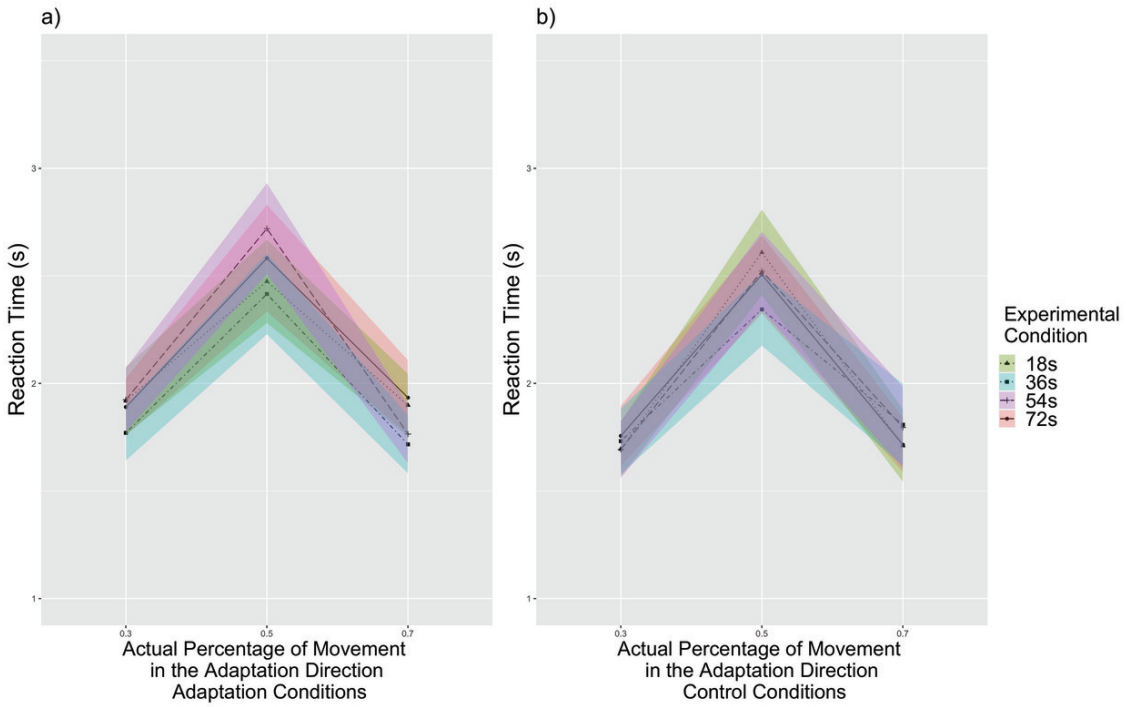

Figure A.38: Experiment 4: Reaction times compared with the actual percentage for filtered subjects, separated by experimental conditions (n = 27). The reaction time increased as the actual percentage approached 50% in both experimental conditions. a) Reaction times for adaptation conditions. b) Reaction times for control conditions. Solid lines indicate the grand average value, and the shaded area indicate 1 standard error of means. Tukey correction.

A.16 Experiment 4: Strategies

A.16.1 Task Difficulty

Raw Data

As for the rated difficulty of each condition, participants rated the adaptation session ($M = 3.90 \pm 0.26$) to be more difficult than the control session ($M = 3.42 \pm 0.23$)($t(30)$ = -2.18, p = 0.037, $Cohen's\, d$ = -0.358, 95%CI = [-0.697, -0.019]).

Filtered Data

As for the rated difficulty of each condition, participants rated the adaptation session ($M = 3.93 \pm 0.29$) to be more difficult than the control session ($M = 3.37 \pm 0.25$)($t(26)$ = -2.20, p = 0.037, $Cohen's\, d$ = -0.394, 95%CI = [-0.767, -0.021]).

A.16.2 Task Difficulty in Different Strategies.

Raw Data

For the task difficulty, we conducted an *experimental condition*(adaptation, control) × *strategy*(counting strategies, focusing on part of the environment, unique strategies) mixed-subjects repeated measures ANOVA. There was no main effect of strategy ($F(2,\ 28) = 1.49$, $p = 0.242$, $\eta_p^2 = 0.096$, 95%$CI = [0.000, 0.307]$, ns) or interaction between strategy and condition ($F(2,\ 28) = 0.37$, $p = 0.692$, $\eta_p^2 = 0.026$, 95%$CI = [0.000, 0.178]$, ns). There was a marginally significant main effect of experimental condition ($F(1,\ 28) = 3.91$, $p = 0.058$, $\eta_p^2 = 0.123$, 95%$CI = [0.000, 0.362]$).

Filtered Data

Then we conducted the same ANOVA analyses on filtered data. There was no main effect of strategy ($F(2,\ 24) = 1.26$, $p = 0.302$, $\eta_p^2 = 0.095$, 95%$CI = [0.000, 0.321]$, ns)

or interaction between strategy and condition ($F(2,\ 24) = 0.33,\ p = 0.723,\ \eta_p^2 = 0.027,\ 95\%CI = [0.000, 0.192],\ ns$). We found a marginally significant main effect of the experimental condition ($F(1,\ 24) = 3.94,\ p = 0.059,\ \eta_p^2 = 0.141,\ 95\%CI = [0.000, 0.400]$) that people reported the adaptation session ($M = 3.75 \pm 0.33$) to be more difficult than the control session ($M = 3.16 \pm 0.29$).

A.16.3 Reported Rate in Different Strategies.

Raw Data

For the perceived percentage, we conducted an *experimental condition*(adaptation, control) $\times$ *actual percentage*(30%, 50%, 70%) *adaptation time periods* (18s, 36s, 54s, 72s) *strategy*(counting strategies, focusing on part of the environment, unique strategies) mixed-subjects repeated measures ANOVA. There was a main effect of condition ($F(1,\ 28) = 5.23,\ p = 0.030,\ \eta_p^2 = 0.135,\ 95\%CI = [0.000, 0.376]$) where people reported more toward the adaptation direction in the adaptation session ($M = 0.555 \pm 0.019$) than in the control session ($M = 0.503 \pm 0.020$). As expected, there was also a main effect of the actual percentage ($F(1.46,\ 40.91) = 570.20,\ p < 0.001,\ \eta_p^2 = 0.972,\ 95\%CI = [0.948, 0.982]$) that showed the perceived percentage increased with the actual percentage. There was a significant interaction between the experimental condition and the actual percentage ($F(1.57,\ 43.96) = 3.87,\ p = 0.038,\ \eta_p^2 = 0.121,\ 95\%CI = [0.000, 0.279]$). Post-hoc Tukey analyses revealed that adaptation increased perceived percentage at 30% ($p = 0.038$) and 50% ($p = 0.016$). All other main effects and interactions were not significant (all $p > 0.08$).

Filtered Data

For the perceived percentage, we conducted an *experimental condition*(adaptation, control) $\times$ *actual percentage*(30%, 50%, 70%) *adaptation time periods* (18s, 36s, 54s, 72s) *strategy*(counting strategies, focusing on part of the environment, unique strategies) mixed-subjects repeated measures ANOVA. There was a main effect of condition ($F(1,\ 24) = 4.93,$

$p = 0.036$, $\eta_p^2 = 0.123$, $95\%CI = [0.000, 0.381]$) where people reported more toward the adaptation direction in the adaptation session ($M = 0.542 \pm 0.018$) than in the control session ($M = 0.503 \pm 0.006$). As expected, there was also a main effect of the actual percentage ($F(1.49, 35.67) = 579.28$, $p < 0.001$, $\eta_p^2 = 0.980$, $95\%CI = [0.962, 0.988]$) that showed the perceived percentage increased with the actual percentage. There was a significant interaction between the experimental condition and the actual percentage ($F(1.67, 40.17) = 4.89$, $p = 0.017$, $\eta_p^2 = 0.169$, $95\%CI = [0.010, 0.346]$). Tukey HSD post-hoc analyses revealed that people had increased Reported Rate in the adaptation condition than the control condition at 50% ($p = 0.032$) and 50% ($p = 0.019$). All other main effects and interactions were not significant (all $p > 0.08$).

A.16.4 Reaction Time in Different Strategies.

Raw Data

For the reaction time, we conducted an *experimental condition*(adaptation, control) × *actual percentage*(30%, 50%, 70%) *adaptation time periods* (18s, 36s, 54s, 72s) *strategy*(counting strategies, focusing on part of the environment, unique strategies) mixed-subjects repeated measures ANOVA. We observed a main effect of the actual percentage ($F(1.14, 31.92) = 34.57$, $p < 0.001$, $\eta_p^2 = 0.185$, $95\%CI = [0.000, 0.411]$) such that the reaction time increased with actual percentage, peaking at 50%. There was a significant interaction between the strategy and the experimental condition ($F(2, 28) = 3.79$, $p = 0.035$, $\eta_p^2 = 0.065$, $95\%CI = [0.000, 0.260]$). Post-hoc Tukey paired t-tests did not found difference between any pairs of strategies and conditions. There was also a marginally significant interaction among the experimental condition, the actual percentage, and adaptation time periods ($F(4.57, 128.02) = 2.11$, $p = 0.074$, $\eta_p^2 = 0.070$, $95\%CI = [0.000, 0.128]$). Because this interaction was only marginally significant, we did not conduct further posthoc analyses. All other main effects and interactions were not significant (all $p > 0.08$).

Filtered Data

Then we conducted the same ANOVA analyses on filtered data. Again, we observed a main effect of the actual percentage ($F(1.13,\ 27.04) = 33.88$, $p < 0.001$, $\eta_p^2 = 0.204$, $95\%CI = [0.000, 0.446]$) such that the reaction time increased with actual percentage, peaking at 50%. There was a significant interaction between the strategy and the experimental condition ($F(2,\ 24) = 3.95$, $p = 0.033$, $\eta_p^2 = 0.078$, $95\%CI = [0.000, 0.296]$). Post-hoc Tukey paired t-tests found that people with the strategy of focusing on part of the environment responded slower in the adaptation condition than the control condition ($p = 0.024$). There was also a marginally significant interaction among the experimental condition, the actual percentage, and adaptation time periods ($F(4.59,\ 110.13) = 2.26$, $p = 0.059$, $\eta_p^2 = 0.086$, $95\%CI = [0.000, 0.153]$). Because this interaction was only marginally significant, we did not conduct further posthoc analyses. All other main effects and interactions were not significant (all $p > 0.08$).

A.17 Comparison Across Experiments

When comparing difficulty ratings across experiments, there was a main effect of experimental condition that people overall rated adaptation condition to be more difficult than control condition ($F(1,\ 145) = 4.57$, $p = 0.034$, $\eta_p^2 = 0.031$, $95\%C.I. = [0.000,\ 0.104]$), and Experiment 3 was rated more difficult than Experiment 1 ($p = 0.003$) (Appendix Section A.17.1 Figure A.39, Appendix Section A.17.1 Figure A.40). However, the effect of experimental condition disappeared after controlling for other factors such as age, gender, and session sequence (Appendix Section A.19.3). There was also no influence of age, gender, session sequence, or strategy on people's evaluations of task difficulty (all $p > 0.08$)(Appendix Section A.19.3). Filtered data showed the same result patterns except that people with unique strategy rated the task being easier than people with counting strategy ($p = 0.018$)(Appendix Section A.19.3).

A.17.1 Experiment 1-4: Difficulty

Raw Data

For the task difficulty, we conducted an *experimental condition* (adaptation, control) × *Experiments* (Experiment 1, Experiment 2, Experiment 3, Experiment 4) mixed-subjects repeated measures ANOVA. We found a main effect of the experimental condition ($F(1, 145) = 4.57$, $p = 0.034$, $\eta_p^2 = 0.031$, $95\%C.I. = [0.000, 0.104]$) such that subjects found the adaptation condition ($M = 3.93\% \pm 0.12\%$) to be more difficult than the control condition ($M = 3.68\% \pm 0.12\%$). There was also a main effect of the experiments ($F(3, 145) = 4.16$, $p = 0.007$, $\eta_p^2 = 0.079$, $95\%CI = [0.007, 0.162]$). Pairwise t-tests showed people rated Experiment 3 to be more difficult than Experiment 1 ($p = 0.003$) and Experiment 3 to be slightly more difficult than Experiment 4 ($p = 0.079$). There was no interaction between the experimental condition and experiments ($F(3, 145) = 1.82$, $p = 0.146$, $\eta_p^2 = 0.036$, $95\%CI = [0.000, 0.099]$, ns). See Figure A.39.

Sidak post-hoc analyses revealed that people rated the adaptation session in Experiment 3 to be more difficult than the adaptation session in Experiment 1 ($p = 0.018$). People rated the control session in Experiment 3 to be marginally more difficult than the control session in Experiment 1 ($p = 0.051$). No difference in difficulty ratings were found between adaptation and control conditions within each experiment (all $p > 0.08$).

Filtered Data

Then we conducted same analyses for task difficulty on filtered data. We found a main effect of the experimental condition ($F(1, 122) = 4.99$, $p = 0.027$, $\eta_p^2 = 0.039$, $95\%C.I. = [0.000, 0.127]$) such that subjects found the adaptation condition ($M = 3.95\% \pm 0.14\%$) to be more difficult than the control condition ($M = 3.67\% \pm 0.13\%$). There was also a main effect of the experiments ($F(3, 122) = 3.31$, $p = 0.023$, $\eta_p^2 = 0.075$, $95\%CI = [0.001, 0.164]$). Pairwise t-tests showed people rated Experiment 3 to be more difficult than Experiment 1

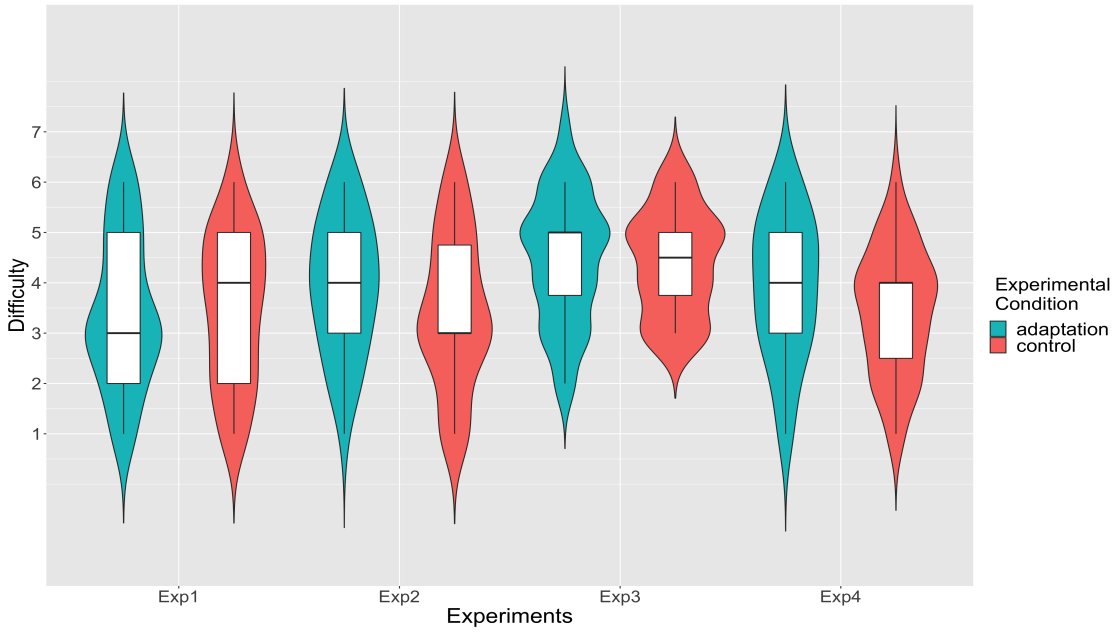

Figure A.39: Task difficulty, separated by experiments and adaptation conditions. People reported the adaptation condition to be around the same as the control condition in Experiment 1 ($p = 0.992$), Experiment 2 ($p = 0.164$), Experiment 3 ($p = 0.998$), and Experiment 4 ($p = 0.176$). Note: Experiment 1 (n = 60), Experiment 2 (n = 30), Experiment 3 (n = 28), Experiment 4 (n = 31)

($p = 0.014$). There was a interaction between the experimental condition and experiments ($F(3, 122) = 2.91$, $p = 0.037$, $\eta_p^2 = 0.067$, $95\%CI = [0.000, 0.152]$). See Figure A.40.

Sidak post-hoc analyses revealed that people rated the adaptation session in Experiment 3 to be more difficult than the adaptation session in Experiment 1 ($p = 0.041$). In Experiment 2, people rated the adaptation session to be only marginally more difficult than the control session ($p = 0.067$).

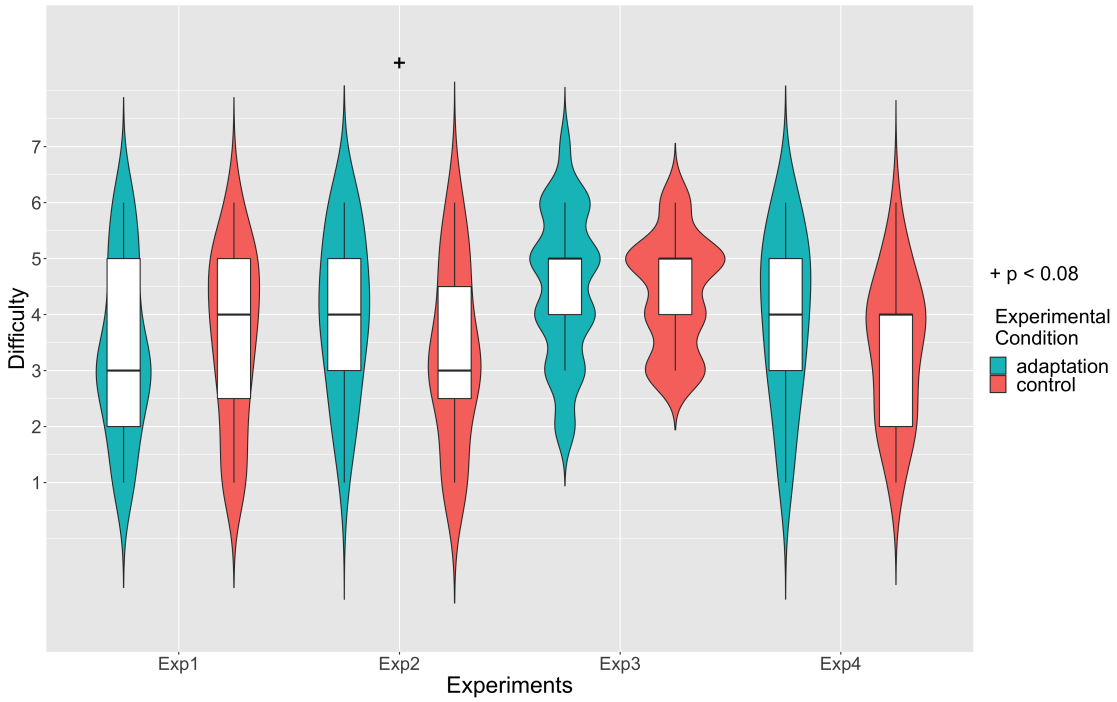

Figure A.40: Task difficulty, separated by experiments and adaptation conditions. People reported the adaptation condition to be marginally more difficult than the control condition in Experiment 2 ($p = 0.067$), but not in Experiment 1 ($p = 0.836$), Experiment 3 ($p = 0.997$), or Experiment 4 ($p = 0.146$) (Sidek corrected). Note: Experiment 1 (n = 51), Experiment 2 (n = 23), Experiment 3 (n = 24), Experiment 4 (n = 27)

A.17.2 Experiment 1-4: Reported Rate

Raw Data

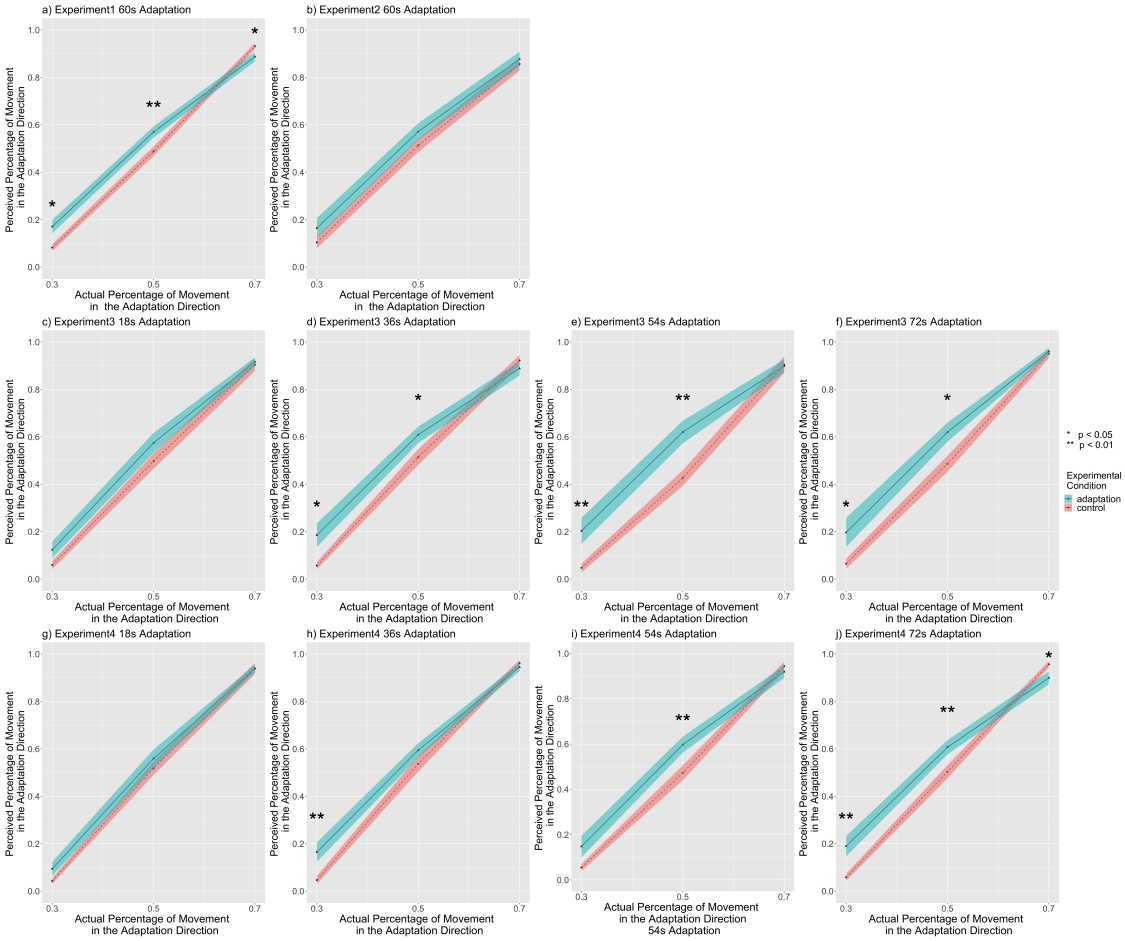

Figure A.41: The perceived percentage of movement in the adaptation direction compared with the actual percentage for all subjects, separated by experiments and adaptation time periods. a) The Reported Rate for 60s adaptation trials in Experiment 1 (n = 60). b) The Reported Rate for 60s adaptation trials in Experiment 2 (n = 30). c) The Reported Rate for 18s adaptation trials in Experiment 3 (n = 28). d) The Reported Rate for 36s adaptation trials in Experiment 3 (n = 28). e) The Reported Rate for 54s adaptation trials in Experiment 3 (n = 28). f) The Reported Rate for 72s adaptation trials in Experiment 3 (n = 28). g) The Reported Rate for 18s adaptation trials in Experiment 4 (n = 31). h) The Reported Rate for 36s adaptation trials in Experiment 4 (n = 31). i) The Reported Rate for 54s adaptation trials in Experiment 4 (n = 31). j) The Reported Rate for 72s adaptation trials in Experiment 4 (n = 31). Solid lines indicate the grand average value, and the shaded area indicate 1 standard error of means. * $p < 0.05$, ** $p < 0.01$, Tukey correction.

Filtered Data

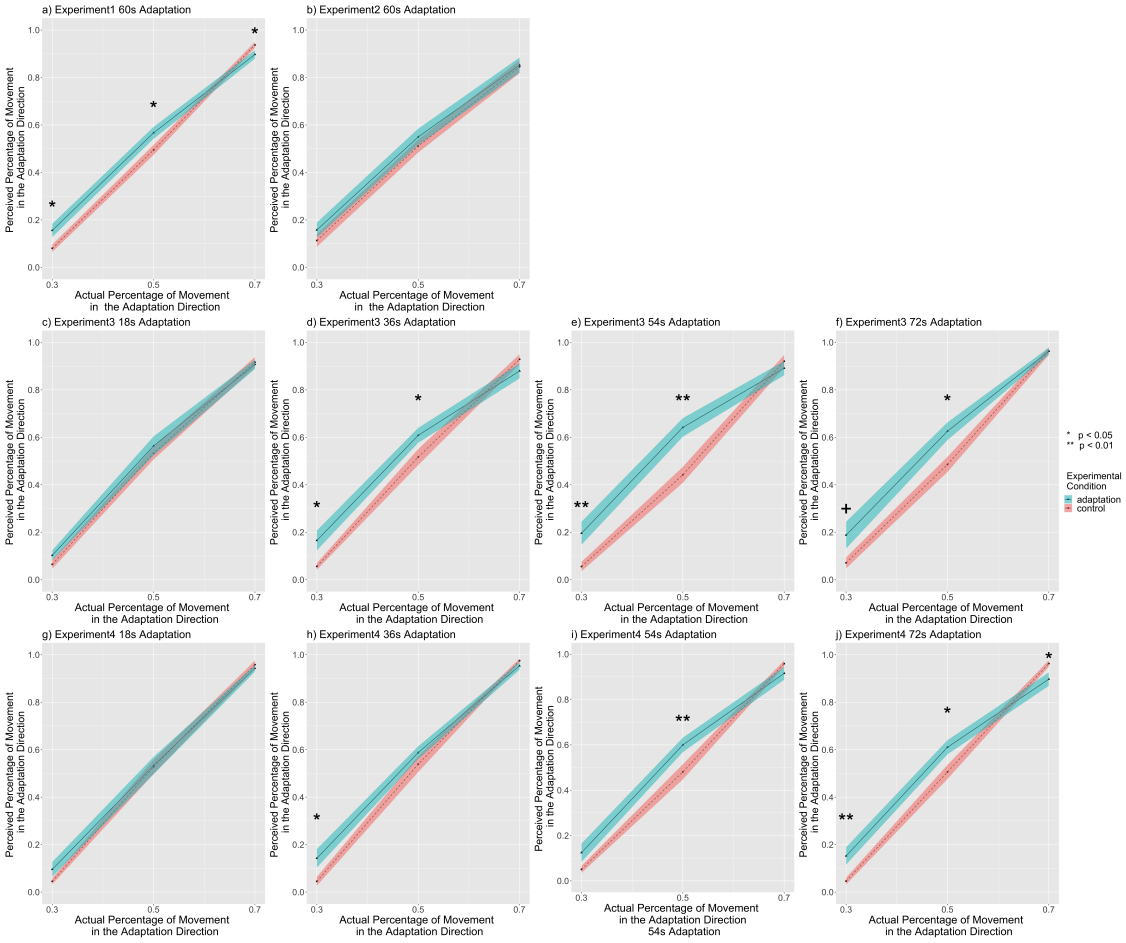

Figure A.42: The perceived percentage of movement in the adaptation direction compared with the actual percentage for all subjects, separated by experiments and adaptation time periods. a) The Reported Rate for 60s adaptation trials in Experiment 1 (n = 51). b) The Reported Rate for 60s adaptation trials in Experiment 2 (n = 23). c) The Reported Rate for 18s adaptation trials in Experiment 3 (n = 24). d) The Reported Rate for 36s adaptation trials in Experiment 3 (n = 24). e) The Reported Rate for 54s adaptation trials in Experiment 3 (n = 24). f) The Reported Rate for 72s adaptation trials in Experiment 3 (n = 24). g) The Reported Rate for 18s adaptation trials in Experiment 4 (n = 27). h) The Reported Rate for 36s adaptation trials in Experiment 4 (n = 27). i) The Reported Rate for 54s adaptation trials in Experiment 4 (n = 27). j) The Reported Rate for 72s adaptation trials in Experiment 4 (n = 27). Solid lines indicate the grand average value, and the shaded area indicate 1 standard error of means. + $p < 0.08$, * $p < 0.05$, ** $p < 0.01$, Tukey correction.

A.17.3 Experiments 1-4: Reaction Times

Raw Data

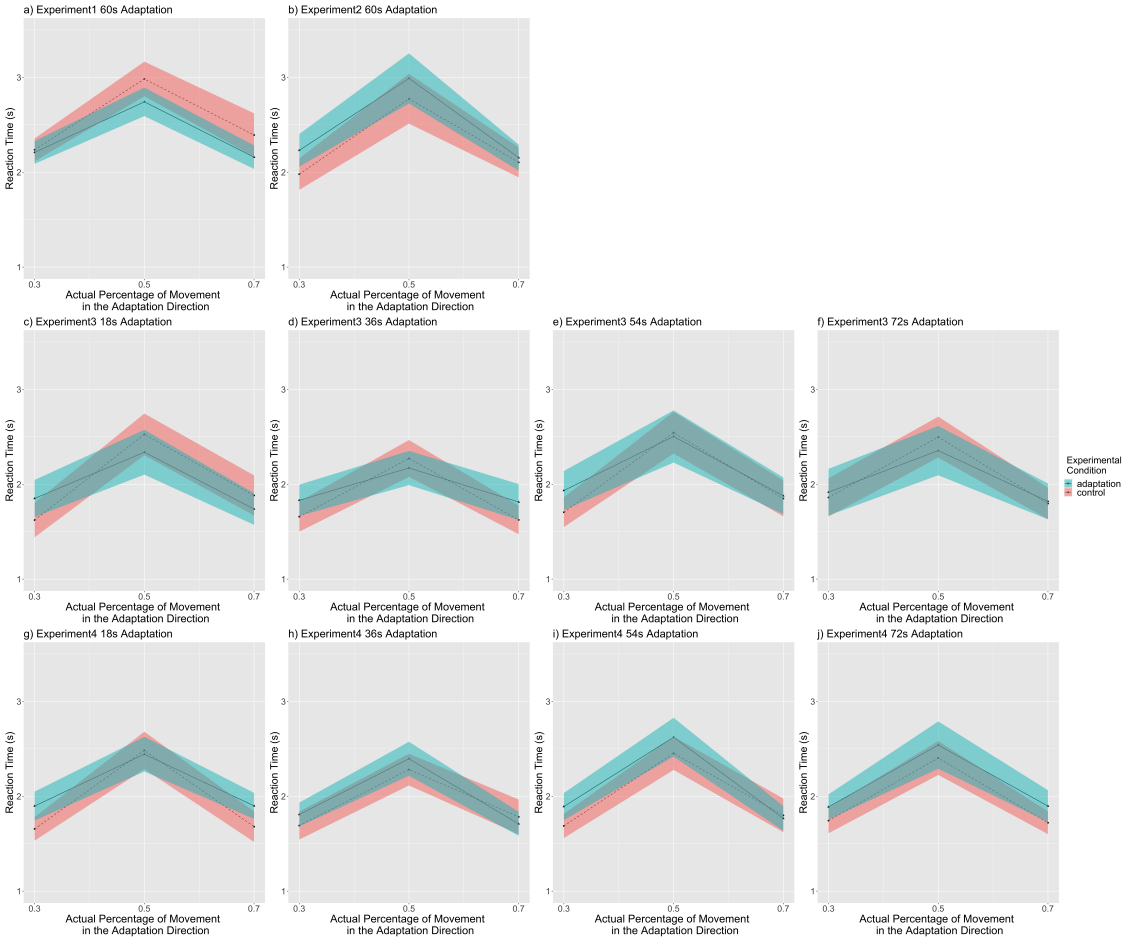

Figure A.43: Reaction times compared with the actual percentage for all subjects, separated by experiments and adaptation time periods. a) Reaction times for 60s adaptation trials in Experiment 1 (n = 60). b) Reaction times for 60s adaptation trials in Experiment 2 (n = 30). c) Reaction times for 18s adaptation trials in Experiment 3 (n = 28). d) Reaction times for 36s adaptation trials in Experiment 3 (n = 28). e) Reaction times for 54s adaptation trials in Experiment 3 (n = 28). f) Reaction times for 72s adaptation trials in Experiment 3 (n = 28). g) Reaction times for 18s adaptation trials in Experiment 4 (n = 31). h) Reaction times for 36s adaptation trials in Experiment 4 (n = 31). i) Reaction times for 54s adaptation trials in Experiment 4 (n = 31). j) Reaction times for 72s adaptation trials in Experiment 4 (n = 31). Solid lines indicate the grand average value, and the shaded area indicate 1 standard error of means.

A.18 D. Strategy Across Experiments

A.19.1 Raw Data

We compared the frequency distribution of all three strategies among different experiments with chi-square test of independence. The result showed that strategies and experiments were significant associated ($\chi^2 = 18.74$, $p < 0.001$). Post-hoc tests (with Bonferroni correction) revealed that Experiment 1 ($p < 0.001$), Experiment 3 ($p = 0.01$), and Experiment 4 ($p < 0.001$) had significantly different distributions of strategy distribution within each experiment, but the frequency of different strategies in Experiment 3 were pretty similar ($p = 0.41$). See Figure A.44.

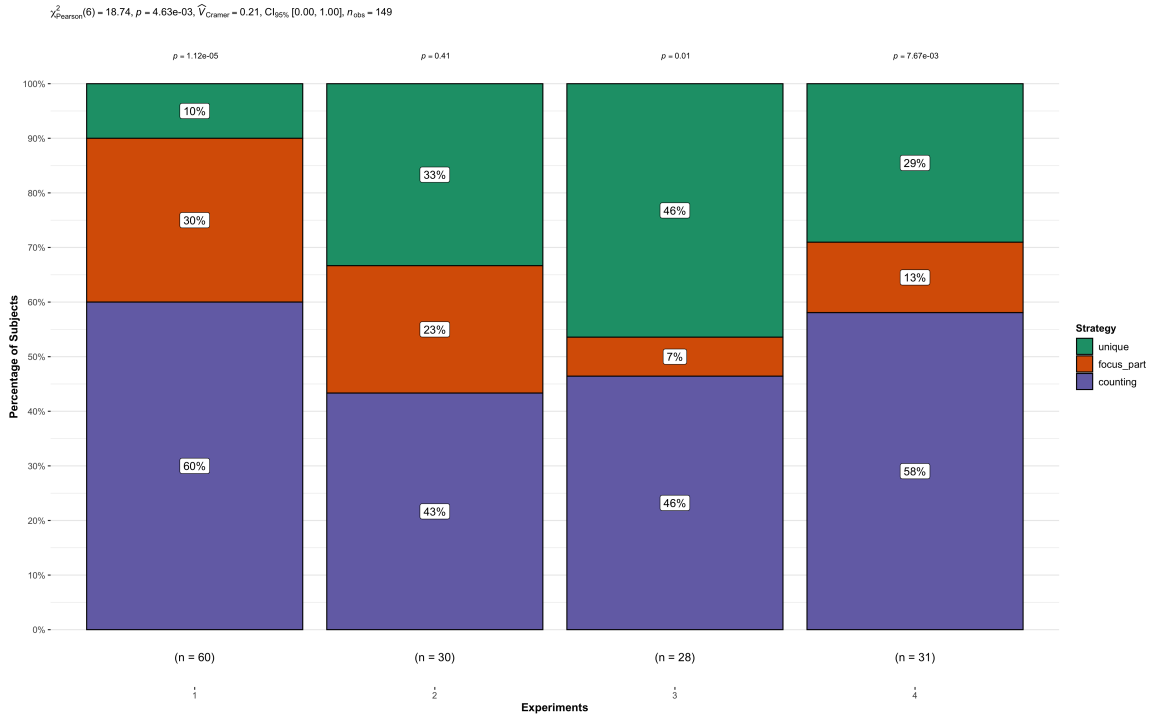

Figure A.44: Proportions of subjects using each strategy, separated by experiments. Note: Experiment 1 (n = 60), Experiment 2 (n = 30), Experiment 3 (n - 28), Experiment 4 (n = 31)

A.19.2 Filtered Data

Then we conducted same analyses for filtered data. The result showed that strategies and experiments were marginally significantly associated ($\chi^2 = 11.89$, $p = 0.06$). Post-hoc tests (with Bonferroni correction) revealed that Experiment 1 ($p < 0.001$), Experiment 3 ($p = 0.03$), and Experiment 4 ($p = 0.03$) had significantly different distributions of each strategy within each experiment, but the frequency of different strategies in Experiment 3 were pretty similar ($p = 0.12$). See Figure A.45.

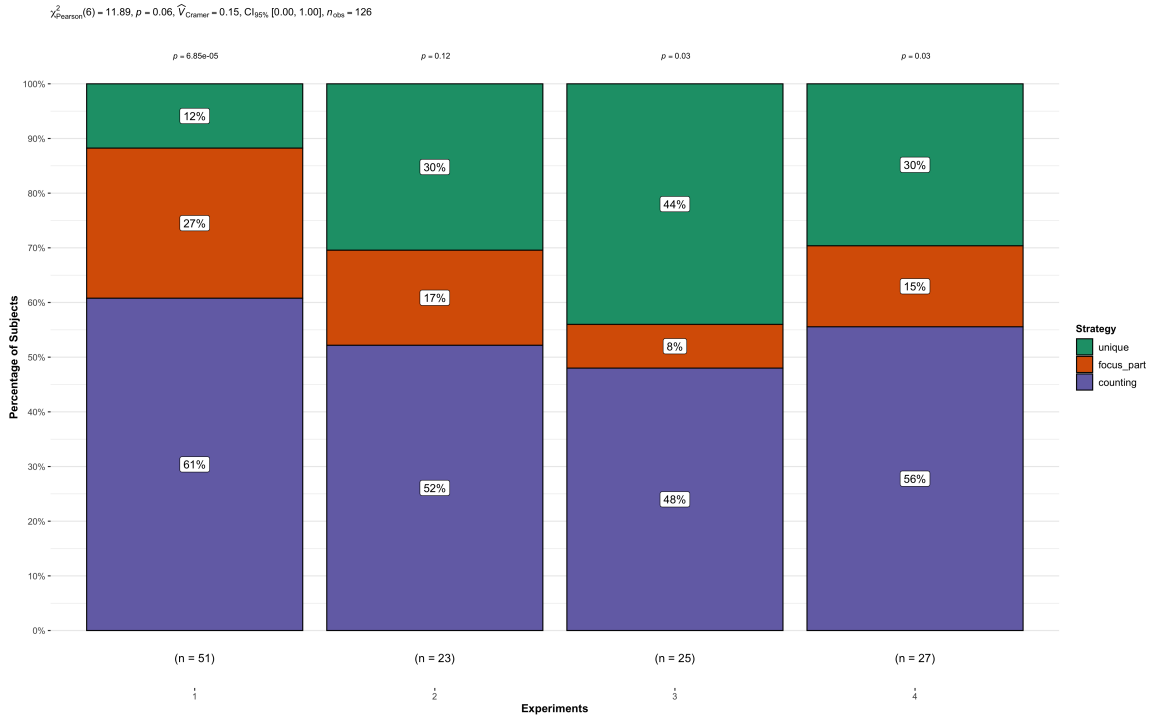

Figure A.45: Proportions of subjects using each strategy, separated by experiments. Note: Experiment 1 (n = 51), Experiment 2 (n = 23), Experiment 3 (n - 25), Experiment 4 (n = 27)

Filtered Data

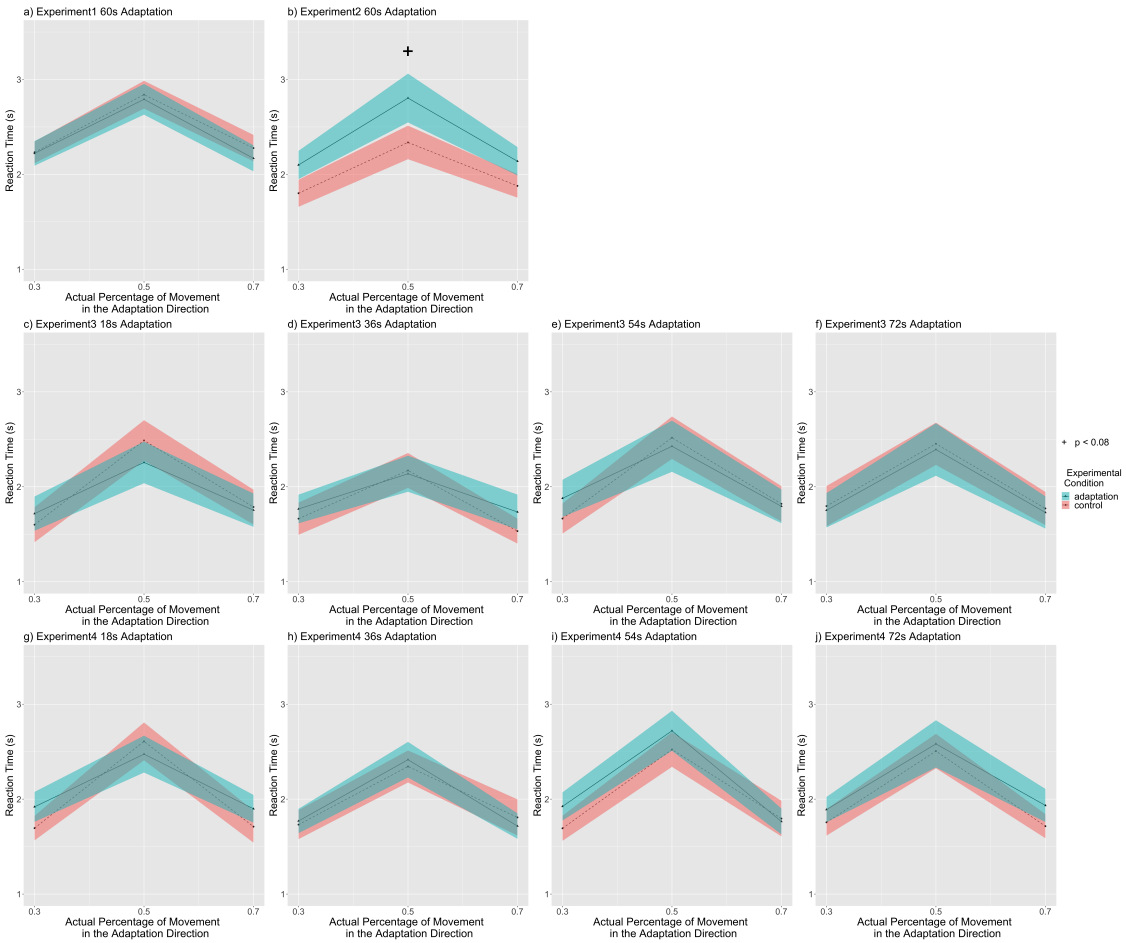

Figure A.46: Reaction times compared with the actual percentage for all subjects, separated by experiments and adaptation time periods. a) Reaction times for 60s adaptation trials in Experiment 1 (n = 51). b) Reaction times for 60s adaptation trials in Experiment 2 (n = 23). c) Reaction times for 18s adaptation trials in Experiment 3 (n = 24). d) Reaction times for 36s adaptation trials in Experiment 3 (n = 24). e) Reaction times for 54s adaptation trials in Experiment 3 (n = 24). f) Reaction times for 72s adaptation trials in Experiment 3 (n = 24). g) Reaction times for 18s adaptation trials in Experiment 4 (n = 27). h) Reaction times for 36s adaptation trials in Experiment 4 (n = 27). i) Reaction times for 54s adaptation trials in Experiment 4 (n = 27). j) Reaction times for 72s adaptation trials in Experiment 4 (n = 27). Solid lines indicate the grand average value, and the shaded area indicate 1 standard error of means.

A.19.3 Experiment 1-4: Effects of Age, Gender, Strategy, Session sequence, and Experiments on Task Difficulty

Raw Data

To approach the effects of age, gender, strategy, session sequence (i.e., control first or adaptation session first), and experiments (i.e., Experiment 1 - 4) on task difficulty, a linear mixed model analyses was conducted. In the model we constructed $Difficulty \sim Age + Gender + Strategy + Session\ Sequence + Experiments + Experimental\ Conditions + (1\|Subjects)$, age, gender, strategy, session sequence, experiments were set as fixed effects, while subject number were set as the random effect.

We only found a significant effect of experiments $power = 0.540$[1], $95\%CI = [0.437, 0.640]$) that people in Experiment 3 reported higher difficulty level than people in Experiment 1 ($t(149) = 3.72$, $p < 0.001$), but no difference in the effect on difficulty levels between Experiment 1 and Experiment 2 ($t(149) = 1.10$, $p = 0.273$, ns) or between Experiment 1 and Experiment 4 ($t(149) = 1.28$, $p = 0.204$, ns). This result was consistent with the result observed in Section A.17.1. However, different from result in Section A.17.1, we did not observe significant effect of experimental conditions ($t(149) = -1.68$, $p = 0.094$, $power = 0.880$, $95\%CI = [0.800, 0.936]$, ns).

Further, we did not observe significant effect of age ($t(149) = 1.03$, $p = 0.306$, $power = 0.910$, $95\%CI = [0.836, 0.958]$, ns), gender ($t(149) = -1.15$, $p = 0.251$, $power = 0.940$, $95\%CI = [0.874, 0.978]$, ns), or session sequence ($t(149) = -1.68$, $p = 0.489$, $power = 0.960$, $95\%CI = [0.901, 0.989]$, ns). In terms of strategy, there was no difference in effect on difficulty levels between the strategy of focusing on part of the environment and the counting strategy ($t(149) = 0.56$, $p = 0.579$, ns) or between the unique strategy and the counting strategy ($t(149) = -1.37$, $p = 0.173$, ns) ($power = 0.920$, $95\%CI = [0.887, 0.984]$).

Therefore, there were no effect of age, gender, experimental conditions, strategy, or session

[1]The power in linear mixed model was calculated based on Monte Carlo based power simulation of 100 times using the simr R package

sequences on difficulty levels and power analyses showed that the results were of practical significance.

Filtered Data

We then conducted the same linear mixed model analyses on filtered data. We still found effect of experiments ($power$ = 0.700, 95%CI = [0.600, 0.788]) that people in Experiment 3 reported higher difficulty level than people in Experiment 1 ($t(126)$ = 3.58, $p < 0.001$), but no difference in the effect on difficulty levels between Experiment 1 and Experiment 2 ($t(126)$ = 0.71, p = 0.477, ns) or between Experiment 1 and Experiment 4 ($t(126)$ = 0.90, p = 0.368, ns). This result was consistent with the result observed in Section A.17.1. However, different from result in Section A.17.1, we did not observe significant effect of experimental conditions ($t(126)$ = -1.50, p = 0.136, $power$ = 0.900, 95%CI = [0.824, 0.951], ns).
Further, we did not observe significant effect of age ($t(126)$ = 0.517, p = 0.606, $power$ = 0.970, 95%CI = [0.915, 0.994], ns), gender ($t(126)$ = -1.46, p = 0.146, $power$ = 0.920, 95%CI = [0.848, 0.965], ns), or session sequence ($t(126)$ = 0.59, p = 0.559, $power$ = 0.930, 95%CI = [0.861, 0.971], ns). In terms of the effect of strategy ($power$ = 0.910, 95%CI = [0.836, 0.958]), there was no difference in effect on difficulty levels between the strategy of focusing on part of the environment and the counting strategy ($t(126)$ = -0.23, p = 0.819, ns), but people with unique strategy rated the experiment to be easier than people with counting strategy ($t(126)$ = -2.40, p = 0.018) .
Therefore, there were no effect of age, gender, experimental conditions, or session sequences on difficulty levels and power analyses showed that results were of practical significance.

Appendix B

Chapter 4: A Neural Model of Travel Direction

B.1 Experiment 1 Predicted By the Original Model Separated By the Adaptation Group

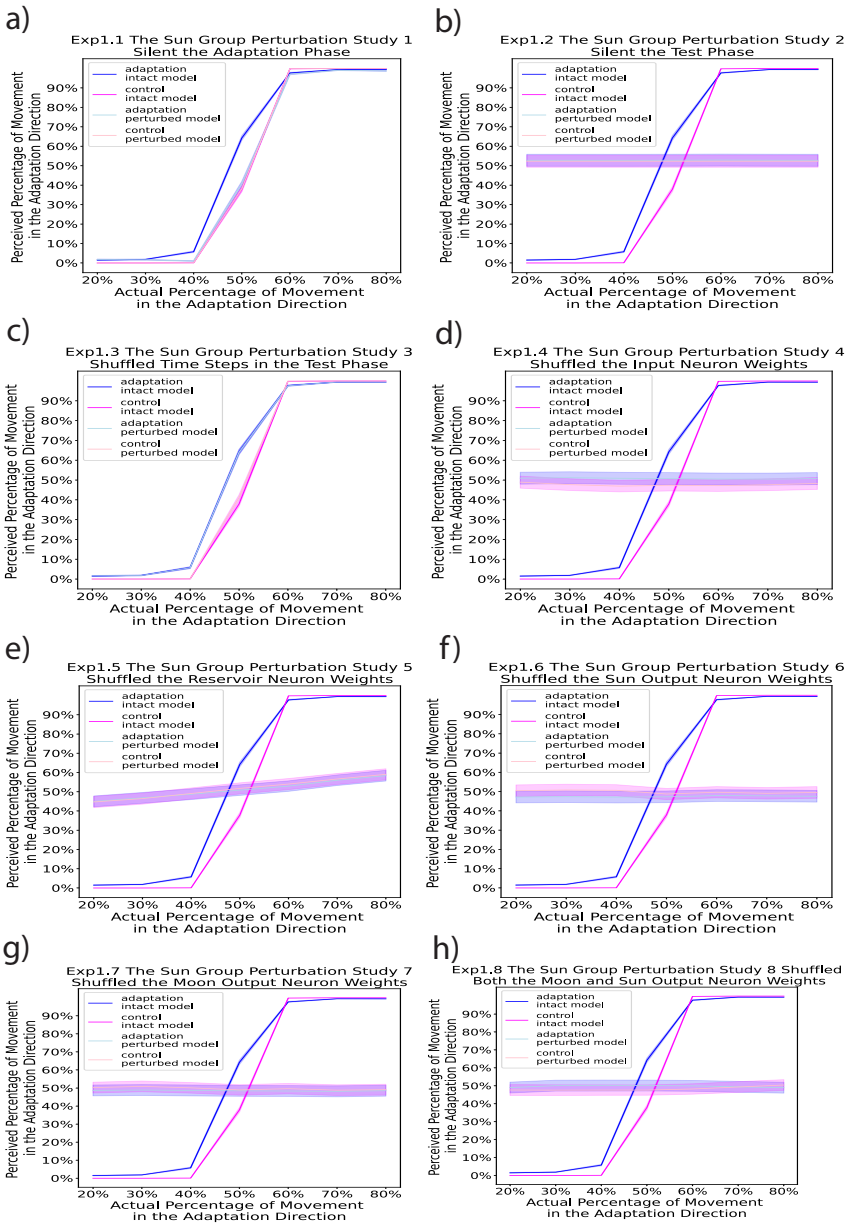

Figure B.1: Experiment 1 modeled reported rates predicted by the perturbed model and the intact model for the sun group: a) Perturbation study 1 - silent the adaptation phase b) Perturbation study 2 - silent the test phase c) Perturbation study 3 - shuffled time steps in the test phase b) Perturbation study 4 - shuffled the input neuron weights b) Perturbation study 5 - shuffled the reservoir neuron weights b) Perturbation study 6 - shuffled the sun output neuron weights b) Perturbation study 7 - shuffled the moon output neuron weights b) Perturbation study 8 - shuffled both the sun and moon output neuron weights

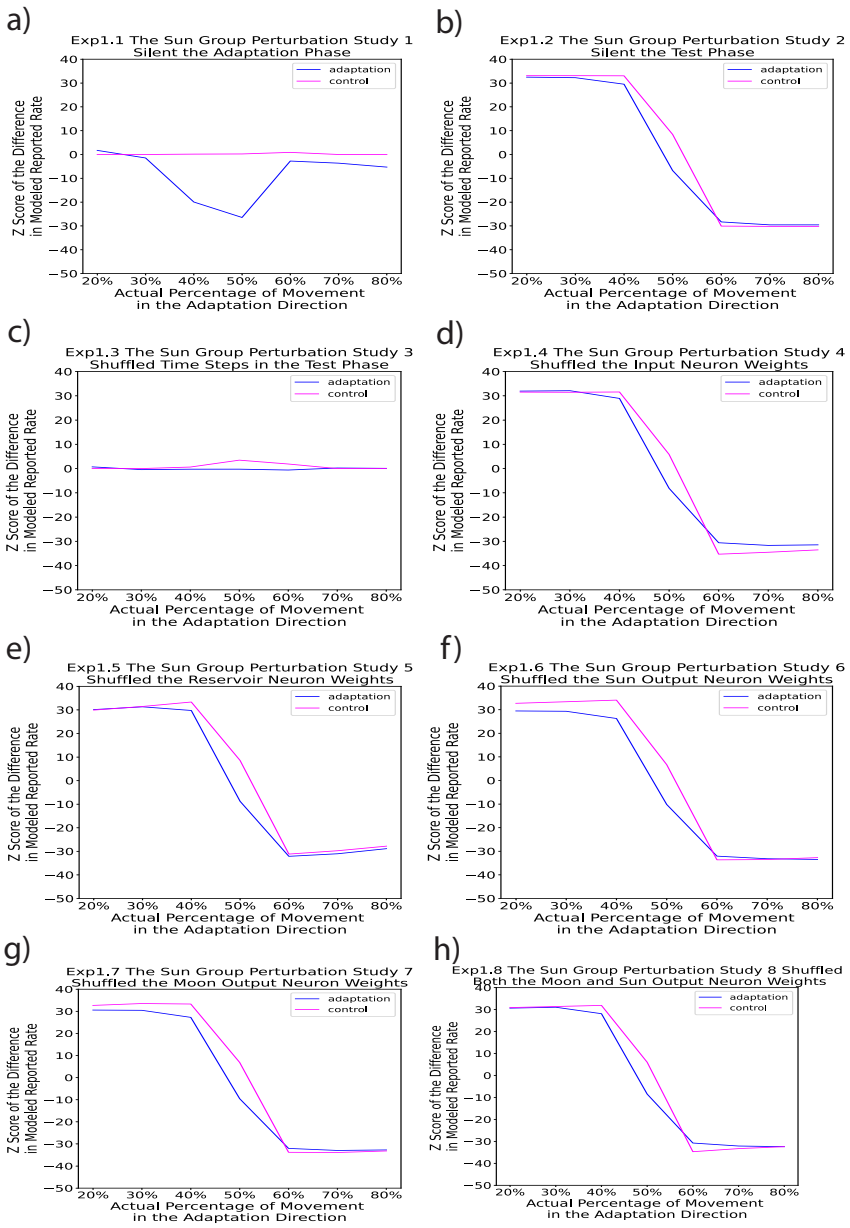

Figure B.2: Experiment 1 normalized difference in modeled reported rate between the perturbed model and the intact model for the sun group: a) Perturbation study 1 - silent the adaptation phase b) Perturbation study 2 - silent the test phase c) Perturbation study 3 - shuffled time steps in the test phase b) Perturbation study 4 - shuffled the input neuron weights b) Perturbation study 5 - shuffled the reservoir neuron weights b) Perturbation study 6 - shuffled the sun output neuron weights b) Perturbation study 7 - shuffled the moon output neuron weights b) Perturbation study 8 - shuffled both the sun and moon output neuron weights

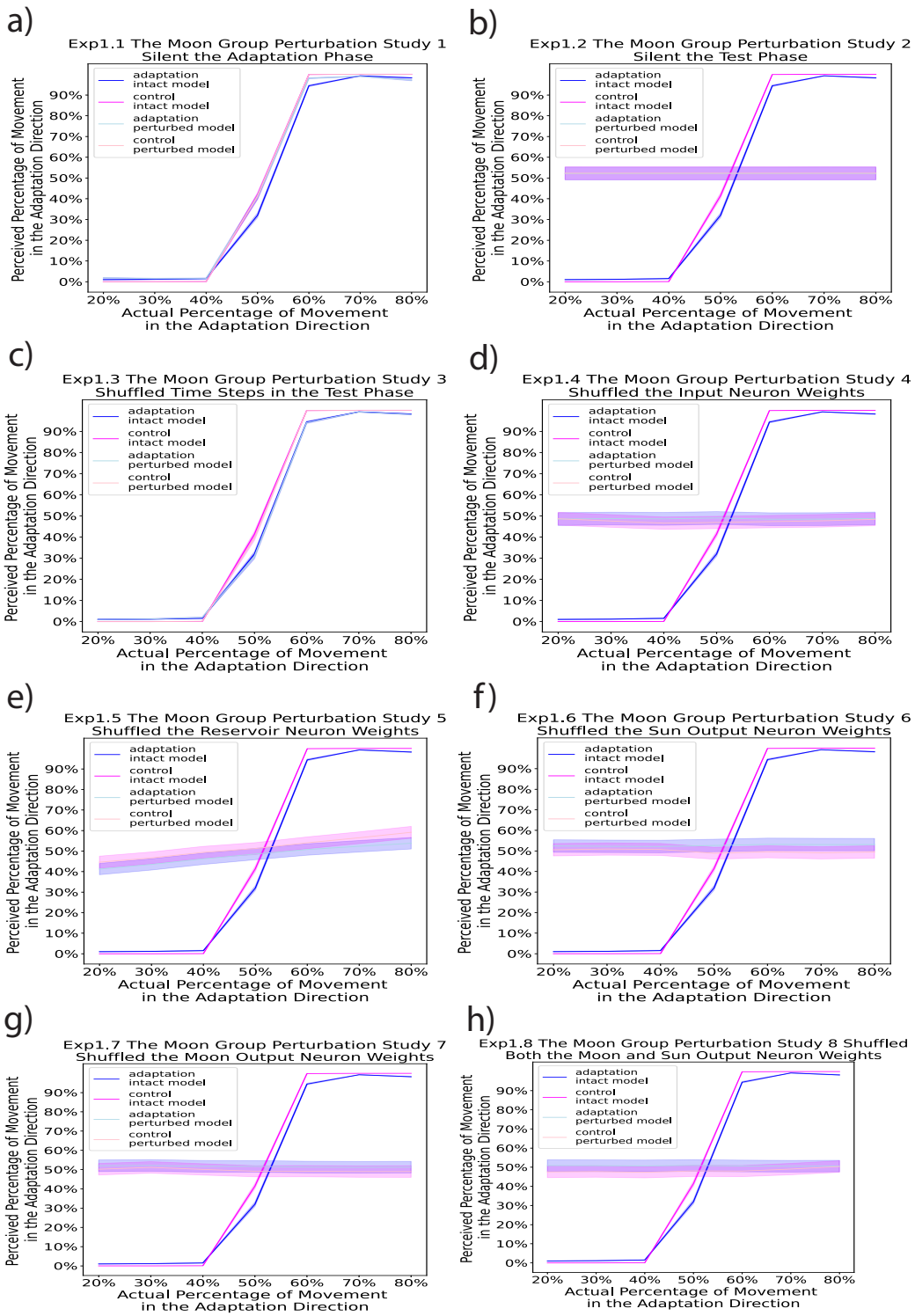

Figure B.3: Experiment 1 modeled reported rates predicted by the perturbed model and the intact model for the moon group: a) Perturbation study 1 - silent the adaptation phase b) Perturbation study 2 - silent the test phase c) Perturbation study 3 - shuffled time steps in the test phase b) Perturbation study 4 - shuffled the input neuron weights b) Perturbation study 5 - shuffled the reservoir neuron weights b) Perturbation study 6 - shuffled the sun output neuron weights b) Perturbation study 7 - shuffled the moon output neuron weights b) Perturbation study 8 - shuffled both the sun and moon output neuron weights

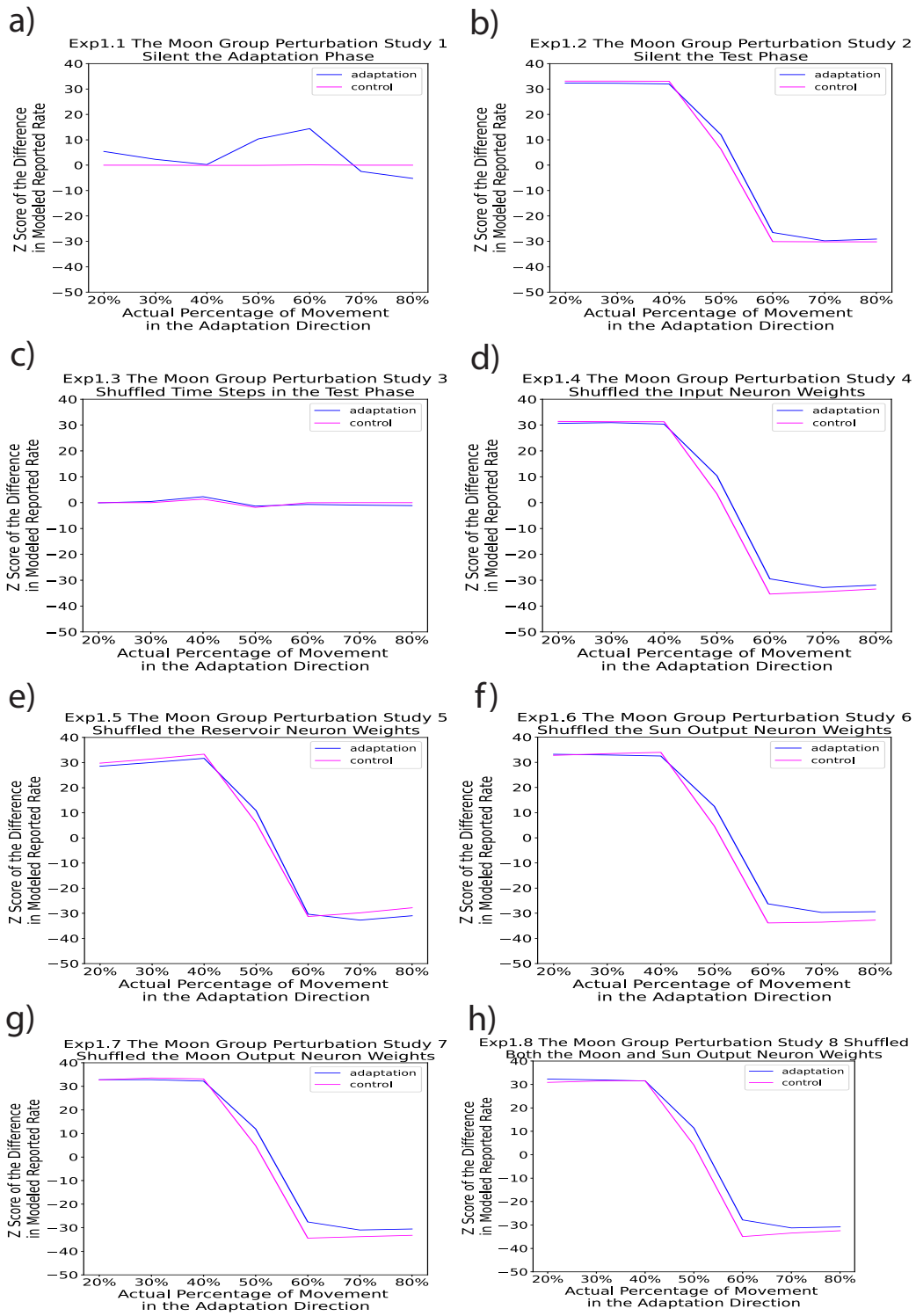

Figure B.4: Experiment 1 normalized difference in modeled reported rate between the perturbed model and the intact model for the moon group: a) Perturbation study 1 - silent the adaptation phase b) Perturbation study 2 - silent the test phase c) Perturbation study 3 - shuffled time steps in the test phase b) Perturbation study 4 - shuffled the input neuron weights b) Perturbation study 5 - shuffled the reservoir neuron weights b) Perturbation study 6 - shuffled the sun output neuron weights b) Perturbation study 7 - shuffled the moon output neuron weights b) Perturbation study 8 - shuffled both the sun and moon output neuron weights

B.2 Experiment 2 Predicted By the Original Model

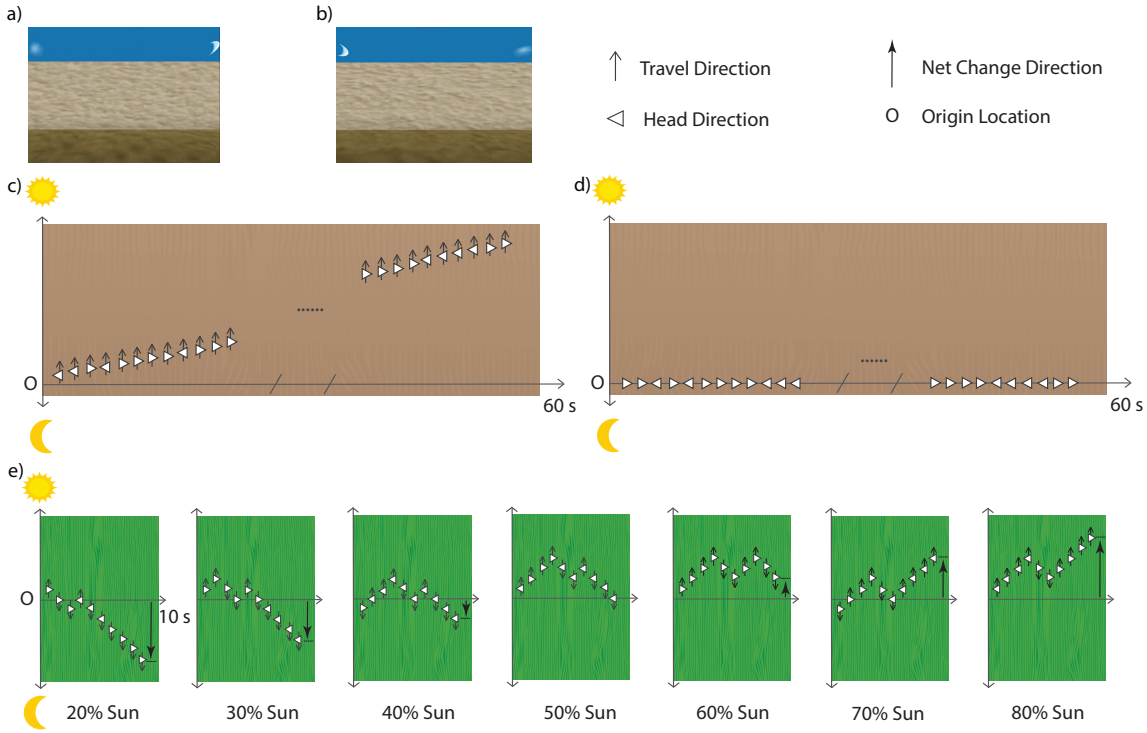

Figure B.5: Experiment 2. a) Hallway during the adaptation phase, adapting to the sun direction. b) Hallway during the adaptation phase, adapting to the sun direction, opposite facing direction than a). The ground for the hallways turned green during the test phase to provide a visual cue for when to start tracking movement direction. c) The 60-second adaptation phase for the experimental condition. During the adaptation phase, visual movement traveled toward the sun while the facing direction occasionally changed. d) The 60-second initial phase for the control session. There was no visual travel, but the facing direction randomly changed. e) The test phase, which was the same for all sessions in all conditions. Visual movement traveled back-and-forth between the sun and the moon during a 10-second interval. Participants were asked to decide whether the total movement was more toward the sun or more toward the moon in that interval. The facing direction randomly changed during the test phase. Here we show one example from each of the seven test phase conditions of the percent of net movement toward the adaptation direction (20%, 30%, 40%, 50%, 60%, 70%, 80%).

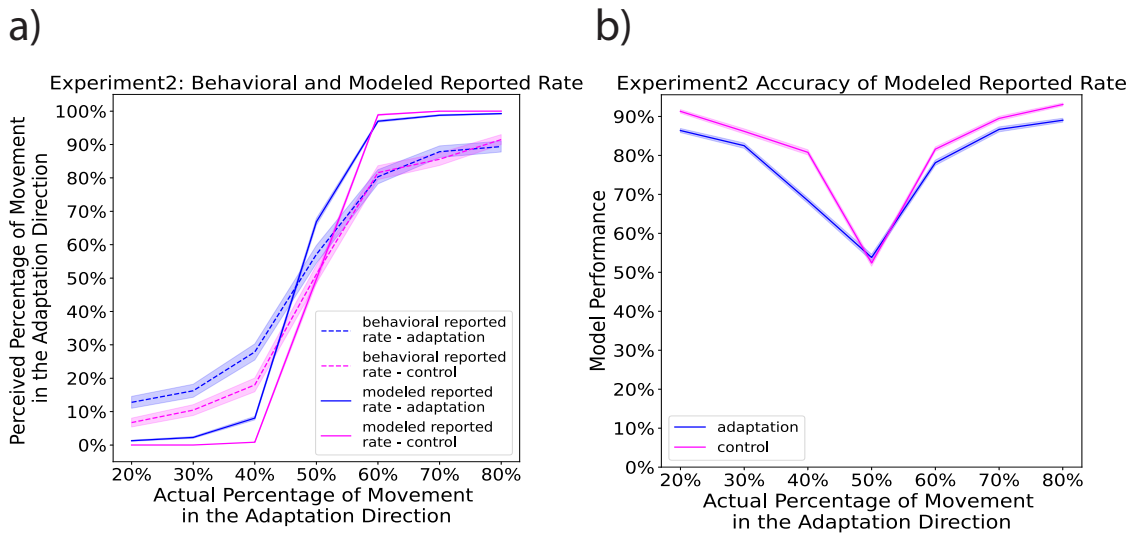

Figure B.6: Experiment 2 The Modeled and Behavioral Reported Rates: a) The modeled reported rate compared with the behavioral reported rate (30 subjects). Similar to the behavioral data, for the modeled data, the adaptation condition showed significantly higher reported percentages than the corresponding control conditions at 20%, 30%, 40%, and 50%, supporting the aftereffect (all $ps < 0.001$). This result suggests an aftereffect in the same direction of travel. Solid lines indicate the grand average value for the modeled reported rate, while dashed lines indicate the grand average for the behavioral reported rate. The shaded areas indicate 95% confidence interval of the mean. b) Accuracy of the modeled reported rate (averaged trial-based classification accuracy across all simulations). The prediction accuracy decreased as the actual percentage of movement in the adaptation direction gets closer to 50%, which aligns with the task difficulty levels. The task gets more difficult as the actual percentage of movement in the adaptation direction gets closer to 50%. The shaded areas indicate 95% confidence interval of the mean.

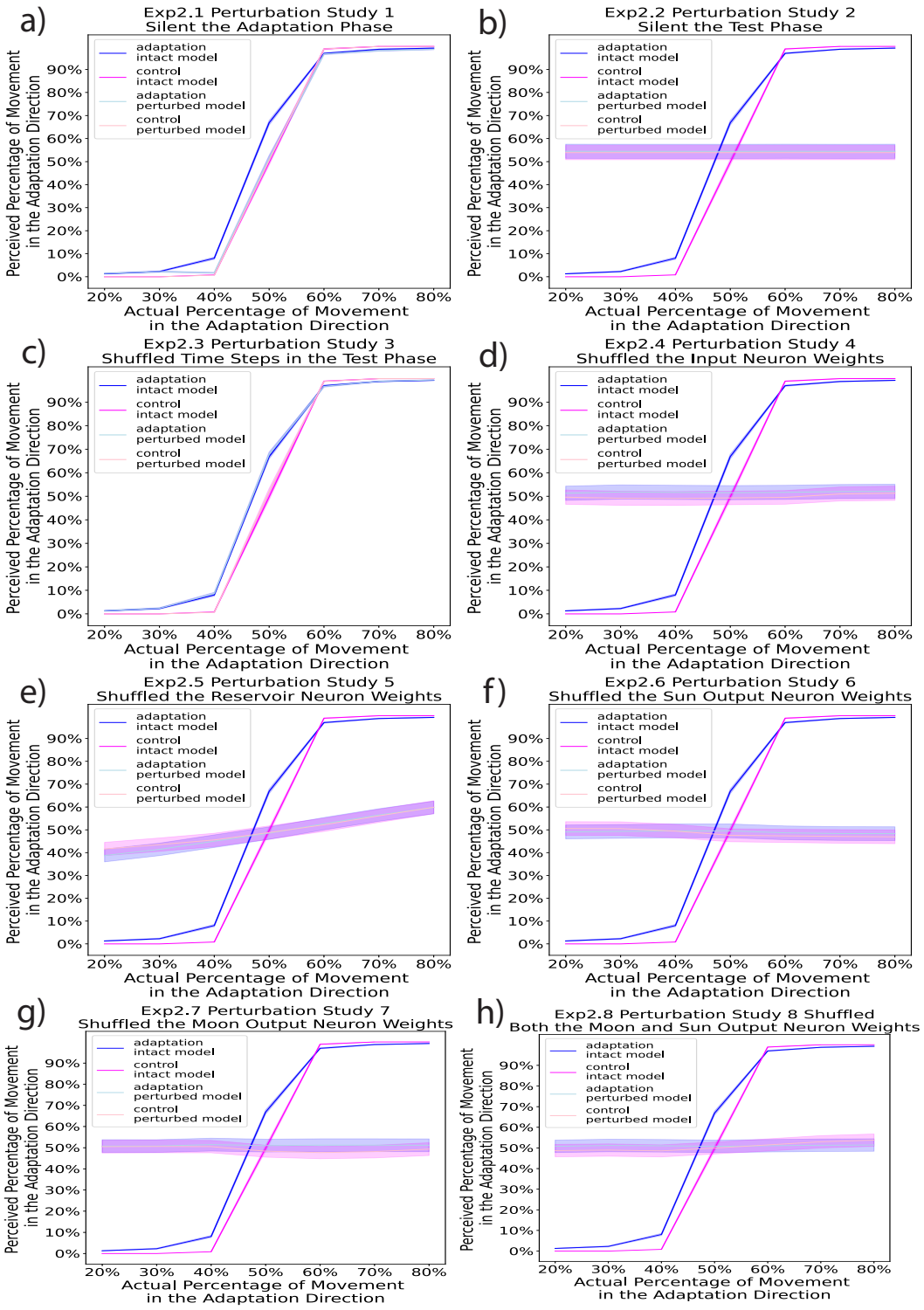

Figure B.7: Experiment 2 modeled reported rates predicted by the perturbed model and the intact model: a) Perturbation study 1 - silencing the adaptation phase b) Perturbation study 2 - silencing the test phase c) Perturbation study 3 - shuffled time steps in the test phase b) Perturbation study 4 - shuffled the input neuron weights b) Perturbation study 5 - shuffled the reservoir neuron weights b) Perturbation study 6 - shuffled the sun output neuron weights b) Perturbation study 7 - shuffled the moon output neuron weights b) Perturbation study 8 - shuffled both the sun and moon output neuron weights

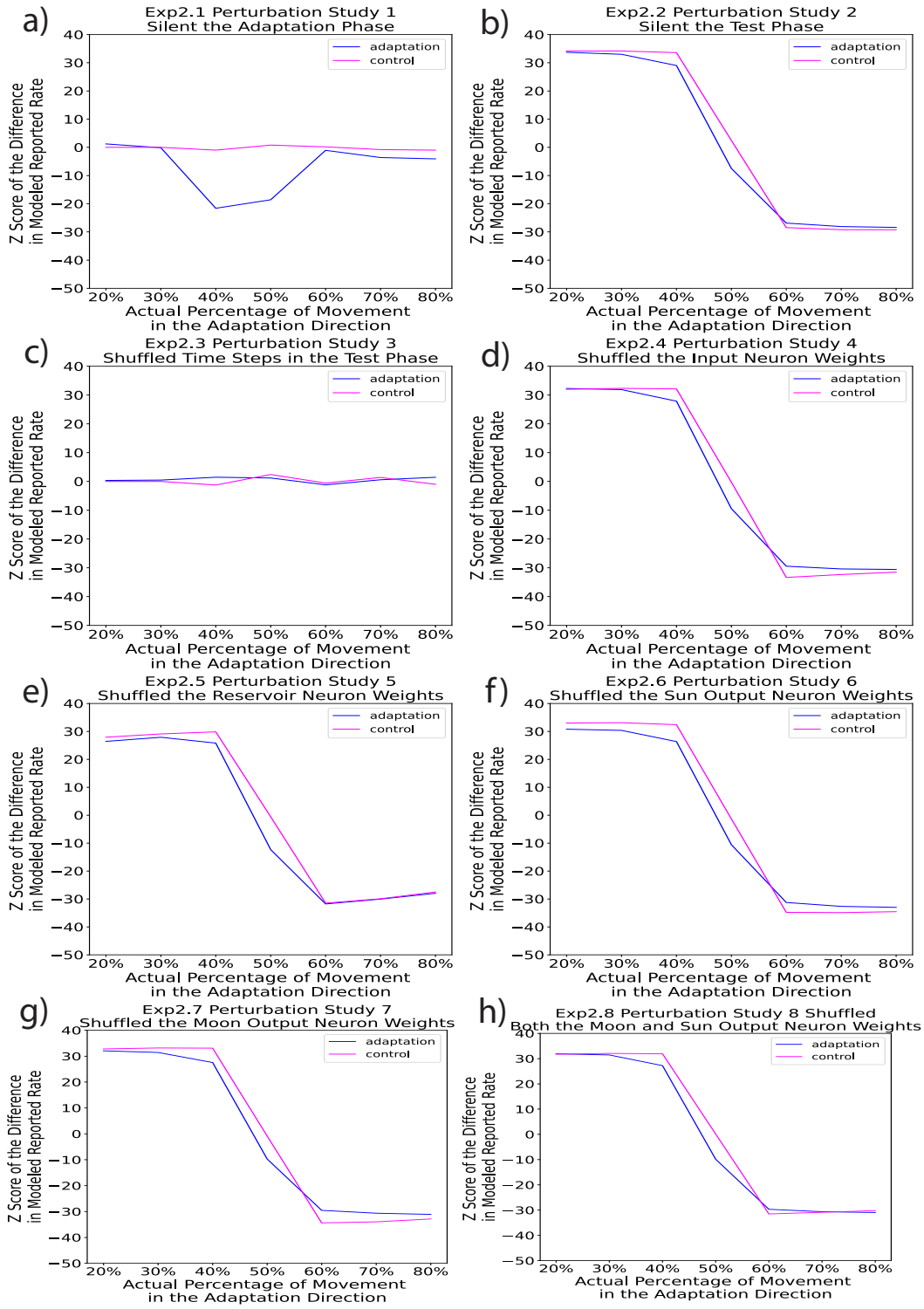

Figure B.8: Experiment 2 normalized difference in modeled reported rate between the perturbed model and the intact model: a) Perturbation study 1 - silencing the adaptation phase b) Perturbation study 2 - silencing the test phase c) Perturbation study 3 - shuffled time steps in the test phase b) Perturbation study 4 - shuffled the input neuron weights b) Perturbation study 5 - shuffled the reservoir neuron weights b) Perturbation study 6 - shuffled the sun output neuron weights b) Perturbation study 7 - shuffled the moon output neuron weights b) Perturbation study 8 - shuffled both the sun and moon output neuron weights

B.3 Experiment 3 Predicted By the Original Model

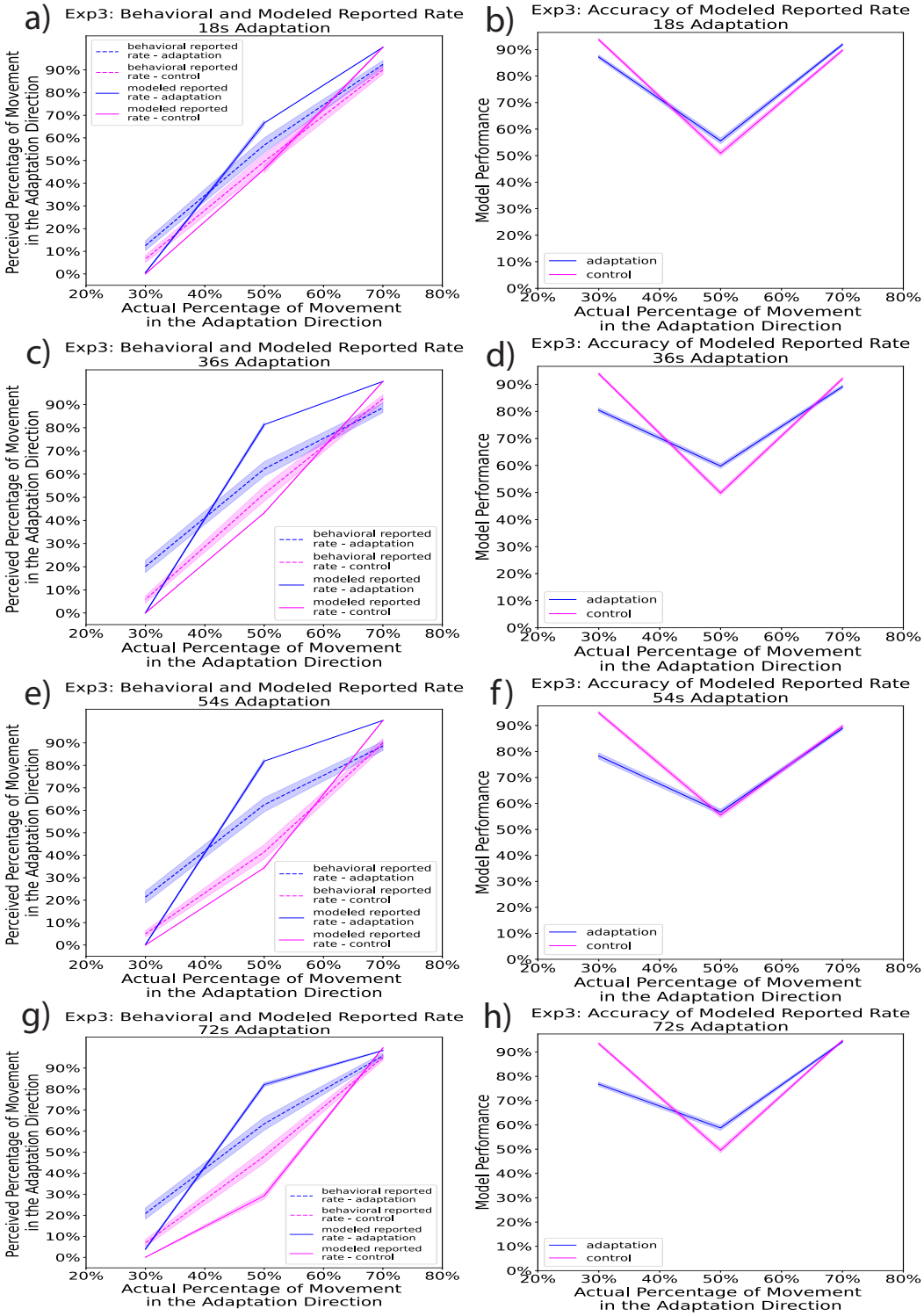

Figure B.9: Experiment 3 The Modeled and Behavioral Reported Rates Separated by Adaptation Duration: a) The modeled reported rate compared with the behavioral reported rate (28 subjects) for 18s adaptation. Solid lines indicate the grand average value for the modeled reported rate, while dashed lines indicate the grand average for the behavioral reported rate. The shaded areas indicate 95% confidence interval of the mean. b) Accuracy of the modeled reported rate (averaged trial-based classification accuracy across all simulations) for 18s adaptation. The prediction accuracy decreased as the actual percentage of movement in the adaptation direction gets closer to 50%, which aligns with the task difficulty levels. The task gets more difficult as the actual percentage of movement in the adaptation direction gets closer to 50%. The shaded areas indicate 95% confidence interval of the mean. c) similar to a), for 36s adaptation. d) similar to b), for 36s adaptation. e) similar to a), for 54s adaptation. f) similar to b), for 54s adaptation. g)similar to a), for 72s adaptation separately. h) similar to b), for 72s adaptation.

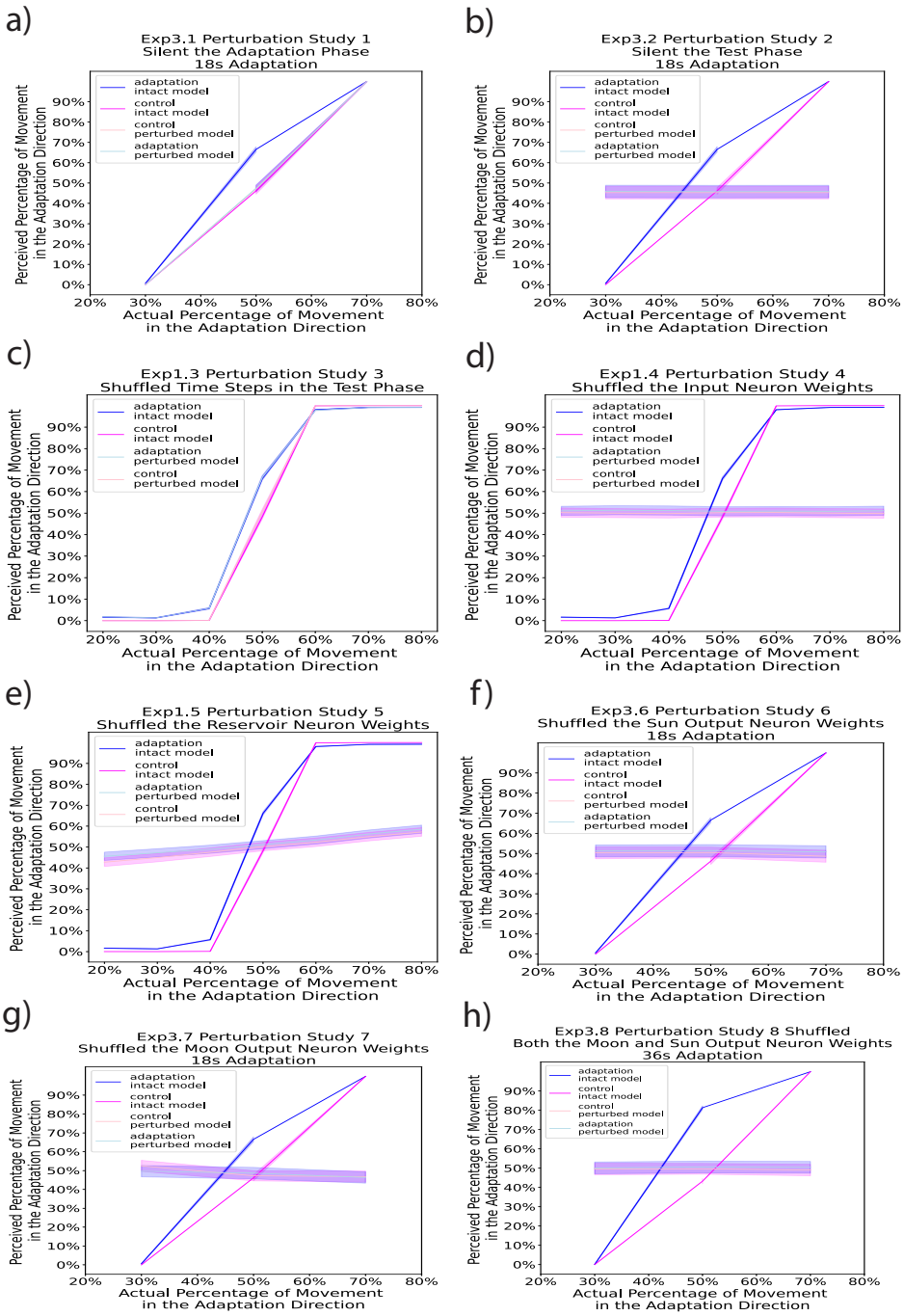

Figure B.10: Experiment 3 modeled reported rates predicted by the perturbed model and the intact model for the 18s Adaptation: a) Perturbation study 1 - silent the adaptation phase. The perturbed adaptation line overlaps with the condition lines. b) Perturbation study 2 - silent the test phase c) Perturbation study 3 - shuffled time steps in the test phase b) Perturbation study 4 - shuffled the input neuron weights b) Perturbation study 5 - shuffled the reservoir neuron weights b) Perturbation study 6 - shuffled the sun output neuron weights b) Perturbation study 7 - shuffled the moon output neuron weights b) Perturbation study 8 - shuffled both the sun and moon output neuron weights

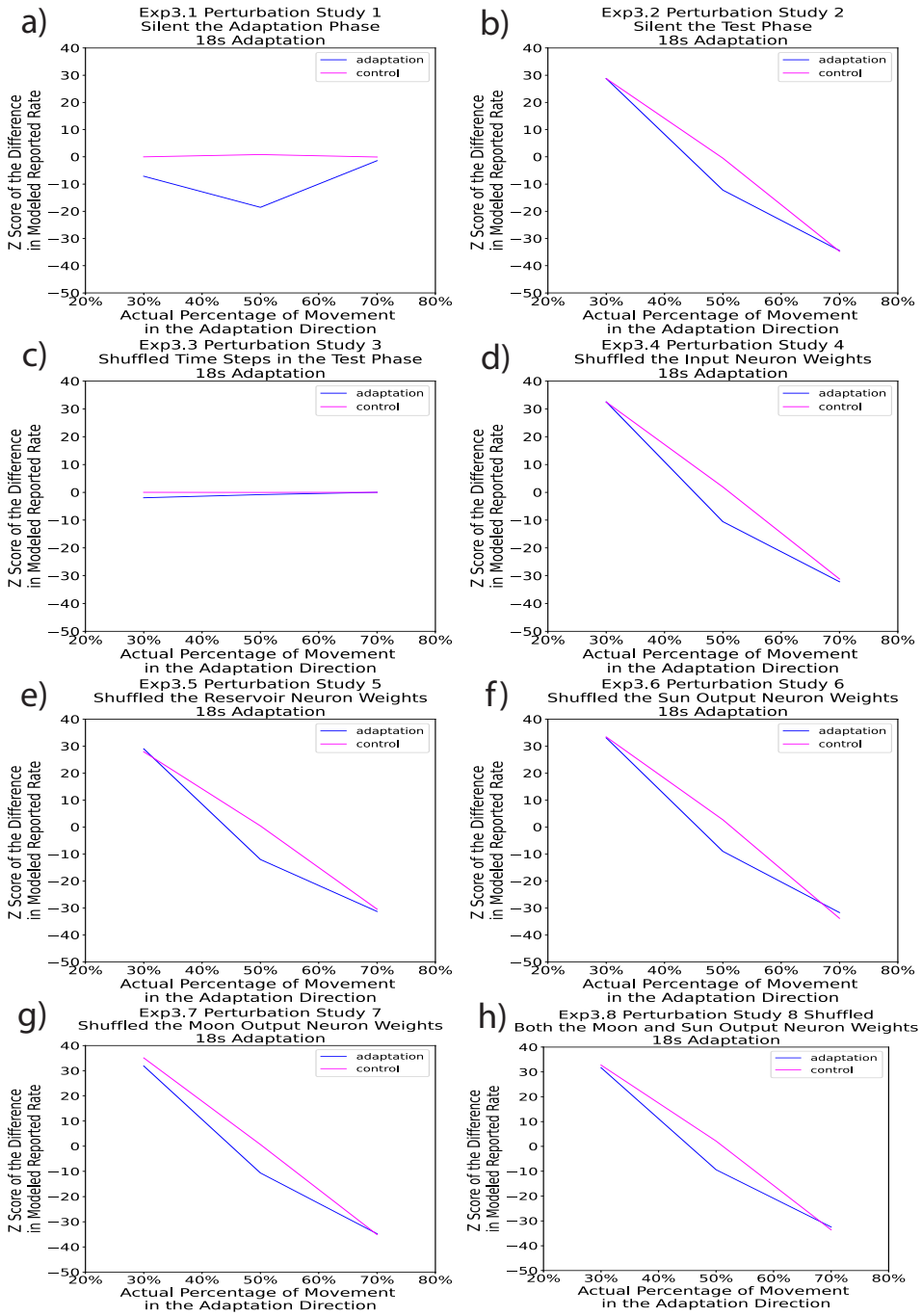

Figure B.11: Experiment 3 normalized difference in modeled reported rate between the perturbed model and the intact model for the 18s Adaptation: a) Perturbation study 1 - silent the adaptation phase. The perturbed adaptation line overlaps with the condition lines. b) Perturbation study 2 - silent the test phase c) Perturbation study 3 - shuffled time steps in the test phase b) Perturbation study 4 - shuffled the input neuron weights b) Perturbation study 5 - shuffled the reservoir neuron weights b) Perturbation study 6 - shuffled the sun output neuron weights b) Perturbation study 7 - shuffled the moon output neuron weights b) Perturbation study 8 - shuffled both the sun and moon output neuron weights

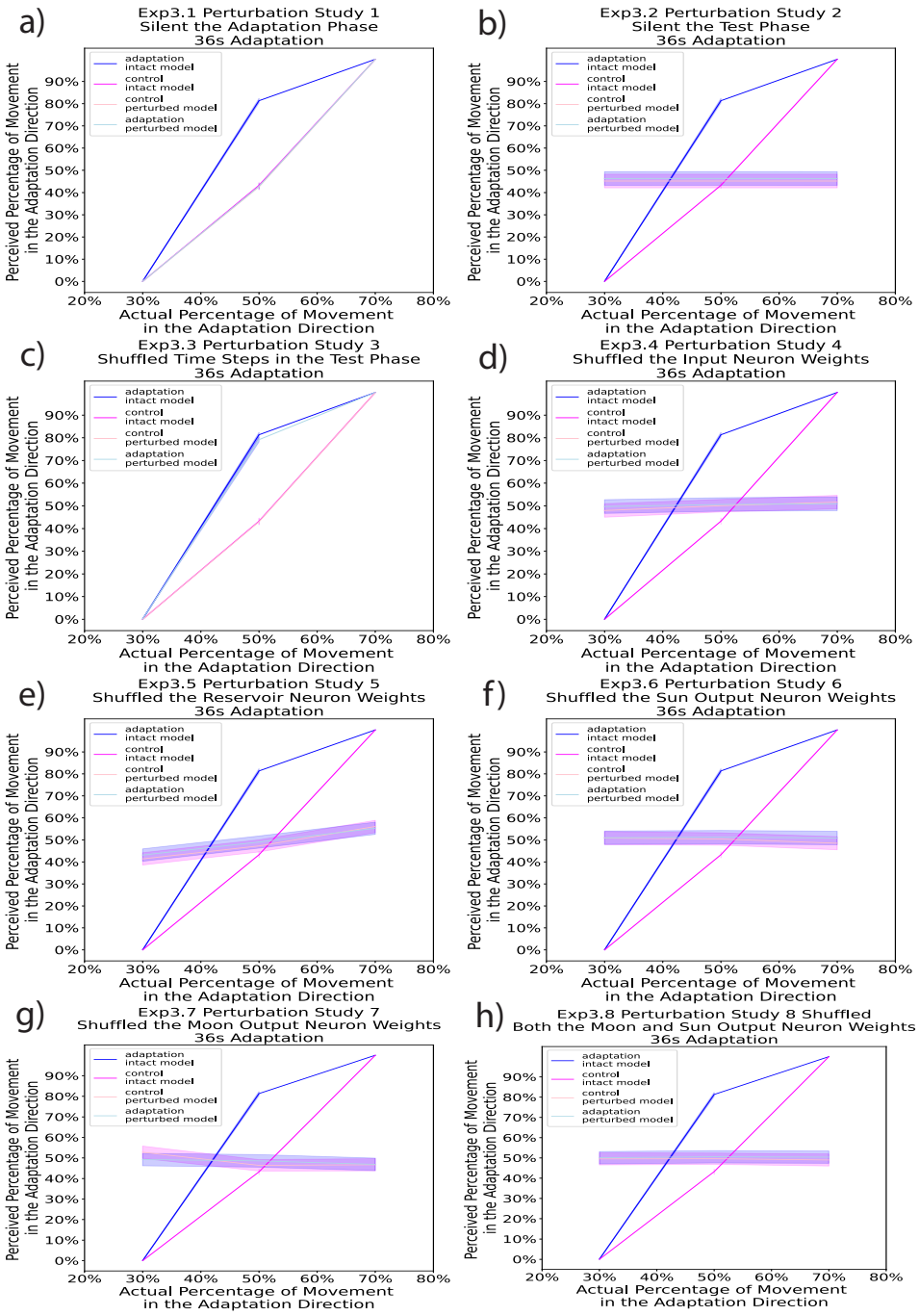

Figure B.12: Experiment 3 modeled reported rates predicted by the perturbed model and the intact model for the 36s Adaptation: a) Perturbation study 1 - silent the adaptation phase. The perturbed adaptation line overlaps with the condition lines. b) Perturbation study 2 - silent the test phase c) Perturbation study 3 - shuffled time steps in the test phase b) Perturbation study 4 - shuffled the input neuron weights b) Perturbation study 5 - shuffled the reservoir neuron weights b) Perturbation study 6 - shuffled the sun output neuron weights b) Perturbation study 7 - shuffled the moon output neuron weights b) Perturbation study 8 - shuffled both the sun and moon output neuron weights

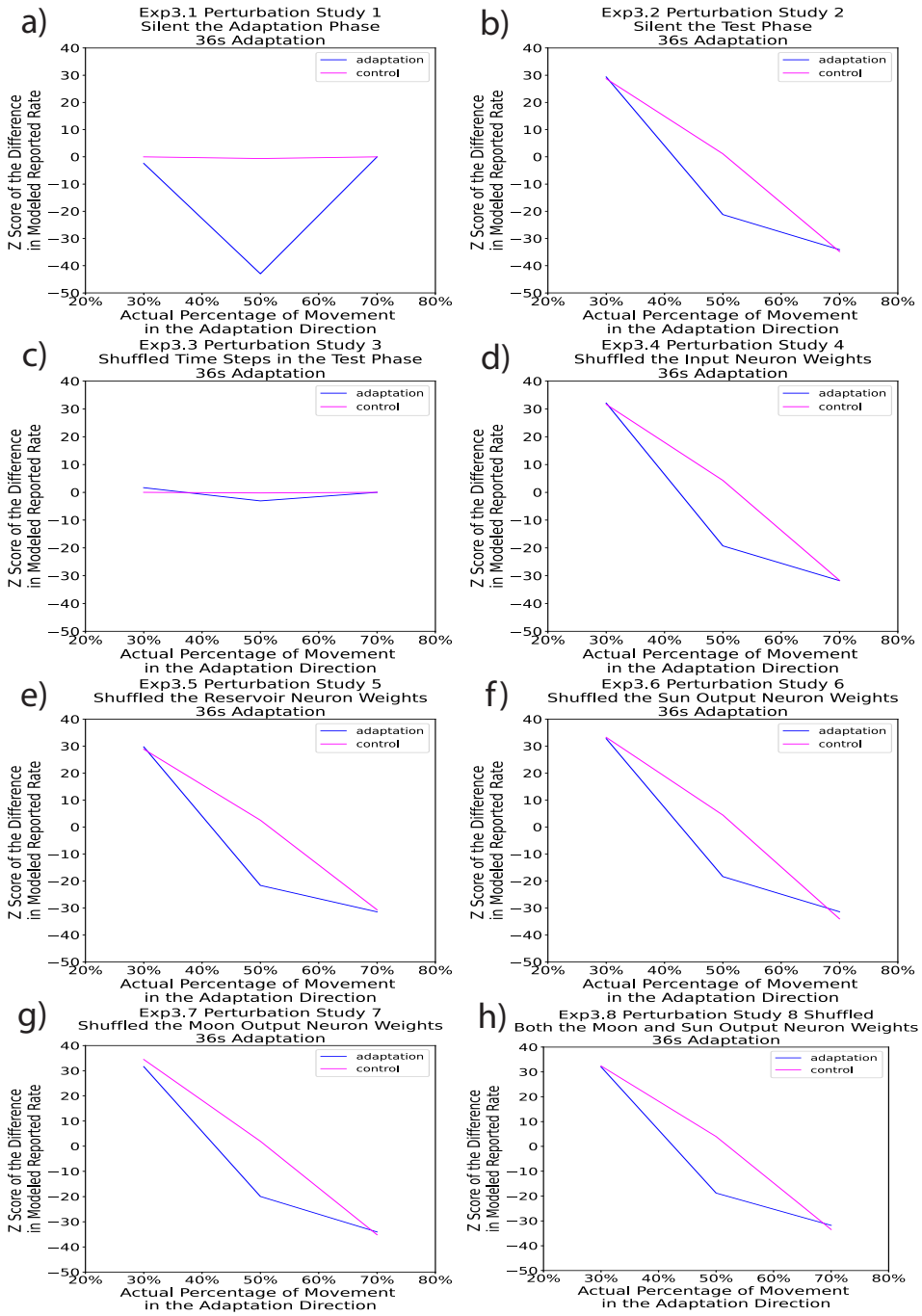

Figure B.13: Experiment 3 normalized difference in modeled reported rate between the perturbed model and the intact model for the 36s Adaptation: a) Perturbation study 1 - silent the adaptation phase. The perturbed adaptation line overlaps with the condition lines. b) Perturbation study 2 - silent the test phase c) Perturbation study 3 - shuffled time steps in the test phase b) Perturbation study 4 - shuffled the input neuron weights b) Perturbation study 5 - shuffled the reservoir neuron weights b) Perturbation study 6 - shuffled the sun output neuron weights b) Perturbation study 7 - shuffled the moon output neuron weights b) Perturbation study 8 - shuffled both the sun and moon output neuron weights

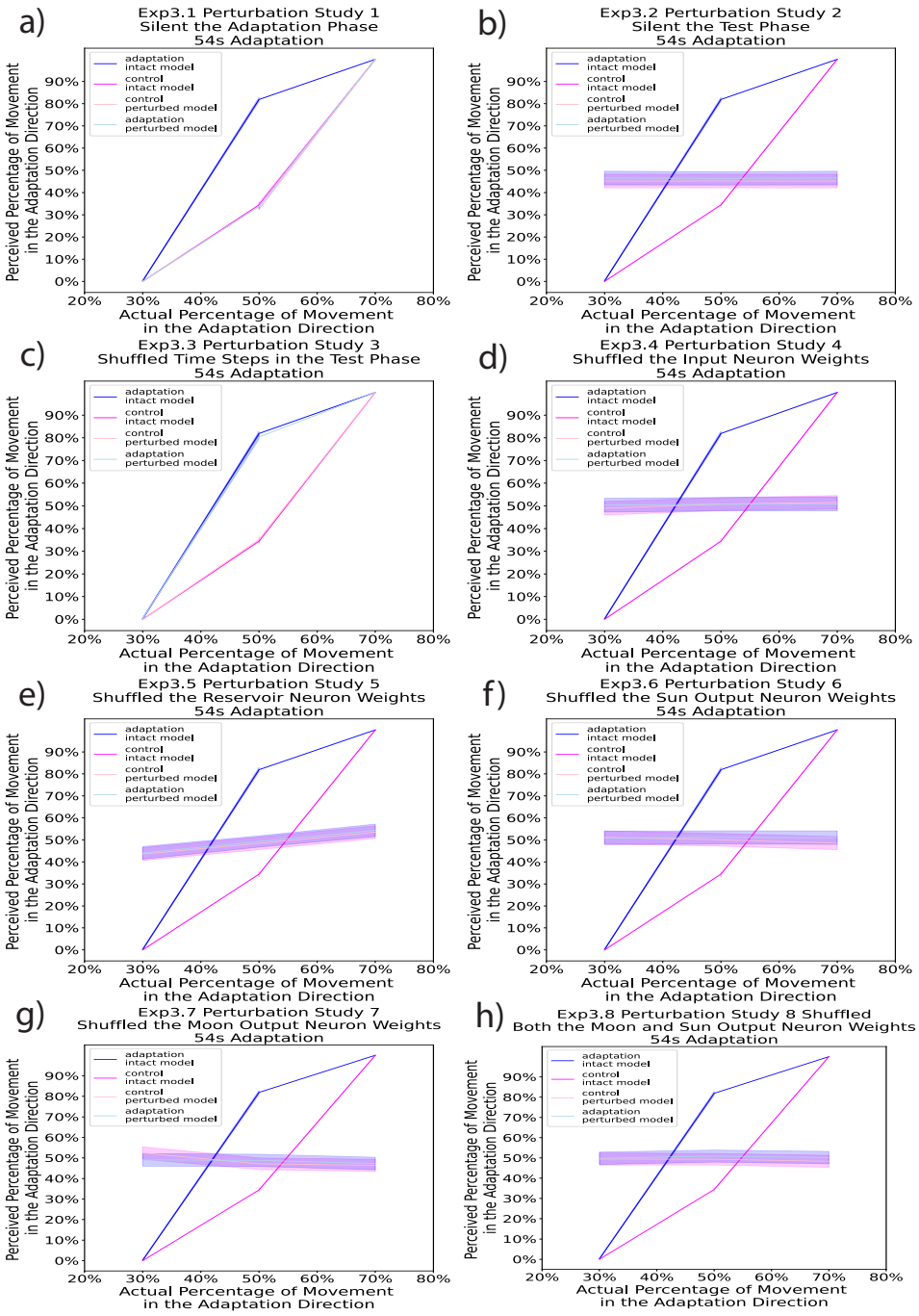

Figure B.14: Experiment 3 modeled reported rates predicted by the perturbed model and the intact model for the 54s Adaptation: a) Perturbation study 1 - silent the adaptation phase. The perturbed adaptation line overlaps with the condition lines. b) Perturbation study 2 - silent the test phase c) Perturbation study 3 - shuffled time steps in the test phase b) Perturbation study 4 - shuffled the input neuron weights b) Perturbation study 5 - shuffled the reservoir neuron weights b) Perturbation study 6 - shuffled the sun output neuron weights b) Perturbation study 7 - shuffled the moon output neuron weights b) Perturbation study 8 - shuffled both the sun and moon output neuron weights

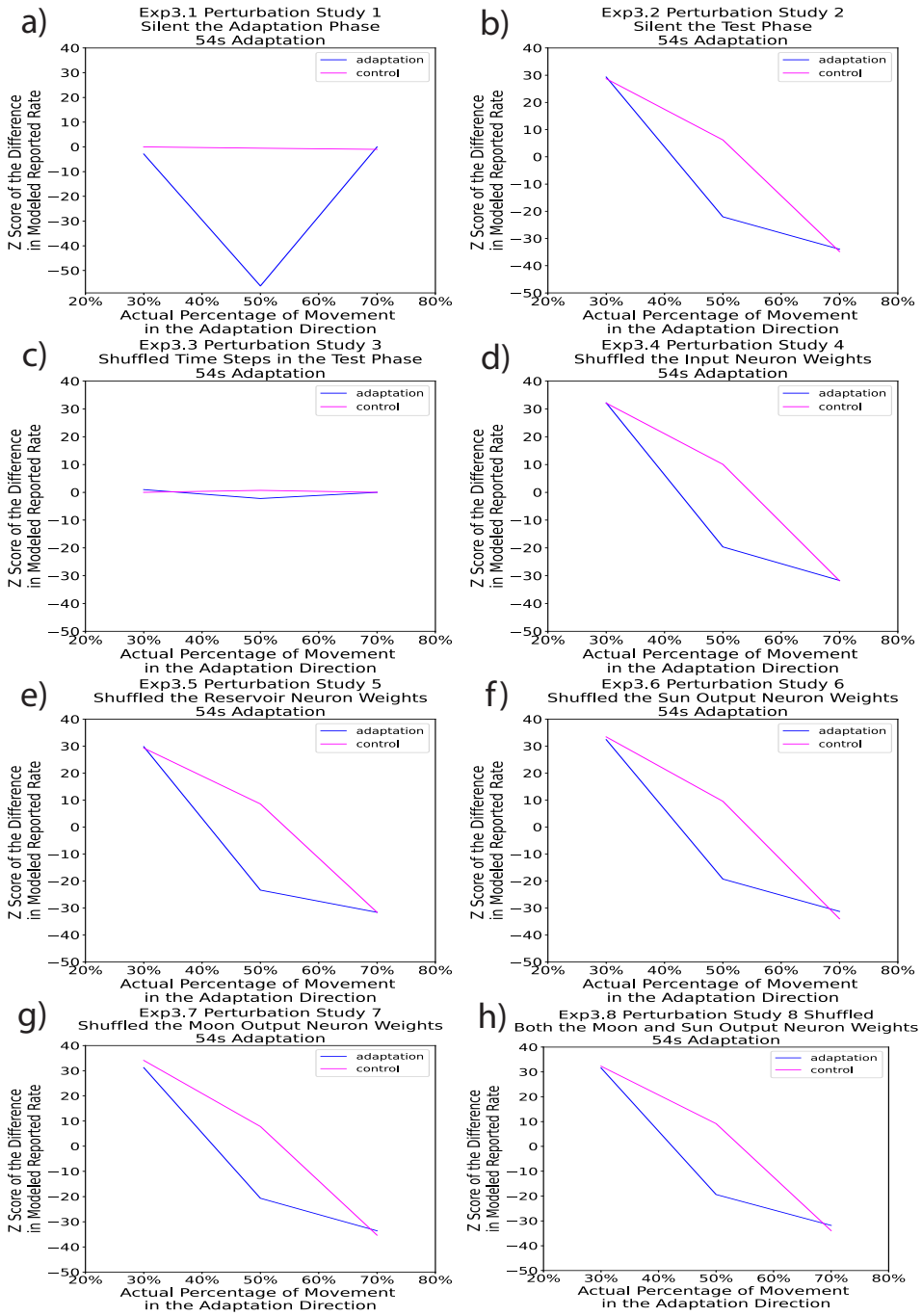

Figure B.15: Experiment 3 normalized difference in modeled reported rate between the perturbed model and the intact model for the 54s Adaptation: a) Perturbation study 1 - silent the adaptation phase. The perturbed adaptation line overlaps with the condition lines. b) Perturbation study 2 - silent the test phase c) Perturbation study 3 - shuffled time steps in the test phase b) Perturbation study 4 - shuffled the input neuron weights b) Perturbation study 5 - shuffled the reservoir neuron weights b) Perturbation study 6 - shuffled the sun output neuron weights b) Perturbation study 7 - shuffled the moon output neuron weights b) Perturbation study 8 - shuffled both the sun and moon output neuron weights

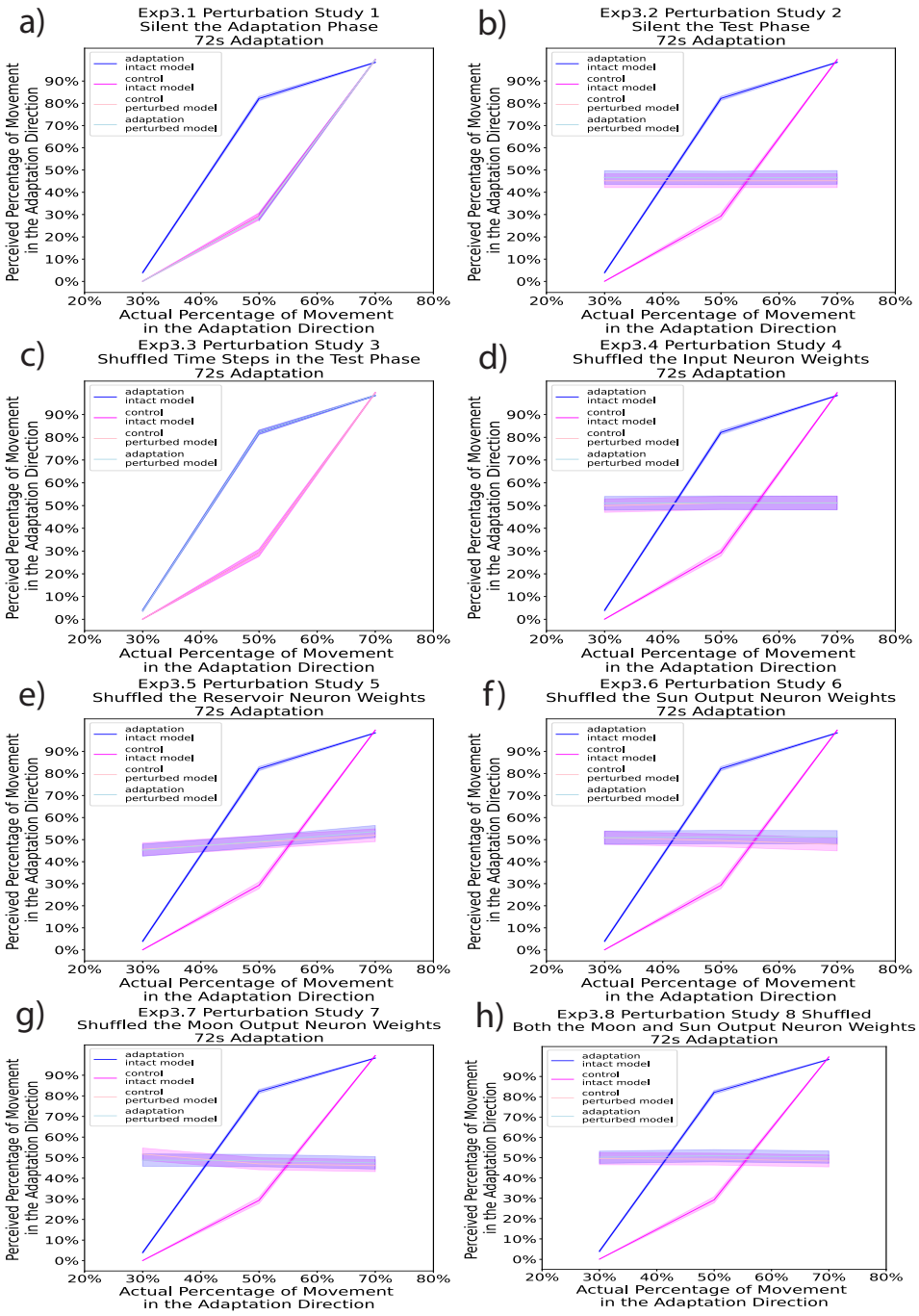

Figure B.16: Experiment 3 modeled reported rates predicted by the perturbed model and the intact model for the 72s Adaptation: a) Perturbation study 1 - silent the adaptation phase. The perturbed adaptation line overlaps with the condition lines. b) Perturbation study 2 - silent the test phase c) Perturbation study 3 - shuffled time steps in the test phase b) Perturbation study 4 - shuffled the input neuron weights b) Perturbation study 5 - shuffled the reservoir neuron weights b) Perturbation study 6 - shuffled the sun output neuron weights b) Perturbation study 7 - shuffled the moon output neuron weights b) Perturbation study 8 - shuffled both the sun and moon output neuron weights

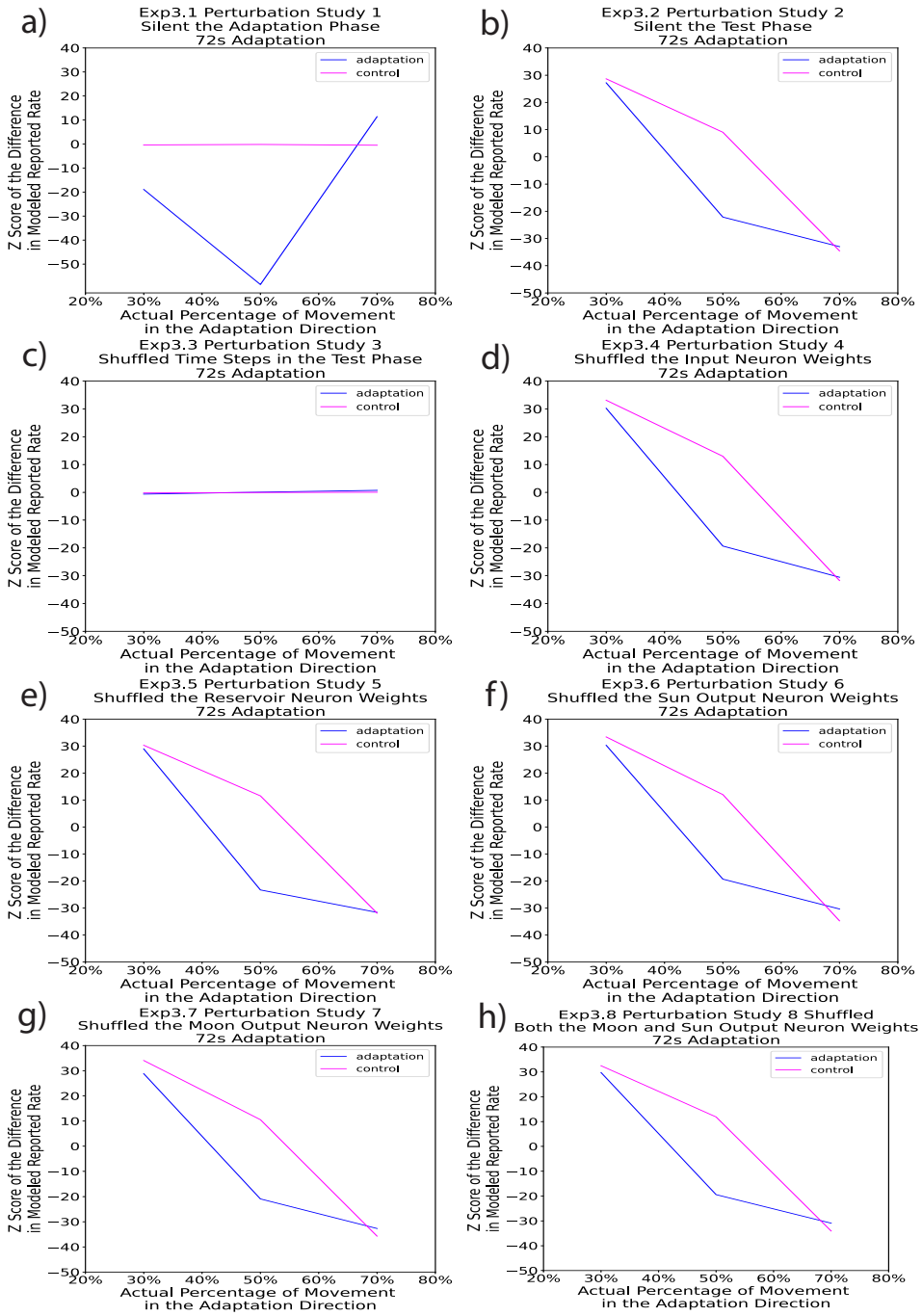

Figure B.17: Experiment 3 normalized difference in modeled reported rate between the perturbed model and the intact model for the 72s Adaptation: a) Perturbation study 1 - silent the adaptation phase. The perturbed adaptation line overlaps with the condition lines. b) Perturbation study 2 - silent the test phase c) Perturbation study 3 - shuffled time steps in the test phase b) Perturbation study 4 - shuffled the input neuron weights b) Perturbation study 5 - shuffled the reservoir neuron weights b) Perturbation study 6 - shuffled the sun output neuron weights b) Perturbation study 7 - shuffled the moon output neuron weights b) Perturbation study 8 - shuffled both the sun and moon output neuron weights

B.4 Experiment 1 Predicted By the Alternative Model

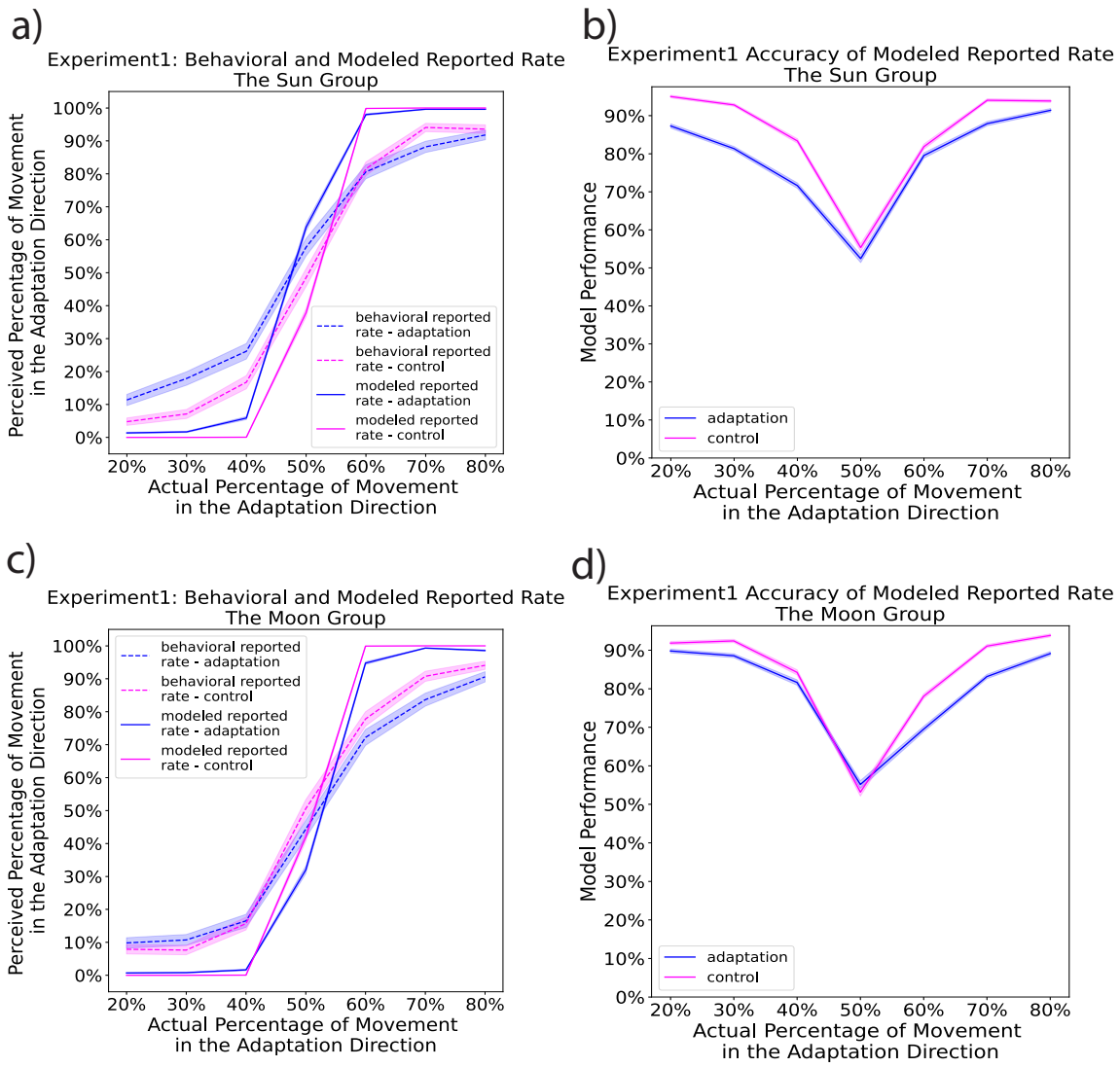

Figure B.18: Experiment 1 The Behavioral Reported Rate and the Modeled Reported Rate Using the Alternative Model Separated by Adaptation Groups: a) The modeled reported rate compared with the behavioral reported rate for the sun group (30 subjects). Similar to the behavioral data, for the predicted data, the adaptation condition showed significantly higher reported percentages than the corresponding control conditions at 20%, 30%, 40%, and 50%, supporting the aftereffect (all $ps < 0.001$). This result suggests an aftereffect in the same direction as the travel adaptation. Solid lines indicate the grand average value for the modeled reported rate, while dashed lines indicate the grand average for the behavioral reported rate. The shaded areas indicate 95% confidence interval of the mean. b) Accuracy of the modeled reported rate for the sun group (averaged trial-based classification accuracy across all simulations). The prediction accuracy decreased as the actual percentage of movement in the adaptation direction gets closer to 50%, which aligns with the task difficulty levels. The task gets more difficult as the actual percentage of movement in the adaptation direction gets closer to 50%. The shaded areas indicate 95% confidence interval of the mean. c) similar to a), The modeled reported rate compared with the behavioral reported rate for the moon group (30 subjects). d) similar to b), Accuracy of the modeled reported rate for the moon group (averaged trial-based classification accuracy across all simulations).